Surface and bulk characterisation of selected coals, bitumens and polymers as revealed by esca and other analytical techniques

Rosemary Wilson

A thesis entitled

'SURFACE AND BULK CHARACTERISATION OF SELECTED COALS, BITUMENS AND POLYMERS AS REVEALED BY ESCA AND OTHER ANALYTICAL TECHNIQUES'

Submitted by

Rosemary Wilson, M.Sc. (Dunelm)

A candidate for the Degree of Doctor of Philosophy

The Graduate Society,
University of Durham.

March 1984

Acknowledgements

I would like to express my sincere gratitude to Professor David T. Clark for his continued support throughout this research.

I am grateful to my colleagues and those members of the University who have assisted during this research. In particular I thank Dr W.J. Feast, Dr J.H. Edwards and Dr F. Steltzer (University of Graz, Austria) for their help and advice relating to the study of polyacetylene; Dr J.M.E. Quirke (now at Florida International University, U.S.A.), for many valuable discussions; and Dr J. Howard and Ms J. Nichol for performing the IINS analyses presented in Chapter Five. Dr G.A.L. Johnson is to be thanked for his advice, and the x-ray diffraction data presented in this thesis are due to the expertise of Mr R. Hardy; the use of weather records (Chapter Five), collated by Dr R. Harris is much appreciated. Dr P.J. Stephenson (whilst at the University of Guelph, Ontario, Canada) was responsible for the solid-state ^{13}C nmr spectra shown in Chapter Five.

The coal studies have been made possible through collaboration with a number of people to whom I remain indebted. They are: Dr A.G. Douglas, Dr J.M. Jones, Professor D.G. Murchison, Dr P.M.R. Smith and Mrs L. Summerbell (Organic Geochemistry Unit, University of Newcastle-upon-Tyne); Dr D. Blythe, Dr A. Gilbertson, Mr G.J. Liposits, Dr A. Mills and Dr R. Westerman (National Coal Board, U.K.); Dr H. Marsh (Northern Carbon Research Laboratories, University of Newcastle-upon-Tyne); Professor P.H. Given (Pennsylvania State University, PA, U.S.A.); Dr M.L. Gorbaty (Exxon Research and Engineering Company, Linden, N.J., U.S.A.); Dr J.M. Hunt (Woods Hole Oceanographic Institution, MASS, U.S.A.); and Dr H.L. Retcofsky (Pittsburgh Energy Technology Center, PA, U.S.A.).

Financial support was provided by the Science and Engineering Research Council. I am grateful to NATO and the British Vacuum Council for the provision of travel fellowships.

Finally, may I extend my thanks to Mrs R.L. Reed for her professional skills and patience in typing this manuscript.

Rosemary Wilson

Abstract

Electron spectroscopy for chemical applications (ESCA) has been used to study aspects of the surface chemistry of some polymeric materials of well defined composition, and in the characterisation of some naturally occurring carbonaceous materials, with particular attention to coal.

The selective surface modification of polymers by means of both straight hydrogen and oxygen plasmas and sequential plasma treatments has been studied. A detailed account of the changes in functional group distribution upon treatment is presented.

The surface treatment of polyvinyl alcohol with trifluoroacetic anhydride has been monitored using the non-destructive depth profiling capabilities of ESCA. Experimental results are complemented by data from computer simulation. The trifluoroacetylation of the surface hydroxyl functionalities of cellulose has been investigated.

Aspects of the preparation and surface chemistry of polyacetylene have been explored, with special reference to its passification towards atmospheric oxidation. The application of a mild hydrogen plasma treatment, prior to air contact, was found to produce an essentially hydrocarbon-like overlayer, more resistant to atmospheric oxidation than the untreated polyacetylene. Oxidation of the material beneath the overlayer did occur, possibly due to poor oxygen barrier properties of the overlayer.

A critical account of the use of ESCA in the understanding of the structure, bonding and reactivity of coal and coal-related materials has been presented. The value of ESCA in the characterisation of surface specific reactions has been exemplified by studies of surface oxidation reactions, both naturally occurring through weathering processes, and

artificially induced via irradiation with ultra-violet light. Other analytical techniques, including optical microscopy, solid state nuclear magnetic resonance and incoherent inelastic neutron scattering spectroscopies have been employed and provide supplementary data.

Memorandum

The research described in this thesis was carried out whilst the author was a research student at the University of Durham between October 1981 and October 1983. It has not been submitted for any other degree and is the original work of the author except where acknowledged by reference.

Work in this thesis has formed the whole, or part of the following publications.

1. 'Selective Surface Modification of Polymers by Means of Hydrogen and Oxygen Plasmas'. D.T. Clark and R. Wilson, J. Polym. Sci., Polym. Chem. Edn., 21, 837-853 (1983).
2. 'An Evaluation of the Potential of ESCA (Electron Spectroscopy for Chemical Applications) (and Other Spectroscopic Techniques) in the Surface and Bulk Characterisation of Kerogens, Brown Coal, and Gilsonite'. D.T. Clark, R. Wilson and J.M.E. Quirke, Chemical Geology, 39, 215-239 (1983).
3. 'ESCA Applied to Aspects of Coal Surface Chemistry'. D.T. Clark and R. Wilson, a paper presented (by RW) at the Society for Chemical Industry, Industrial Carbon and Graphite Group Symposium, 'Analytical Methods for Coals, Cokes, and Carbons', 28-29th April, 1983, London. Fuel, 62, 1034-1040 (1983).
4. 'Aspects of the Surface Chemistry of Coal, Kerogen and Bitumen as Revealed by ESCA'. D.T. Clark and R. Wilson, a poster presented (by RW) at the 11th International Meeting on Organic Geochemistry, 12-16th September, 1983, The Hague, Netherlands. Advances in Organic Geochemistry / J. Org. Geochem. (in press).

Contents

CHAPTER ONE

ELECTRON SPECTROSCOPY FOR CHEMICAL APPLICATIONS (ESCA)

CHAPTER ONE

ELECTRON SPECTROSCOPY FOR CHEMICAL APPLICATIONS (ESCA)

1.1 Introduction

The ESCA experiment involves the measurement of binding energies of electrons ejected by interactions of a molecule with a monoenergetic beam of soft X-rays. In common with most other spectroscopic methods, X-ray photoelectron spectroscopy is a technique originally developed by physicists and is now extensively utilized in the fields of inorganic, organic and physical chemistry providing valuable information on structure bonding and reactivity. [1]

Although independent investigations by De Broglie [2,3] and Robinson [4-6] into the photoelectric effect studied the X-ray induced electron emission from a variety of materials ranging from thin metal films to inorganic salts in the early part of the 20th century, only in the 1950s was the technique developed by Siegbahn and co-workers at the Institute of Physics, Uppsala University, Sweden. [7,8] Much of the pioneering work into high resolution X-ray photoelectron spectroscopy was carried out by Siegbahn, who christened the technique ESCA (Electron Spectroscopy for Chemical Analysis) which he later amended to Electron Spectroscopy for Chemical Applications. Siegbahn's two books 'ESCA Atomic, Molecular and Solid State Structure Studied by Means of Electron Spectroscopy' [9] and 'ESCA Applied to Free Molecules' [10] provide extensive documentation of his early work.

The development of electron spectroscopy pre-Siegbahn is covered in a review by Jenkin, Leckey and Liesengang. [11]

The technique of ESCA is also known as:

(1) X-ray Photoelectron Spectroscopy (XPS)

(2) High Energy Photoelectron Spectroscopy (HEPS)

(3) Induced Electron Emission Spectroscopy (IEES)

(4) Photoelectron Spectroscopy of the Inner Shell (PESIS)

At this point it is worth mentioning that a multitude of approaches are available by which electrons, characteristic of the material from whence they originated, may be generated. These distinct techniques, based upon the analysis of electron energies following a collision between an impacting particle or photon and an atom, molecule or solid, may be classified under the generic term 'electron spectroscopy'. Types of electron spectroscopy are listed in Table 1.1. A detailed description of individual techniques is beyond the scope of this thesis; however the interested reader is referred to recent reviews by Baker and Brundle [106] and Rhodin and Gadzuk [107] and references therein.

1.2 Fundamental Electronic Processes Involved in ESCA

1.2.1 Photoionisation

Irradiation of a molecule with X-rays causes electrons with binding energies less than that of the exciting radiation to be photo-ejected. [9] X-ray sources in common use today are $MgK\alpha_{1,2}$ and $A\ell K\alpha_{1,2}$ with photon energies of 1253.7eV and 1486.6eV respectively. The electrons ejected may be either core or valence electrons (Figure 1.1) though the latter are usually studied using ultra-violet photoelectron spectroscopy (UPS) [12] with He(I) radiation (21.22eV), or He(II) radiation (40.8eV).

Table 1.1 Types of Electron Spectroscopy [106]

Name of technique		Basis of Technique
Photoelectron spectroscopy (Ultraviolet excitation)	PES or UPS	Electrons ejected from materials by monoenergetic ultraviolet photons are energy analysed.
Photoelectron spectroscopy (x-ray excitation)	ESCA or XPS	Electrons ejected from materials by monoenergetic X-ray photons are energy analysed.
Auger electron spectroscopy	AES	Auger electrons ejected from materials following initial ionisation by electrons or photons (not necessarily monoenergetic) are energy analysed.
Ion neutralisation spectroscopy	INS	Auger electrons ejected from surfaces following impact of a noble gas ion are energy analysed.
Penning ionisation spectroscopy	PIS	Metastable atoms are used to eject electrons from materials. The electrons are then energy analysed.
Autoionisation electron spectroscopy		Similar to Auger electron spectroscopy. Electrons ejected in an auto-ionising decay of super-excited states are measured. Electron or photon impact can be used to produce the super-excited state.
Resonance electron capture Electron transmission spectroscopy	)	The elastic scattering cross-section for electrons is measured as a function of the energy of the electron beam and the scattering angle.

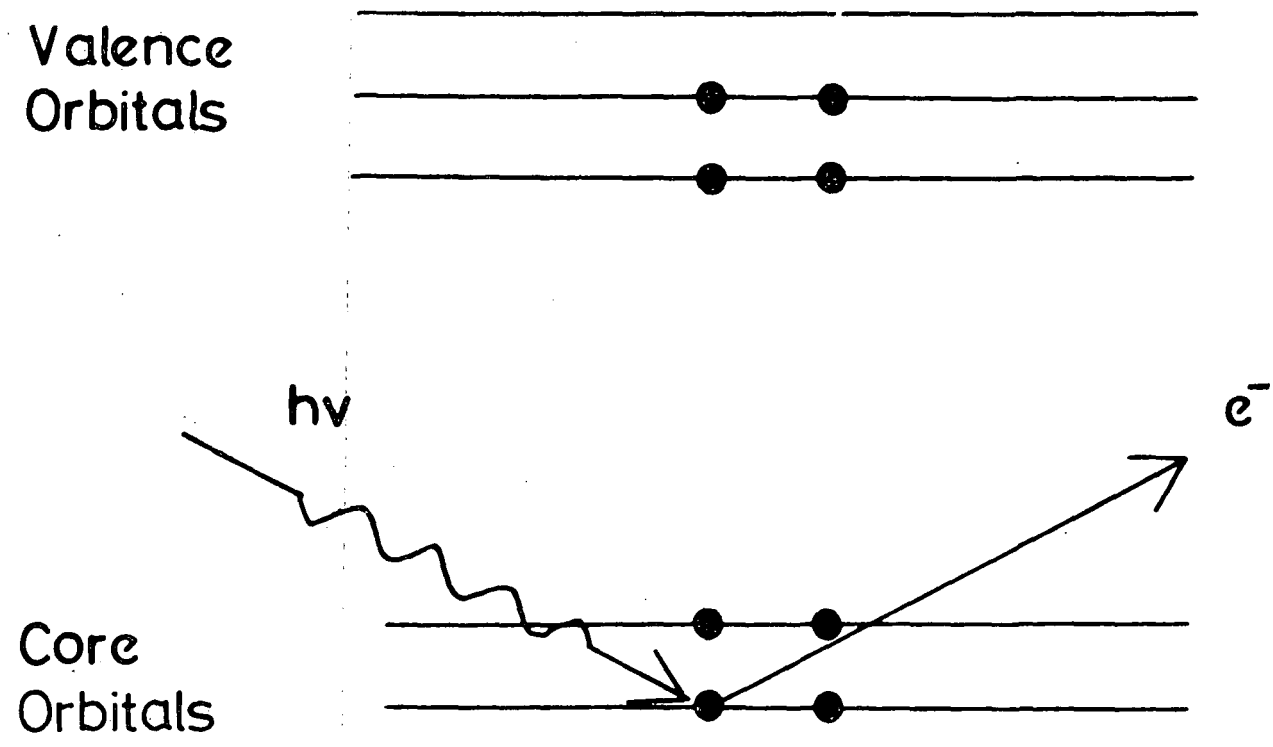

Figure 1.1 The photoionisation of a core level electron

It has been shown that the relative intensities of various peaks in the valence electron spectrum vary with differences in the incident excitation energy, not only between X-ray and U.V., but between X-ray photons of different energies.[26] These effects are attributed to differences in photoionisation cross-section involved in the various electron states in the valence band region. (The cross-section for photoionisation for a particular level is a measure of the probability of the level being ionised when irradiated by a photon of known energy, and is discussed more fully in Section 1.6.) Figure 1.2 demonstrates the striking difference between X-ray and U.V. valence band studies on carbon monoxide. The photon sources used are $A\ell K\alpha_{1,2}$ (1486.6eV) and He(1) (21.2eV): note the difference in relative peak intensities between the two spectra.

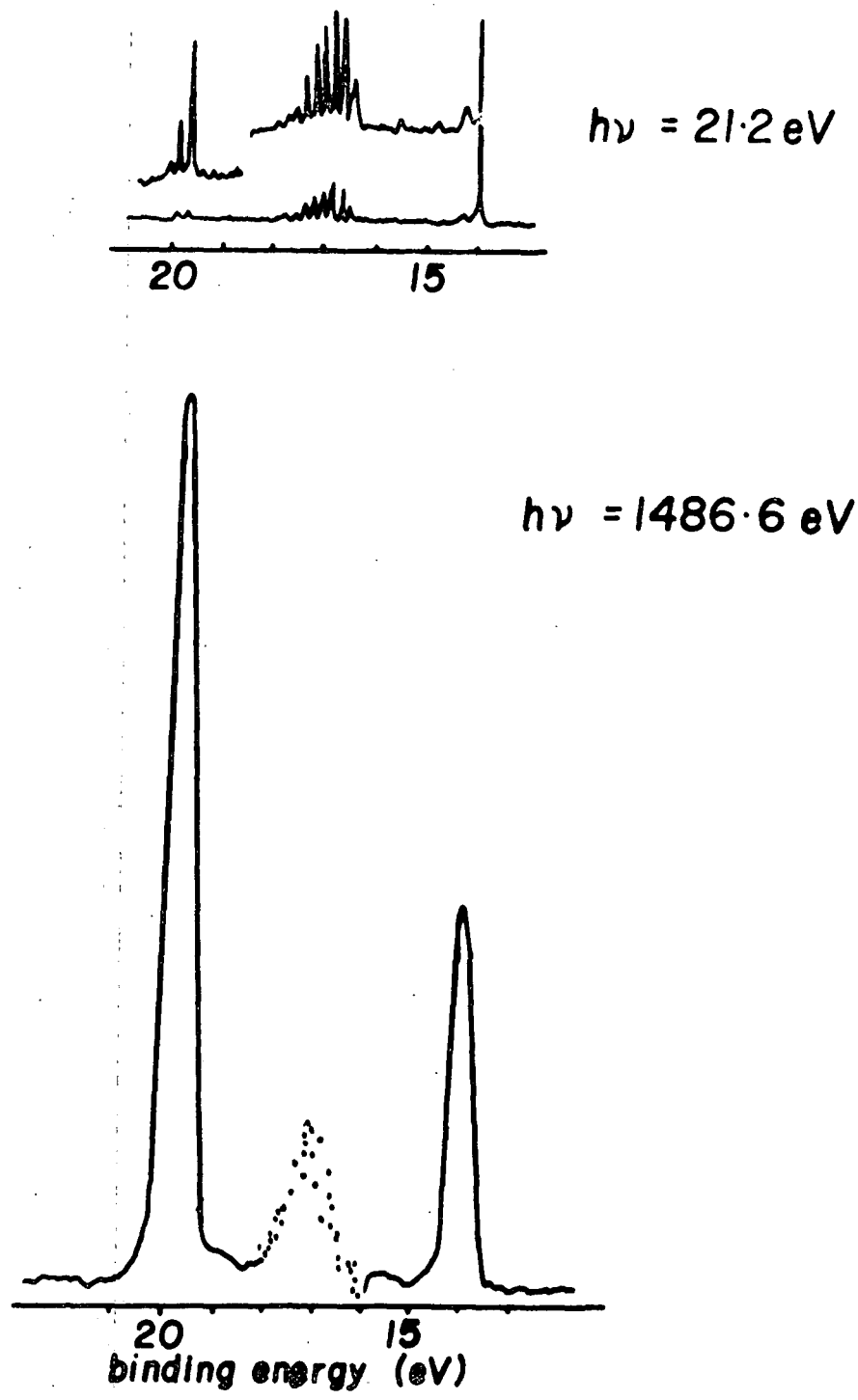

Figure 1.2 Valence band spectra of CO using He(1) and $A\ell K\alpha_{1,2}$ photon sources

The photoemission process is complete in typically $\sim 10^{-17}$ seconds.[13]

The total kinetic energy of an emitted photoelectron (K.E., which may include the contributions from the vibrational, rotational and translational motions, as well as electronic) is given by the equation 1.1.

$$K.E. = h\nu - B.E. - E_r \qquad (1.1)$$

where $h\nu$ is the energy of the incident photon; h is Planck's constant and ν is the frequency of the X-ray radiation. B.E. is the binding energy of the emitted electron which is defined as the positive energy required to remove an electron to infinity with zero kinetic energy, and E_r is the recoil energy of the atom. Siegbahn and co-workers[9] have shown that the recoil energy is usually negligible for light atoms when using typical X-ray sources, for example $MgK\alpha_{1,2}$ and $A\ell K\alpha_{1,2}$. This is not the case however where high energy X-rays, for example AgKα (22000eV) are employed, and recoil energies for light elements must be taken into account. Recent studies by Cederbaum and Domcke[14] show that these effects can lead to modifications of the vibrational band envelopes of light atoms and hence recoil energies for light elements must be considered. With the present resolution of typical ESCA spectra the excitations from the translational, vibrational and rotational motions are seldom observed to contribute to the final K.E. Therefore the equation for a free molecule reduces to equation 1.2.

$$K.E. = h\nu - B.E. \qquad (1.2)$$

It is important to understand the relationship that exists between the binding energies observed experimentally by ESCA for solids versus free molecules when compared with values calculated theoretically by *ab initio* and semi-empirical LCAO - MO - SCF treatments.

The most convenient reference level for a conducting sample is the Fermi level.[15] In a metal this level, sometimes referred to as the 'electron chemical potential', is defined as the highest occupied level at absolute zero.

The work function, $\emptyset_s$, for a solid is defined as the energy gap between the free electron (vacuum) level and the Fermi level in the solid, and is represented diagramatically in Figure 1.3. The vacuum

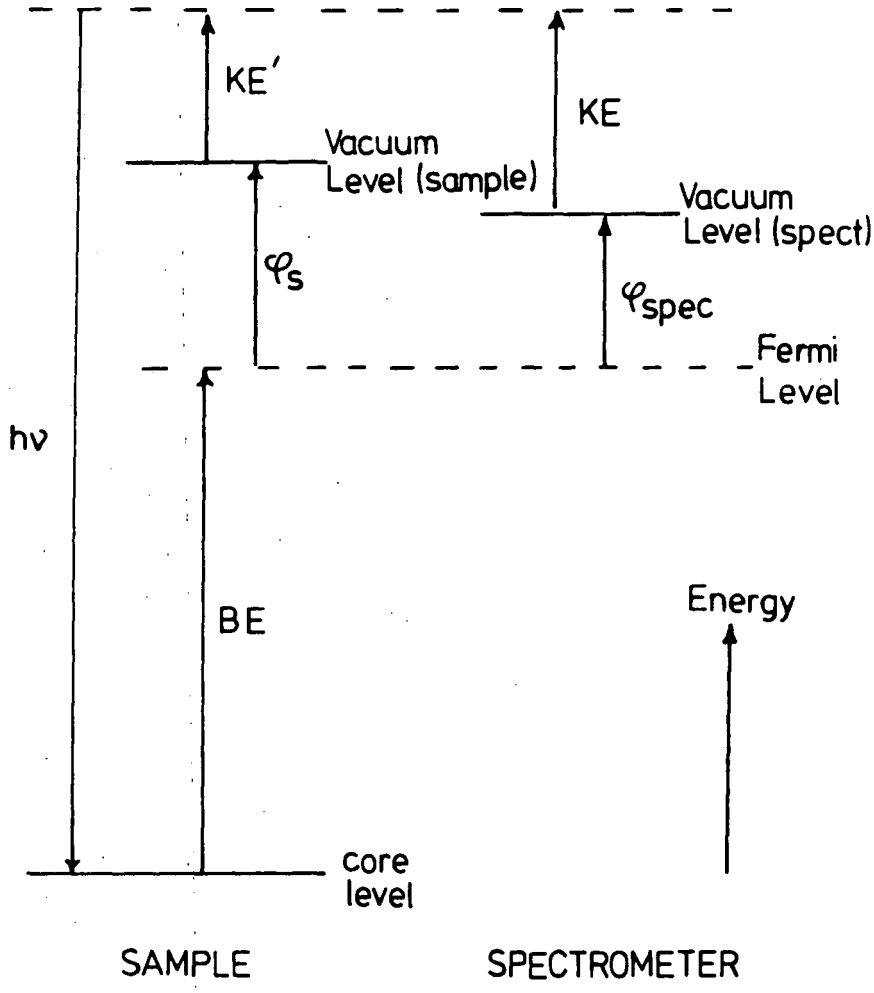

Figure 1.3 Relationship between vacuum level and Fermi level for a sample isolated from spectrometer

levels for the solid sample and the spectrometer may however be different and the electron will experience either a retarding or accelerating potential equal to $\phi_s - \phi_{spec.}$ where $\phi_{spec.}$ is the work function of the spectrometer.[9] In the ESCA experiment it is the kinetic energy of the electron when it enters the analyser that is measured, and taking zero binding energy to be the Fermi level of the sample, the following equation results

$$B.E. = h\nu - K.E. - \phi_{spec.} \qquad (1.3)$$

The binding energy referred to the Fermi level does not depend on the work function of the sample but on that of the spectrometer and this represents a constant correction to all binding energies. Energy referencing and sample charging effects will be considered in Section 1.5.

1.2.2 Processes Accompanying Photoionisation

Several processes may accompany photoionisation and these may be divided into two main categories depending upon whether they are slow compared to the original photoionisation or occur within a similar time span. Electron relaxation, shake-up and shake-off occur within a similar time span and result in modification of the kinetic energy of the photoelectrons. Auger emission and X-ray fluorescence however are comparatively slow processes and cause little effect on the kinetic energy of the photoelectrons.

1.2.3 Electronic Relaxation

Accompanying the photoionisation process, which is complete within a time span of approximately 10^{-17} seconds, there is a substantial electronic relaxation of the valence electrons.[16-18] It has been

shown by theoretical and experimental studies that the relaxation energy is a sensitive function of the electronic environment of a molecule [19-23] and hence is responsible for shifts in binding energies. Relaxation energies associated with core ionisations of first row elements have been found to be considerable [23,24] and are caused by the reorganisation of the valence electrons in response to the decreased shielding of the nuclear charge. This reorganisation changes the spatial distribution of the remaining electrons. The differences between relaxation energies for closely related molecules are small and therefore they cause only small changes in binding energies.

The theory of the chemical shift in core electron binding energies has received much attention.[18,26,27] Whereas the ionisation energies of core electrons in small molecules can be calculated by *ab initio* methods, this procedure is unrealistic when dealing with polyatomic molecules. [28] It is then necessary to resort to approximate semi-empirical methods. These take many forms. The use of Koopmans' Theorem [29] in the calculation of binding energies does not account for electronic relaxation, whereas self-consistent field (ΔSCF) calculations do take account of the relaxation energy (R.E.). This provides a method by which relaxation energies may be investigated, equation 1.4

$$\text{R.E.} = \text{B.E. (Koopmans)} - \text{B.E. (}\Delta\text{SCF)} \qquad (1.4)$$

1.2.4 Shake-up and Shake-off Phenomena

The removal of a core electron, which is almost completely shielding as far as the valence electrons are concerned, is accompanied by substantial reorganisation (relaxation) of the valence electrons in response to the effective increase in nuclear charge. This perturbation gives rise to a finite probability for photoionisation to be accompanied

by simultaneous excitation of a valence electron from an occupied to an unoccupied level (shake-up) or ionisation of a valence electron (shake-off) as shown in Figure 1.4. These relaxation processes result in excited states of the core ionised species. Since these phenomena

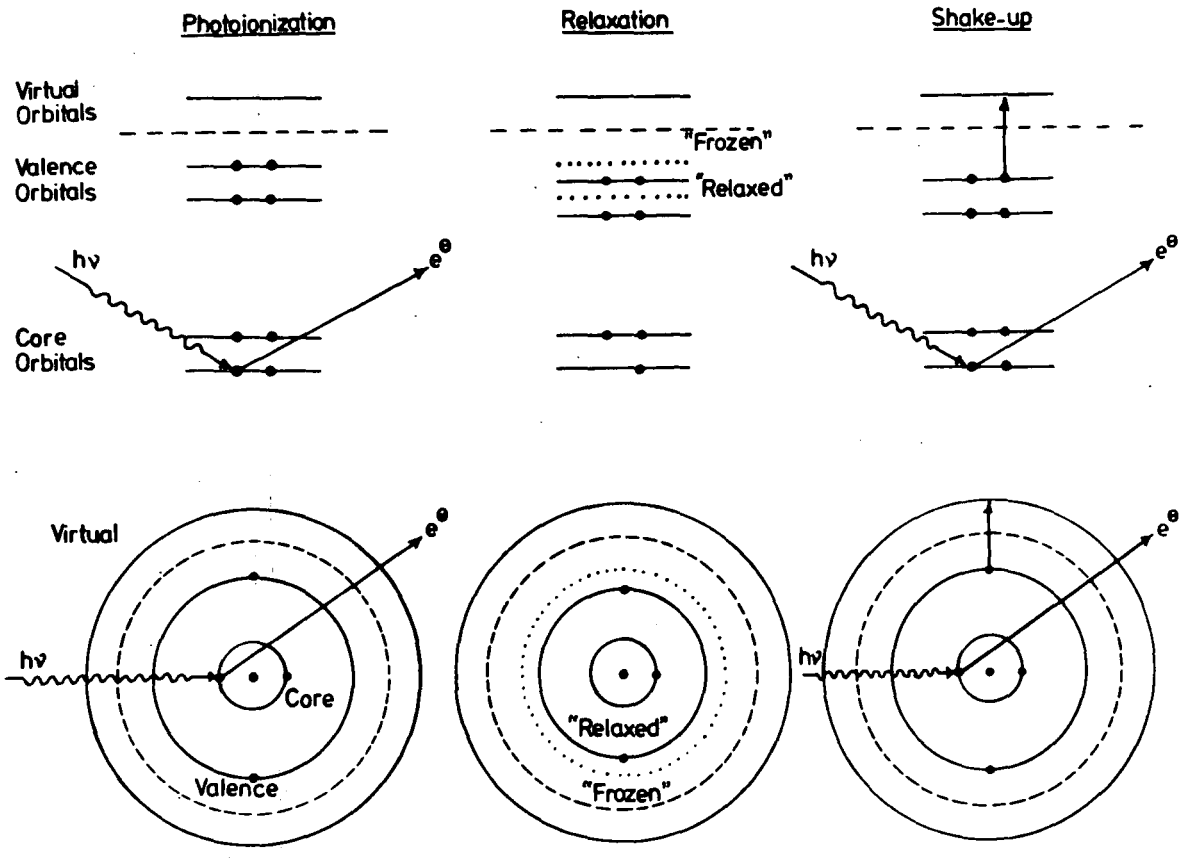

Figure 1.4 Photoionisation, shake-up and shake-off

take place on a similar time scale to photoionisation they result in a modification of the primary photoelectron signal producing satellite peaks occurring to the lower kinetic energy side of the main core signal. The shake-up process obeys monopole selection rules and may be viewed as an analogue of ultra-violet (U.V.) spectroscopy.

These processes have received much attention both from the experimental and theoretical standpoint. The theoretical relationship between shake-up and shake-off satellite intensities to the relaxation energy has been discussed by Manne and Åberg.[30] They showed that the weighted mean of the direct photoionisation, shake-up and shake-off peaks corresponds to the binding energy of the unrelaxed system (Figure 1.5).

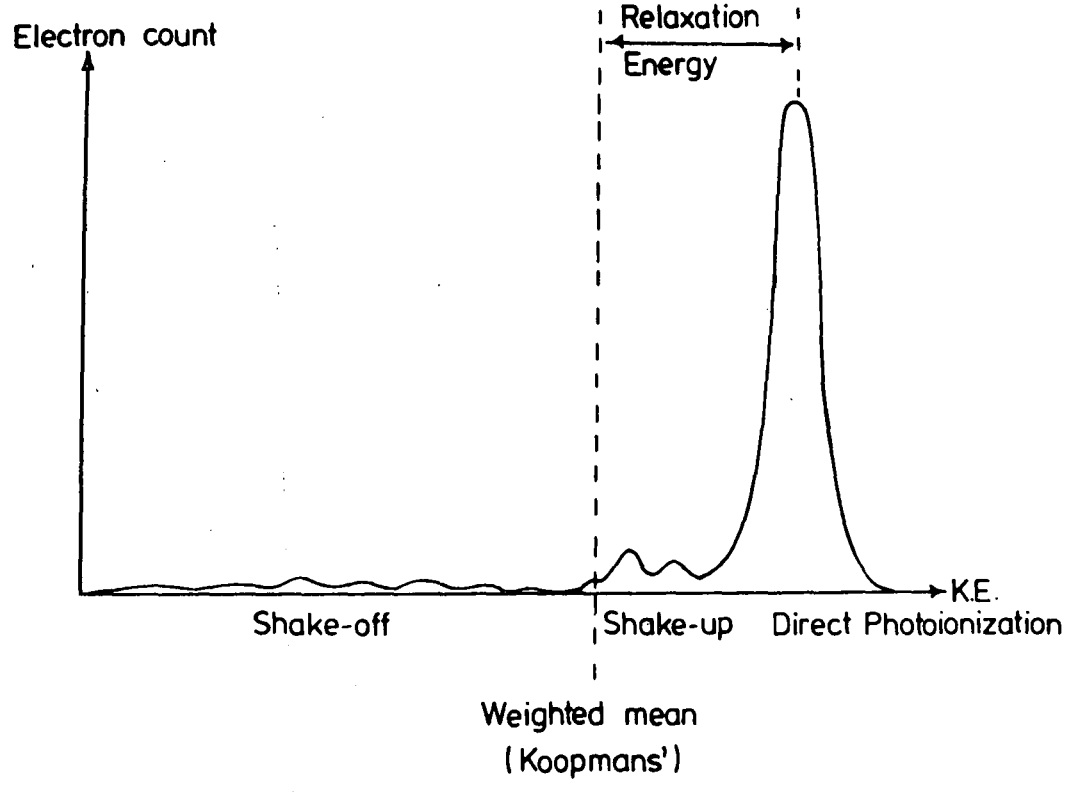

Figure 1.5 Relationship between relaxation energy, Koopmans' Theorem (mean) and the relative intensities of direct photoionisation, shake-up and shake-off

Shake-up and shake-off structure has been studied in a range of organic [31,32] and inorganic [33,34] materials, particular attention being paid to 'd' block elements. [104] The intensity of shake-up satellites varies from material to material, and the 3d spectra of the oxides La_2O_3 and CeO_2, for example, show satellite structure of comparable intensity to the main photoelectron signals. [35,36] In such cases difficulty is encountered in distinguishing satellite and parent signals. Shake-up peaks are most difficult to identify the stronger they are and may be mistakenly interpreted in terms of a chemical shift effect.

The phenomenon of shake-up has proved to be of use in elucidating fine details of structure and bonding in polymer systems which are not directly attainable from the primary information levels in ESCA. [37-39]

Shake-up effects have been the subject of a review. [40]

1.2.5 Auger Emission and X-ray Fluorescence

There are two principal processes through which de-excitation of the hole produced in a core sub-shell normally decays, namely X-ray fluorescence [41] and Auger electron emission. Both these processes, which are shown schematically in Figure 1.6, are comparatively slow compared to photoionisation and so they have little effect on the kinetic energy of the original photoelectron.

The probability for each process is a function of the atomic number of the atom as shown in Figure 1.7, Auger emission predominating for lighter atoms [8] while X-ray fluorescence is more important for heavier elements.

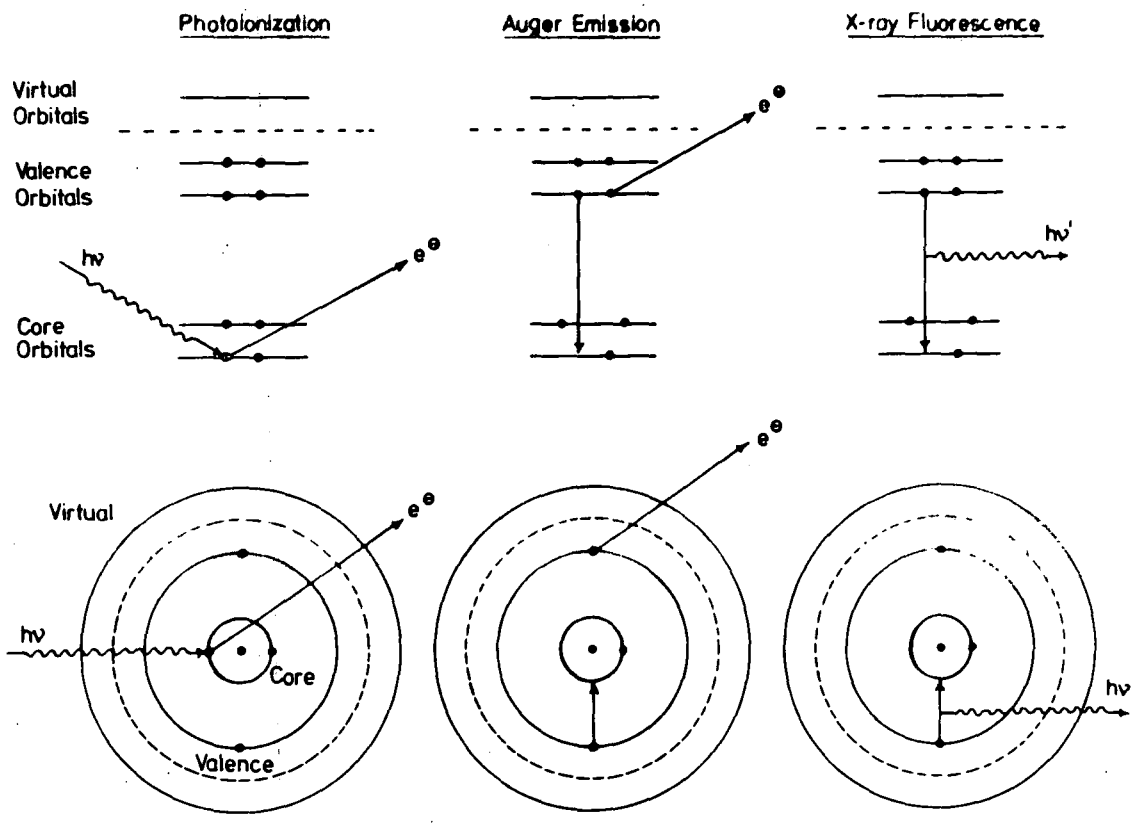

Figure 1.6 Photoionisation, Auger Emission and X-ray Fluorescence

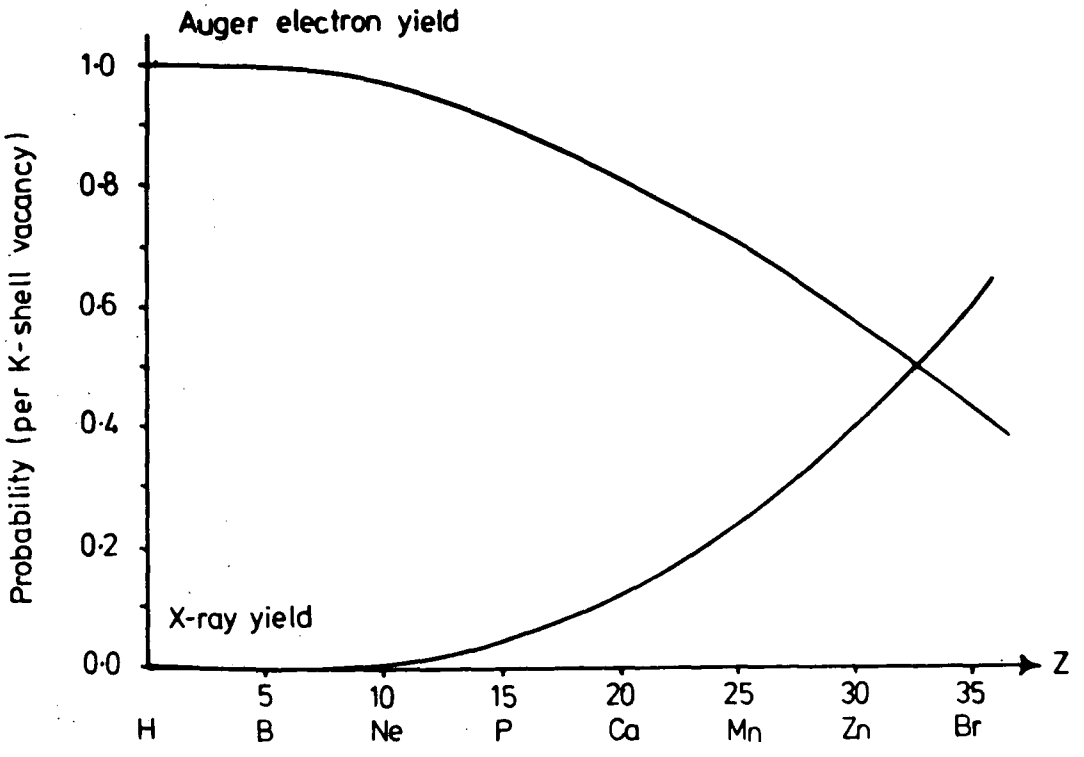

Figure 1.7 Efficiency of Auger and X-ray Fluorescence processes as a function of atomic number

Auger emission may be viewed as a two-step process in which the ejection of an electron from an inner shell by a photon is followed by an electron dropping down from a higher level to the vacancy in the inner shell with simultaneous emission of a second electron.[42-47] When the electron drops from a valence orbital, the Auger spectrum is related to the energies of both the valence and core orbitals. When the electron drops from an inner orbital, a Coster-Kronig[46] transition,

the Auger spectrum is related to the inner orbital transition. Such spectra are often very well resolved but unfortunately lead to broadening of the ESCA spectrum due to the very short lifetime of the process. For a Coster-Kronig process to occur, the difference in binding energies of the two inner shells must be sufficiently large to eject an electron from an orbital in the higher shell. These processes only occur in elements of atomic number <40. [119]

Auger Emission Spectroscopy (AES) is itself an important analytical technique in its own right and has found particular application to the study of the surfaces of metals and semi-conductors. Commercial Auger spectrometers use an electron beam as the source of excitation radiation of typically 2 keV rather than X-ray photons. The technique is highly surface-sensitive since the sampling depth of the exciting electrons is only about five atomic layers [48] or $\sim 1 \times 10^{-9}$m. It should be noted that the flux dosage of the incident electron beam used in AES is approximately three orders of magnitude larger than a normal ESCA photon beam and radiation damage caused to organic material poses a severe problem. [49,50]

Due to the complexity of the Auger electron signal, chemical information is not so straightforwardly extracted as in ESCA. However, in the case of metal oxides, for example, the Auger chemical shift is much larger than the photoelectron chemical shift because of polarisation screening effects; the direction of the shift being such that the kinetic energy of Auger electrons from more polarisable salts is increased more than is the energy of the photoelectrons.

From the work of Shirley, Kowalczyk, Ley, McFeely and Pollak [51-54] in their studies of systems of Cu, Zn, Li and Na, and from the independent investigations by Wagner [108] and with co-worker Bilden [25], a relationship

between shifts in Auger energy and the shifts in photoionisation peaks was derived. [54]

Wagner [55] has since developed the concept of the Auger Parameter, which is taken as the kinetic energy of the sharpest Auger line minus that of the most intense photoelectron peak, and is of considerable value to analytical chemists because it is a quantity independent of sample charging effects. Chemical state scatter plots [56,105,161] on which photoelectron and Auger data are represented for a given element are likely to be of considerable importance in the use of ESCA for identification of chemical states.

1.3 Chemical Shifts

The core electrons of an atom are essentially localised and do not take part in bonding. Their energies are characteristic of the particular element and are sensitive to the electronic environment of the atom. [1] While the absolute binding energy of a given core level on a given atom will be characteristic of the element (Table 1.2), differences in electronic environment of a given atom in a molecule give rise to a small range of binding energies, 'chemical shifts', often representative of a particular structural feature; the classical illustration being the C_{1s} spectrum of ethyl trifluoroacetate [159] shown in Figure 1.8. Shifts in core levels as a function of substituent for a wide range of polymers which have been investigated experimentally are shown in Table 1.3, and similar information exists for other core levels. [105] Such data taken in conjunction with relative cross-sections for photoionisation (to be covered in Section 1.6) from the relative core levels forms the basis for quantitative analysis by ESCA. This aspect will be treated in Section 1.11.

Table 1.2 Approximate core binding energies (eV)

	Li	Be	B	C	N	O	F	Ne
1s	55	111	188	284	399	532	686	867
	Na	**Mg**	**Aℓ**	**Si**	**P**	**S**	**Cℓ**	**Ar**
1s	1072	1305	1560	1839	2149	2472	2823	3203
2s	63	89	118	149	189	229	270	320
$2p_{1/2}$	31	52	74	100	136	165	202	247
$2p_{3/2}$	31	52	73	99	135	164	200	245

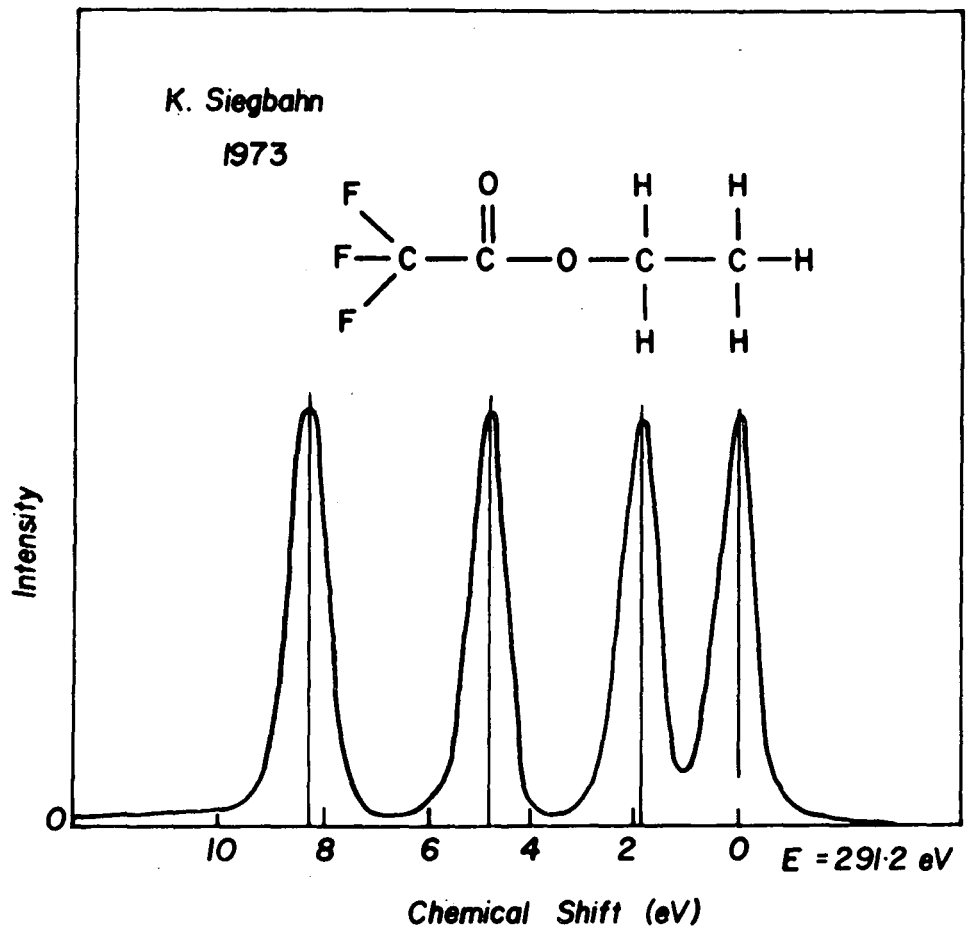

Figure 1.8 C_{1s} spectrum of ethyl trifluoroacetate [159]

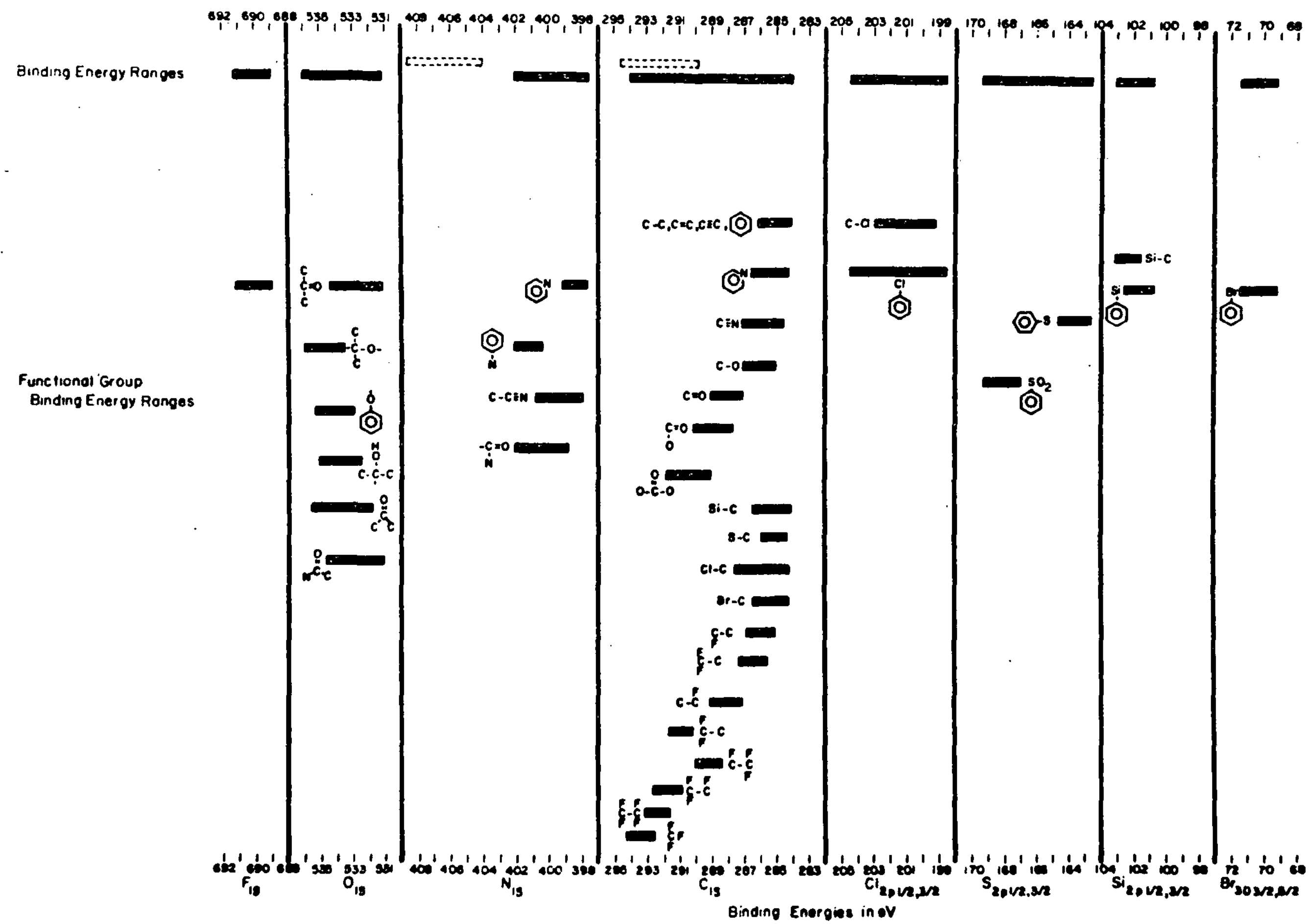

Table 1.3 Characteristic core level binding energies for various structural features in polymers

When choosing a core level for study, the following factors are worthy of consideration:

(1) The core level should have a high cross-section for photoionisation to give a high intensity spectrum.

(2) The escape depth of the electrons should be taken into account (see Sections 1.6 and 1.11).

(3) Levels should be chosen which are free from interference from other peaks in the same region of kinetic energy. This interference may be caused by either core level photoionisation peaks (e.g. Hg_{4f}/Si_{2p}) or Auger electron signals. An example of the latter is given by Figure 1.9 which shows wide scan ESCA spectra for a polymer sample studied with both $MgK\alpha_{1,2}$ and $Al k\alpha_{1,2}$ radiation. The change in photon energy allows a ready identification to be made of the direct photoionisation peaks and those arising from Auger processes since the kinetic energy of the latter are independent of the way in which the initial hole is created. Thus the well-developed fluorine Auger spectrum is readily identified whilst the distinctive core-level spectra show that the material contains fluorine and carbon.

(4) The line widths should be sufficiently narrow so as not to obscure subtle chemical shifts.

(5) The peak should be well removed from high background signals, that is, there should be a high signal to noise ratio.

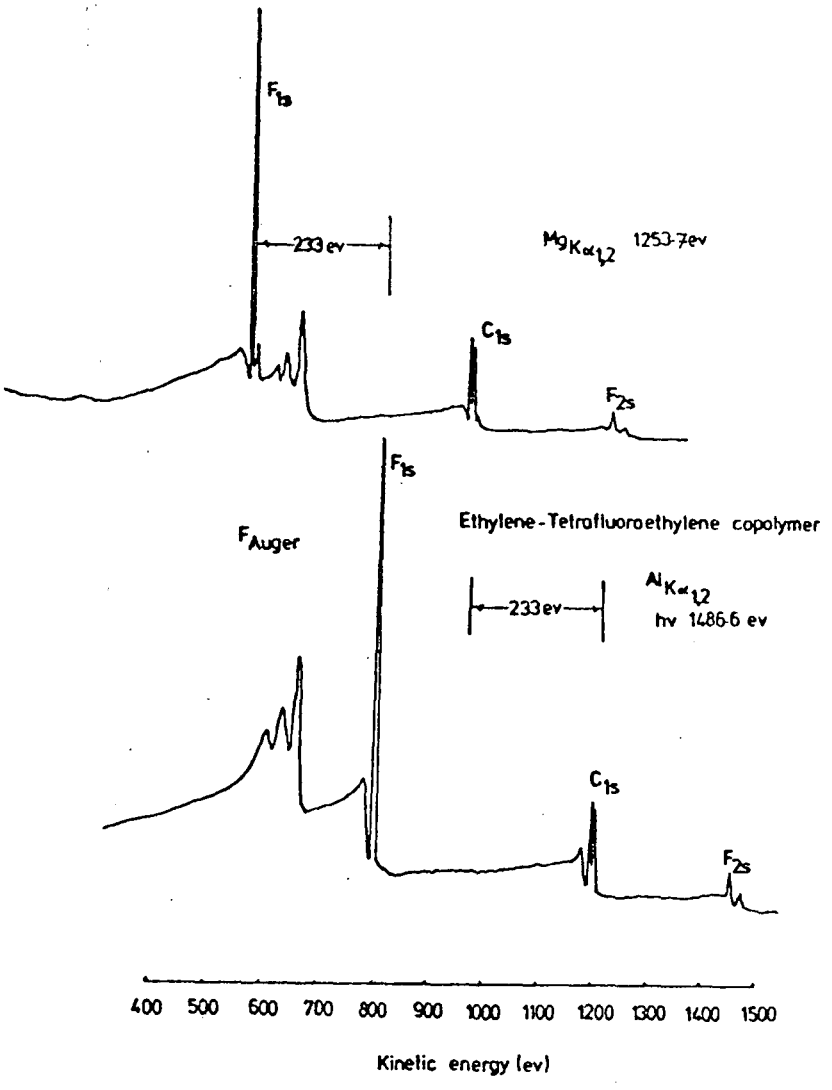

Figure 1.9 Wide-scan ESCA spectra for an ethylene-tetrafluoroethylene copolymer with $MgK\alpha_{1,2}$ and $A\ell K\alpha_{1,2}$ photon sources showing differentiation between photoionisation and Auger peaks

Much attention has been paid to the theoretical interpretation of the chemical shift phenomenon observed experimentally. The following distinct but interrelated approaches have been used:

(1) Koopmans' Theorem [29]

(2) Core Hole Calculations [58,59] - linear combination of atomic orbitals - molecular orbital - self-consistent field method (LCAO MO SCF)

(3) Equivalent Cores Model [57]

(4) Charge Potential Model [10]

(5) Quantum Mechanical Potential Model [60-62]

(6) Many body formalism

An account of the physical processes involved in electron photoemission and their effects for a theoretical standpoint has been given by Fadley. [63]

1.4 Fine Structure

1.4.1 Multiplet Splitting

Multiplet splitting of core levels is the result of spin interaction between an unpaired electron resulting from the photoionisation process and other unpaired electrons present in the system. Examples can be found in the core level spectra of transition element compounds.[64,65] The theoretical interpretation of multiplet effects is relatively straightforward only for s-hole states and is based on Van Vlecks' vector coupling model. [66] The magnitude of the splitting provides information concerning the localisation or delocalisation of unpaired electrons in a compound, since the greater the localisation and spin densities on an atom the greater will be the observed splitting. Multiplet splittings in photoelectron spectroscopy have been reviewed in some detail by Fadley.[67]

1.4.2 Spin Orbit Splitting

When photoionisation occurs from an orbital which has an orbital quantum number (ℓ) greater than 1, i.e. from a p, d or f orbital, then coupling can occur between the spin (S) and orbital angular momentum (L) to yield a total momentum (J). A doublet, which is usually well-resolved, is then observed in the spectrum instead of a single peak.[9] The relative intensities of the component peaks of the doublet are proportional to the ratio of the degeneracies of the states which is quantum mechanically defined as $2J + 1$. The relative intensities of the J states for s, p, d and f orbitals are shown in Table 1.4 and illustrated in Figure 1.10.

Table 1.4 J states for s, p, d and f orbitals

Orbital	Orbital Quantum No.	Total Quantum No.	Intensity Ratio
	ℓ	$J = (\ell \pm S)$	$2J+1) : (2J^{1}+1)$
s	0	$^1/_2$	singlet
p	1	$^1/_2$, $^3/_2$	1 : 2
d	2	$^3/_2$, $^5/_2$	2 : 3
f	3	$^5/_2$, $^7/_2$	3 : 4

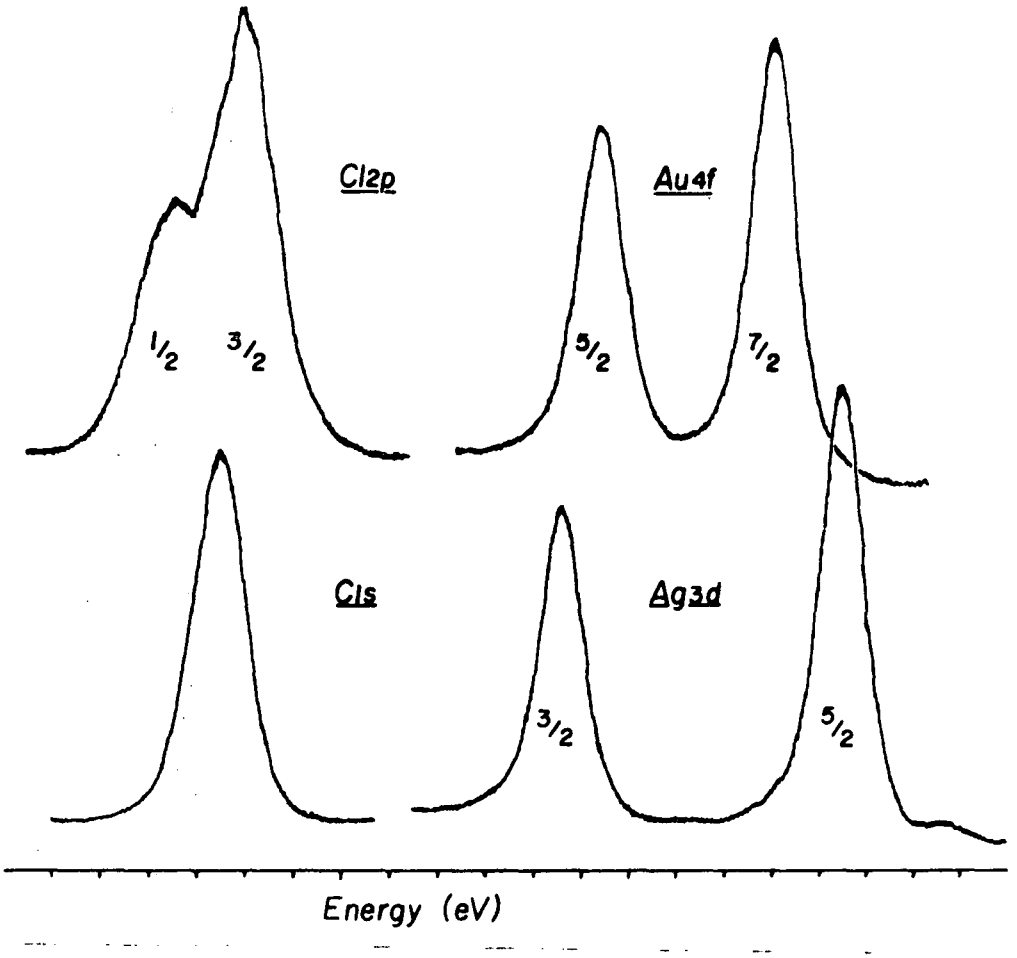

Figure 1.10 Spin-orbit splittings in C_{1s}, $C\ell_{2p}$, Ag_{3d} and Au_{4f} core levels

1.4.3 Electrostatic Splitting [68-70]

This is caused by the differential interaction between the external electrostatic field and the spin states of the core level being investigated. It has been observed for a number of systems,

for example, the $5p_{3/2}$ levels of uranium and thorium and in some compounds of gold.[71,72] Correlation has been observed between electrostatic splitting and the quadrupole splittings obtained from Mössbauer spectroscopy,[73] which arise from the interaction of the nuclear quadrupole moment with an inhomogeneous electric field.

A summary of the type of splitting encountered in ESCA is given in Figure 1.11.

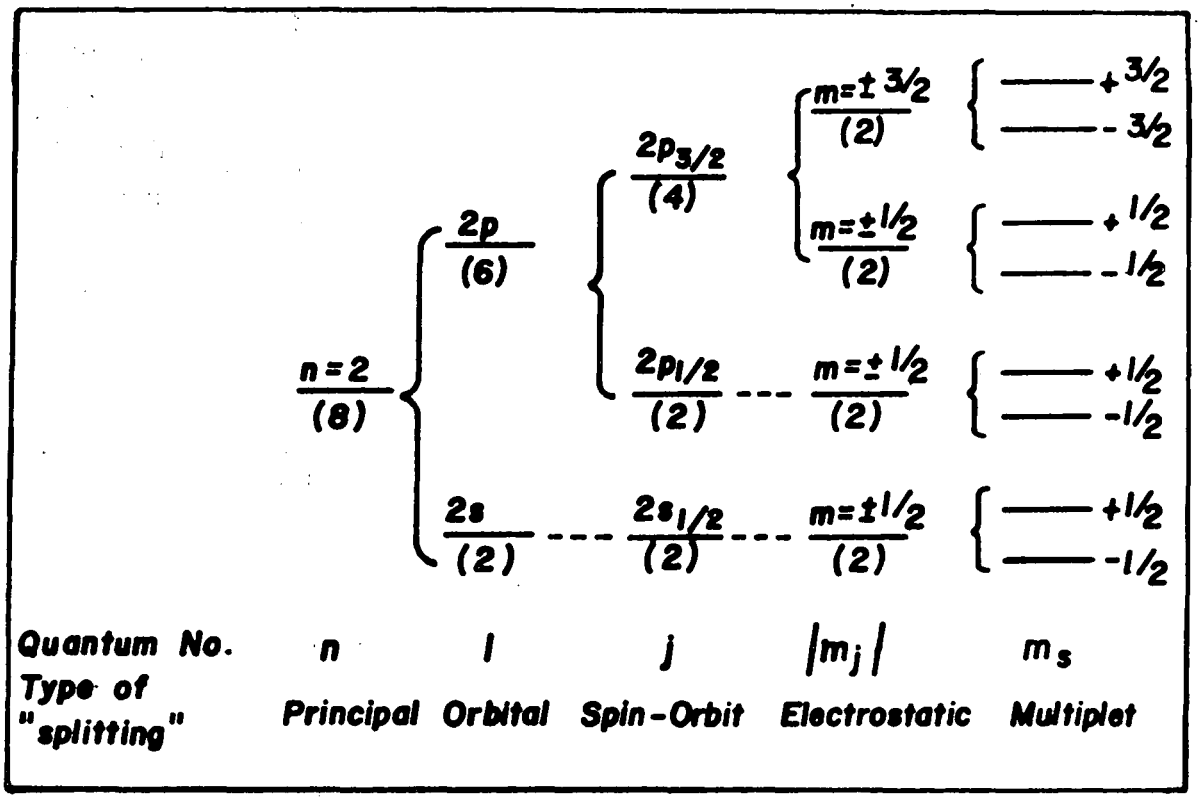

Figure 1.11 Schematic of the types of splitting encountered in ESCA

1.5 Sample Charging and Energy Referencing

As mentioned previously, for conducting samples in electrical contact with the spectrometer, the Fermi level serves as a convenient level for energy referencing. However, with insulating samples or samples not in contact with the spectrometer, the Fermi level is not so well-defined and some calibration procedure must be adopted in order to correct for this.

The phenomenon of 'sample charging' associated with insulating samples arises from the inability of the sample to replace electrons at the surface from the surroundings in contact with the sample, either through conduction from the sample backing or by capture of stray electrons from the vacuum system.[74-76] This stray electron flux, which comprises slow electrons photoemitted from the sample, from photoelectrons generated by X-ray impact on the X-ray window and on the chamber walls, for example, has been shown to amount to 99% of the total photoemitted flux for an insulating sample.[76] Photoemitted electrons from the surface experience a net retardation and therefore larger binding energies are measured. All photoelectrons are affected by the same retardation voltage and are shifted in energy by the same amount.

For a sample with a uniformly distributed positive surface charge, the energy equation for a solid becomes:

$$K.E. = h\nu - B.E. - \phi_S - \Delta \qquad (1.5)$$

where Δ is the energy shift due to the positive sample charge.

A non-uniform distribution or non-equivalent positive potential ('differential sample charging') over the surface of the sample will lead to a broadening of the primary photoelectron peak.

This is because the electrons from core levels of atoms of different charge will experience different retardation potentials at the surface.

One method by which charging may be detected is to vary the incident electron flux by means of an electron 'flood gun'.[120] Additional low energy electrons are released into the sample region: if the photoelectron peaks move to lower apparent binding energy, charging effects are present. Indeed, the use of such flood guns has found application in the study of the complex charging effects arising from conducting and insulating catalyst sites in industrial catalysts.[121]

The prime motivation for the use of electron flood guns is the very large sample charging for thick insulating samples in spectrometers employing monochromatic X-ray sources. The removal of bremsstrahlung as a source of secondary electrons can lead to shifts in kinetic energy scale in the hundred eV range and can be compensated by flooding the sample with low energy electrons. Samples can become negatively charged however, and the method needs great care to achieve an accuracy comparable with that of other methods.

An alternative source of low energy electrons is to illuminate the sample region with U.V. radiation from a low pressure, low power mercury lamp via a quartz viewing port in the source region of the spectrometer. Sufficient secondaries are generated from photoemission, from the metal surfaces of the sample analysis chamber, that sample charging is reduced to a low level.[122]

The most convenient method for overcoming the problems of sample charging connected with energy referencing employed in routine analyses is to use a suitable reference peak. A correction factor calculated from the observed kinetic energy of the photoelectrons

corresponding to the reference peak is then used to find the binding energies of the other peaks. The two most commonly used calibration lines are the C_{1s} peak from $(\underline{C}H_2)_n$ environments at 285.0 eV binding energy, either inherent in the sample or arising from hydrocarbon contamination within the spectrometer, [77-78] and the $Au_{4f\ 7/2}$ level at 84.0 eV, if the sample has been deposited on a gold substrate. [1]

A study by Clark, Dilks and Thomas [123] into the sample-charging phenomena arising in the ESCA experiment for a series of polymers has shown sample charging to be of importance as an information level in its own right. For samples studied as films or powders mounted insulated from the spectrometer probe and for gold under similar conditions, it has been shown that over a wide range of operating conditions, equilibrium charging shifts are characteristic of the sample and show a strong dependence on the theoretically calculated total photoionisation cross-sections. The surface sensitivity of the phenomenon has been demonstrated by monitoring changes in changing shifts as a function of hydrocarbon contamination, or in the case of thin films deposited on gold. The time-dependent behaviour of charging shifts for polymer films mounted directly in contact with the spectrometer was also reported. The utility of studying sample-charging shifts was demonstrated by reference to changes which occur upon surface modification of an ethylene-tetrafluoroethylene copolymer system in radio frequency plasmas excited in inert gases. Detailed ESCA analyses of both the core and valence spectra for the polymer system under similar reaction conditions have shown that the chemical changes which occur produce a surface which has a greatly reduced fluorine content. [124-127] The considerable difference existing between the charging characteristic of the fluorine

containing copolymer and of a solely hydrocarbon based polymer such as polyethylene made it possible for the change in surface composition to be monitored by sample charging measurements.

1.6 Signal intensities

The geometry employed in the ES200B spectrometer with a fixed arrangement of analyser and X-ray source is depicted in Figure 1.12.

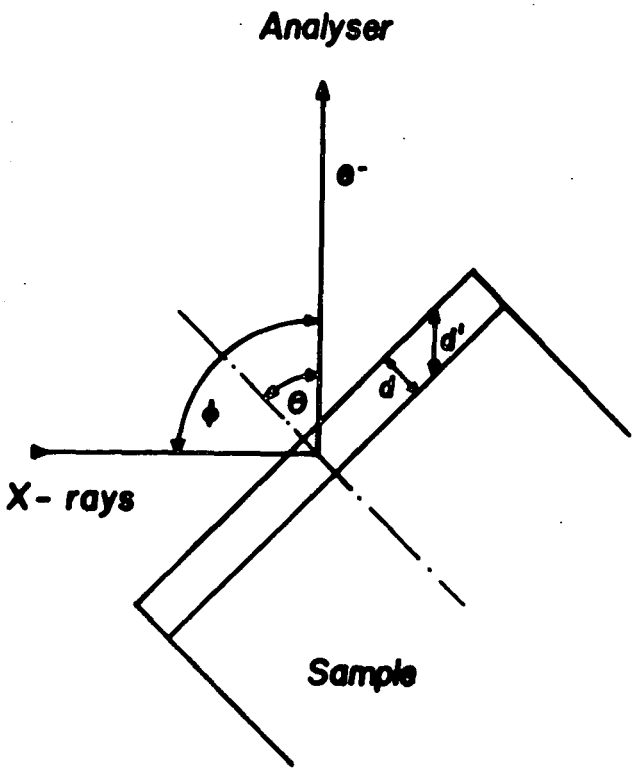

Figure 1.12 Schematic of the sample geometry relative to the X-ray gun and analyser

$h\nu$ represents the incident photon beam and e^- is the fraction of photoemitted electrons entering the analyser, $\emptyset$ is the angle between the X-ray source and the analyser entrance slit and θ describes the angle of the sample in relation to the analyser. If the photoelectrons are emitted from a depth, d, of the sample, their true path length will be d^1 where

$$d^1 = d \text{ cosec } \theta \qquad (1.6)$$

Due to the short mean free paths of electrons (for K.E. > 50eV) in solids it is possible to enhance surface features with respect to bulk and subsurface by conducting experiments involving grazing exit of the photoemitted electrons which are analysed, that is with θ approaching 90^o. Angular dependence studies are only feasible on uniform flat surfaces (e.g. films or coatings) and is not applicable to samples with rough surface topography, such as is the case for powders.

For an infinitely thick homogeneous sample the intensity (I) of the elastic (no energy loss) photoionisation peak corresponding to photoionisation from a core level i may be expressed as: [79,80]

$$dI_i = F\alpha_i N_i k_i e^{-x/\lambda_i} dx \qquad (1.7)$$

where: I_i is the intensity arising from core level i,

F is the exciting photon flux,

α_i is the cross section for photoionisation in a given shell of a given atom for a given X-ray energy,

N_i is the number of atoms per unit volume on which the core level i is localised,

k_i is the spectrometer factor,

λ_i is the electron mean free path.

On integration the equation 1.7 becomes:

$$I_i = \int_0^\infty F\alpha_i N_i k_i e^{-x/\lambda_i} dx \qquad (1.8)$$

$$I_i = F\alpha_i N_i k_i \lambda_i \qquad (1.9)$$

The parameters affecting the intensity of a given signal in ESCA are discussed more fully below.

The X-ray flux, F, is primarily dependent on the power applied to and the efficiency of the X-ray gun. However, the angle of incidence $\emptyset$ of the X-rays and the analyser and θ do have an effect on the intensity of the photoionisation peak.

The cross-section for photoionisation of core level i, α_i, is a parameter which describes the probability of the core level being ionised when irradiated by a photon of known energy [81] and includes only the fraction of the total number of electrons photoemitted within the angle of acceptance of the analyser focussing lens. α_i is a function of the core level to which it relates and the energy of the incident photon. Values of α_i may be calculated from the fundamental properties of the atom [82] or determined experimentally from gas phase ESCA experiments. [10] The geometry of the X-ray source with respect to the analyser entrance slit affects α_i values, but for a particular spectrometer and using the same X-ray source and with a fixed value of $\emptyset$ then α_i is normally a constant. With $MgK\alpha_{1,2}$ and $A\ell K\alpha_{1,2}$ the cross-sections for photoionisation for core levels of most elements of the periodic table are within two orders of magnitude of that for the C_{1s} levels, therefore ESCA has a convenient sensitivity range for all elements. The cross-sections for core levels are normally considerably higher than those for valence levels.

The spectrometer factor, k_i, includes contributions due to detector efficiencies, analyser transmission characteristics which are both dependent on the kinetic energy of the core electrons being analysed, and geometric factors such as the solid angle of acceptance of the analyser.

The inelastic mean free path of photoemitted electrons (sometimes referred to as the escape depth) λ_i, is defined as the distance in the solid through which the electrons will travel before $^1/_e$th of them have not suffered energy loss through inelastic collisions. Both experimental [83,84] and theoretical [85] calculations of λ_i have been undertaken. λ_i is related to the kinetic energy of the photoionised electrons and ranges from ~4Å. for electrons of about 80eV K.E. to ~30Å. for electrons of about 1500eV. This variation is presented graphically in Figure 1.13.

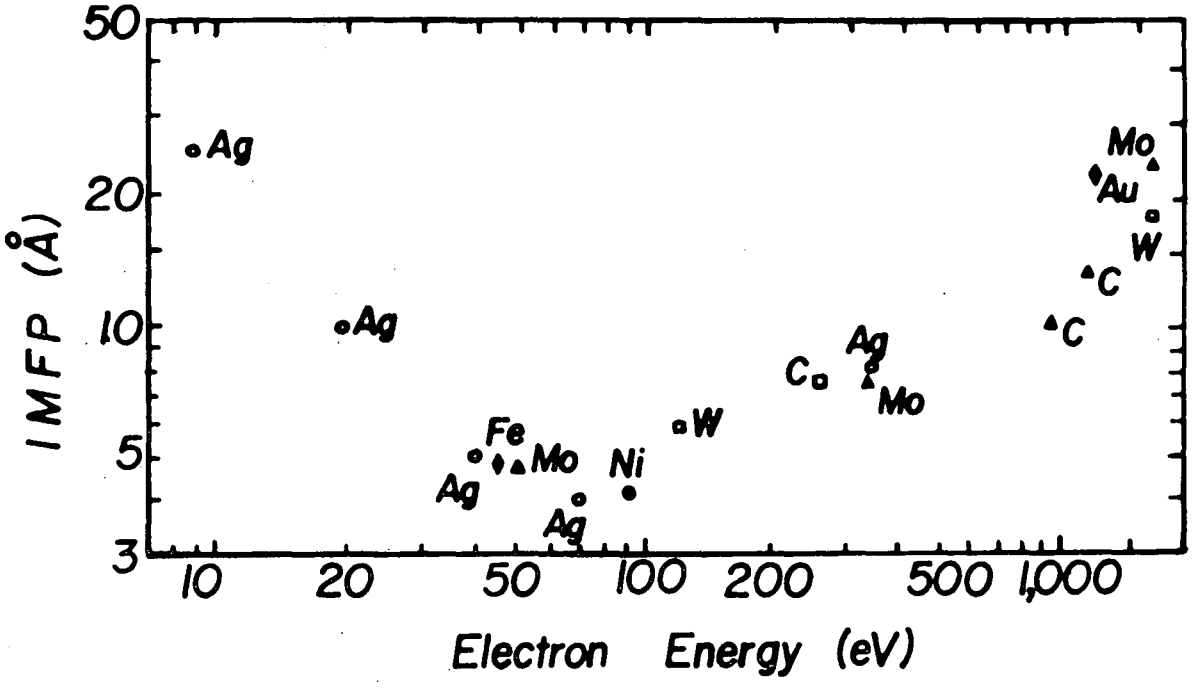

Figure 1.13 Mean free paths of photoemitted electrons

The sampling depth (not to be confused with the electron mean free path) is defined as the depth from which 95% of the signal, arising from a given core level, derives and may be related to λ by

$$\text{Sampling depth} = -\lambda \ln 0.05 \qquad (1.10)$$

$$\simeq 3\lambda \qquad (1.11)$$

As an example, for carbon 1s levels studied by a $MgK\alpha_{1,2}$ X-ray source the kinetic energy of the photoelectrons is ~960eV and the mean free path of the electrons is ~15Å. 50% of the signal seen by ESCA derives from the outermost 10Å. of the sample and 95% from the top 45Å. This illustrates the high surface sensitivity of ESCA.

It has been noted that the sampling depth varies with λ and this effect is clearly illustrated by the high and low kinetic energy germanium peaks (Ge 3d 1222eV and Ge 2p 268eV) from a sample of germanium with a passive oxide surface, as shown in Figure 1.14.

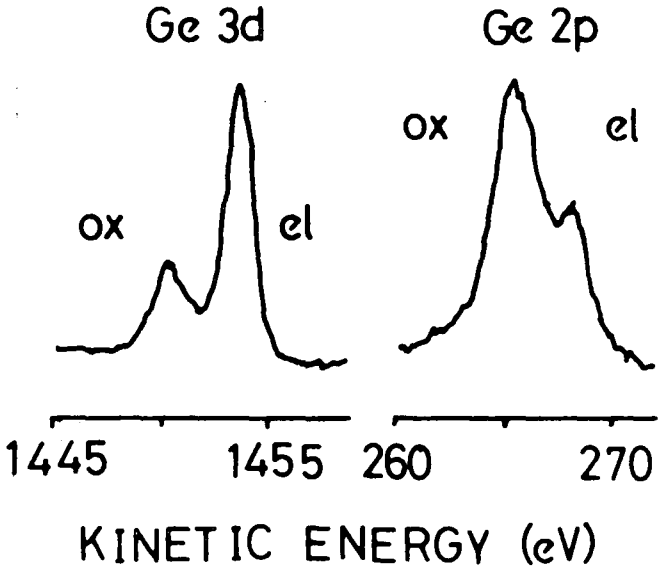

Figure 1.14 Ge core level spectra from Ge metal with a passive oxide overlayer, illustrating the greater sampling depth of the higher K.E. photoelectron

In general, a departure from homogeneity within the sample region will be indicated by a marked deviation in the intensity ratio of widely spaced peaks (on the kinetic energy scale) from that obtained from homogeneous standards. The ratio of the intensities I_{low}/I_{high} for the high and low kinetic energy peaks provides an alternative method for analytical depth profiling. This may be used to monitor overlayer and modification effects; the intensity ratio tending to a minimum as the modification depth tends to $3\lambda_{high}$.

Although the number density N_i is not directly related to the density of the sample, it is generally the case that for similar materials the ESCA signal for a given core level will be more intense for the higher density material.[78] The most important consequence of N_i is that the relative signal intensities for core levels in a homogeneous sample are directly related to the overall stiochiometries of the atoms sampled. Thus for two core levels i and j,

$$\frac{I_i}{I_j} = \frac{F\alpha_i N_i k_i \lambda_i}{F\alpha_j N_j k_j \lambda_j} \qquad (1.12)$$

If i and j correspond to the same core level in differing chemical environments, then

$$k_i \alpha_i \lambda_i = k_j \alpha_j \lambda_j \text{ and } \frac{N_i}{N_j} = \frac{I_i}{I_j}.$$

If however i and j are different core levels, then $k_i \alpha_i \lambda_i \neq k_j \alpha_j \lambda_j$ and

$$\frac{N_i}{N_j} = \frac{I_i k_j \alpha_j \lambda_j}{I_j k_i \alpha_i \lambda_i}.$$ The ratio $\frac{k_j \alpha_j \lambda_j}{k_i \alpha_i \lambda_i}$ may be determined experimentally from standard samples of known stiochiometry containing i and j. Since k_i and k_j vary from one spectrometer to another, as does $(\phi + \theta)$, these ratios, known as sensitivity factors, must be determined for the particular spectrometer.[86]

Quantitative aspects of ESCA are to be discussed in Section 1.11.

1.6.1 The Surface/Overlayer Model

A situation commonly met with in ESCA studies relating to surface analysis concerns the case of a single homogeneous component or of a surface coating of thickness d on a homogeneous base. This is illustrated in Figure 1.14a. The intensity for a film A of

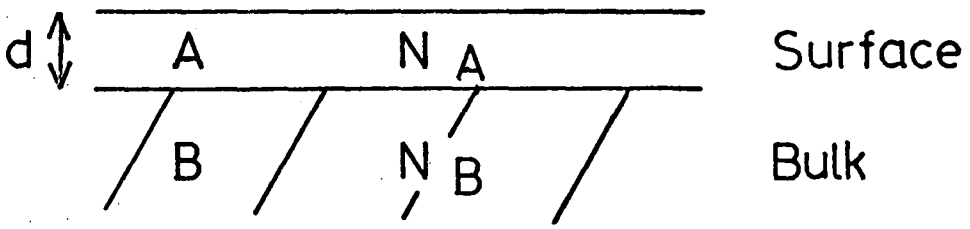

Figure 1.14a The Substrate/Overlayer Model

thickness d may be expressed as

$$I^A = I^A_\infty \ (1 - e^{-d^1/\lambda_A}), \qquad (1.12a)$$

whereas for the base B (considered infinitely thick), on the surface of which A is located, the intensity I^B, is given as

$$I^B = I^B_\infty e^{-d^1/\lambda_B} \qquad (1.12b)$$

(with $N_A = N_B$).

The full derivation is presented below:

$$I_\infty = \int_0^d F \alpha N K e^{-x/\lambda} . \, dx = F \alpha N K \lambda \qquad (1.9)$$

$$I^A = \int_0^d F \alpha N_A K e^{-x/\lambda_A} . \, dx = F \alpha N_A K \lambda_A (1-e^{-d^1/\lambda_A})$$

$$= I_\infty^A (1-e^{-d^1/\lambda_A})$$

$$I^B = \int_d^\infty F\alpha N_B K e^{-(x-d^1)/\lambda_B} e^{-d^1/\lambda_A} . dx$$

$$= F\alpha N_B K \lambda_B e^{-d^1/\lambda_A}$$

if $N_A = N_B$, $\lambda_A \approx \lambda_B$

$$I^B = I_\infty^B e^{-d^1/\lambda_A}$$

Equations 1.12a and 1.12b form the basis of computational models of varying sophistication which have been used to interpret experimental data of a substrate/overlayer nature.[156,165-7] Such a model has been applied in Chapter 3 of this thesis.

1.7 Line Shape Analysis

The need for line shape analysis (deconvolution) arises when the chemical shift of a level is smaller than the linewidth of that level. The measured linewidths of component peaks for a core level may be expressed as

$$(\Delta E_m)^2 = (\Delta E_x)^2 + (\Delta E_s)^2 + (\Delta E_\ell)^2 + (\Delta E_{ss})^2 \qquad (1.13)$$

ΔE_m is the measured width at half height, the so-called full width at half maximum (FWHM).

ΔE_x is the FWHM of the X-ray photon source. This is the dominant contributor to the observed line widths, typical values being

0.7eV for $MgK\alpha_{1,2}$ and 0.9eV for $A\ell K\alpha_{1,2}$ [9] and may be reduced using monochromatisation techniques. [10]

ΔE_s is the contribution due to spectrometer abberations and is dependent on the emission energy and the choice of analyser slits.

ΔE_{ss} is the contribution due to solid state effects in the sample.

ΔE_ℓ is the natural width of the core level under investigation and is related, via the uncertainty principle, to the lifetime of the core hole state. [72,92] Small changes in line widths of the order of 0.1eV have been found to be caused by chemical effects which have a small effect on the lifetime of the core hole state. This emphasises the need to estimate peak intensities by area and not by height.

The contribution to ΔE_m from ΔE_x for the commonly used photon sources (i.e. Mg and Aℓ) are essentially Lorentzian line shapes. The characteristics for the energy distribution in MgKα radiation are essentially comprised of four major component lines; α_1, α_2, α_3 and α_4, the relative positions to the α_1 line are -0.33, +8.4 and +10.2eV, with relative intensities of 100, 50, 12.8 and 6.9. [87] The α_3 and α_4 lines are significantly removed from the α_1 and α_2 lines and manifest themselves as satellite peaks to the high kinetic energy side of the intense primary photoionisation signal in the ESCA spectrum. A similar situation is true for the AℓKα radiation. [87]

The contribution to ΔE_m from ΔE_s is considered to be Gaussian, whereas that from ΔE_ℓ is Lorentzian.

The convolution of these line shapes produces a hybrid shape with a Gaussian distribution dominating the overall line shape and with Lorentzian character in the tails. The use of pure Gaussian shapes introduces only small errors into the line shape analysis. [10]

Deconvolution procedures may be grouped into two main categories:

(1) Deconvolution by mathematical methods which have been reviewed by Carley and Joyner.[88]

(2) Curve fitting by simulation, either in analogue or digital fashion.

Figure 1.15 is an example of a complex spectrum which has been deconvoluted using this approach into its individual components with area ratios shown.

For much of the work in this thesis, deconvolution was performed by analogue simulation using a Du Pont 310 curve resolver (and the accuracy is of the order of a few percent). On this instrument, the binding energy, line width and peak height are controlled by the operator as is also the line shape, though this is usually set for a Gaussian form. The underlying philosophy in such a technique is outlined in Table 1.5. When dealing with complex line shapes, a detailed knowledge of prototype systems becomes increasingly more important.

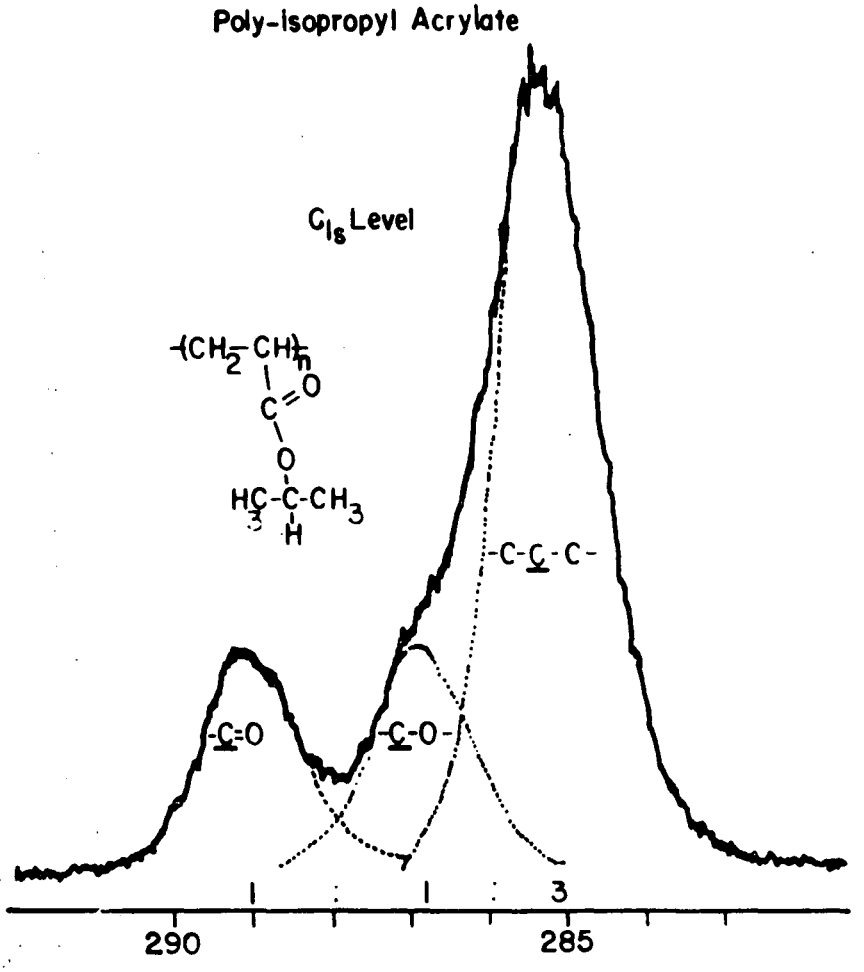

Figure 1.15 Deconvoluted C_{1s} spectrum of Poly-isopropyl Acrylate

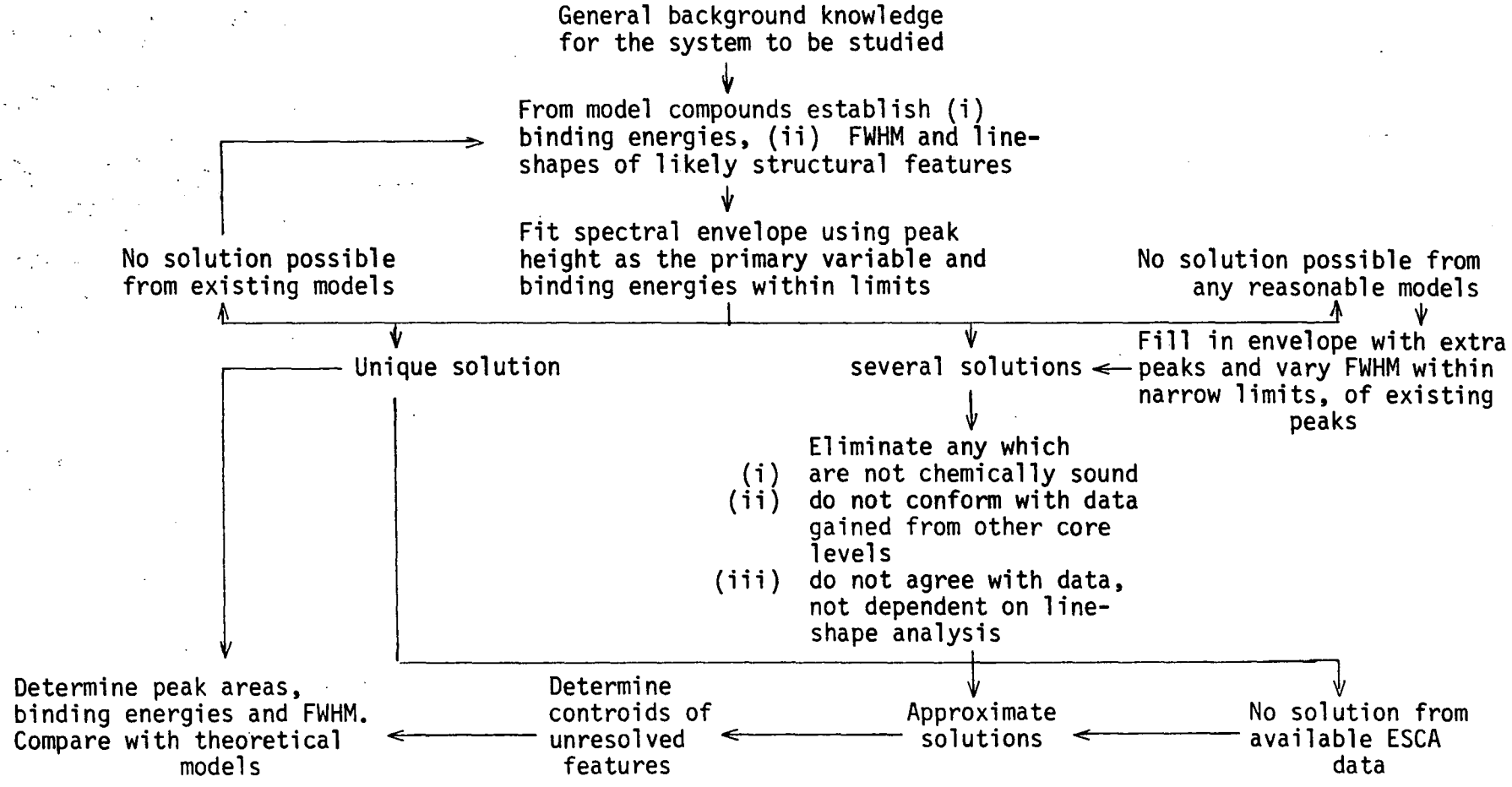

Table 1.5 Line-shape analysis by curve fitting; schematic of logic procedure[1]

1.8 ESCA Instrumentation

Instrumentation used in the ESCA experiment may be conveniently considered in four parts:

(1) X-ray source,

(2) Sample chamber,

(3) Electron energy analyser,

(4) Electron detection.

The work in this thesis was carried out using either an A.E.I. ES200B spectrometer or a custom-designed Kratos ES300 spectrometer.

A schematic of the basic experimental set-up is given in Figure 1.16.

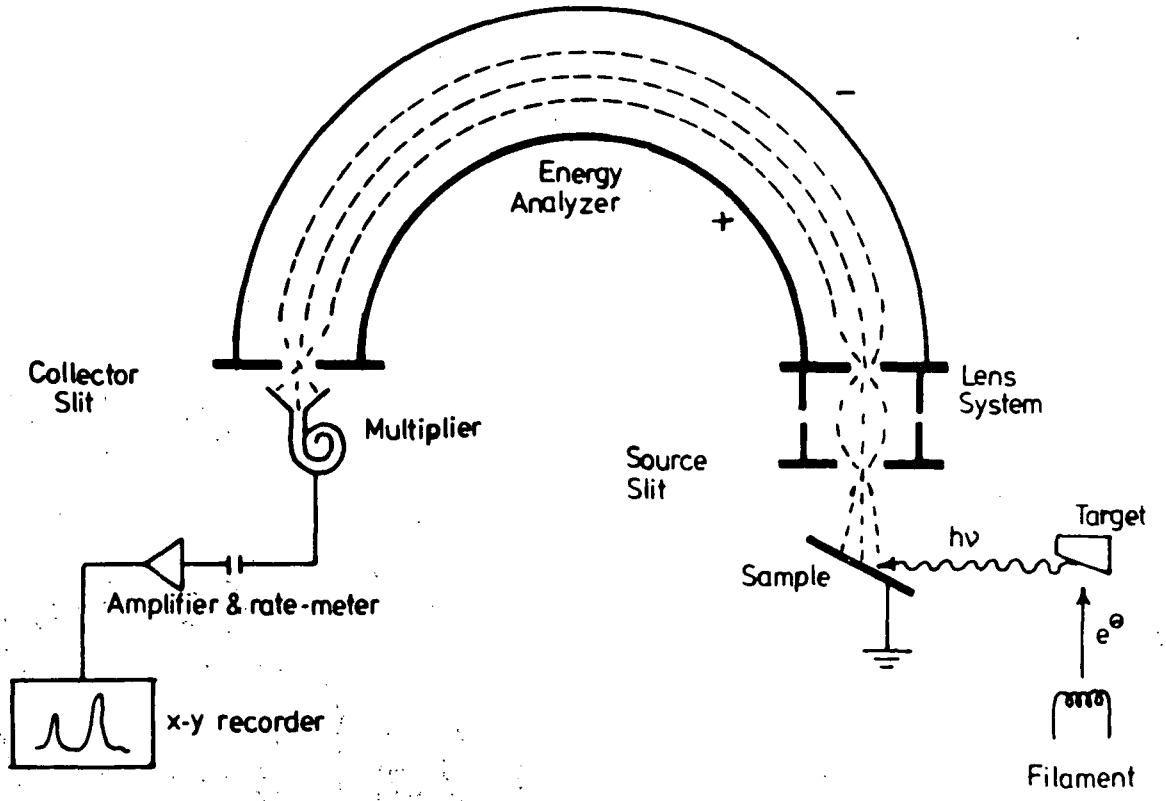

Figure 1.16 Schematic of the ESCA instrumentation

1.8.1 X-ray source

The X-ray beam is commonly produced by the bombardment of a target (or anode) with high energy electrons. A typical, non-monochromatic X-ray spectrum is shown in Figure 1.17, which illustrates the appearance of emission lines, characteristic of the anode material

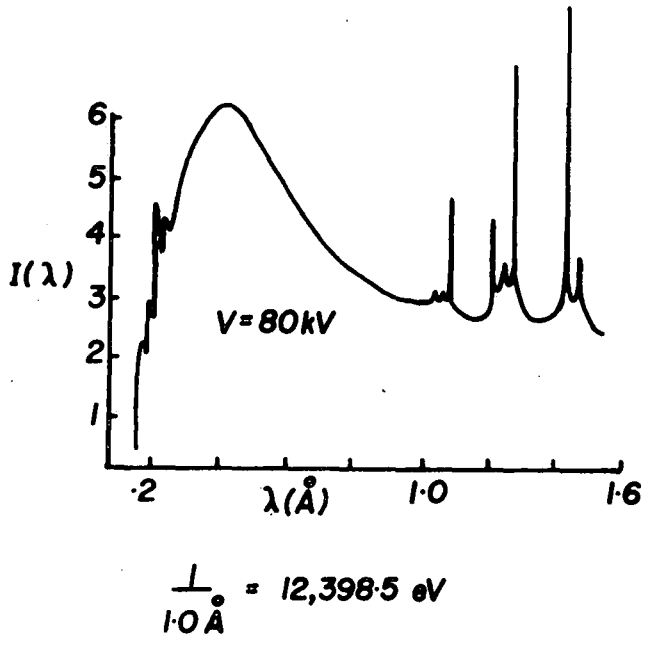

Figure 1.17 X-ray spectrum of a tungsten anode

superimposed on a continuous spectrum (Bremsstrahlung).[89] The continuum's shape depends only on the energy of the incident electrons on the anode, and not on the nature of the anode material.

Soft X-ray sources are most commonly employed in ESCA, for example, the MgKα ($h\nu$ = 1253.7eV) and AℓKα ($h\nu$ = 1486.6eV) lines; only very occasional use being made of harder X-rays such as $CuK\alpha_1$ ($h\nu$ = 8048eV) and $CrK\alpha_1$ ($h\nu$ = 5415eV). Other sources intermediate in energy are SiKα (1739.5eV)[90] and TiKα X-rays (4510eV) and it is likely that these harder X-ray sources will be employed in future Auger work.[91,92]

The ES200B spectrometer has a Marconi Elliott GX5 high voltage supply unit with integrally variable voltage, 0-60kV and current, 0-80mA. The X-ray source comprises an unmonochromatised magnesium anode of Henke design[93] with hidden filament; this reduces risks of contamination of the target by evaporated tungsten from the electron gun filament. Normal source operating conditions are 12kV and 15mA. The X-ray flux is of the order of 0.1 millirad s^{-1},[94] which causes little or no radiation damage to the majority of systems. The target is isolated from the sample chamber by a thin aluminium window (~0.003" thick) to prevent interference due to electrons from the filament. The risk of scattered electrons exciting X-radiation from the aluminium window is reduced by operating the filament at near ground potential (+ 10V) and the anode at high positive voltage. Aluminium impurity, sometimes found in magnesium targets, is known to cause satellites due to AℓKα excitation of the sample under investigation. These satellites, which have intensities a few percent of the primary peaks, particularly affect attempts to detect peaks from elements present in trace amounts.

The ES300 spectrometer is equipped with a dual-anode[95] with magnesium and titanium targets and a monochromatised $A\ell K\alpha_{1,2}$ X-ray source, their usual operating conditions being (9kV, 8mA), (13.5kV, 18mA) and (15kV, 35mA) respectively. The monochromator for the $A\ell K\alpha_{1,2}$ uses slit filtering[19] and diffraction from the (100) plane

of quartz [10] at the Bragg angle of 78.3°. Other monochromators may use dispersion compensation or 'fine focussing' systems. [96]

The titanium anode probes further into the surface yielding data on bulk composition. [97] The typical sampling depth using the titanium target is ~130 Å, compared with a sampling depth in the region of 50 Å when a magnesium X-ray source is employed. Hence analytical depth profiling at three levels is available at the flick of a switch.

An idealised photon source for photoelectron spectroscopy would be a monochromatised source of continuously tunable energy and high intensity. Synchrotron radiation [98] has been developed since the 1960s and facilities for its use are becoming available. [99] The phenomenon results naturally from the centripetal acceleration of charged particles moving at relativistic velocities inside an accelerator: storage ring systems are also in use. The tunable polarised source so produced is capable of supplying exciting photons in the ultrasoft X-ray region. The use of synchrotron radiation sources would enable the study of, for example, the variation of the cross-section behaviour of different core levels as a function of photon energy.

1.8.2 Sample Analysis Chamber

Figure 1.18 is a drawing of the ES200B spectrometer equipped with monochromator showing the relative positions of the sample, X-ray sources and analyser.

The source chamber has several access ports for sample introduction and treatments. Sample entry is via fast-entry insertion locks allowing for rapid sample turn round and angular dependent studies. Purpose-built reaction chambers may be attached onto the source chamber via an insertion lock and this provides facilities for 'in situ' treatment of samples.

Typical operating pressures for the ES200B are $<10^{-7}$ torr for samples of low volatility and a pressure in the 10^{-9} torr range is obtainable after baking. These pressures are achieved using cold-trapped diffusion pumps backed by rotary pumps.

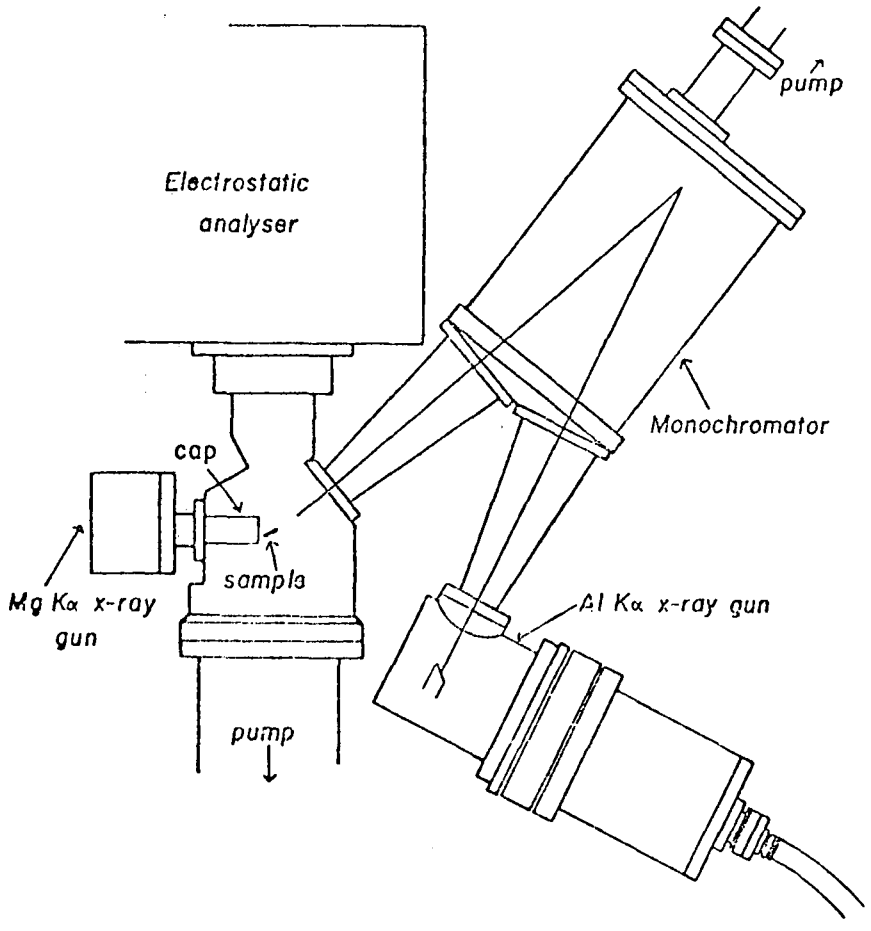

Figure 1.18 General layout of the A.E.I. ES200B spectrometer

The ES300, which has a specially designed preparation chamber attached permanently to the sample analysis chamber to cater for the needs of the polymer research interests of the laboratory, has separately pumped analyser and source regions. Pumping for the source region of the spectrometer is by means of an Alcatel 350 ℓs^{-1} electrically driven turbomolecular pump, whilst the analyser is pumped by a 140 ℓs^{-1} pump of the same design. The base pressure for normal operating conditions is ~ 5×10^{-9} torr.

1.8.3 Electron Energy Analyser

The ES200B has a hemispherical double focussing analyser based on the principle described by Purcell [100] which is screened from external magnetic interference by means of mu-metal shields.

The resolution of the analyser, $\Delta E/E$, where E is the energy of the electrons, should be 1 in 10^4 for ESCA studies and is related to the mean radius of the hemispheres (R), and the combined width of the source and collector slits (W) by the equation 1.14:

$$\Delta E/E = \frac{R}{W} \qquad (1.14)$$

The resolution may be improved by:

(1) Reducing the slit width, which reduces the signal intensity,

(2) Increasing the radius of the hemisphere, thereby increasing engineering costs and pumping requirements,

(3) Retarding the electrons before entry into the analyser

In practice a compromise is made on the slit widths to obtain sufficient signal intensity and on the size of the hemisphere so as to

prevent mechanical distortion and keep costs down. The ES200B uses a retarding lens to slow the electrons down before entry into the analyser and cuts down on the resolution requirements of the analyser.[101] This lens assembly also serves to remove the sample region from the analyser and hence more flexible sample handling can be employed.

Focussing of the electrons at the detector slit may take place by either of two methods:

(1) Scanning the retarding potential applied to the lens and keeping a constant potential between the hemispheres, or

(2) Scanning the retarding potential and the potential between the analyser hemisphere simultaneously maintaining a constant ratio between the two.

The first method of fixed analyser transmission (FAT) has greater sensitivity at low kinetic energies (<500eV) and the second, fixed retardation ratio (FRR) has greater sensitivity at higher electron kinetic energies. The FRR mode is employed in this work.

1.8.4 Electron detection and data acquisition

Electrons of pre-selected energy pass from the analyser into an electron multiplier via the collector slit. The output from the multiplier undergoes amplification and is fed into a data handling system. ESCA spectra may then be generated in two ways:

(1) The continuous scan, where the electrostatic field is increased from the starting kinetic energy continuously, a ratemeter monitoring the signal from the amplifier. In this way a graph of electron count rate versus the kinetic energy of the electrons may be recorded on an X-Y plotter.

(2) The step scan, where the field is increased by preset increments (typically 0.1eV) and at each increment (a) counts may be measured for a fixed length of time or (b) a fixed number of counts may be timed. The data so obtained may be stored in a multichannel analyser. Alternatively, specially designed data acquisition/ manipulation mini computer systems are available. Such a data system (Kratos DS 300) is attached to the ES 300 spectrometer. Many scans can be accumulated to average random fluctuations in background, thereby enhancing signal to noise ratio.

It should be borne in mind that where data acquisition is a lengthy procedure (greater than say 1 hour) sample changes, such as hydrocarbon build-up or sample charging effects, may lead to erroneous spectra.

1.9 Sample Handling

1.9.1 Solid Samples

Solids may be mounted onto the spectrometer probe tip using double-sided adhesive insulating tape. Here sample charging effects will occur and a more satisfactory technique involves depositing a thin layer of the sample onto a gold substrate as a film by evaporation from a suitable solvent, or sublimation, for example. Small strips and wires may be held in a chuck and powdered samples may be mounted by pressing into a metal gauze or piece of soft metal foil such as lead or indium.

A typical probe has facilities for temperature dependence studies, heating being achieved by means of conduction from a thermo-

statically controlled resistance heater. Cooling is carried out by pumping liquid nitrogen through the probe, thus enabling solids which are slightly volatile to be studied. More volatile solids are usually sublimed from a capillary tube, which may be heated, onto a cooled probe tip.

1.9.2 Liquids

Although the technique of ESCA may be applied to the analysis of solids, liquids and gases, the development of liquid studies is still in its infancy. [118] The only technique that is at present viable on commercially available instruments involves the injection of the liquid into a heatable (25°C to 150°C) evacuated reservoir shaft followed by diffusion of the vapour through a metrosil leak and subsequent condensation onto a cooled gold plate on the tip of the sample probe. The sample surface is continually renewed and contamination and radiation damage effects are thereby reduced.

Two techniques for studying liquids and solutions have been developed by Siegbahn where samples are studied as submillimeter beams [102] or as a film on a wire passing through the X-ray beam parallel to the analyser entrance slit. [89]

1.9.3 Gases

Gases may be studied either in condensed phase using a cooled probe or in the gaseous phase for which purpose gas cells have been developed. Studies using molecules in the gas phase have the following advantages: [19]

(1) No inherent broadening of the levels due to solid state effects.

(2) Problems of sample charging are removed.

(3) Increased signal to background ratio.

(4) Radiation damage, if it occurs, is of no importance unless the sample is recirculated.

(5) By mixing with standard gases, peaks may be readily calibrated.

(6) Inelastic losses and shake-up or shake-off processes may be distinguished by varying the sample pressure.

(7) Direct comparison with theoretical calculations is simplified.

1.10 General Aspects of ESCA

ESCA is an extremely powerful tool with wide-ranging applicability. The principal advantages of the technique may be summarised as follows:

(1) The sample may be solid, liquid or gas, and sample sizes are small e.g. in favourable cases 1mg solid, 0.1μℓ liquid and 0.5cm^3 of a gas at STP.

(2) The high sensitivity of the technique is such that a fraction of a monolayer coverage may be detected.

(3) The process is virtually non-destructive, since the X-ray flux is small (0.1 millirad sec^{-1}). This is especially advantageous over Auger spectroscopy where the electron beam produces many surface changes, particularly in polymeric systems where cross-linking and degradation can occur.

(4) The technique is independent of the spin properties of the nucleus and can be used to study any element of the periodic table with the exception of hydrogen and helium. These are the only elements for which the core levels are also the valence levels.

(5) Materials may be studied 'in situ' in their working environments with a minimum of preparation.

(6) The technique provides a large number of information levels from a single experiment and these are listed in Table 1.6.

(7) ESCA has a higher sensitivity than many other analytical techniques, as shown in Table 1.7.

(8) The data is often complementary to that obtained by other techniques and has unique capabilities centred to the development of a number of important fields.

(9) For solids, ESCA has the capability of differentiating the surface from subsurface and bulk phenomena, allowing analytical depth profiling.

(10) The information relates directly to bonding and molecular structure and applies to both inner and valence orbitals of the molecule. This enables a thorough analysis of electronic structure of the system to be made.

(11) The information levels are such that 'ab initio' investigations are possible and the theoretical basis is well understood, resulting in considerable interest to theoreticians.

The following aspects should also receive consideration:

(1) The overall costs are quite high, being comparable to Fourier Transform I.R., laser Raman and conventional Mass Spectrometers, and considerably more expensive than standard I.R. equipment.

(2) The vacuum system associated with ESCA instrumentation means that routine sample handling requires provision of vacuum interlocks and also implies that it is not possible to switch the spectrometer on to routinely investigate a sample.

(3) Although ESCA has the capability of studying solids, liquids and gases, it is only for solids and gases that the requisite instrumentation is routinely available. Whilst the technique has excellent depth resolution (in the range of ~ 100 Å), the spatial resolution is poor and an area of $0.3cm^2$ is normally sampled.

(5) If the surface differs from the bulk, then it is not possible to say anything about the bulk structure by means of ESCA without sectioning the sample.

(6) With conventional unmonochromatised X-ray sources and slitted designs, two features are of importance in studying thick samples, namely sample charging and the polychromatic nature of the X-ray source. The former, arising from a distribution of positive charge over the sample surface under the conditions of X-ray bombardment can be a severe problem for thick insulating samples and needs careful consideration. The latter leads to a relatively poor signal to background ratio; however this has been alleviated considerably by the development of efficient monochromatisation schemes and multiple collector assemblies.

(7) To take full advantage of the technique often requires a relatively high level of theoretical competence. However, it must be emphasised that the technique has capability for exploitation at many levels, for example from routine trouble shooting problems where only a straightforward comparison is required, to investigations of a phenomenom at a fundamental level.

It is the composite nature of the large range of available information levels which endows ESCA with such wide-ranging capabilities and this hierarchy of information levels is set out in Table 1.6.

Table 1.6 The Hierarchy of Information Levels available in ESCA

(1) Absolute binding energies, relative peak intensities, shifts in binding energies. Elemental mapping for solids, analytical depth profiling, identification of structural features, etc. Short-range effects directly, longer-range indirectly.

(2) Shake-up - shake-off satellites. Monopole excited states; energy separation with respect to direct photoionisation peaks and relative intensities of components of 'singlet and triplet' origin. Short and longer range effects directly (Analogue of U.V.).

(3) Multiplet effects. For paramagnetic systems, spin state, distribution of unpaired electrons (Analogue of e.s.r.).

(4) Valence energy levels, longer range effects directly.

(5) Angular dependent studies. For solids with fixed arrangement of analyser and X-ray source, varying take-off angle between sample and analyser provides means of differentiating surface from subsurface and bulk effects. For gases with variable angle between analyser and X-ray source, angular dependence of cross-sections, asymmetry parameter β [103], symmetries of levels.

A comparison of analytical techniques is shown in Table 1.7.

Table 1.7 Sensitivities of Various Analytical Techniques

Bulk Techniques	Minimum Detectable Quantity (g)
Infrared absorption	10^{-6}
Atomic absorption	10^{-9} - 10^{-2}
Vapour phase chromatography	10^{-3} - 10^{-7}
High pressure liquid chromatography	10^{-6} - 10^{-9}
Mass spectroscopy	10^{-9} - 10^{-15}
Surface Techniques	
ESCA	10^{-10}
Neutron activation analysis	10^{-12}
Ion scattering spectrometry	10^{-15}
X-ray fluorescence	10^{-7}
Auger emission spectroscopy	10^{-14}
Secondary ion mass spectrometry	10^{-13}

1.11 Quantitative Analysis

Having presented an outline of the nature of the processes involved in the ESCA experiment together with instrumentation details with particular reference to the qualitative viewpoint, for a thorough appreciation of the data which is to follow in subsequent chapters of this thesis, it is necessary to highlight certain aspects of the procedures used in deriving elemental analytical information at the quantitative level.

As mentioned previously, the first information level available from the ESCA experiment includes the relative intensities of the photoionisation peaks within a spectrum. These may be used in conjunction with a knowledge of certain other factors, which will be expanded upon in the following discussion, to yield a quantitative analysis.

In order that ESCA, essentially a surface sensitive technique, may be applied successfully to problems of quantitative elemental analysis, it is of prime importance that the outermost monolayers of the sample under investigation be representative of the bulk composition of the material as a whole. Knowledge of the degree of homogeneity of the material sampled is therefore important.

A common situation of vertical inhomogeneity is caused by the presence of a layer of surface contamination. The depth of material sampled ($\sim 3\lambda$, where λ is the inelastic mean free path of the photoelectron) depends upon the core level studied since λ is a function of the kinetic energy. A contamination layer therefore leads to errors in quantitative analysis especially when peaks of widely different kinetic energy are used.

For homogeneous samples, elemental analysis is as follows. The area of the most intense core level peak of each element, together with associated structure (shake-up for example) where this can be assigned, is measured. These figures are divided by the appropriate sensitivity factors, derived using compounds of known stiochiometry to yield atomic ratios.

Tables of relative elemental sensitivities have been formulated from experimental work using model compounds by a number of research workers,[108-110] and are unaffected by chemical environment.[116]

These results which are reported in the literature refer to instruments used in the FAT mode of electron detection and are not strictly applicable to raw data obtained from FRR type instrumentation. Theoretical calculations of photoionisation cross-sections have been performed [81-2, 109, 111-2] and the methods employed form the subject of a review by Huang and Rabalis. [113] Discrepancies between results obtained using theoretical cross-sections and experimentally derived sensitivity factors stem from the assumption that X-ray photoionisation in solids should be essentially an atomic process. In some cases the processes accompanying core ionisation which detract from the main photoionisation peak may be difficult to assess experimentally.

Crystallinity effects have been found to be important when dealing with materials containing inorganic solids. The solid state matrix phenomenon was first noted by Wagner [108] in his study of a variety of sodium and fluorine-containing compounds. Swingle, [111] Wyatt and co-workers, [114] and Ng and Hercules [115] have studied the effect on relative peak intensities of matrix effects, especially for ionic compounds. Nearest neighbour inelastic scattering effects in certain systems appear to play an important role, causing a variation of escape probability with change in chemical composition. [115]

Evans, Adams and Thomas, in their studies aimed at the development of ESCA as a quantitative surface analytical technique, have reported a means of probing the surface structure and composition of layered silicate minerals using X-ray photoelectron diffraction, together with energy-dispersive X-ray (K-emission) analyses and X-ray diffraction and extensive chemical analyses. [128] X-ray photoelectron diffraction patterns were obtained from monocrystalline mineral flakes cleaved 'in situ'; a set of spectra being produced at 5^{o} increments

of take-off angle. The diffraction of the outgoing photoelectrons by the atoms surrounding the emitting site allows differentiation between equivalent, near-equivalent, and non-equivalent sites occupied by two or more elements either in one single crystal or in crystals of closely similar structure. This is found to apply even when the element(s) concerned comprise only a small fraction of the crystal and when the sub-lattice lacks both long and short range order.

Despite these factors, reproducible, quantiative, instrument-independent ESCA analyses to within 10% are possible provided that the necessary calibration procedures for voltage scales and intensity response are followed. [117]

CHAPTER TWO

SELECTIVE SURFACE MODIFICATION OF POLYMERS BY MEANS OF HYDROGEN AND OXYGEN PLASMAS

CHAPTER TWO

SELECTIVE SURFACE MODIFICATION OF POLYMERS BY MEANS OF HYDROGEN AND OXYGEN PLASMAS

2.1 Introduction

The surface modification of polymers, particularly those in film form, is an area of considerable technological and industrial importance. In the particular case of polyolefins for example a variety of chemical treatments have been described to change the wettability, printing and laminating characteristics of films and performed items. [323] Such treatments fall into two general categories depending on whether a wet chemical process is involved, or whether the interaction occurs at the gas-solid interface, as would be the case in a flame or electrical discharge treatment.

The advent of surface sensitive forms of spectroscopy has, in recent years, allowed considerable progress to be made in the investigation of changes in surface chemistry brought about by a variety of surface treatments of polymers. [324] Thus chromic acid etching of polyolefins [129,130,148] and Na/NH_3 etching of fluorocarbons [131] have been the subject of detailed ESCA investigations. Electrical discharge treatments ranging from plasma to corona functionalisation [130,132,324] and to surface crosslinking by the CASING technique [126,325] have also been studied in some detail. The clear picture to emerge from such studies is that the most efficient surface sensitive mode of controlling the surface chemistry is by means of gas-solid interactions involving 'cool' plasmas. [133] Thus, whilst wet chemical and flame techniques provide convenient means of functionalising polymers, the reactions are by no means confined to the outermost few monolayers and it is difficult

to exercise control over the extent and depth of the modification. [132] Wet chemical treatments also have the limitation that any impurities may well segregate at the surface so that minor changes in etching technique can lead to difficulties in effecting reproducibility. Corona techniques are widely employed in industry since continuous treatment processing is readily accomplished. [326] However, the degree of functionalisation is relatively low and typically extends to depths of $\sim 100\text{Å}$. [132]

Previous work in the Durham ESCA laboratory demonstrated [126,132-5,169] the use of inductively coupled radiofrequency plasmas to effect functionalisation at polymer surfaces in a controlled manner, both in terms of extent of reaction, and the depth range over which functionalisation occurs. In the particular case of oxygen plasmas it has been shown that a range of functionalities may be introduced and studies of polyethylene (high and low density), polypropylene and polystyrene indicated the surface sensitivity and selectivity of the process. [135] The selective surface modification of III - V semiconductors [174] may also be accomplished by plasma means and reactions involving both oxygen and hydrogen plasmas are surface specific. In addition the data for hydrogen plasma treatments of semiconductor surfaces suggest that surface sensitive reductive functionalisations should be feasible.

Here the scope of such studies is extended by considering not only the reactions of hydrogen and oxygen plasmas with a representative cross section of polymers (high density polyethylene (HDPE), polystyrene, polyethylene terephthalate (PET) and bisphenol-A polycarbonate, but also the effects of sequential treatments involving both types of plasma.

As will be discussed in the following chapter, there is considerable interest in the production of substrates with a well-defined

distribution of surface functionality and differing from the bulk structure, on which specific surface chemical reactions may be performed. Apart from probing the reactivities of different polymers towards straight hydrogen and oxygen plasmas and of sequential hydrogen/oxygen and oxygen/hydrogen plasma treatments, the final distribution of surface functionality was studied with interest.

2.2 Experimental

2.2.1 Samples

This investigation involved oxygen plasma and hydrogen plasma treatments of high density polyethylene, polystyrene, polyethylene terephthalate and bisphenol-A polycarbonate polymer samples studied in the form of thin films. Details of the origins of the polymer samples are as follows:

(1) High density polyethylene TFE 554 was supplied by the Metal Box Company and was known to contain the antioxidant Irganox 1076 (Octadecyl 3-(3,5-ditertbutyl-4-hydroxylphenyl) propionate) at the 0.016% level;

(2) Polystyrene film was supplied by Dr A. Davis of the Ministry of Defence;

(3) Polyethylene terephthalate, 'Mylar' film was supplied by Dr T. Kent of the Home Office (PSDB);

(4) Bisphenol-A polycarbonate film was cast onto glass from a 12% wt/vol solution in chloroform.

2.2.2 Sample Preparation

All films were used in their 'as received' forms without pre-treatment. Prior to plasma modification, samples were mounted on

a copper probe tip (7mm x 21mm) by means of double-sided adhesive 'Scotch' insulating tape.

2.2.3 Plasma Instrumentation and Reactor Configuration

Plasmas were excited in all cases using a Tegal corporation radiofrequency generator capable of delivering a power output from 0.05 - 100 watts, continuously variable and operating at a frequency of 13.56 MHz. The system includes a pulsing facility which may be employed on a microsecond time scale to give greater stability to the plasma at low average power loadings (< 1 W). Tuning of the radiofrequency power was achieved by an L-C matching network in an inductively coupled mode and monitored by the standing wave ratio using a Heathkit HM102 R.F. power meter.

The plasma reactor was mounted in a greaseless vacuum system, pumped by a two-stage rotary pump with a nominal pumping speed of 50 $l.min.^{-1}$. Pressures were monitored using a Pirani vacuum gauge and the gas was introduced via a leak valve.

The reactor consisted of 6cm diameter Pyrex tubing in an inverted 'T' shape configuration, as shown in Figure 2.1a. The overall dimensions were 37cm long and 30cm high, with inlet and outlet tubes ½" and 1" diameter respectively, the inlet tube being at the top. The discharge was excited in the vertical limb by a 9 turn, 6μH copper coil electrode wound externally and centred 18cm from the inlet tube.

The premounted sample was positioned on a glass slide resting on the wall of the reactor such that the sample was positioned along the length of the reactor, its surface horizontal and facing uppermost and lying 1.5cm from the reactor floor at the centre of the 'T'. (Since there is a concentration profile of ions, radicals and neutral species extending through the glow region of the reactor, the spatial

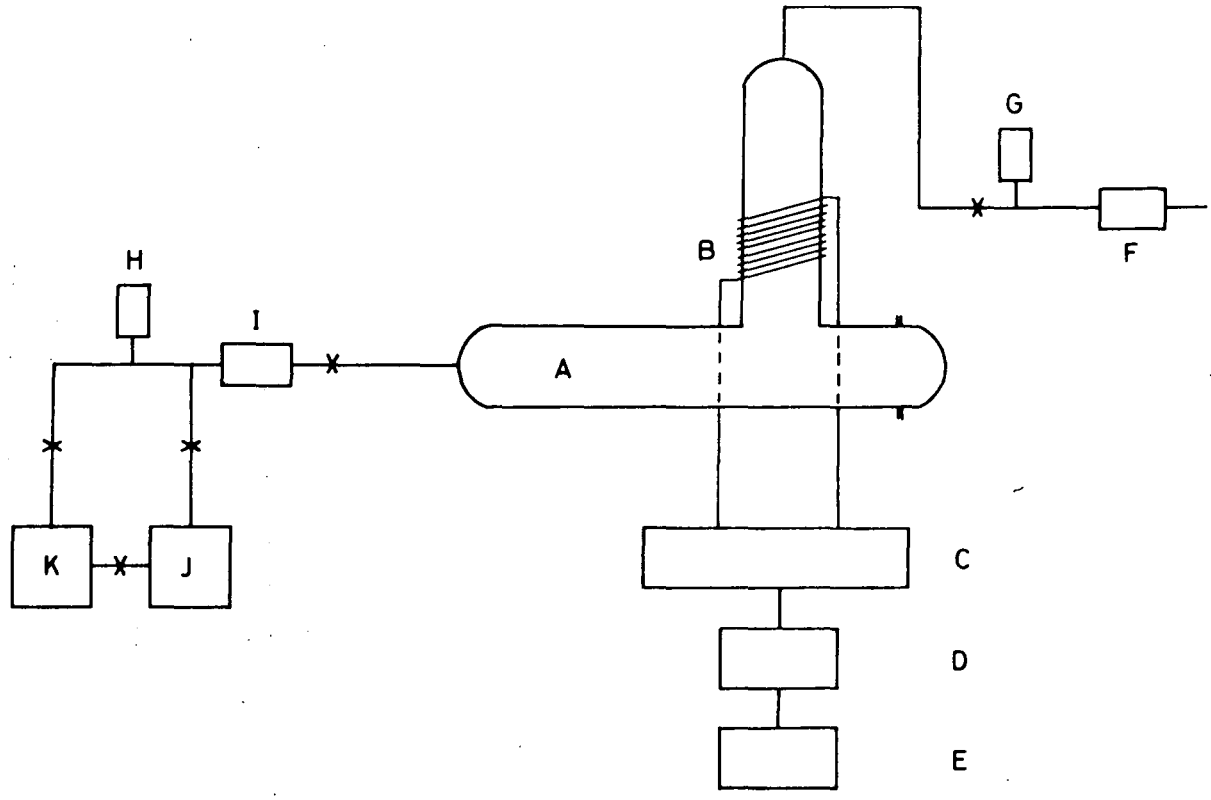

Figure 2.1a Schematic diagram of the inductively coupled RF plasma instrumentation : A, reactor; B. RF coil; C, matching unit; D, standing-wave ratio bridge; E, RF source; F, leak valve; G, Pirani gauge; H, Penning gauge; I, cold trap; J, backing pump; K, diffusion pump; X, vacuum valve

position of the sample in relation to the reactor geometry becomes important if processing under reproducible conditions is to be affected.)

2.2.4 Experimental Procedure

2.2.4a Oxygen Plasma Treatment

The sample, mounted on the probe-tip, was positioned in the plasma reactor and the system evacuated to a pressure in the region of 5×10^{-2} torr. Oxygen gas from standard laboratory cylinders, obtained from the British Oxygen Corporation, was used without further purification. The vacuum line was flushed with oxygen gas, evacuated, and then let up to the required pressure (0.2 torr) via a leak valve. The system was purged for approximately 20 minutes before the glow discharge was initiated. The characteristic electromagnetic output in the visible region gave a pale white tinge to the oxygen plasma and was sometimes difficult to observe.

2.2.4b Hydrogen Plasma Treatment

Care was taken to remove atmospheric oxygen from the plasma environment. To this end the reactor was pumped down to a pressure of $\sim 10^{-4}$ torr (as monitored using a Penning gauge) by means of a diffusion pump for a period of approximately 30 minutes before leaking in hydrogen gas (supplied by the British Oxygen Corporation and used without further purification) to a pressure of 0.2 torr. The system was allowed to equilibrate before the plasma was initiated. The characteristic electromagnetic radiation in the visible region gave rise to a lilac glow.

The respective treatment times and powers for oxygen and hydrogen plasma modifications chosen for this study were 5 seconds at 0.4 W and 10 seconds at 0.4 W. In all cases the glow region extended throughout the length of the vertical coil region and for a substantial distance on either side of the sample position in the horizontal portion of the reactor.

2.2.5 ESCA Analysis

Once treated, the polymer was removed from the reactor, attached to the spectrometer probe and introduced into the ESCA spectrometer via a fast insertion lock. Typically ESCA analysis began approximately three minutes after treatment and took 40 minutes to complete. All spectra were recorded on an A.E.I. ES200B spectrometer using $Mg_{K\alpha_{1,2}}$ radiation, with a base pressure of $\sim 5 \times 10^{-8}$ torr, and typical operating parameters of 12kV and 15mA. Under the experimental conditions employed, the $Au_{4f_{7/2}}$ level (at 84eV binding emergy) used for calibration purposes, had a full width at half maximum height (FWHM) of 1.2eV. Deconvolution and area ratios were determined using a Dupont 310 analogue curve resolver.

The information levels available from the ESCA experiment which are of particular value in this study arise from analyses inter alia of:-

(1) The integrated relative intensities of the C_{1s} and O_{1s} core levels particularly as a function of electron take off angle, θ, (either 30^{o} or 70^{o} to the normal to the sample surface). Comparison of the spectra obtained at these different take off angles provides a means of analytical depth profiling (Section 1.6).

(2) The change in integrated intensity of a given core level (e.g. C_{1s}) as a function of take off angle. In this way it is possible to monitor changes in the number average of carbon atoms sampled by ESCA over different sampling depths.

(3) The component analysis of individual core level band profiles.

2.2.6 Infrared and Laser Raman Analyses

The infrared and laser Raman spectra of HDPE before and after hydrogen plasma treatment were performed using a Perkin Elmer 457 grating infrared spectrophotometer and a Cary 82 laser Raman spectrophotometer respectively.

2.3 Results and Discussion

It is convenient in discussing the results of this study to present an initial survey of the various plasma treatments of the individual polymers and then to draw comparisons between them.

Relative intensity data pertaining to the deconvoluted C_{1s} and O_{1s} core level spectra for all the polymer samples studied in this investigation are presented in Table 2.1.

Table 2.1 Relative intensity data pertaining to the deconvoluted C_{1s} and O_{1s} core level spectra for polymer samples exposed to oxygen plasma (5 sec., 0.4 W, 0.2 Torr), hydrogen plasma (10 sec., 0.4 W, 0.2 Torr) and sequential plasma treatments

Material	Plasma Treatment	θ	C_{1s} Total	C - H	C - O	C = O	$C^{=O}_{-O}$	O-C-O	π→π*	C_{1s}/O_{1s}	C_{1s}^{30}/C_{1s}^{70}
HDPE	Untreated	30°	100	95.2	4.8	-	-	-	-	90.9	1.8
		70°	100	95.9	5.6	0.5	-	-	-	90.9	
	Oxygen	30°	100	84.0	10.1	3.4	1.7	0.8	-	5.4	1.6
		70°	100	80.0	11.2	4.0	3.2	1.6	-	3.7	
	Hydrogen	30°	100	95.2	4.8	-	-	-	-	62.5	2.0
		70°	100	92.5	6.4	1.2	-	-	-	62.5	
	Hydrogen/Oxygen	30°	100	80.0	9.7	4.8	4.1	1.4	-	3.8	1.8
		70°	100	74.6	12.7	5.2	5.2	2.2	-	2.8	
	Oxygen/Hydrogen	30°	100	82.0	9.8	3.3	2.5	2.5	-	4.3	1.9
		70°	100	78.1	12.5	4.7	3.9	0.8	-	3.4	

Table 2.1 (continued)

Material	Plasma Treatment	θ	C_{1s} Total	$\underline{C}$ - H	$\underline{C}$ - O	$\underline{C}$ = O	$\underline{C}(=O)-O$	O-$\underline{C}$-O	$\pi \rightarrow \pi^*$	C_{1s}/O_{1s}	C_{1s}^{30}/C_{1s}^{70}
Polystyrene	Untreated	30°	100	90.1	4.5	-	-	-	5.4	52.6	1.9
		70°	100	89.8	5.1	-	-	-	5.1	40.0	
	Oxygen	30°	100	73.5	11.8	5.9	3.7	2.9	2.2	2.5	1.7
		70°	100	61.3	15.3	11.0	7.4	4.3	0.6	1.5	
	Hydrogen	30°	100	84.8	12.1	1.5	-	-	1.5	11.2	2.0
		70°	100	90.1	8.1	0.9	-	-	0.9	7.4	
	Hydrogen/Oxygen	30°	100	80.0	8.8	4.0	2.4	3.2	1.6	2.7	1.9
		70°	100	68.5	15.1	6.9	4.8	4.1	0.7	2.0	
	Oxygen/Hydrogen	30°	100	73.5	14.0	5.1	2.2	2.9	2.2	2.6	1.8
		70°	100	65.8	17.8	6.6	3.9	4.6	1.3	2.0	

Table 2.1 (continued)

Material	Plasma Treatment	θ	C_{1s} Total	C - H	C - O	C = O	C^{O}_{O}	$O-C(=O)-O$	$\pi \rightarrow \pi^*$	C_{1s}/O_{1s}	C_{1s}^{30}/C_{1s}^{70}
PET	Untreated	30°	100	59.0	21.2	0.3	17.1	0.6	1.8	1.9	2.0
		70°	100	61.3	17.2	4.9	14.1	0.6	1.8	2.2	
	Oxygen	30°	100	52.4	25.7	-	19.9	1.6	0.5	1.5	2.7
		70°	100	53.2	16.0	11.2	17.0	2.7	-	1.5	
	Hydrogen	30°	100	69.0	16.6	-	13.1	-	1.4	2.9	1.9
		70°	100	78.2	14.1	-	7.7	-	-	3.8	
	Hydrogen/Oxygen	30°	100	53.3	22.6	0.7	19.0	2.9	1.5	1.6	2.3
		70°	100	49.8	20.9	6.0	29.2	2.5	1.0	1.7	
	Oxygen/Hydrogen	30°	100	55.4	22.3	-	19.6	0.9	1.8	1.8	2.0
		70°	100	54.3	24.5	-	19.6	1.1	0.5	1.8	

Table 2.1 (continued)

Material	Plasma Treatment	θ	C_{1s} Total	C - H	C - O	C = O	C^{O}_{O}	$O-\overset{O}{\overset{\|}{C}}-O$	$\pi \rightarrow \pi^*$	C_{1s}/O_{1s}	C_{1s}^{30}/C_{1s}^{70}
Bisphenol-A polycarbonate	Untreated	30°	100	78.1	13.3	-	-	6.3	2.3	4.3	1.7
		70°	100	78.4	13.5	-	-	6.1	2.0	4.1	
	Oxygen	30°	100	66.7	16.7	5.3	4.0	5.3	2.0	2.6	1.4
		70°	100	64.0	19.2	5.9	5.0	5.0	0.8	2.2	
	Hydrogen	30°	100	82.5	12.4	-	-	4.1	1.0	5.5	2.3
		70°	100	85.0	10.6	-	-	3.7	1.4	5.2	
	Hydrogen/Oxygen	30°	100	69.4	17.6	3.5	2.4	5.9	1.2	2.6	1.9
		70°	100	67.1	18.1	4.7	4.0	4.7	1.3	2.2	
	Oxygen/Hydrogen	30°	100	69.9	18.2	2.8	2.1	4.9	2.1	2.6	1.7
		70°	100	69.8	17.4	4.7	3.5	4.7	-	2.4	

2.3.1 High Density Polyethylene

Histograms containing the C_{1s} and O_{1s} core level data for the untreated polymer and for plasma treated high density polyethylene are given in Figure 2.1. The oxygen plasma treatments, either alone or sequentially coupled with hydrogen plasma treatments, clearly give rise to considerable oxidative functionalisation which shows subtle variations dependent on the sequence employed.

Whilst for the untreated material the low level of oxygen functionality (corresponding to $\sim$ 1 carbon in 150) is manifest in terms of a low intensity O_{1s} peak corresponding to $\sim$ 1% of the intensity of the C_{1s} peak; for the oxygen plasma treated sample the O_{1s} levels correspond to $\sim$ 19% and 27% of the C_{1s} intensity at take off angles of 30^{o} and 70^{o} respectively. The distinctive difference for the two take off angles confirms that reaction is confined to the outermost few monolayers and is not therefore detectable by IR or MATR for example or by laser Raman spectroscopy (Figures 2.2 and 2.3). This suggests that the surface reaction is diffusion limited and the time scale of the experiments indicates that the reactive species in the plasma (O, O_2^+ etc) [164] react with very low activation energy even with saturated systems. From a knowledge of the cross sections for photoemission from the C_{1s} and O_{1s} core levels [86] an average C:O stoichiometry over the depth scale appropriate to ESCA of 8:1 is obtained.

Analysis of the C_{1s} levels by standard line shape analysis shows that the oxidative functionalisation provides $\underline{C}$ - O, $\underline{C}$ = O,

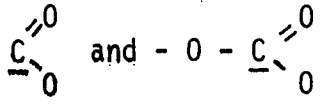

and - O - $\underline{C}$ 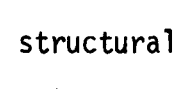 structural features and this is conveniently shown in histogram form for the plasma treated samples as shown in Figure 2.1. For the oxygen plasma treated sample, comparison with

Figure 2.1 Histograms of the deconvoluted C_{1s} and O_{1s} spectra for high density polyethylene exposed to oxygen plasma (5 sec., 0.4 W, 0.2 Torr), hydrogen plasma (10 sec., 0.4 W, 0.2 Torr) and sequential oxygen-hydrogen and hydrogen-oxygen plasma treatments recorded at electron take off angles of 30^{o} and 70^{o}.

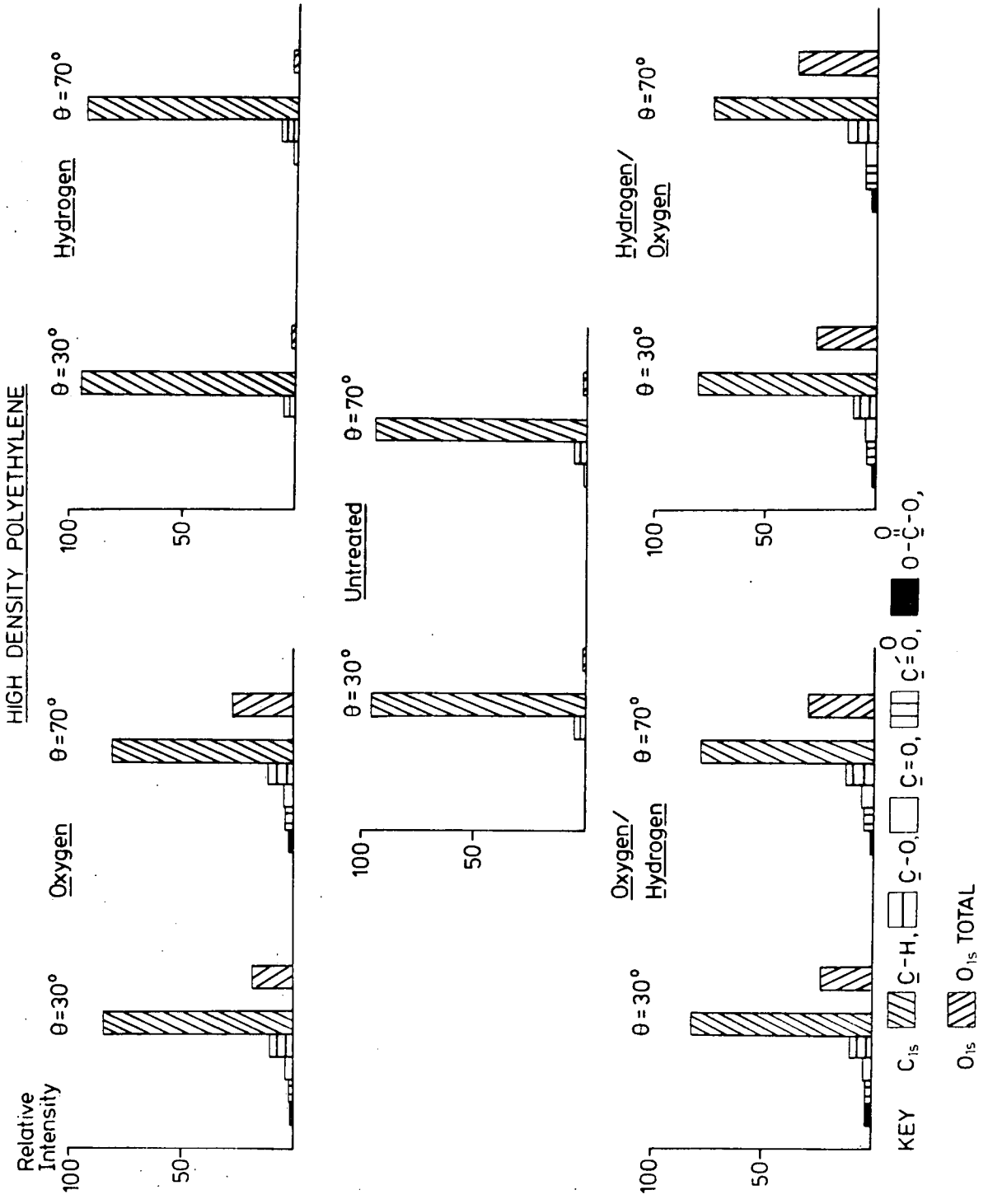

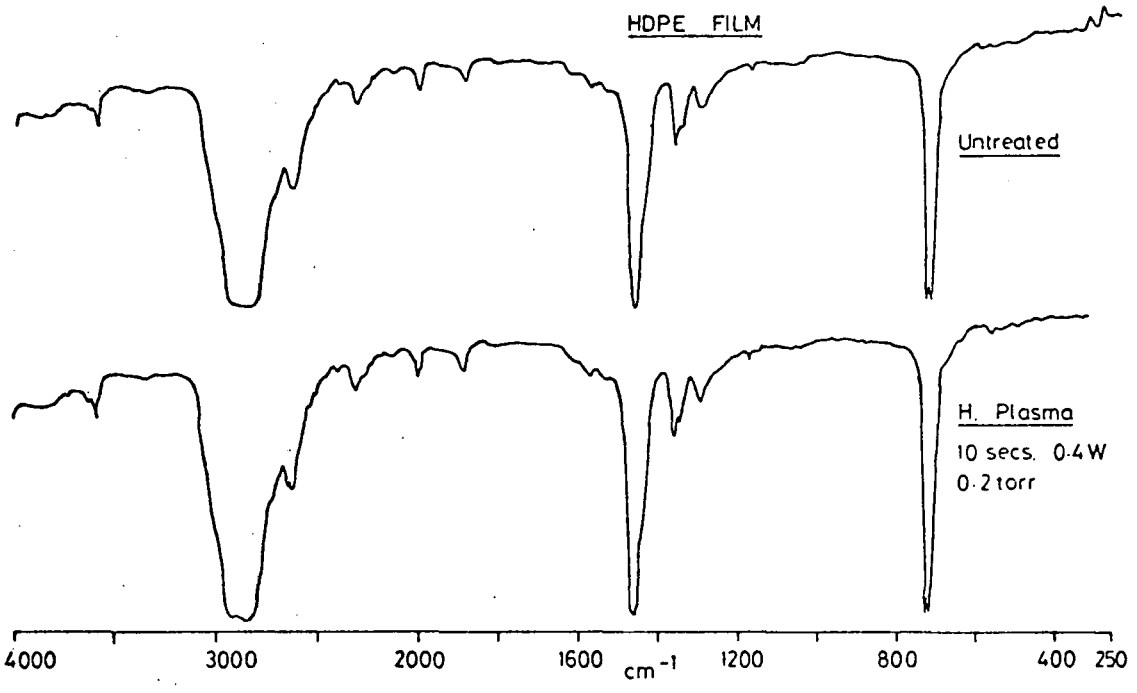

Figure 2.2 IR spectra of high density polyethylene film untreated and after hydrogen plasma treatment.

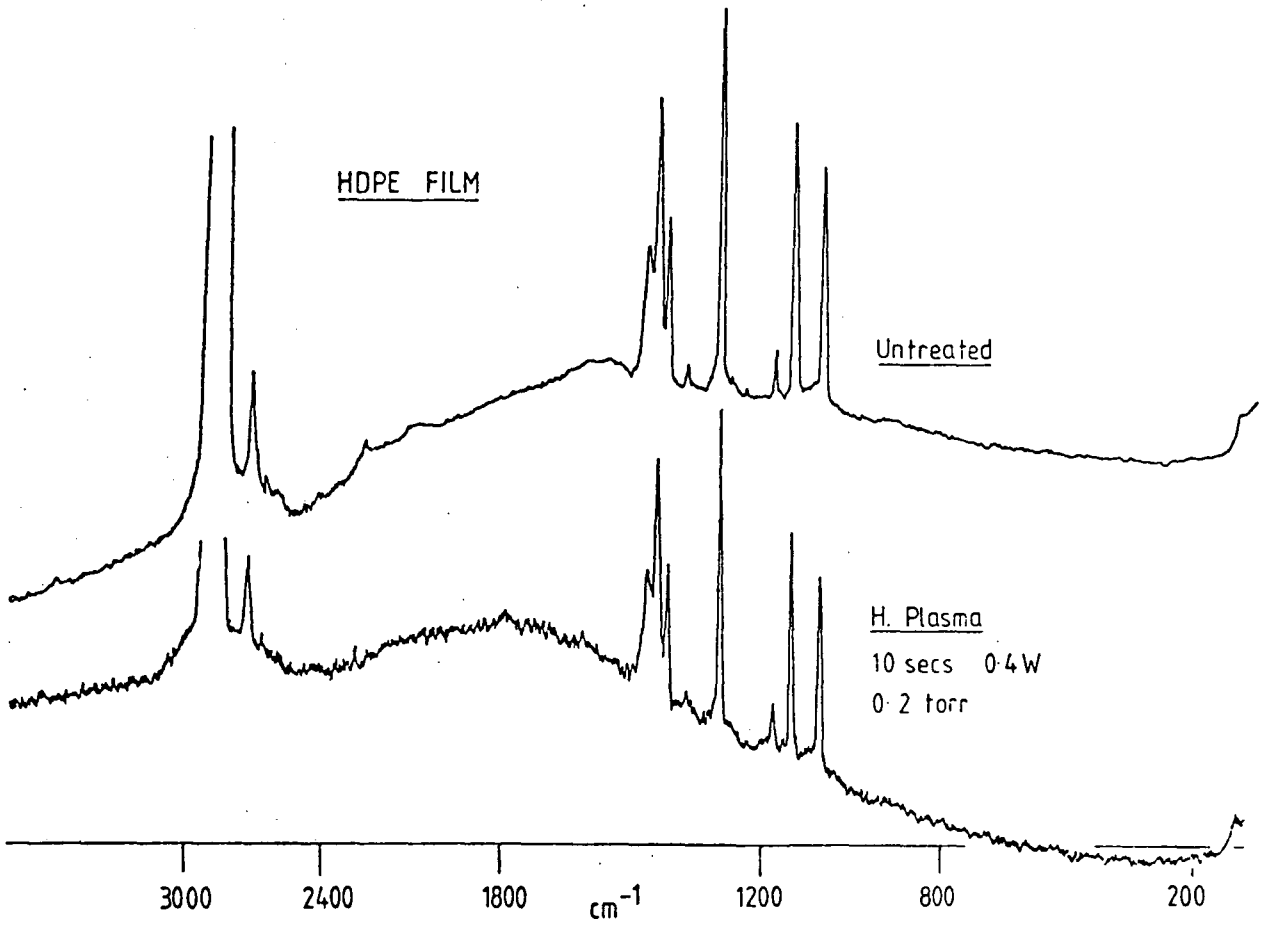

Figure 2.3 Laser Raman spectra (514.4nm) of high density polyethylene film, untreated and after hydrogen plasma treatment.

the integrated C_{1s}/O_{1s} intensity data suggests that the carbon singly bonded to oxygen (~286.4eV) corresponds almost exclusively to ester or ether linkages rather than free hydroxyl groups.

The integrated total intensity of the C_{1s} band profile in principle provides a means of determining the change in number average of carbon atoms sampled by ESCA. Unfortunately accurate measurements of absolute intensities are fraught with difficulty; however, by considering relative changes useful information may still be obtained. The relevant figures have been included in Table 2.1.

For the untreated sample the instrumental and sample dependent factors give rise to a ratio of 1.8 for the total integrated C_{1s} intensity at a take off angle of 30^{o} relative to that at 70^{o}. As will become apparent for the vertically homogeneous starting materials used for these studies (viz. the films of HDPE, polystyrene, PET and bisphneol-A polycarbonate) the dominant factor in determining this ratio is the instrument response function which has been described in detail elsewhere.[167,168] Thus for the untreated polymer films the intensity ratios ($C_{1s}{}^{30}/C_{1s}{}^{70}$) are within 5% the same. The lower power plasma treatments of interest in this work are such that changes in gross surface topography are negligible and changes in intensity ratios should therefore reflect changes in surface chemistry as they influence the number average of core levels statistically sampled by the ESCA experiment (viz. from changes in interchain spacing etc.).

For the oxygen plasma treated sample the $C_{1s}{}^{30}/C_{1s}{}^{70}$ ratio of 1.6 is only slightly smaller than for the untreated sample, perhaps suggesting a small increase in the number average of carbons sampled in the very surface (70^{o}). This could arise from ester or ether linkages between adjacent chains in the oxygen plasma treated surface regions.

Corresponding analyses for the hydrogen plasma treated sample reveal the following:- The low level of oxygen functionality present in the untreated sample remains effectively unchanged by the hydrogen plasma treatment. This low level of functionality appears to be present in the form of oxygen singly bonded to carbon (from the O_{1s} binding energy and the C_{1s} component analysis) and the evidence suggests that the low power hydrogen plasma does not reduce such

linkages. The integrated C_{1s}^{30}/C_{1s}^{70} intensity ratio of 2.0 is slightly higher than for the untreated sample and suggests therefore that surface cross linking is probably not a feature of the plasma treatment.

The small change in surface chemistry evidenced by the ESCA data for the hydrogen plasma treated samples does however lead to subtle changes in the subsequent reaction in an oxygen plasma. Thus the C_{1s}/O_{1s} intensity ratio at 30^{o} and 70^{o} of 1.8 may be compared with the corresponding ratios for the sample treated solely in the oxygen plasma of 1.6. The changes in C_{1s}/O_{1s} intensity ratios as a function of take off angle indicates that there is not a great difference in relative inhomogeneity for the two treatments despite the fact that oxidative functionalisation is significantly higher for the sample which has received hydrogen plasma treatment prior to the oxygen treatment. The relative constancy of the depth dependence of the oxidative functionalisation is revealed by considering the relative intensity of the components of the C_{1s} spectra associated with oxidative functionalisation as a function of take off angle and the relative data are displayed in Table 2.1.

2.3.2 Polystyrene

The histograms containing the core level data for plasma treatments for polystyrene are displayed in Figure 2.4. The diagram provides a direct visual impression of the substantial differences in the net effect of sequential plasma treatments for an aromatic as opposed to an aliphatic system.

Previous ESCA studies [135,169] have shown that polystyrene typically has a low level of surface oxidative functionalisation and detailed studies have also shown how the relatively high intensity $\pi \rightarrow \pi^{*}$

Figure 24 Histograms of the deconvoluted C_{1s} and O_{1s} spectra for polystyrene exposed to oxygen plasma (5 sec., 0.4W, 0.2 Torr), hydrogen plasma (10 sec., 0.4 W, 0.2 Torr) and sequential oxygen-hydrogen and hydrogen-oxygen plasma treatments, recorded at electron take off angles of 30^0 and 70^0.

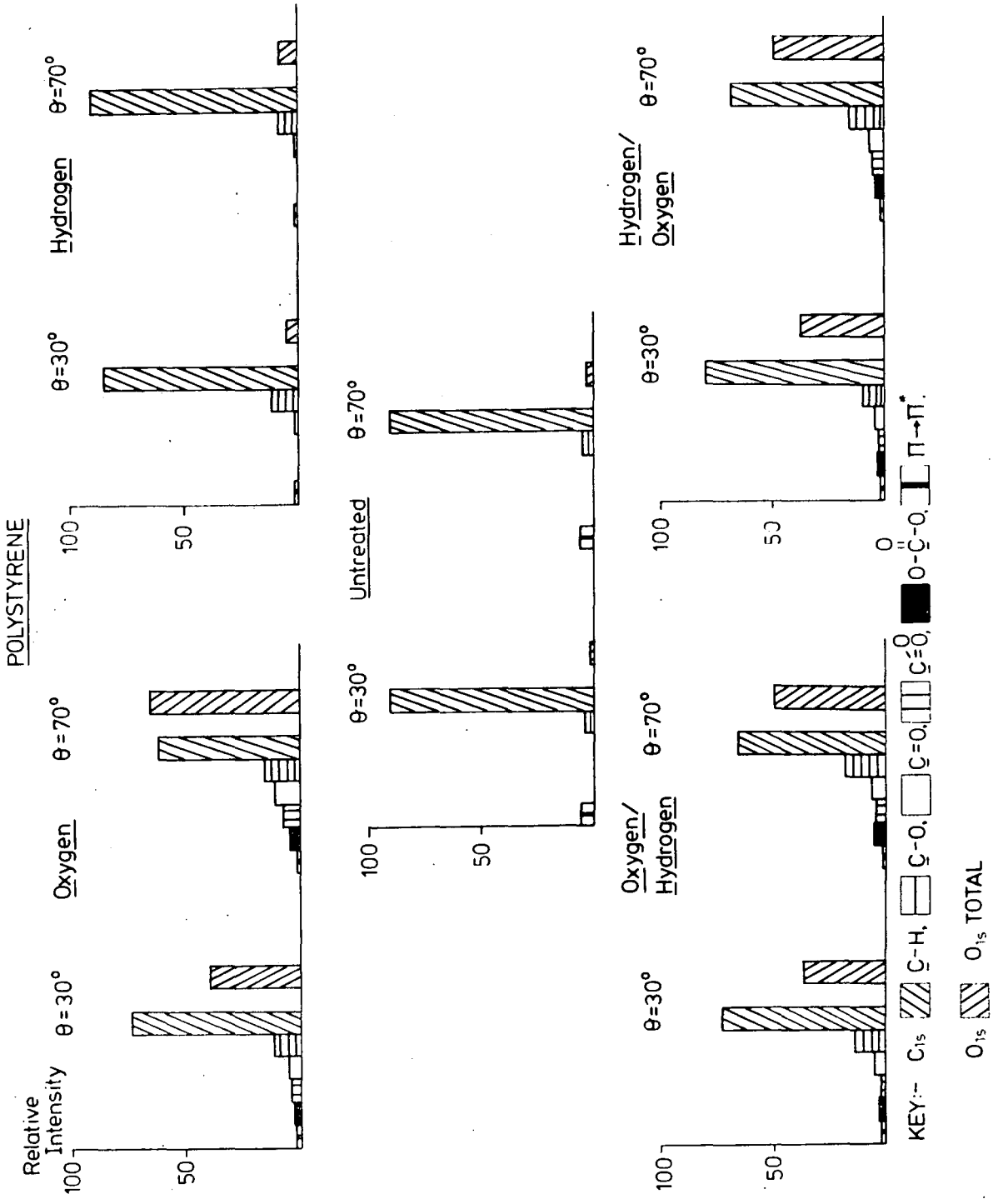

shake up component ($\sim$ 6.7eV from the main C_{1s} photoionisation peak) may be used to monitor the aromatic system.[38,135,170]

The effect of the hydrogen plasma is to drastically reduce the shake up structure indicating a substantial loss of aromatic character, this being greater at the very surface (70^{o} take off angle) than at 30^{o}. The C_{1s}^{30}/C_{1s}^{70} intensity ratio 1.9 remains essentially the same which would be consistent with hydrogenation to cyclohexyl side chains in a largely amorphous surface region with little change in interchain spacing. In contrast to the aliphatic system the hydrogen plasma seems to slightly increase the level of oxidative functionalisation although part at least of this arises from the silicone contamination inherent in the polymer and for which plasma treatment may well enhance diffusion to the surface. In addition it seems likely that some at least of the oxidative functionalisation may arise from the low levels of oxygen dissolved in the polymer sample. The difference with respect to HDPE can then be explained both in terms of the greater reactivity of the polystyrene and the increased solubility of oxygen in the latter.[171] Comparison of the relative intensities of the oxidative functionalisation at two different take off angles reveals that relatively there is less oxidative functionalisation at the very surface for the hydrogen plasma treated sample than for the 'as received' sample. This is consistent with the idea that part of the functionalisation arises from dissolved oxygen.
A further manifestation of the vertical inhomogeneity of the hydrogen plasma treatment is the increased FWHM of the component contributions to the line shape, particularly as a function of take off angle. This almost certainly arises from two effects. First there will be a small difference in binding energy for the C_{1s} levels in saturated and unsaturated environments; and second, there may well be a

broadening effect arising from differences in interchain contributions to relaxation energies (Section 1.2.3). [172]

Previous studies by Clark and Dilks, [135] and Wilson [169] on the plasma oxidation of polystyrene have shown the vertical inhomogeneity of the resulting oxidative functionalisation and have indicated the much greater reactivity of this polymer system compared with HDPE. The C_{1s} and O_{1s} core level spectra of Wilson [169] for polystyrene and polyethylene films, taken at both 30^{o} and 70^{o} take off angles, before and after oxygen plasma treatments are reproduced in Figures 2.5 and 2.6.

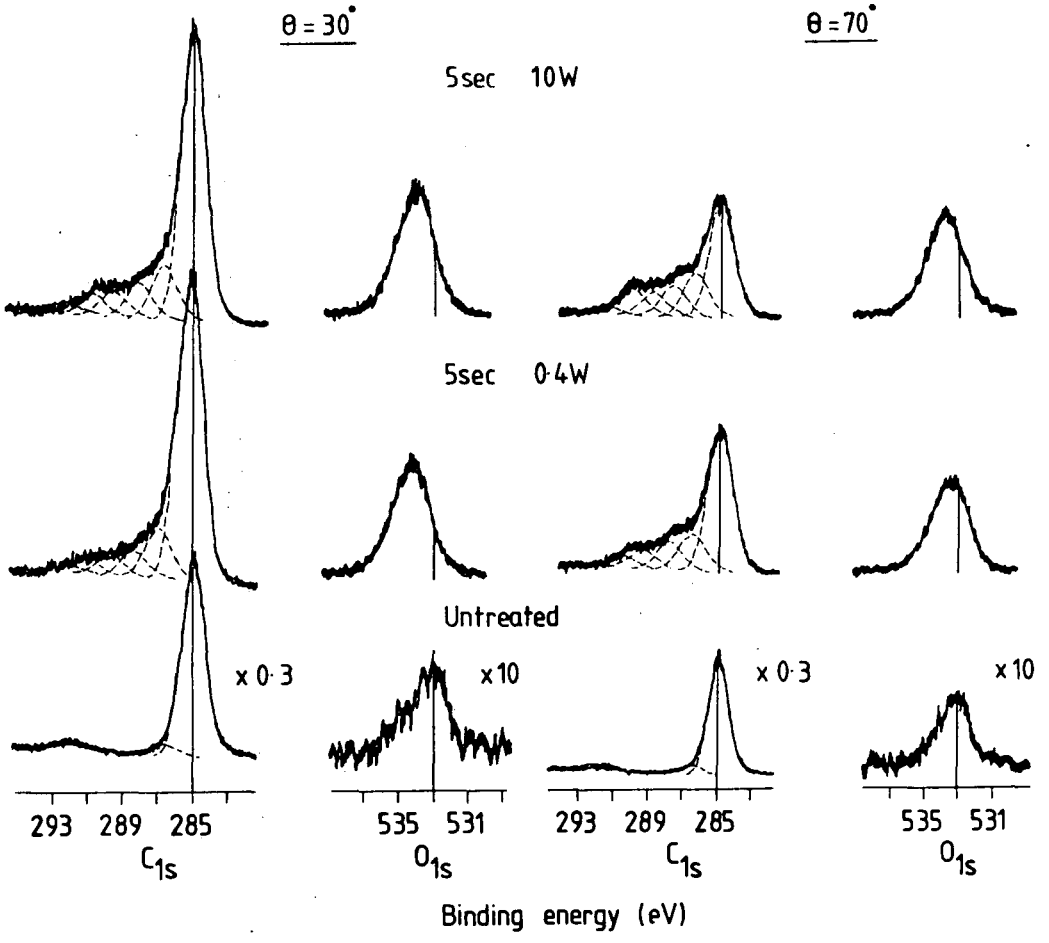

Figure 2.5 C_{1s} and O_{1s} spectra of polystyrene before and after oxygen plasma treatment (0.2 torr). [169]

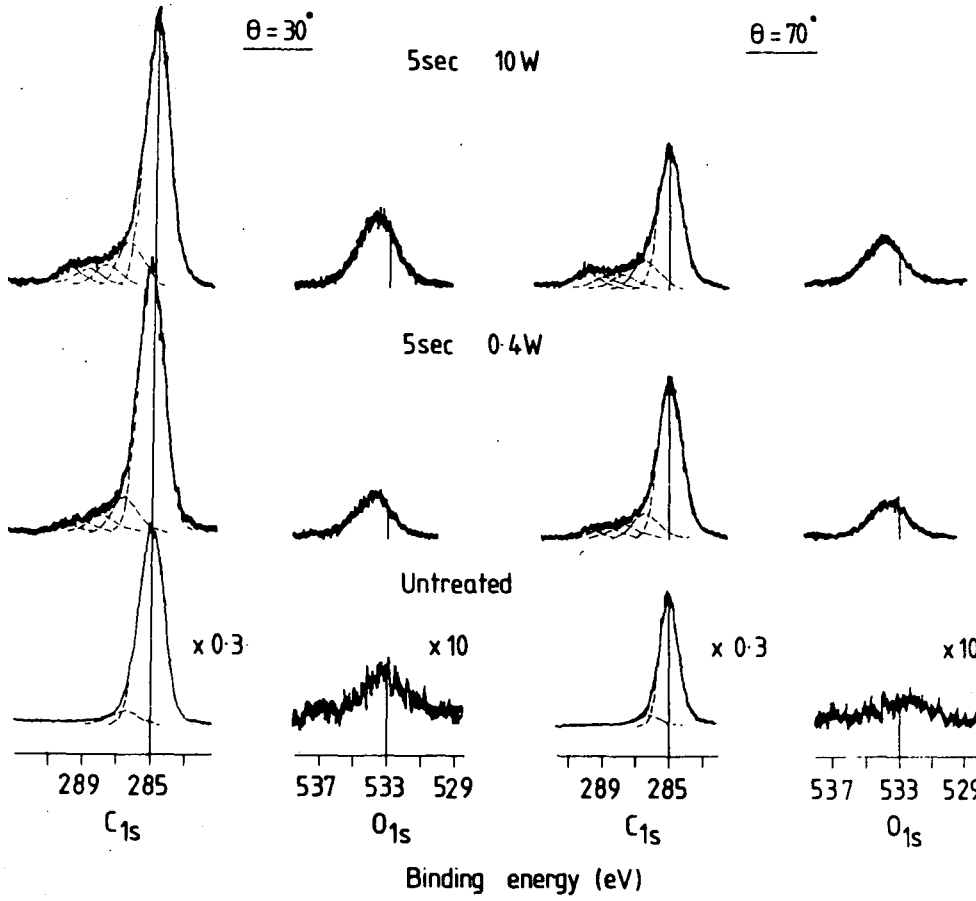

Figure 2.6 C_{1s} and O_{1s} spectra of high density polyethylene before and after oxygen plasma treatment (0.2 torr). [169]

These figures illustrate the marked differences between the aromatic and aliphatic polymer systems.

The histograms shown in Figures 2.1 and 2.4 mirror these differences for the polymer samples now under discussion. The oxygen

plasma results in the introduction of $\underline{C}$ - O, > $\underline{C}$ = O, -$\underset{\underset{O}{|}}{\underline{C}}$ = O and O-$\underset{\underset{O}{||}}{\underline{C}}$-O structural features and there is a substantial loss of shake up structure indicating transformations of the pendant phenyl groups. The effect of an oxygen plasma subsequent to a hydrogen plasma treatment is significantly different as is evident from the data in Figure 2.4. The main difference is in the distribution of oxidative functionalisation features, the overall depth profile being somewhat similar cf. Table 2.1. The integrated C_{1s} intensity ratios reveal little change in number average of carbons sampled (Table 2.1). The oxygen followed by hydrogen sequential plasma treatment leads overall to a very similar effect to the oxygen plasma, the main difference being that in the very surface region (70^{o}) there is evidence for reduction of > C = O and -$\underset{\underset{O}{|}}{\underline{C}}$ = O functionalities, however the carbonate functionality remains essentially unchanged.

2.3.3 Polyethylene terephthalate

The histograms containing the core level data for polyethylene terephthalate are shown in Figure 2.7 and reveal the striking chemical changes effected by the various plasma treatments: core level spectra are presented in Figure 2.8. For the sake of convenience in direct visual interpretation the O_{1s} core levels which exhibit fine structure are also displayed as single components in Figure 2.7. For the untreated sample the C_{1s} core levels at 30^{o} take off angle exhibit a four component structure corresponding in increasing binding energy to $\underline{C}H$, $\underline{C}$ - O, $\underset{\underset{O}{|}}{\underline{C}}$ = O and $\pi \rightarrow \pi^{*}$ shake up components whilst the O_{1s} levels are a 1:1 doublet corresponding to the two oxygen electronic environments, the component occurring at higher binding energy corresponding to oxygen singly bonded to carbon. The untreated PET shows a slightly

Figure 2.7 Histograms of the deconvoluted C_{1s} and O_{1s} spectra for polyethylene terephthalate exposed to oxygen plasma (5 sec, 0.4W, 0.2 torr), hydrogen plasma (10 sec, 0.4W, 0.2 torr) and sequential oxygen-hydrogen and hydrogen-oxygen plasma treatments, recorded at electron take off angles of 30° and 70°.

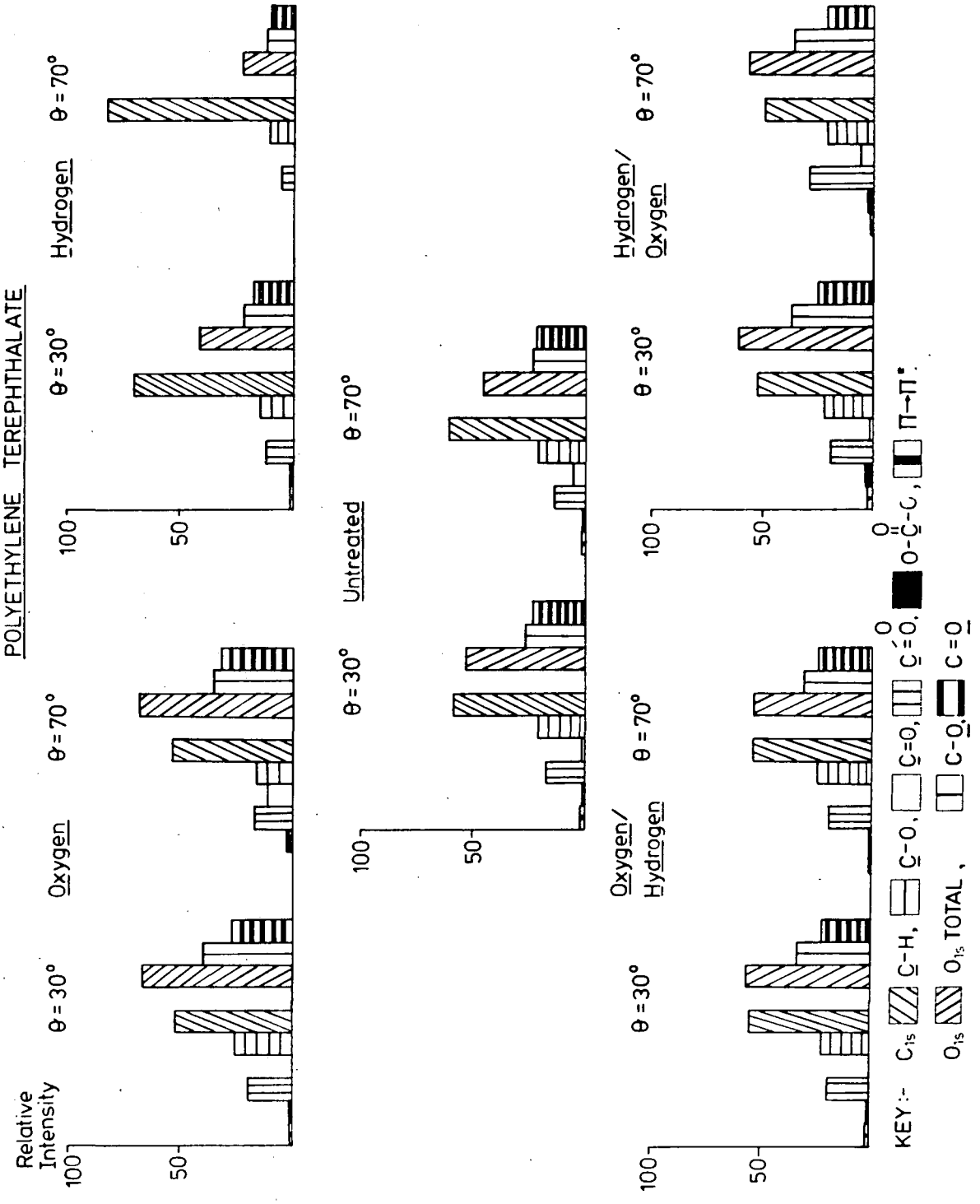

Figure 28 C_{1s} and O_{1s} spectra for polyethylene terephthalate exposed to oxygen plasma (5 sec, 0.4W, 0.2 torr), hydrogen plasma (10 sec, 0.4W, 0.2 torr) and sequential oxygen-hydrogen and hydrogen-oxygen plasma treatments, recorded at electron take off angles of 30^{0} and 70^{0}.

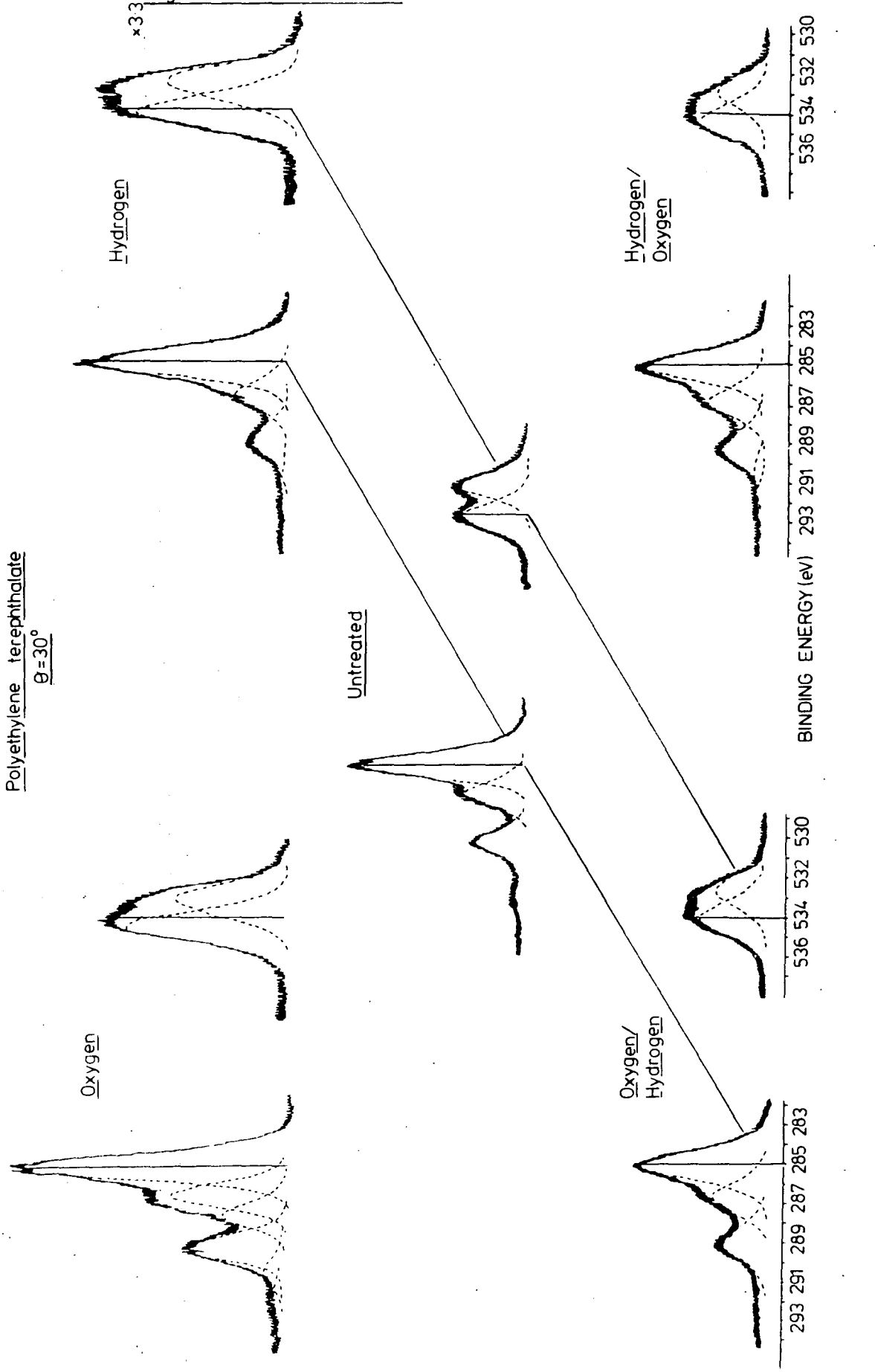

more intense peak at 285eV at 70^{o} compared with the corresponding peak at 30^{o} take off angle. This would tend to point to an enrichment of hydrocarbon at the very surface which would mask surface oxygen functionality. Comparing the carbon: oxygen atomic ratios obtained from considering the C_{1s} and O_{1s} peak areas at 70^{o} and 30^{o} take off angle reveals some depletion of surface oxygen. The respective values are 100:28.8 and 100:33.4, in contrast to the predicted value of 100:40 from the stoichiometry of PET. Two factors which may account for the apparent surfeit of hydrocarbon are a build-up of surface hydrocarbon contamination arising on storage of the film prior to ESCA analysis, or originating from extraneous contamination of the ESCA vacuum system;‡ alternatively, the hydrocarbon enriched surface may be due to a 'turning in' of the polar oxygen functional groups to reduce the surface energy of the system.[173] The effect of the hydrogen plasma is clear from the data in Figure 2.7, there being a substantial reduction in oxygen functionality, particularly in the surface regions, the relative intensity of the oxidatively functionalised contribution to the C_{1s} spectrum measured at 30^{o} relative to 70^{o} increasing significantly on treatment (1.1 → 1.4). The component analysis of the C_{1s} spectrum reveals a reduction in the $\pi \rightarrow \pi^{*}$ shake up intensity indicating lack of aromaticity in the surface regions and a substantial reduction in $-\underset{\underset{O}{\|}}{C} = O$ and $\underline{C} - O$ structural features. Analysis of the O_{1s} line profile also shows the change in relative proportions of oxygen singly and doubly bonded to carbon. The total relative integrated intensity of the C_{1s} levels at 30^{o} and 70^{o} take off angles changes very little on hydrogen plasma treatment (Table 2.1). This implies little change in the number average of carbon atoms sampled

in the ESCA experiment thus suggesting little change in interchain spacing. †

---

† The behaviour of PET on exposure to hydrogen plasma has also been studied as a function of exposure time. Two plasma powers were used, 0.4W and 1.0W, and treatment times of up to 50 seconds were chosen. All plasmas were initiated as described earlier (Section 2.2.4b). The relevant data are presented in Tables 2.2 and 2.3 and Figures 2.9 - 11. It has been noted that hydrogen plasma treatment (10 sec, 0.4W, 0.2 torr) leads to a substantial reduction in the oxygen content of the surface regions of PET film, as revealed by O_{1s} and O_{2s} core level spectra. This trend extends throughout the range of conditions used. The surface specificity is immediately apparent on consideration of the angular dependent data displayed graphically in Figure 2.9. It is also clear that the stronger plasma treatment (at 1W) yields a surface slightly more oxygen deficient than is found for the 0.4W plasma treatment. The variation in intensity of the C_{1s} component peaks with hydrogen plasma treatment at 0.4W and 1.0W power is shown in Figures 2.10 and 2.11. Again the surface specificity of modification is apparent, and it is interesting to note that the carbon singly bonded to oxygen and carboxylate moieties of the C_{1s} envelope show similar intensity variation with treatment time. This would seem to suggest that the PET ester functionality undergoes chemistry resulting in its elimination from the surface; or alternatively, the hydrogen plasma may allow a reorientation of the ester groups away from the surface regions.

‡ Calculations, based on the substrate/overlayer model described in Section 1.6.1, suggest that the contaminant hydrocarbon overlayer, if present, takes the form of a patched overlayer (Figures 2.11a-c).

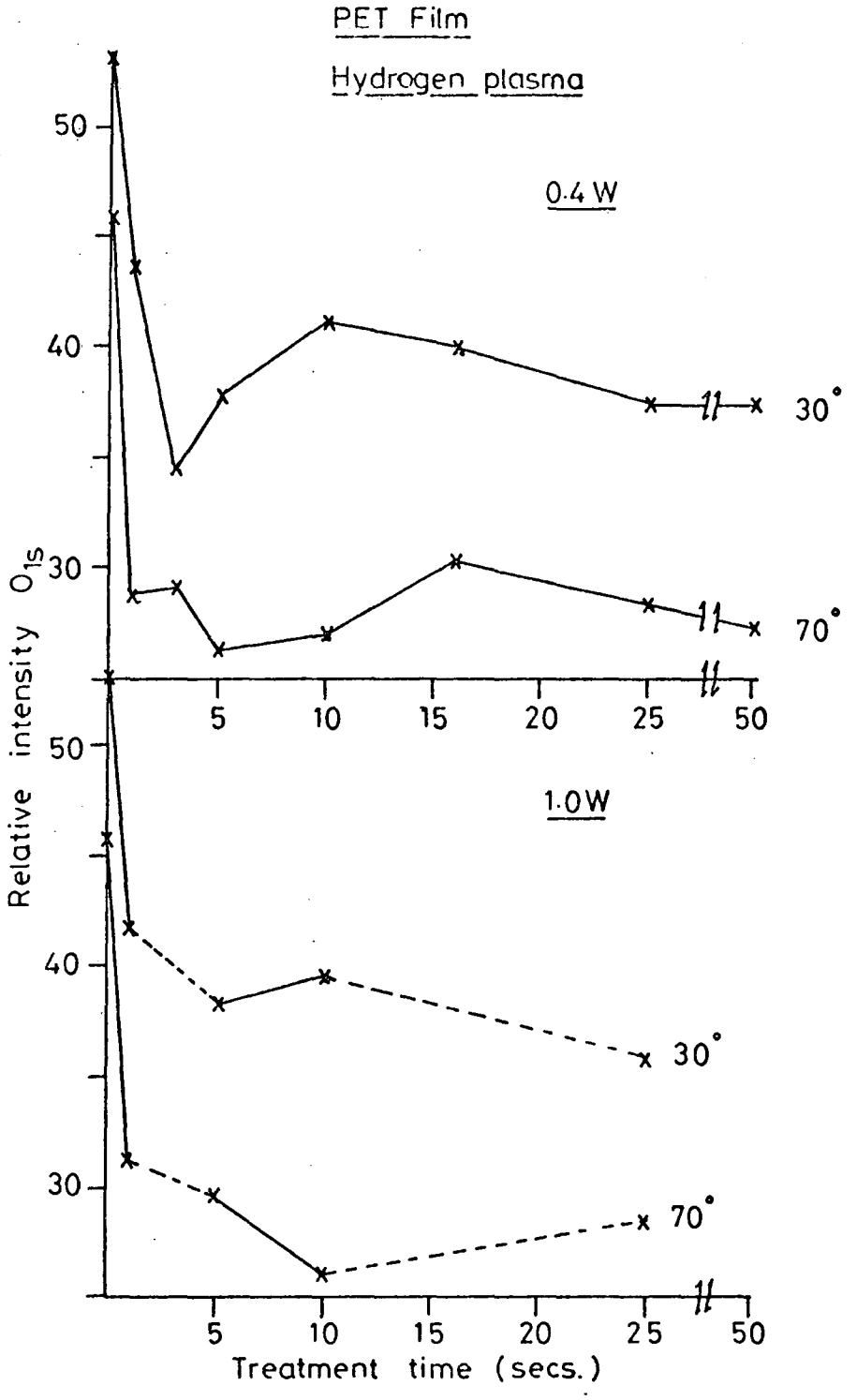

Figure 2.9 Relative intensity of the O_{1s} signal of PET as a function of time of exposure to hydrogen plasma (0.4W and 1W, 0.2 torr) for spectra recorded at electron take off angles of 30^{o} and 70^{o}.

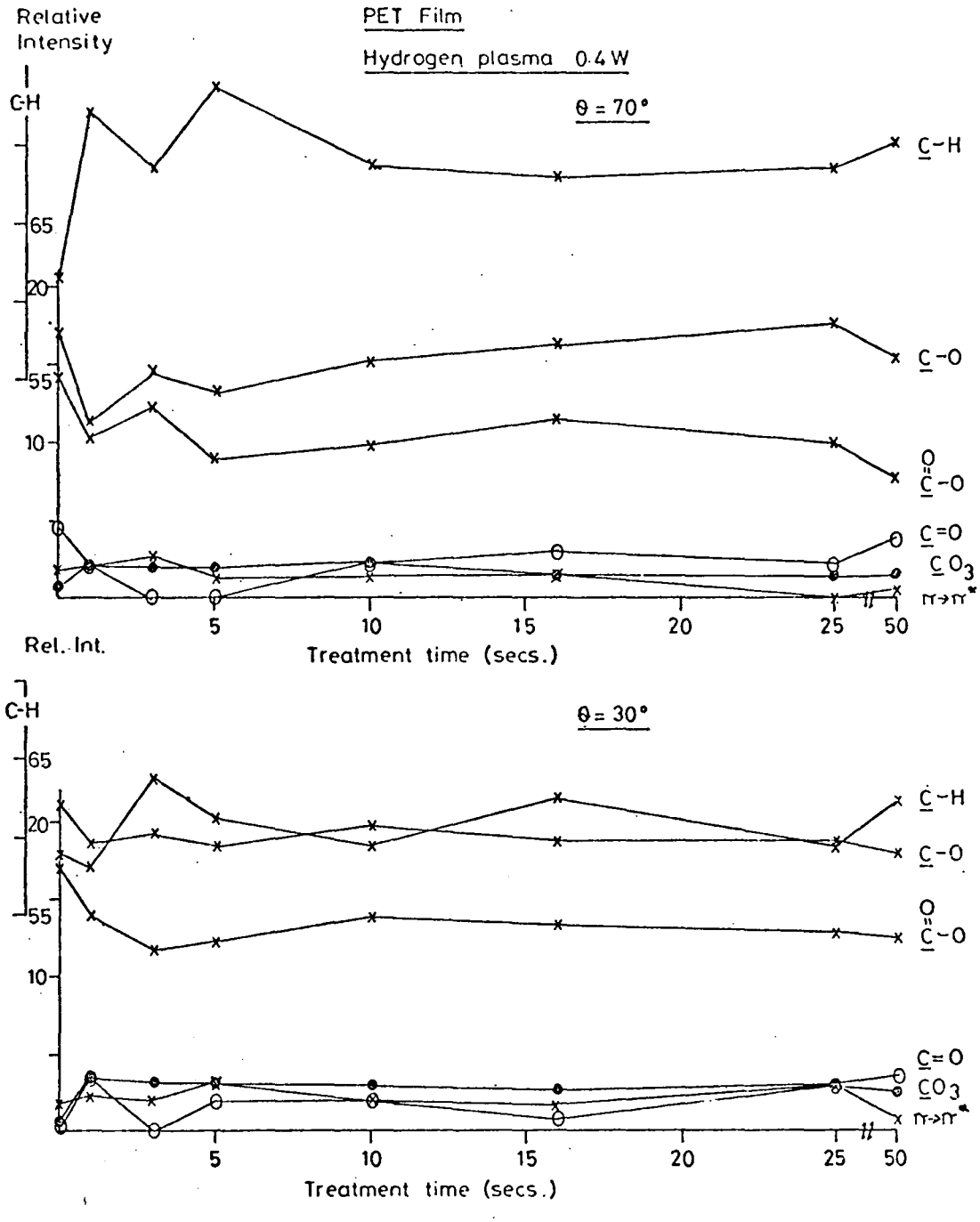

Figure 2.10 Intensities of the individual C_{1s} component peaks (expressed as % of total C_{1s} band intensity) for PET as a function of hydrogen plasma (0.4 W, 0.2 torr) exposure time for $\theta = 30^{o}$ and $\theta = 70^{o}$.

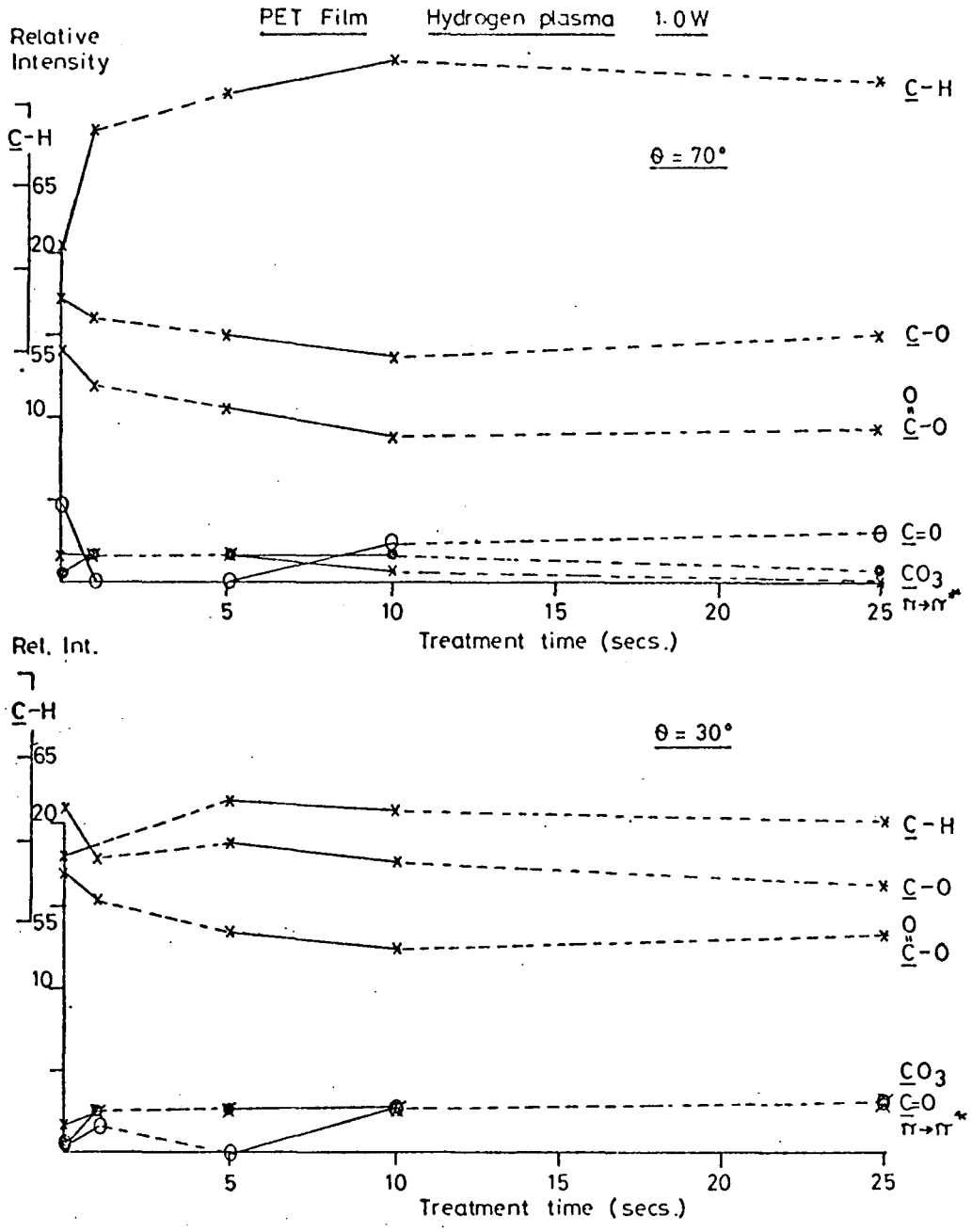

Figure 2.11 Intensities of the individual C_{1s} component peaks (expressed as % of total C_{1s} band intensity) for PET as a function of hydrogen plasma (1.0W, 0.2 torr) exposure time for $\theta = 30^{o}$ and $\theta = 70^{o}$.

Table 2.2 Hydrogen plasma treatment (0.4W, 0.2 torr) of PET film. Relative intensities of core electron signals

Treatment time (secs.)	θ	Total C_{1s}	C - H	C - O	>C = O	O ‖ C - O	O ‖ O-C-O	$\pi \rightarrow \pi^*$	O_{1s}
0	30°	100	59.0	21.2	0.3	17.1	0.6	1.8	53.1
	70°	100	61.3	17.2	4.9	14.1	0.6	1.8	45.8
1	30°	100	58.1	18.6	3.5	14.0	3.5	2.3	43.6
	70°	100	72.2	11.3	2.1	10.3	2.1	2.1	28.9
3	30°	100	63.8	19.1	-	11.7	3.2	2.1	34.5
	70°	100	68.5	14.4	-	12.3	2.1	2.7	29.2
5	30°	100	61.2	18.4	2.0	12.2	3.1	3.1	37.7
	70°	100	73.5	13.2	-	8.9	2.1	1.4	26.3
10	30°	100	59.4	19.8	2.0	13.9	3.0	2.0	41.0
	70°	100	68.7	15.3	2.3	9.9	2.3	1.5	27.0
16	30°	100	62.5	18.8	0.9	13.4	2.7	1.8	39.9
	70°	100	68.0	16.3	3.1	11.5	1.5	1.5	31.3
25	30°	100	59.4	18.8	3.0	12.9	3.0	3.0	37.4
	70°	100	68.7	17.6	2.3	9.9	1.5	-	28.5
50	30°	100	62.5	17.9	3.6	12.5	2.7	0.9	37.5
	70°	100	70.3	15.6	3.9	7.8	1.6	0.8	27.3

Table 2.3 Hydrogen plasma treatment (1.0 W, 0.2 torr) of PET film. Relative intensities of core electron signals

Treatment time (secs.)	θ	Total C_{1s}	C - H	C - O	> C = O	O ‖ C - O	O ‖ O-C-O	$\pi \rightarrow \pi^*$	O_{1s}
0	30°	100	59.0	21.2	0.3	17.1	0.6	1.8	53.1
	70°	100	61.3	17.2	4.9	14.1	0.6	1.8	45.8
1	30°	100	59.8	17.9	1.7	15.4	2.6	2.6	42.1
	70°	100	68.4	16.2	-	12.0	1.7	1.7	31.3
5	30°	100	62.5	18.8	-	13.4	2.7	2.7	38.3
	70°	100	70.8	15.0	-	10.6	1.7	1.7	28.6
10	30°	100	61.9	17.7	2.7	12.4	2.7	2.7	39.6
	70°	100	72.6	13.7	2.4	8.9	1.6	0.8	26.1
25	30°	100	61.2	16.3	3.1	13.2	3.1	3.1	35.8
	70°	100	71.4	15.1	3.2	9.5	0.8	-	28.6

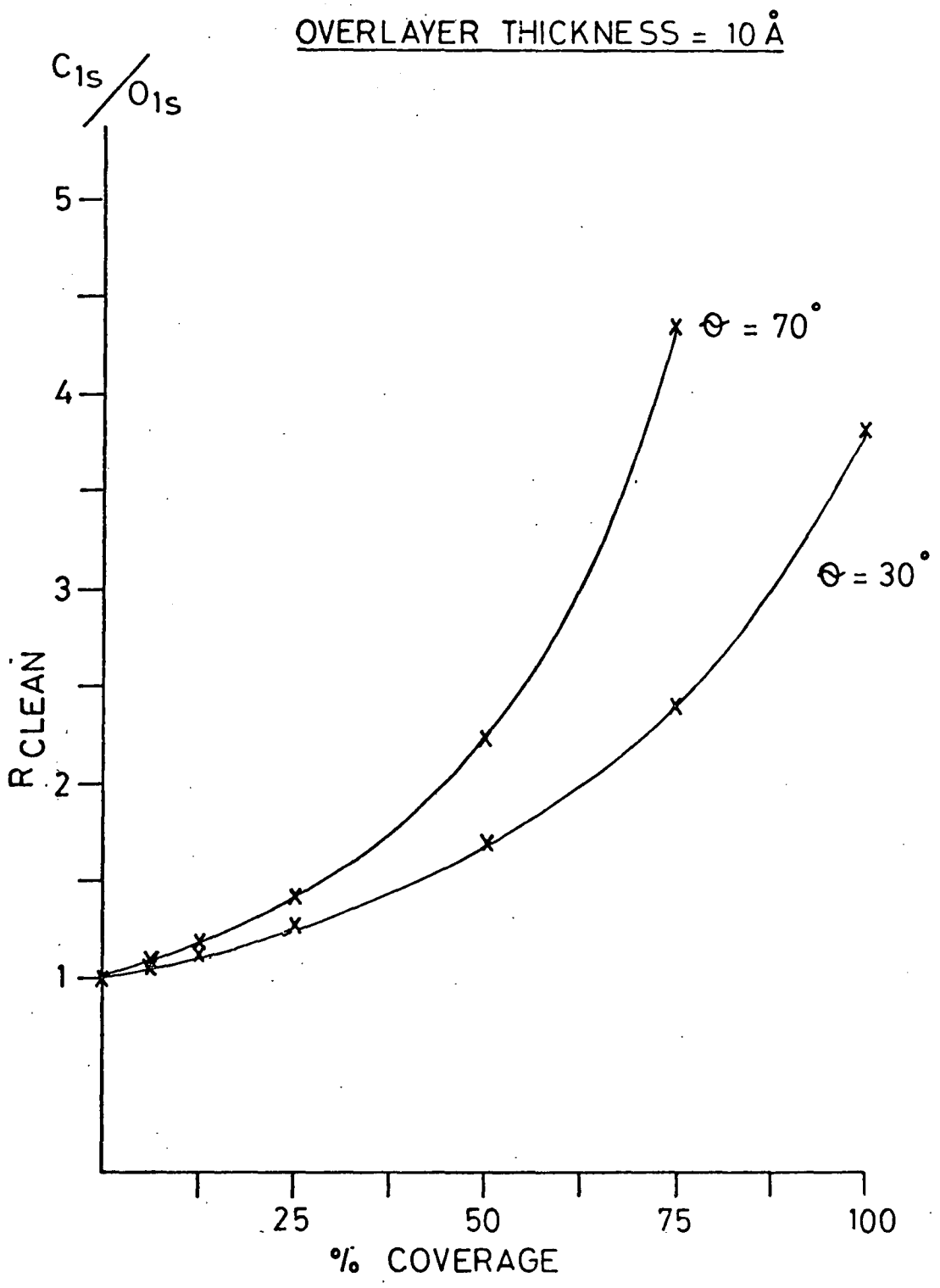

Figure 2.11a Effect of a surface overlayer of hydrocarbon contamination of thickness 10Å on the C_{1s}/O_{1s} ratio, relative to that for the clean substrate, for PET film (C : O atomic ratio = 10 : 4).

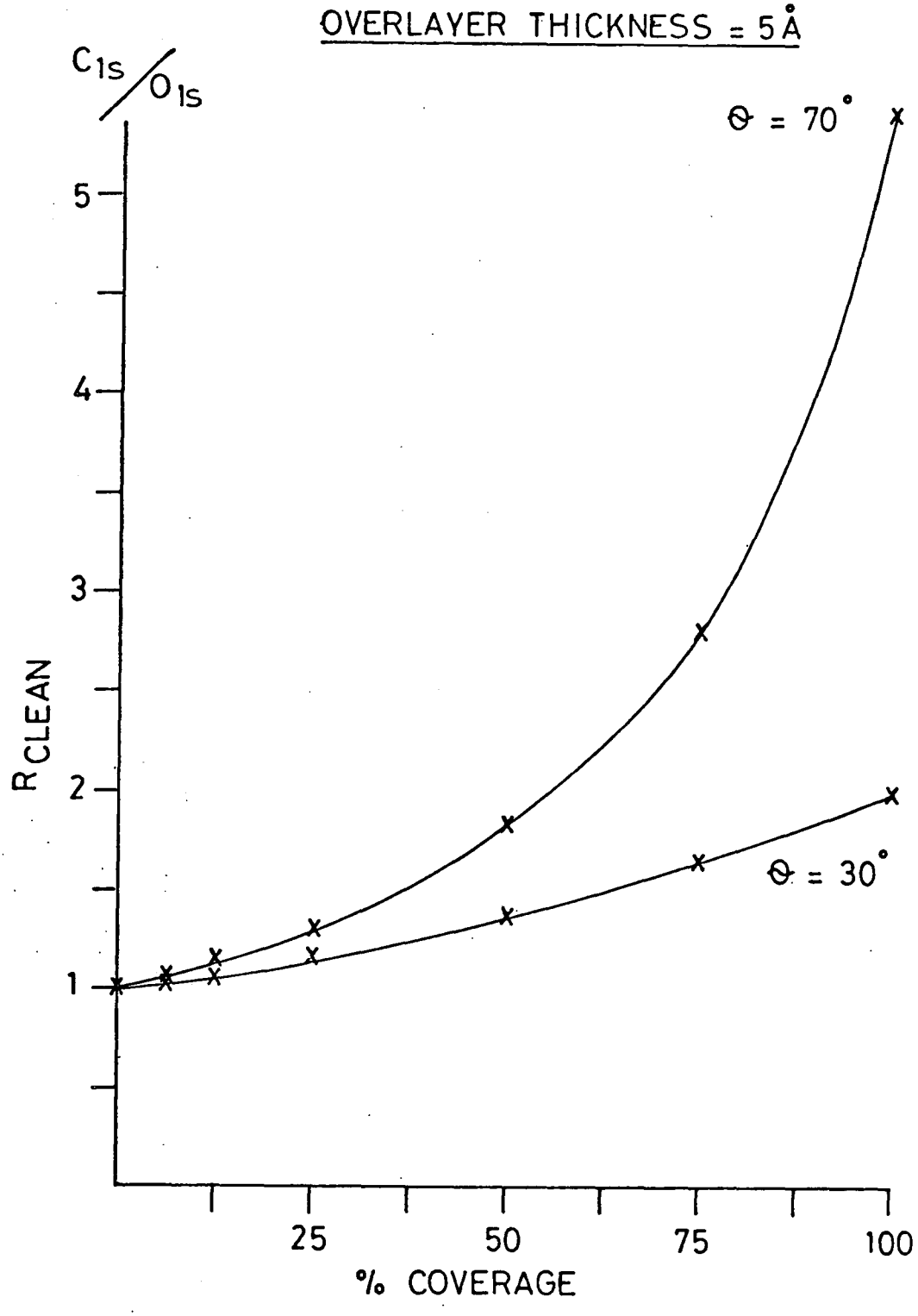

Figure 2.11b Effect of a surface overlayer of hydrocarbon contamination of thickness 5Å on the C_{1s}/O_{1s} ratio, relative to that for the clean substrate, for PET film.

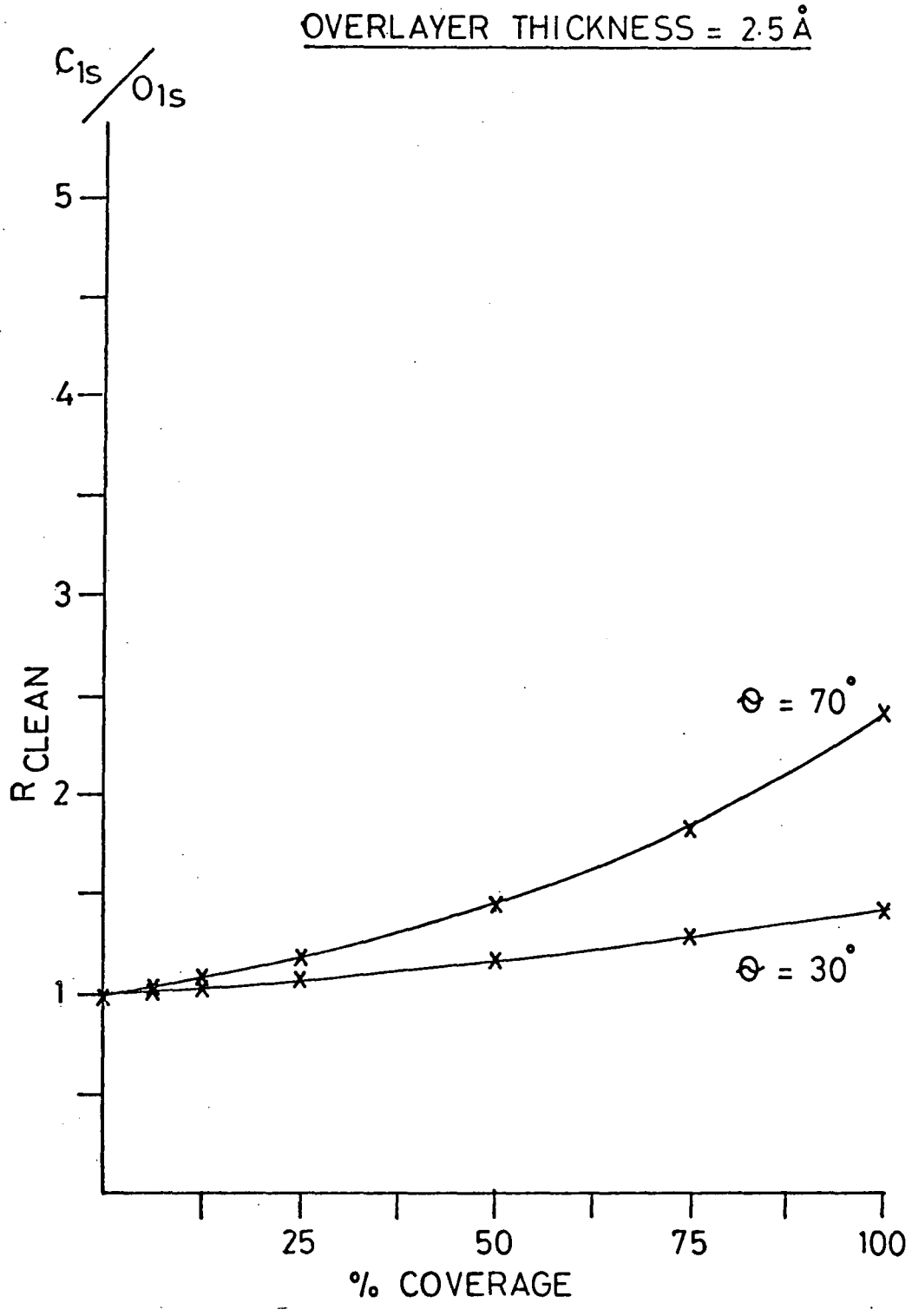

Figure 2.11c Effect of a surface overlayer of hydrocarbon contamination of thickness 2.5Å on the C_{1s}/O_{1s} ratio, relative to that for the clean substrate, for PET film.

The effect of the oxygen plasma is to increase the level of oxidative functionalisation but to only a modest degree, the C:O stoichiometry changing by $\sim$ 25%. The component analysis reveals loss of aromatic character ($\pi \rightarrow \pi^*$ and CH components) with a concomitant increase in carbonyl, carboxylate and carbonate structural features. The relative integrated intensity of the high binding energy components (arising from oxidative functionalisation) with respect to that at low binding energy (CH) shows roughly the same angular dependence as the untreated sample. This indicates the vertical homogeneity in stoichiometry of the treated sample. The change in C_{1s} integrated intensity ratio from 2.0 (untreated) to 2.7 at 30^{o} vs. 70^{o} take off angle indicates a more open surface structure for the plasma treated sample with a greater average interchain spacing.

The sequential plasma treatments show subtle differences between each other and the oxygen plasma treatment and this is evident both from the histograms in Figure 2.7 and the representative C_{1s} and O_{1s} spectra in Figure 2.8.

Comparison of the sequential oxygen-hydrogen plasma treatments with the straight hydrogen plasma treatment reveals the following:

(i) The level of oxidative functionalisation is much higher for the sequentially treated sample.

(ii) The vertical inhomogeneity as evidenced from the angular dependent data indicates a greater level of oxidative functionalisation in the surface as opposed to the subsurface for the sequentially treated sample, the reverse of that found for the straight hydrogen plasma treated sample.

Comparison with the oxygen plasma treated sample shows little difference with respect to the sequentially treated sample. The only distinctive feature being the somewhat greater degree of vertical inhomogeneity in carbon:oxygen stoichiometry and the somewhat more open nature of the surface structure for the oxygen plasma treated sample compared to that which has been sequentially treated.

By contrast the oxygen-hydrogen plasma treated sample is distinctively different from the straight hydrogen plasma treated sample and this is clearly evident from Figures 2.7 and 2.8. The sequentially treated sample retains a much greater degree of oxidative functionalisation than the hydrogen plasma treated sample. Comparison of the two sequentially treated samples shows relatively small differences between them. The level of oxidative functionalisation is very comparable, the main difference being in the distribution of unfunctionalised (CH), carbonyl and carbonate structural features.

The histogram data in Figure 2.7 reveals the proportion of high to low binding energy oxygen components. Thus, from the roughly 50:50 distribution (C-O to C=O) for the starting material the plasma treatments in general give rise to an increasing proportion of oxygen singly bonded to carbon functionalities compared to the lower binding energy component arising from oxygen doubly bonded to carbon.

2.3.4 Bisphenol-A polycarbonate

The C_{1s} and O_{1s} core level spectra for untreated bisphenol-A polycarbonate are very distinctive with components arising from $\underline{C}H$, $\underline{C}-O$, $O-\underline{C}(=O)-O$ and $\pi \rightarrow \pi^*$ structural features (Fig. 2.12). The effect of hydrogen plasma treatment is to significantly reduce the level of oxygen functionalities and the relative intensity of the high to low binding energy components of the C_{1s} levels at 30^0 and 70^0 take off angles indicates vertical inhomogeneity with the level of oxidative functionality being lower in the very surface regions (Table 2.1). The integrated relative intensity of the C_{1s} levels at 30^0 and 70^0 take off angles changes from 1.7 for the untreated sample to 2.3 for the hydrogen plasma treated sample indicating a greater interchain spacing.

Comparison of the component contributions to the overall C_{1s} band profile (Figure 2.13) shows that hydrogen plasma treatment leads to a reduction in the $\pi \rightarrow \pi^*$ shake up satellite consistent with hydrogenation of the aromatic rings and the carbonate structural features are also reduced. It is significant that reduction of carbonate is not to either carbonyl or carboxylate structural features. This could arise from reductive cleavage resulting in the loss of CO_2.

Oxygen plasma treatment results in both carbonyl and carboxylate structural features with both the $\pi \rightarrow \pi^*$ shake up and carbonate components being reduced in intensity and this is particularly evident for the spectra recorded at 70^0 take off angle (Figure 2.12). The integrated total intensity ratio of the C_{1s} levels at 30^0 and 70^0 changes from that for the untreated sample in a sense indicating an increase in number average of carbon atoms in the oxygen plasma treated sample and the most ready explanation for this would be

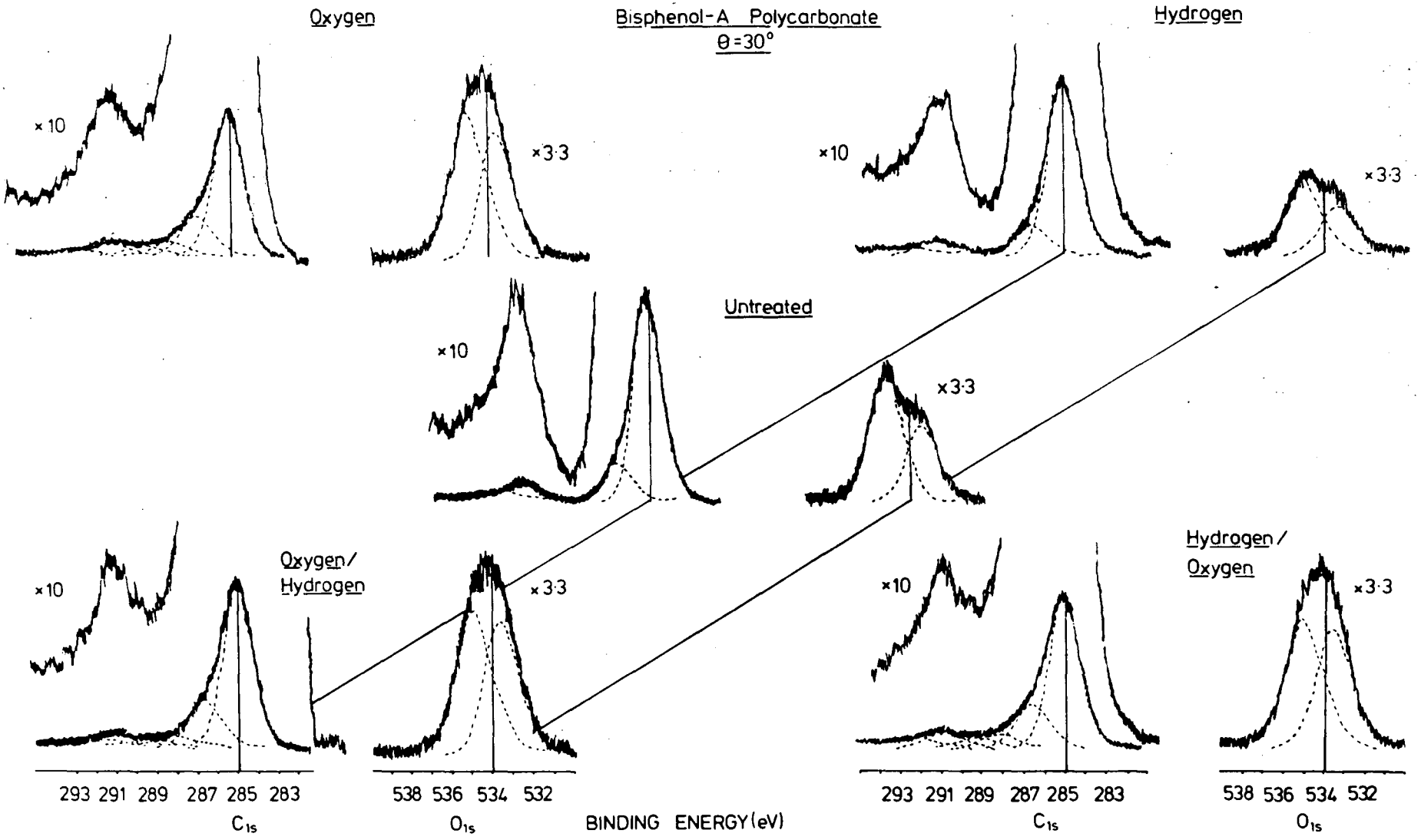

Figure 2.12 C_{1s} and O_{1s} spectra for bisphenol-A polycarbonate exposed to oxygen plasma (5 sec, 0.4 W, 0.2 torr), hydrogen plasma (10 sec, 0.4 W, 0.2 torr) and sequential oxygen-hydrogen and hydrogen-oxygen plasma treatments, recorded at electron take off angles of 30° and 70°.

Figure 2.13 Histograms of the deconvoluted C_{1s} and O_{1s} spectra for bisphenol-A polycarbonate exposed to oxygen plasma (5 sec, 0.4 W, 0.2 torr), hydrogen plasma (10 sec, 0.4 W, 0.2 torr) and sequential oxygen-hydrogen and hydrogen-oxygen plasma treatments, recorded at electron take off angles of 30° and 70°

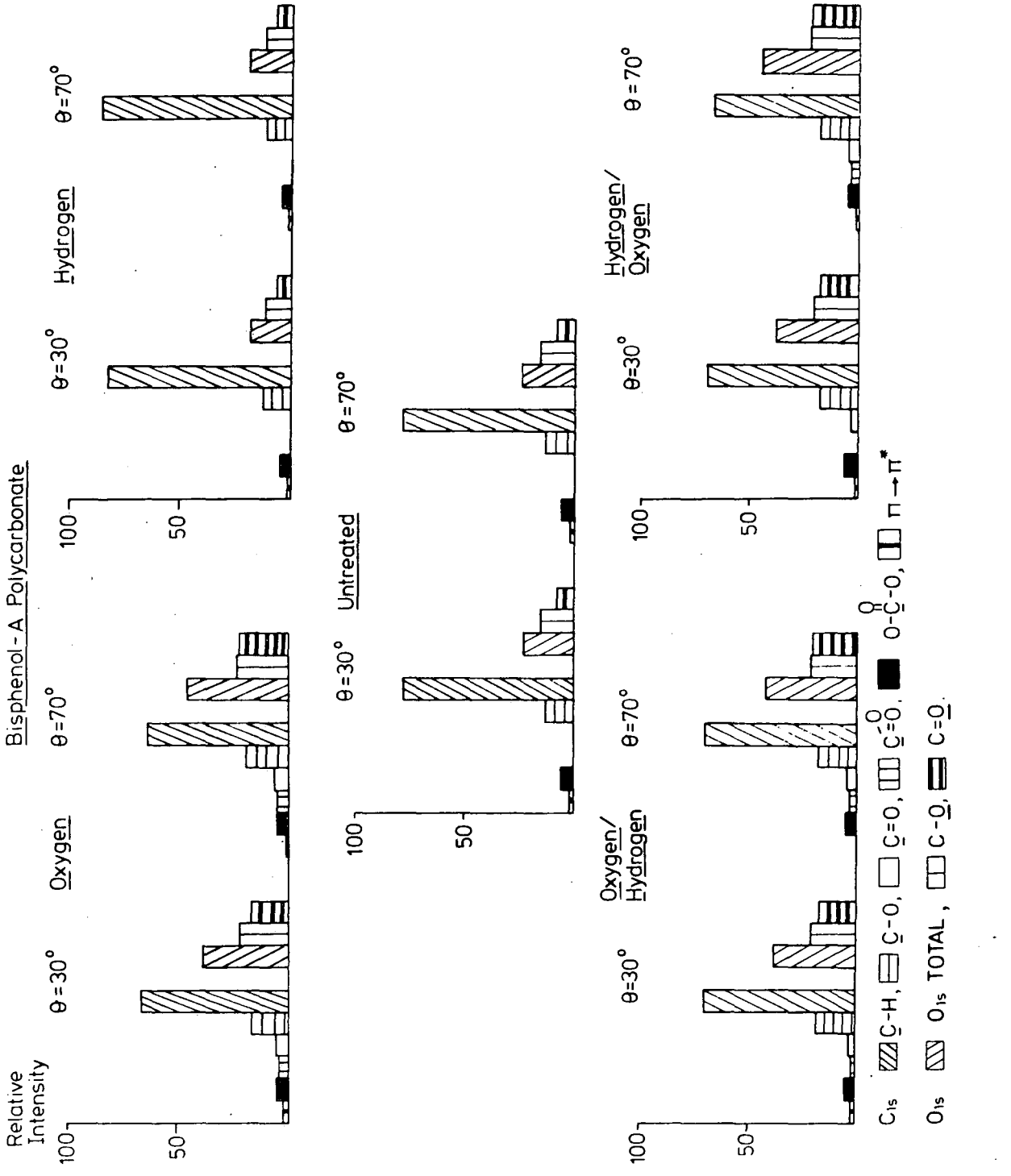

a degree of cross linking. The C_{1s}/O_{1s} intensity ratios suggest a change in overall C:O stoichiometry on plasma treatment from 100:14 for the starting material to 100:23 for the treated sample.

The histograms reveal the similarities between the sequentially plasma treated samples (Figure 2.13). The stoichiometries and distribution of structural features for the hydrogen/oxygen and oxygen/hydrogen treatments are closely similar as are the vertical homogeneities. The total relative integrated intensities of the C_{1s} levels at 30^{o} and 70^{o} take off angles also differ very little from that for the starting polymer.

2.3.5 Comparison of data

The angular dependent data reveal the surface specific nature of the changes in chemistry effected with the low powered plasmas. Oxygen plasma treatment in each case leads to an increase in oxidative functionality and it is of interest to compare HDPE and polystyrene for which low levels of adventitious oxidative functionality exists for the starting materials and also PET and polycarbonate for both of which oxidative functionalities are an integral part of the repeat unit.

For HDPE and polystyrene we may compare the relative change in signal intensity for the components of the C_{1s} signal associated with oxidative functionalities as a function of oxygen plasma treatment under identical conditions. The data are displayed in Table 3.4 and the increase is seen to be greatest for the aromatic polymer (5.4 vs. 3.3 at 30^{o} take off angle) indicating the greater reactivity of the polystyrene. The data also show the greater vertical inhomogeneity of the oxidative functionalisation in the aromatic system.

Table 2.4 A measure of the relative change in signal intensity for the components of the C_{1s} signal associated with oxidative functionalities as a function of plasma treatment, $[C_{1s}\ oxid/C_{1s}\ total]_{Treated} / [C_{1s}\ oxid/C_{1s}\ total]_{Untreated}$.†

Material	θ	Untreated	Oxygen	Hydrogen	Hydrogen/Oxygen	Oxygen/Hydrogen
HDPE	30°	1.0	3.3	1.0	4.2	3.8
	70°	1.0	3.6	1.3	6.2	5.3
Polystyrene	30°	1.0	5.4	3.0	4.1	5.4
	70°	1.0	7.5	1.8	6.0	6.5
PET	30°	1.0	1.2	0.8	1.2	1.1
	70°	1.0	1.3	0.6	1.3	1.2
Bisphenol-A polycarbonate	30°	1.0	1.6	0.8	1.5	1.4
	70°	1.0	1.8	0.7	1.6	1.5

† A value of > 1 indicates an increase in oxidative carbon functionality on plasma treatment.

A value of < 1 indicates a decrease in oxidative carbon functionality on plasma treatment.

Comparison of PET and bisphenol-A polycarbonate shows that the latter is somewhat more reactive than the former, both showing less vertical inhomogeneity in oxidative functionalisation than polystyrene.

Hydrogen plasma treatment of the aromatic polymers leads to a decrease in $\pi \rightarrow \pi^*$ shake up structure and hence unsaturation and reduction of functional groups leads overall to a decrease in oxidative functionalisation, this being comparable for PET and the bisphenol-A polycarbonate. The low level of oxidative functionality in polystyrene and HDPE appears to increase slightly during hydrogen plasma treatment and this could arise in the former case from the high inherent reactivity to oxygen and is most probably attributable to reactions involving low levels of dissolved oxygen in the polymer films. To put matters in perspective however the C:O stoichiometry for these hydrogen plasma treatments indicates that approximately 1 carbon in 50 (polystyrene) or 1 carbon in 100 (HDPE) has an oxygen singly bonded to carbon.

For PET and bisphenol-A polycarbonate the sequential plasma treatments lead overall to comparable oxidative functionalisation as for the oxygen plasma treatment alone with a small decrease in level of functionalisation apparent for the treatment which involves hydrogen after oxygen exposure.

The level of oxidative functionalisation for the sequentially treated samples in the particular cases of HDPE and polystyrene is somewhat different. Thus for HDPE sequential treatment actually leads to a higher level of oxidative functionality than for oxygen plasma treatment alone whereas for polystyrene the sequential treatments lead overall to a reduction in the oxidative functionalisation.

2.4 Conclusions

This study has illustrated the complex changes in surface chemistry which occur on the treatment of a selection of polymers with very mild radiofrequency plasmas excited in oxygen and hydrogen. Attention has been paid to the effects of sequential treatments and this is an area which has not been explored previously. These preliminary results would suggest that the fabrication of surfaces containing an enhancement of specific functional groups may be achieved by plasma means, as opposed to wet chemical treatments which have formed the subject of other studies.[162,163] Further development work would be needed to substantiate this supposition.

CHAPTER THREE

THE SURFACE TREATMENT OF POLYVINYL ALCOHOL WITH TRIFLUOROACETIC ANHYDRIDE AS STUDIED BY ESCA

CHAPTER THREE

THE SURFACE TREATMENT OF POLYVINYL ALCOHOL WITH TRIFLUOROACETIC ANHYDRIDE AS STUDIED BY ESCA

3.1 Introduction

The previous chapter has highlighted the important role of the surface properties of materials in their potential usage, special attention being paid to organic polymers. It has been shown that a wide variety of surface treatments, both wet chemical [129-31] and those occurring at gas-solid interfaces, [126, 132-136, 168] may be used to modify the wettability, printing and laminating characteristics of a polymer without affecting the bulk properties of the solid. Grafting processes are of prime importance in the textile manufacture and finishing industries [137] thereby reducing static charging, [138] shrinkage and biological attack. [139]

The philosophy of current research is towards ascertaining functional group distribution analyses of these surfaces for correlation with properties of interest. This it is hoped will lead to the development of surfaces tailored to specific needs. [162, 163] ESCA has an important part to play in this area.

Quantitative ESCA analysis of specific surface functional groups is often hindered by the proximity of photoemission signals arising from atoms of the same element in differing chemical environments. The single most important example of this concerns functional groups arising during oxidation.† Although the C_{1s}/O_{1s}

† Many organic nitrogen species are overlapping, including amide, amine and nitrogen in certain heterocyclic structures, [141] Carbon-carbon unsaturation, as well as phenyl groups, are difficult to distinguish from saturated species, although shake-up structure may be used as a distinguishing feature [38, 142, 143].

intensity ratio provides an overall indication of oxidative functionality, and analysis of C_{1s} line shapes provides direct information on broad structural types, viz. $\underline{C}$-O, >$\underline{C}$=O, -$\underline{C}\lesssim^{O}_{O}$ etc., ambiguities often remain.[58,59,140] Thus signals arising from carbon singly bonded to oxygen can originate from a variety of structural features including peroxides, esters, carbonates, in addition to simple ethers or alcohols. Although the C_{1s} binding energies potentially contain considerable information regarding the nature of the oxidised surface species, the limited resolution and small range of binding energies (typically 532-534eV) preclude the extraction of this information by a unique deconvolution of the O_{1s} envelopes.[58]

In an attempt to overcome this problem, chemical derivatisation techniques have been developed which are not only specific but also enable a degree of signal enhancement to be accomplished. These methods utilise reagents which will react specifically with the chemical functionality in question to produce a new functional group, more readily detectable under the ESCA analysis. Table 3.1 lists methods previously employed in polymer surface derivatisation ESCA studies.

From the recent appraisals to have appeared in the literature,[141,154,155] it is clear that the use of chemical 'tagging' or 'labelling' procedures in the quantification of surface functionalities is fraught with difficulty. Specificity, extent of reaction, stability of tag and mobility of group must be evaluated. Many of the derivatisation techniques employ wet chemical conditions where solvent effects may become important: in gaseous or vapour phase conditions diffusion of unreacted reagent cannot be ignored.

Table 3.1 ESCA studies using Polymer Surface Derivatisation [141]

Substrate	Reaction	
Na treated PTFE	$\succ C = C \prec \xrightarrow{Br_2} -\overset{Br}{\underset{|}{C}} - \overset{Br}{\underset{|}{C}}-$	Riggs and Dwight [131, 144]
Bovine Albumin	$(P)-NH_2 \xrightarrow{Et\text{-}S\text{-}C(O)\text{-}CF_3} (P)-\overset{H}{N}-\overset{O}{\overset{\|}{C}}-CF_3$	Millard and Masri [145]
Plasma initiated Polyacrylic acid grafts on polypropylene	$-CO_2H \xrightarrow[H_2O]{Ba\,C\ell_2} -CO_2^- \; Ba^{2+}$ (2)	Bradley and Czuha [146, 147]
Melting PE on Aℓ	$\succ C = C \prec \xrightarrow{Br_2} -\overset{Br}{\underset{|}{C}} - \overset{Br}{\underset{|}{C}}-$	Briggs *et al.* [148]
Methyl methacrylate + hydroxypropyl methacrylate copolymer	$\overset{OH}{\underset{|}{-CH_2}} \xrightarrow{(CF_3CO)_2O} \overset{O-C(=O)-CF_3}{\underset{|}{-CH_2}}$	Hammond *et al.* [149]
Epoxy/ester primer	$-CO_2^- Na^+ \xrightarrow{Ag\,NO_3} -CO_2^- Ag^+$	" [150]

Continued overleaf

Table 3.1 ESCA studies using Polymer Surface Derivatisation [141] (continued)

Substrate	Reaction		
Corona treated PE	$>C=C<$	$\xrightarrow{Br_2}$ $-\overset{Br}{\overset{|}{C}}-\overset{Br}{\overset{|}{C}}-$	Spell and Christenson [151]
" LDPE	$-CO_2H$	$\xrightarrow{NaOH}$ $-CO_2^- Na^+$	Briggs and Kendal [152]
	$-CH_2-\overset{O}{\overset{\|\|}{C}}-$	$\xrightarrow{Br_2}$ $-\overset{Br}{\overset{|}{C}}-\overset{O}{\overset{\|\|}{C}}-$ (Br)	"
	$>C=O$	$\xrightarrow{C_6F_5-NH-NH_2}$ $>C=N-NH-C_6F_5$	"
	(P)$-CO_2H$	$\xrightarrow{T\ell OEt}$ (P)$-CO_2T\ell$	Batich and Wendt [141]
Photooxidised Bisphenol-A Polycarbonate	$-CH_2-O-OH$	$\xrightarrow{SO_2}$ $-CH_2-O-SO_3H$	Munro [153]

A reaction of considerable current interest is the trifluoroacetylation of hydroxyl groups which has been proposed by Hammond *et al.* [149] as a potential method of chemical tagging for quantification of such functional groups on polymer surfaces.

Everhart and Reilly [154] have applied the use of trifluoroacetic anhydride (TFAA) as a means of labelling hydroxyl groups introduced onto the surface of low density polyethylene film on exposure to radiofrequency inductively coupled N_2 and Ar plasmas. Their method involved a solution phase reaction in benzene followed by soxhlet extraction in ethyl ether. Trifluoroacetylation was found to occur between TFAA and amine, epoxide and carboxylate functionalities as well as alcohol groups.

The advantages of using TFAA as an ESCA tag are threefold:

1) The introduction of fluorine may be easily detected by monitoring the F_{1s} core level signal (the F_{1s} photoionisation peak is of high cross section (Section 1.6)).
2) Three fluorine atoms are introduced for each functionality labelled.
3) The signal arising from the trifluoromethyl carbon atom ($\underline{C}F_3$) is shifted $\sim$ 8eV to the high binding energy side of the hydrocarbon peak, occurring at 285eV binding energy, and therefore may be distinguished with ease. The ability to monitor the extent of reaction using data from one core level, rather than using relative intensity ratios of two core levels, such as C_{1s}/F_{1s}, eliminates the possible effects of differing sampling depths for the core levels concerned. (This point is illustrated in the results and discussion section of this chapter (Section 3.3)).

A recent study by Dickie *et al.* [156] has involved the surface derivatisation of a series of hydroxyl functional acrylic copolymers by means of trifluoroacetic anhydride vapour. Angle-dependent ESCA studies of samples, which had undergone complete reaction with TFAA, were interpreted using single and multiple overlayer models.

Here is reported the reaction of TFAA vapour with polyvinyl alcohol as monitored by ESCA, the emphasis being placed on following the extent of reaction as a function of time of exposure of the polymer to TFAA vapour. Non-destructive depth profiling is accomplished using $Mg_{K\alpha_{1,2}}$ and $Ti_{K\alpha_{1,2}}$ radiation.

3.2 Experimental

3.2.1 Sample Preparation and Treatment

Polyvinyl alcohol (Cellomer Associates, Webster, NY, USA) in granular form was mounted onto a stainless steel probe tip (dimensions 19 x 7mm sample area) by means of double sided adhesive 'Scotch' insulating tape prior to exposure to TFAA vapour.

The probe tip was then positioned at the bottom of a 'pyrex' glass tube fitted with greaseless taps and connected to a similar 'pyrex' glass tube containing degassed TFAA under its own vapour pressure, sealed by means of a greaseless tap. (The TFAA was prepared by dehydration of trifluoroacetic acid with phosphorous pentoxide). The free volume of this apparatus (~ 150cm^3) was evacuated using a rotary pump to a pressure of < 0.1 torr as monitored by a Pirani vacuum gauge. The reaction vessel was then isolated from the pump and the system was let up to TFAA vapour for reaction to occur. After reaction, the reservoir of TFAA liquid was isolated and the reaction vessel evacuated to a pressure > 0.1 torr to remove unreacted

TFAA vapour. The sample was then removed and mounted on a spectrometer probe for ESCA analysis.

The reactions were carried out at ambient temperature ($16^{o}C$).

3.2.2 ESCA Instrumentation

All spectra were recorded on a custom-designed Kratos ES300 spectrometer, equipped with a magnesium/titanium dual anode. The chosen operating conditions were 12kV, 8mA for the magnesium anode, and 13.5kV, 18mA for the titanium anode. Under the experimental conditions employed for the magnesium anode, the $Au_{4f_{7/2}}$ level (at 84eV binding energy), used for calibration purposes, had a full width at half maximum height (FWHM) of 1.1eV. The base pressure of the spectrometer ($\sim 10^{-9}$ torr) was achieved by means of a 450 ℓs^{-1} electrically driven turbomolecular pump. Measurement of the core level spectra took in the order of 15 minutes to complete using the magnesium anode, followed by $\sim$ 40 minutes under titanium radiation. The spectra were recorded in analogue fashion. Deconvolution and area ratios were determined to an accuracy of $\sim$ 5% using a Dupont 310 analogue curve resolver. [1]

3.3 Results and Discussion

3.3.1 $Mg_{K\alpha_{1,2}}$ x-ray source

The concept of the electron mean free path and sampling depth in the ESCA experiment has been introduced in Section 1.6. Extensive studies by Clark and coworkers [83,84,157,158] have investigated the magnitude of electron mean free paths as a function

of kinetic energy for a variety of polymeric systems. For linear polymer systems, under $Mg_{K\alpha_{1,2}}$ radiation, typical mean free paths corresponding to photoemission from F_{1s}, O_{1s} and C_{1s} core levels with kinetic energies of ∿ 560eV, ∿ 720eV and ∿ 969eV are ∿ 9Å, ∿ 10Å and ∿ 15Å, giving effective sampling depths of ∿ 27Å, ∿ 30Å and ∿ 45Å respectively.

The $Mg_{K\alpha_{1,2}}$ excited C_{1s}, F_{1s} and O_{1s} core level spectra for PVA samples exposed to the room temperature equilibrium partial pressure of TFAA for varying lengths of time are shown in Figure 3.1. Numerical data is given in Table 3.2. The C_{1s} spectra are quite striking and it is clear that after 15 minutes there is a remarkable correspondence of the overall line profile with that of Siegbahn's oft quoted ethyl trifluoroacetate spectra (Figure 1.8).[159] The fully trifluoroacetylated PVA is seen to produce a direct polymer analogue for this model system. It is also clear from the spectra that the F_{1s} levels increase rapidly in intensity reaching a constant value at an early stage in the exposure. This reflects the somewhat shorter sampling depth of the F_{1s} photoemission process as opposed to that for the C_{1s} core level.

The relative intensities of the components of the C_{1s} photoionisation envelope as a function of exposure time are presented in Figure 3.2 and Table 3.2. The $\underline{C}F_3$ and $\underline{C}(=O)O$ functionalities increase as a proportion of the overall line profile as the reaction proceeds, whilst the low binding energy components, $\underline{C}H_2$ and $\underline{C}$ - O show a proportionate decrease throughout the reaction.

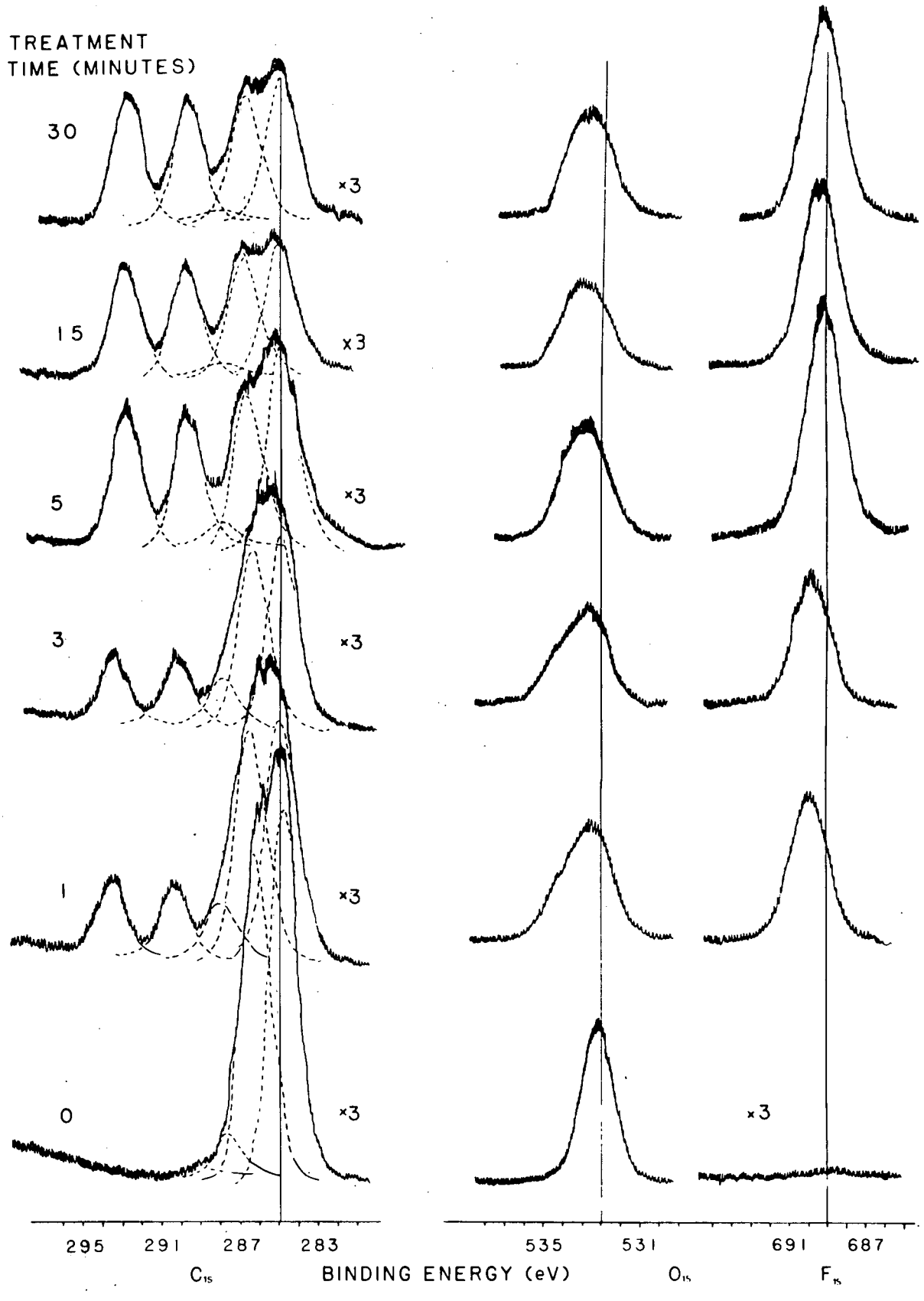

Figure 3.1 $Mg_{k\alpha_{1,2}}$ excited C_{1s}, F_{1s} and O_{1s} core level spectra for polyvinyl alcohol exposed to TFAA for varying lengths of time.

Table 3.2 TFAA treatment of polyvinyl alcohol.

Relative intensities of core electron signals, magnesium anode; figures in brackets indicate binding energies (eV).

Treatment time (mins)	Total C_{1s}	C - H	C - O	>C = O	O ‖ C - O	CF_3	O_{1s}	F_{1s}
0	100	49.5	(286.5) 44.1	(287.7) 5.4	(289.1) 1.0	-	(533.1) 71.3	-
1	100	35.3	(286.5) 34.3	(288.0) 8.1	(290.4) 11.3	(293.5) 11.0	(533.7) 89.0	(689.9) 77.4
3	100	35.1	(286.5) 32.6	(288.0) 8.1	(290.3) 12.3	(293.5) 11.9	(533.8) 92.6	(689.8) 83.2
5	100	29.8	(286.7) 22.6	(288.1) 3.6	(289.7) 20.3	(292.9) 20.8	(534.0) 76.8	(689.3) 125.0
15	100	27.9	(286.8) 24.0	(288.2) 1.7	(289.8) 22.9	(292.8) 23.5	(534.1) 83.8	(689.4) 134.1
30	100	26.9	(256.7) 23.1	(288.0) 2.2	(289.6) 23.1	(292.7) 24.7	(533.9) 88.7	(689.2) 146.8

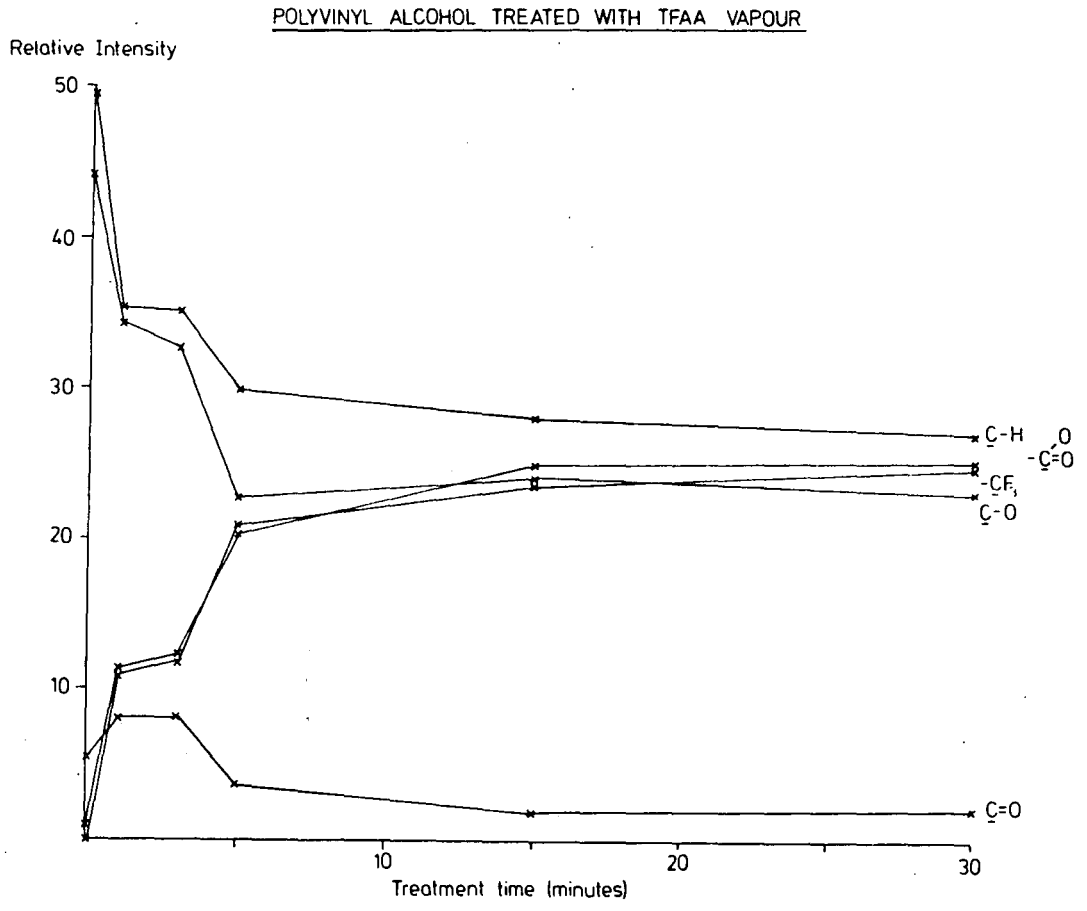

Figure 3.2 Intensities of the individual C_{1s} component peaks (expressed as a % of total C_{1s} band intensity) plotted against treatment time.

It is interesting to note that interaction of trifluoroacetic acid vapour with PVA leads to pronounced swelling of the polymer granules and considerably less extensive trifluoroacetylation is found to occur after an exposure time of one minute than is the case for the anhydride. Line shape analysis reveals that the trifluromethyl peak

amounts to 4.5% of the total C_{1s} envelope for PVA exposed to trifluoroacetic acid vapour for one minute, in contrast to the corresponding value of 11% for treatment with the anhydride. In terms of the degree of labelling of the available hydroxyl functionalities the respective values are 10% and 28%.†

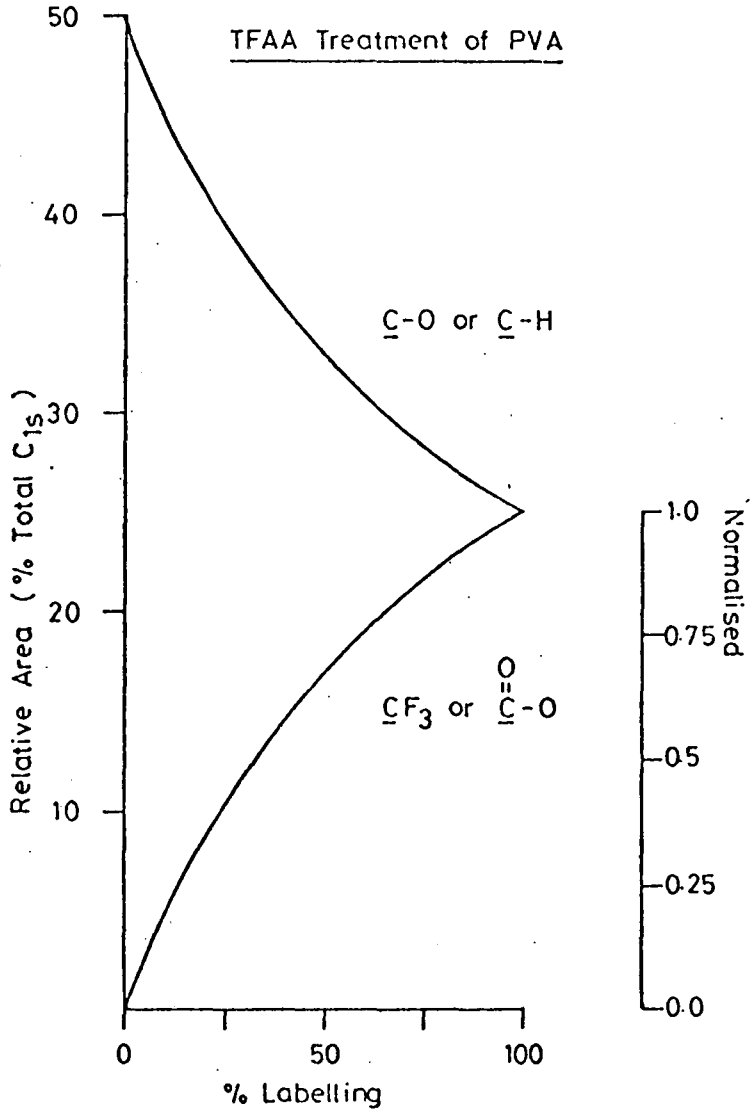

Figure 3.3 Reaction of TFAA with PVA. Variation of contribution to C_{1s} envelope of the individual C_{1s} component peaks with percentage labelling (as calculated).

† Non-linear relationships exist between the relative intensities of the C_{1s} component peaks and the percentage labelling of the polymer. This is also the case for F_{1s}/O_{1s} core level intensity data. Conversion graphs are provided in Figures 3.3 and 3.4.

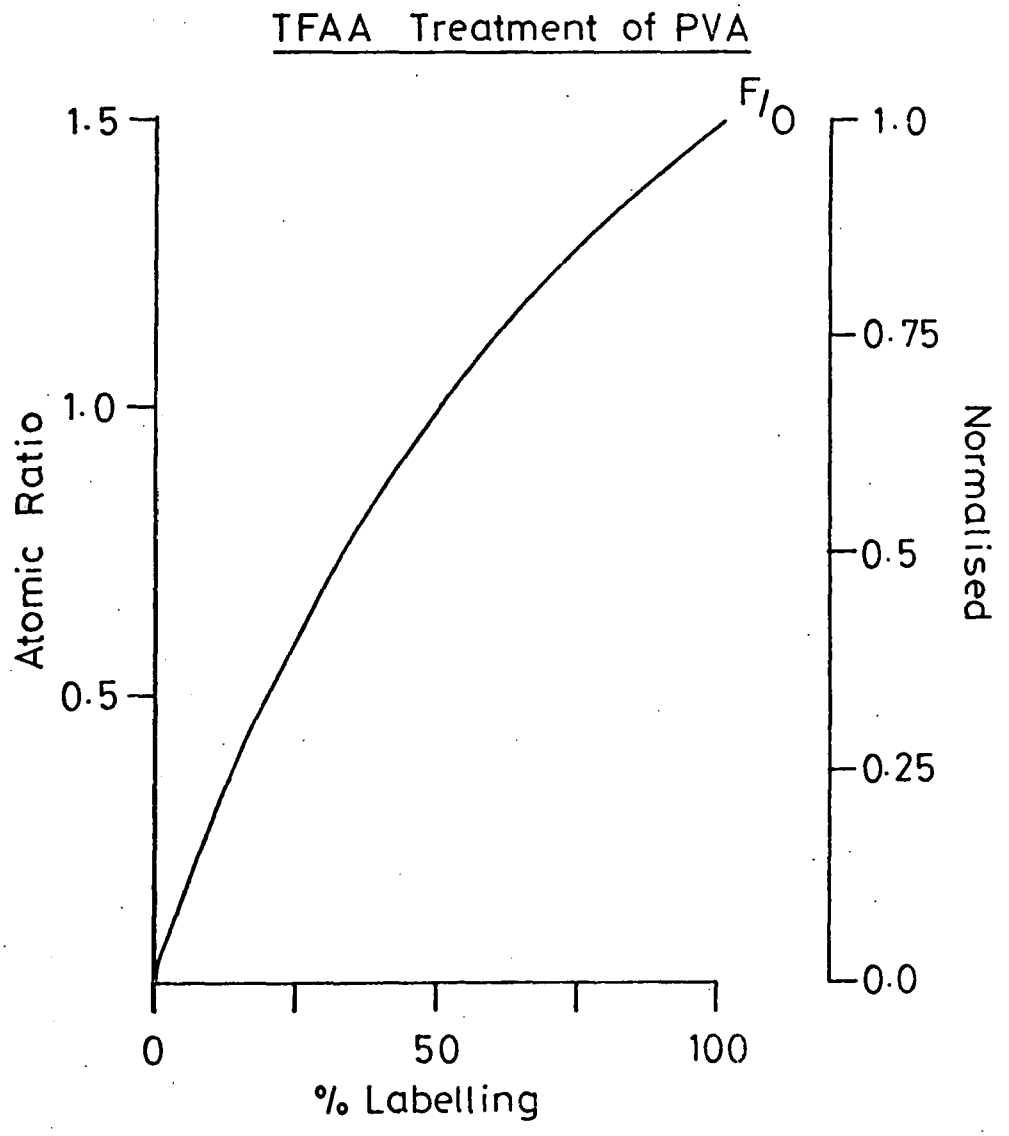

Figure 3.4 Reaction of TFAA with PVA. F/O atomic ratio calculated for varying degree of percentage labelling.

The close correspondence of sampling depth for the F_{1s} and O_{1s} levels provides a convenient means of monitoring the extent of reaction. Figure 3.5 shows how the F_{1s}/O_{1s} ratio changes as a function of exposure time at a sampling depth of $\sim$ 27 - 30 Å appropriate to the core level spectra excited with $Mg_{K\alpha_{1,2}}$ radiation. Comparison

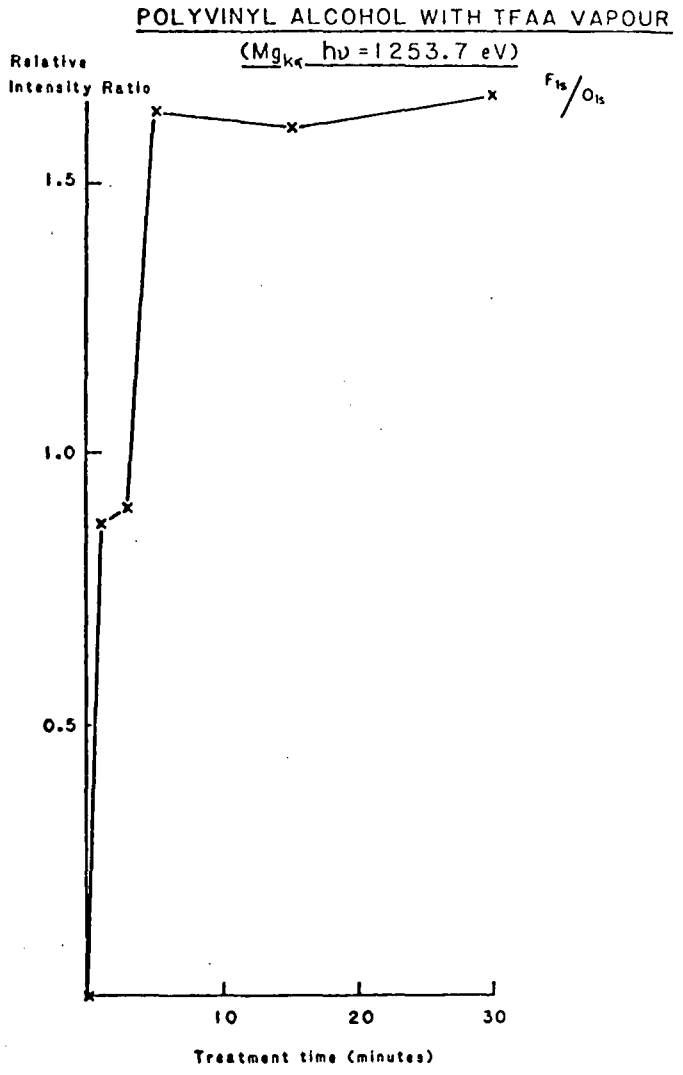

Figure 3.5 The F_{1s}/O_{1s} ratio for $Mg_{K\alpha_{1,2}}$ excited spectra of PVA treated with TFAA for varying lengths of time.

of the data presented in Figures 3.5 and 3.6, which presents the corresponding $\underline{C}F_3/\underline{C}$ - O data demonstrates the depth profiling capabilities of the ESCA experiment. The F_{1s}/O_{1s} data reveal a somewhat more extensive reaction within the initial five minutes of exposure than is found on examination of the corresponding changes

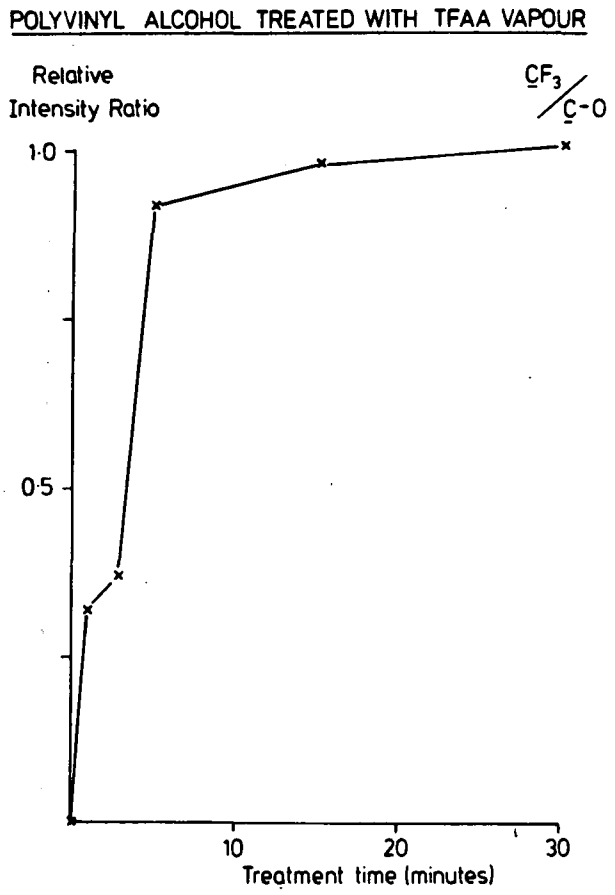

Figure 3.6 The $\underline{CF_3}/\underline{C}$ - O ratio for $Mg_{K\alpha_{1,2}}$ excited spectra of PVA treated with TFAA for varying lengths of time.

in the C_{1s} envelope profile (Figures 3.2 and 3.6). This is entirely reasonable in view of the slightly longer mean free path for photoemission from the C_{1s} core level, compared with those of O_{1s} and F_{1s} photoelectrons.

The phenomenon of sample charging encountered during the ESCA examination of thick insulating samples has been shown to be

a potential source of information in its own right.[123] The charging behaviour of a polymer sample is dependent on the surface composition of the material. It has been demonstrated for the case of the surface modification of an ethylene-tetrafluoroethylene copolymer by means of radio frequency plasmas excited in inert gases that the reaction, which results in a loss of fluorine in the surface regions, may be monitored by sample charging measurements. As reaction proceeds the degree of sample charging decreases and approaches that for a solely hydrocarbon based polymer. The interaction of TFAA vapour with PVA yields a progressive increase in surface fluorination. It would be expected that the uptake of fluorine would lead to an increase in sample charging for the fluorinated surface compared with the degree of charging for untreated PVA. This is indeed found to be the case as is shown in Figure 3.7.

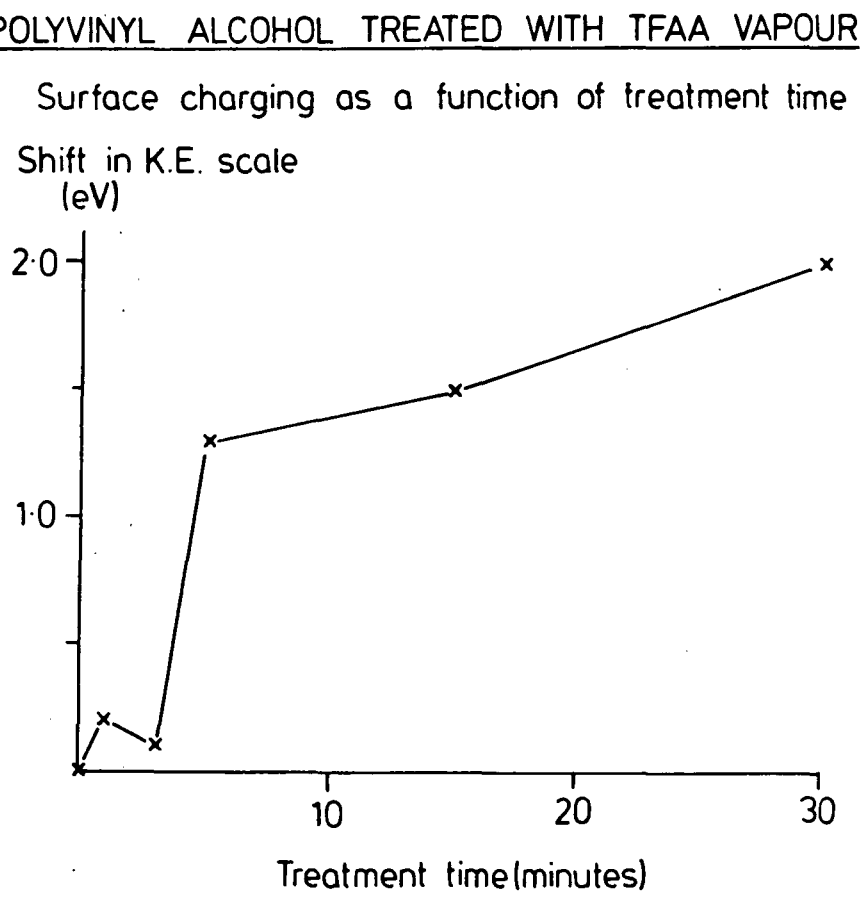

Figure 3.7 The change in surface charging, relative to untreated PVA, plotted against exposure time to TFAA.

3.3.2 $Ti_{K\alpha_{1,2}}$ x-ray source

The use of the harder $Ti_{K\alpha_{1,2}}$ x-ray source for which the photon energy is 4510eV has been of particular value for the straightforward interrogation of the vertical homogeneity of those samples, such as granules, powders and fibres, for which angular dependent

studies are not feasible. The sampling depth for C_{1s} levels photoemitted with $Ti_{K\alpha_{1,2}}$ radiation is in the order of 130Å, [160] thus providing a convenient intermediate depth sampling scale between the ESCA experiment employing $Mg_{K\alpha_{1,2}}$ radiation and multiple attenuated total internal reflectance IR spectroscopy.

The $Ti_{K\alpha_{1,2}}$ excited core level spectra which follow the reaction of TFAA vapour with PVA granules as a function of exposure time are shown in Figure 3.8 and the relative intensity C_{1s}, O_{1s} and F_{1s} data are tabulated in Table 3.3. The F_{1s}/O_{1s} intensity ratios are presented in graphical form in Figure 3.9.

Table 3.3 TFAA treatment of polyvinyl alcohol. Relative intensities of core electron signals, titanium anode.

Treatment time (mins.)	C_{1s}	O_{1s}	F_{1s}
0	100	130.2	0
1	100	133.3	66.7
3	100	140.0	75.0
5	100	142.9	208.6
15	100	115.8	292.1
30	100	113.5	270.3

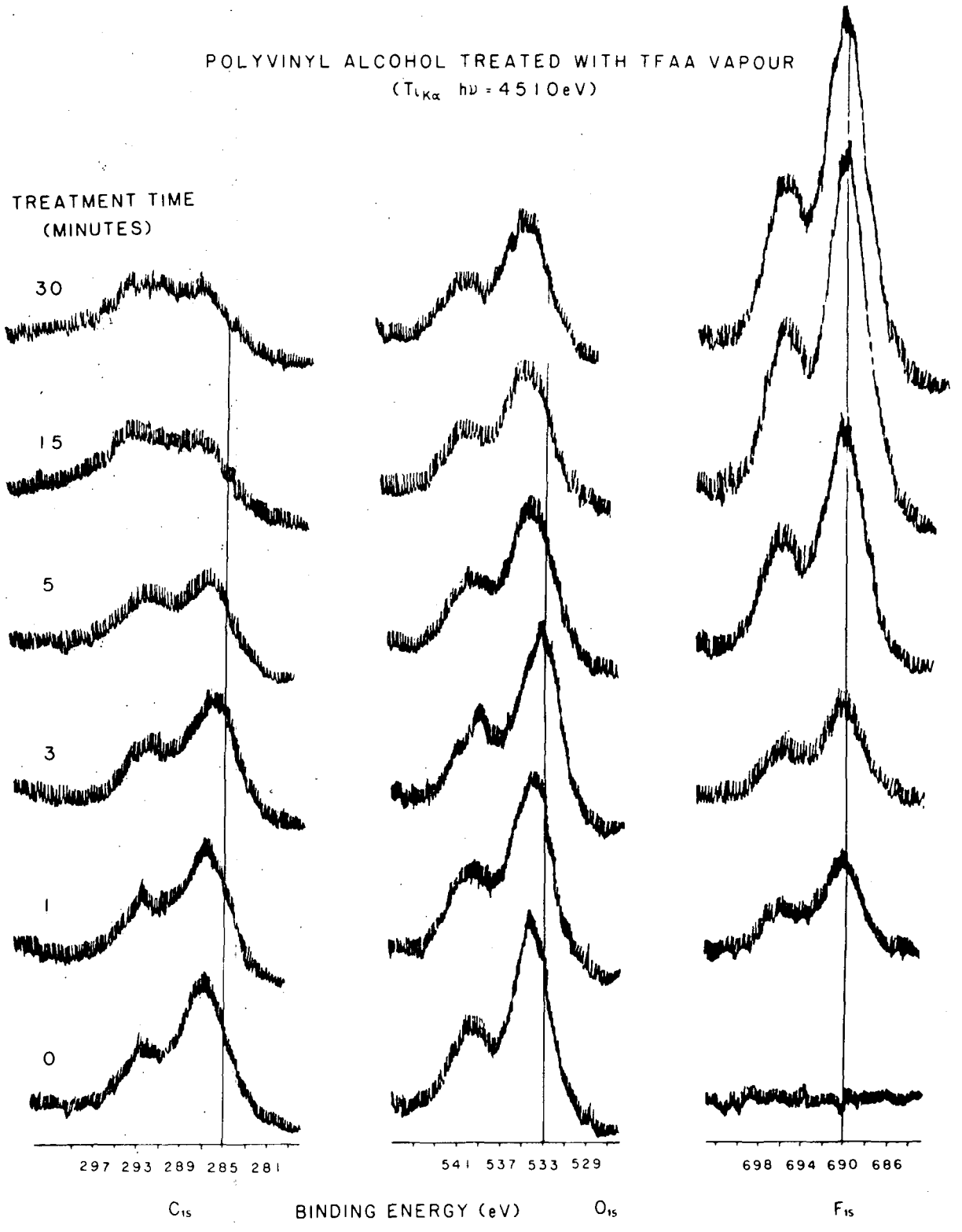

Figure 3.8 $Ti_{K\alpha_{1,2}}$ excited C_{1s}, F_{1s} and O_{1s} core level spectra for polyvinyl alcohol exposed to TFAA for varying lengths of time.

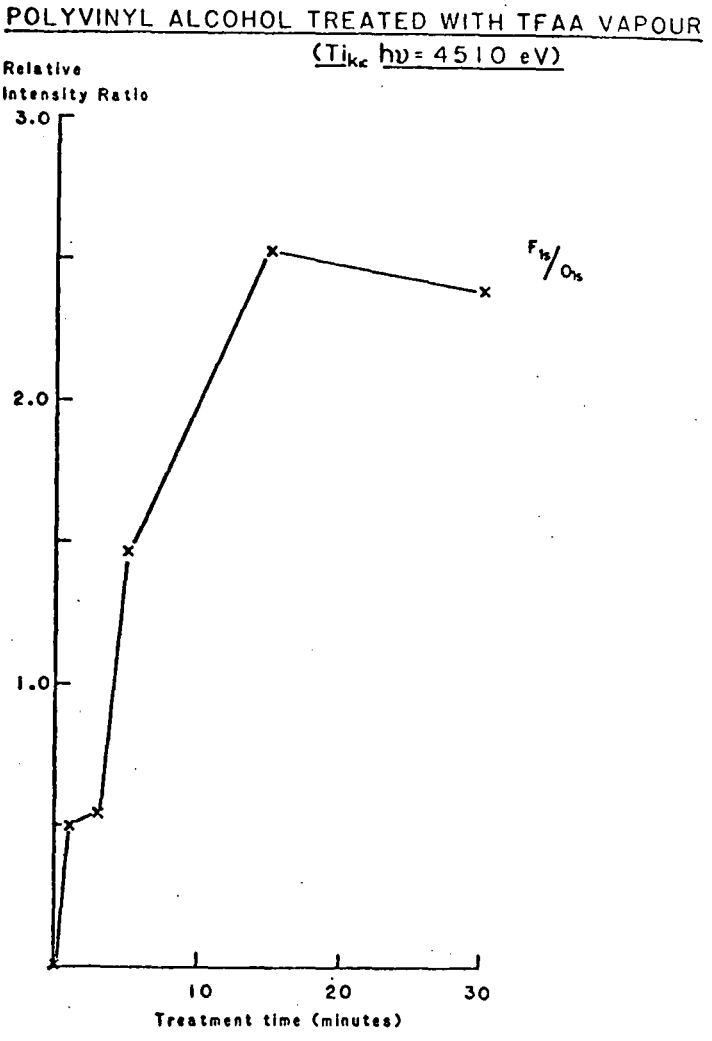

Figure 3.9 The F_{1s}/O_{1s} ratio for $Ti_{K\alpha_{1,2}}$ excited spectra for PVA treated with TFAA for varying lengths of time.

Deconvolution has not been performed on the core level envelopes since for the C_{1s} envelope this would involve at least eight component peaks. Nonetheless it is clear that substantial changes occur in the overall shape of the C_{1s} envelope, components to higher binding energy of the C - H and C - O peaks of the starting material.

The broadening of the O_{1s} core level signal as treatment time increases is a direct result of the incorporation of the trifluoroacetyl label, $CF_3 C\overset{O}{\underset{O-}{<}}$.

After one minute's treatment a substantial F_{1s} photoionisation signal is present in the ESCA spectrum. This peak grows in intensity as a function of increasing treatment time at a more gradual rate than was found for the $Mg_{K\alpha_{1,2}}$ excited spectra. This illustrates the diffusion controlled nature of the reaction at the $Ti_{K\alpha_{1,2}}$ sampling depth. Comparison of the changes in F_{1s}/O_{1s} intensity ratios as a function of treatment time for the $Mg_{K\alpha}$ and $Ti_{K\alpha}$ excited spectra (Figures 3.2 and 3.9) show that the equilibrium substitution in the former case is established to a sampling depth of $\sim 45\text{Å}$ in some 5 minutes whilst for the deeper sampling $Ti_{K\alpha}$ source the equilibrium is established to a depth of $\sim 130\text{Å}$ after $\sim$ 12.5 minutes.

3.4 A model for the reaction

As mentioned in Section 1.6.1, comparison of experimentally observed ESCA data with computed intensity ratios, derived from models of surface structure, provides a useful basis for the interpretation of experimental results on a semiquantitative level. Such models take many forms and have tended to make use of the depth profiling capabilities of angular dependent ESCA data.[156,165,166]

To recap, the signal intensity for a core level in a modified surface layer (A), of thickness d, which overlays an unmodified bulk (B), is given by

$$I^A = I^A_\infty \left(1 - e^{-d/\lambda \cos \theta}\right) \qquad (1.12a)$$

The corresponding signal for the bulk material is given by

$$I^B = I^B_\infty \quad e^{-d/\lambda \cos \theta} \qquad (1.12b)$$

More complex cases, encompassing multiple overlayers, partial coverage and vertically inhomogeneous situations have formed a subject for discussion by Dilks. [167]

Recently, Hutton [175] has developed an algorithm for modelling the variation in ESCA signal intensity as a reaction proceeds for a reaction involving the diffusion of a reactant into a substrate surface followed by reaction with the substrate matrix. This model has been tested for suitability as a means of simulating the ESCA data for the interaction of TFAA vapour with polyvinyl alcohol at the $Mg_{K\alpha}$ and $Ti_{K\alpha}$ sampling depths.

Full details of the algorithm are to be given elsewhere, [175] however an outline of the methodology is as follows. The algorithm assumes a concentration gradient of reacting species (x) with depth into substrate which remains constant with time. Due to this concentration gradient the extent of reaction at a given time will also vary with depth. The substrate surface is divided into a series of monolayers of thickness D. The algorithm then calculates the relative intensities of the various prespecified components of the ESCA spectrum over a given sampling depth as reaction proceeds, assuming a particular reaction pathway.

For the particular case of the interaction of TFAA with PVA (equation 3.1),

$$(CF_3CO)_2\,O + \left(CH(OH)-CH_2\right)_m \rightarrow \left(C(OOCCF_3)-CH_2\right)_m + CF_3CO_2H \qquad (3.1)$$

the extent of reaction, y, as measured by the fraction of reacted alcohol units in the polymer matrix for any one monolayer (i.e. the fraction of ester present), may be related to the rate of reaction, $\frac{dy}{dt}$, as follows,

$$\frac{dy}{dt} = k\,[TFAA]\;\;[PVA] \qquad (3.2)$$
$$= k\,[TFAA]\;\;(1 - y)$$

where k is the rate constant. The concentration of TFAA will depend on the concentration profile chosen for the model and the monolayer of substrate under consideration: it is assumed not to vary with time. In this particular case an exponential decrease of TFAA concentration with depth into the polymer substrate has been used. Hence

$$[TFAA] \quad \alpha \quad e^{-qh} \qquad (3.3)$$

where q is a constant and determines the 'sharpness' of [TFAA] decay, and h is the penetration depth into the polymer. The TFAA concentration over a given layer of polymer between depths d_1 and d_2 will be given by

$$\int_{d_1}^{d_2} e^{-qh}\,.dh = \left[-\frac{1}{q}\,e^{-qh}\right]_{d_1}^{d_2} \qquad (3.4)$$

The algorithm uses as its input for [TFAA] in equation 3.2 the [TFAA] value evaluated from equation 3.4 proportioned such that the concentration in the first monolayer is equal to unity.

Hence, rearranging equation 3.2 and integrating,

$$\int \frac{dy}{(1-y)} = \int k\;[TFAA]\;\;dt \qquad (3.5)$$

Recalling equation 1.7,

$$dI_i = F\,\alpha_i\,N_i\,k_i\,e^{-x/\lambda_i}.\,dx \qquad (1.7)$$

and rewriting the terms F, α_i and k_i as a single constant K, equation 1.7 becomes

$$dI_i = K\,N_i\,e^{-h/\lambda_i \cos\theta}.\,dh \qquad (3.6)$$

In this instance the interest lies in modelling the change in F_{1s}/O_{1s} ratio as the reaction proceeds at the ESCA sampling depths relevant for the $Mg_{K\alpha}$ and $Ti_{K\alpha}$ x-ray fluxes. The values of N_F and N_O for a given monolayer at time t may be expressed in terms of the extent of reaction as follows,

$$N_F^t = 3y_t \qquad (3.7)$$

$$N_o^t = (2 - y)_t \qquad (3.8)$$

The integrated form of equation 3.6 for the F_{1s} core level signal at time t is

$$I^t_{F_{1s}} = K_F \sum_{i=1}^{n} 3y_t \int_{h_i}^{h_i + D} e^{-h/\lambda F_{1s} \cos\theta}.dh \qquad (3.9)$$

Similarly for the O_{1s} core level signal at time t,

$$I^t_{O_{1s}} = K_O \sum_{i=1}^{n} (2-y)_t \int_{h_i}^{h_i + D} e^{-h/\lambda O_{1s} \cos\theta}.dh \qquad (3.10)$$

The values for the inelastic mean free paths for the F_{1s}, O_{1s} and C_{1s} core levels were taken as 9 Å, 10 Å and 15 Å respectively for the magnesium anode, and 35 Å, 37 Å and 40 Å respectively for the titanium anode. For each computer run 30 monolayers each of 5 Å thickness were considered. As stated

previously the model assumed an exponential decrease of TFAA concentration with depth. A series of runs were performed varying the depth into the surface at which the TFAA concentration dropped to 10% of surface value. In this way the magnitude of the constant q in equation 3.4 could be set, and hence the concentration profile with depth evaluated for each particular run. The progress of the reaction was monitored in terms of kt units of 'time'.

The algorithm,written in the Applesoft derivative of BASIC, was run on an Apple II Europlus computer.

It was the aim of this work to obtain a series of computer modelled plots of $Mg_{K\alpha}$ and $Ti_{K\alpha}$ F_{1s}/O_{1s} ratios versus time of reaction, normalized such that the ratio becomes equal to unity for complete trifluoroacetylation, for a range of TFAA concentration depth profiles. These plots were then compared with the experimentally observed results (Figures 3.2 and 3.9), which have been normalized and redrawn in Figure 3.10.

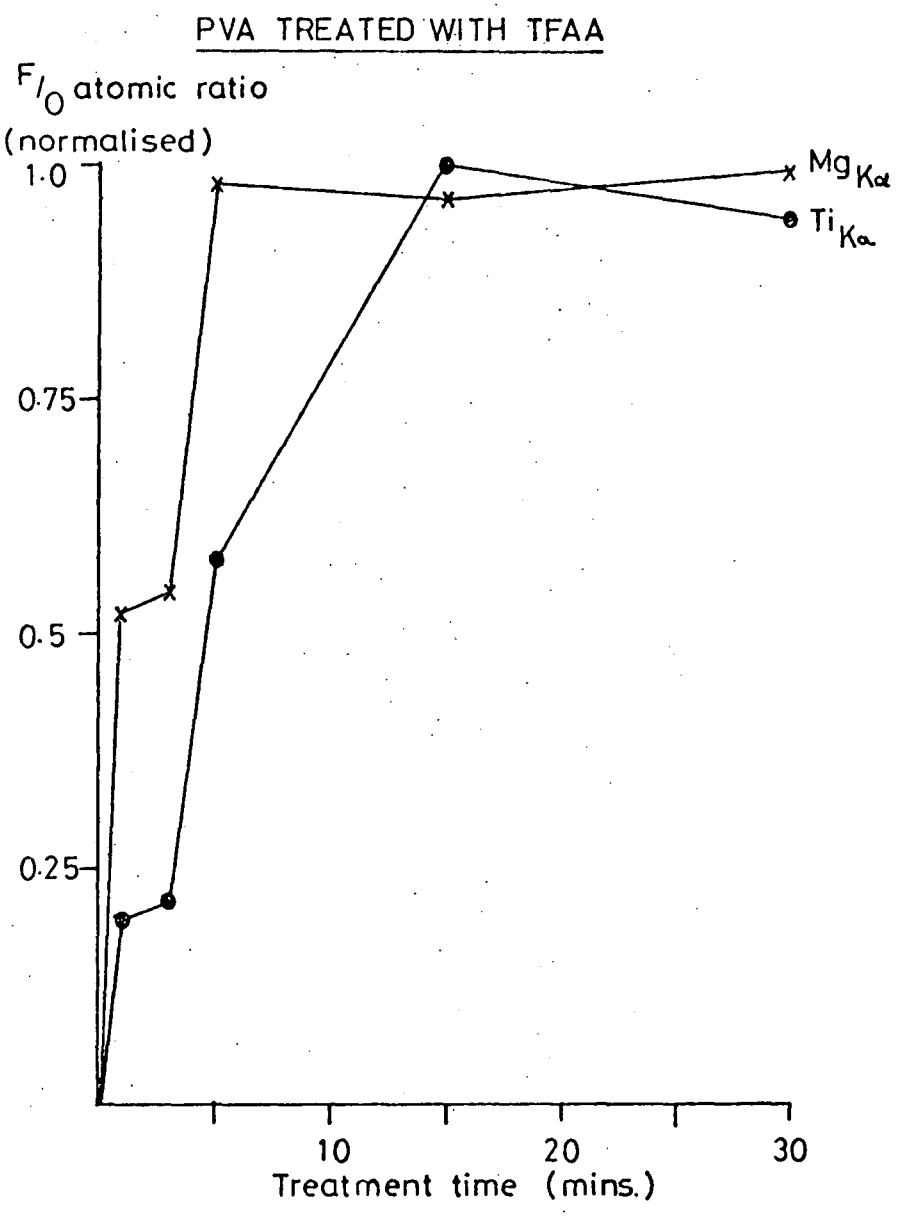

Figure 3.10 Normalized F_{1s}/O_{1s} ratios for $Mg_{K\alpha}$ and $Ti_{K\alpha}$ - excited spectra for PVA treated with TFAA for varying lengths of time.

Figure 3.11 shows the computer modelled plots based on exponential decays of TFAA concentration dropping to 10% of its surface value after 10 Å, 20 Å, 50 Å, 75Å and 100 Å. In each case the reaction proceeds at a faster rate at the $Mg_{K\alpha}$ sampling depth than is found for the more deeply probing $Ti_{K\alpha}$ analysis. For the situations where the TFAA concentration suffers a sharp fall off with depth, there is insufficient TFAA for trifluoroacetylation of all the available alcohol functionalities to occur. Consequently the $Ti_{K\alpha}$ F_{1s}/O_{1s} ratios approach asymptotically values less than that for total reaction. From comparison of the graph in Figure 3.10 with those in Figure 3.11, the experimental observations are most closely matched by a model which assumes an exponential drop in TFAA concentration to 10% of its surface value after $\sim$ 100 Å penetration. Under these conditions, the ratio of the initial gradients of F_{1s}/O_{1s} ratios with time for $Mg_{K\alpha}$ and $Ti_{K\alpha}$ sampling depths is found to be $\sim$ 2 - 3, and this compares favourably with the experimental figure of 2.5 (Section 3.3.2).

It must be borne in mind that the model assumes the reaction to take place at a uniform flat solid surface. The polyvinyl alcohol was used in granular form. Nonetheless, the ESCA sampling depth, coupled with the inherent nature of the technique to statistically sample the averaged composition of the material, is such that the model is still applicable. Here the model may be used to provide an upper estimate of the extent to which the reacting species (TFAA) penetrates the solid (PVA) surface.

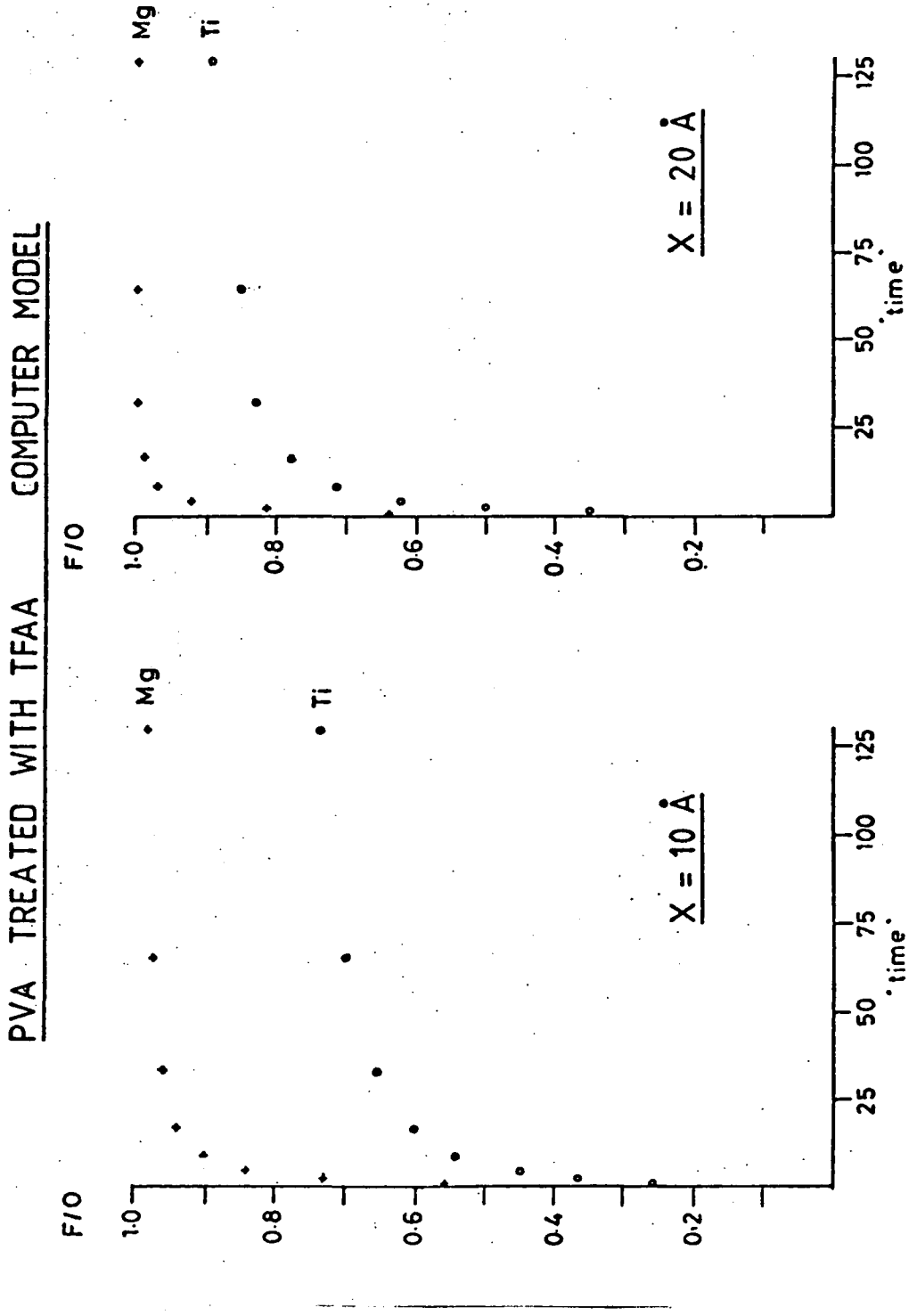

Figure 3.11 Computer modelled F_{1s}/O_{1s} ratios for $Mg_{K\alpha}$ and $Ti_{K\alpha}$ - sampling depths for the reaction between PVA and TFAA. Each plot is based on an exponential decay of [TFAA] dropping to 10% of its surface value after X Å.

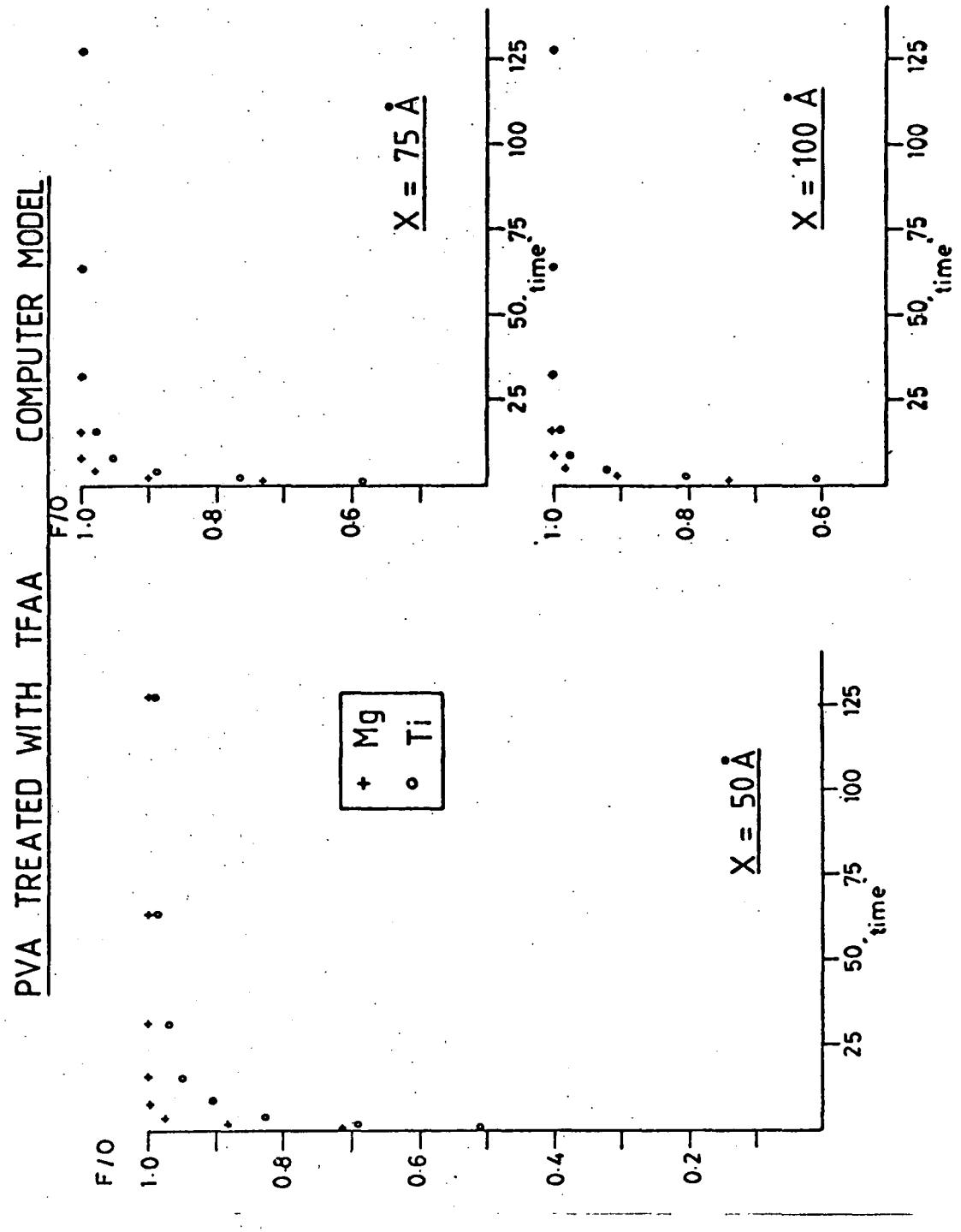

Figure 3.11 (continued)

3.5 Further applications of the TFAA labelling technique

The results presented in the previous discussion have shown that vapour phase trifluoroacetic anhydride may be used as a convenient ESCA tag for monitoring surface C-OH functionality in polyvinyl alcohol, complete reaction being achieved within 15 minutes' exposure. The investigation of the use of TFAA as a derivatisation reagent has been extended to include the following more complex systems:-

1) Cellulose fibres (to be discussed below (Section 3.6)).
2) High density polyethylene film exposed to an oxygen plasma.[321]
3) Oxidized polyacetylene film (Section 4.3).
4) Geochemical materials
   a) Gilsonite 'selects'[322]
   b) Coals of various ranks, before and after exposure to ultraviolet light (Section 5.3.7e).

3.6 The Reaction of Trifluoroacetic Anhydride with Cellulose fibres

3.6.1 Introduction

The reasons for interest in this system are twofold. First, the molecular structure of cellulose contains both primary and secondary hydroxyl groups which may well show different reactivities towards TFAA.[180] Second, there is considerable interest in Durham concerning the nitration of cellulose and the chemistry of cellulose nitrate, as studied for the most part by ESCA and nuclear magnetic resonance techniques.[160, 176-179] Of major concern is the extent of reaction in nitration and denitration processes, and the fate of the hydroxyl functionalities during these conversions.

The nitration of cellulose in the form of cotton linters is usually carried out in mixed acid.[176] On a commercial basis nitric - sulphuric mixes are most commonly employed, although nitric - phosphoric acid mixes may be conveniently used for laboratory scale nitration reactions where recovery expense and corrosion factors are not restrictive. Nitric acid - water mixes are not used since nitration is uneven and degradation and gelatinisation of the product arise at the high percentage nitric mixes required for reaction. The main point of interest in technical nitration in mixed acid is the question of the degree of substitution (D.O.S.) and how this relates to the acid mix composition. Although a theoretical maximum D.O.S. of 3 is feasible, in practice this is never attained and the maximum D.O.S. is $\sim$ 2.8. A definitive answer as to why this should be so has not thus far been given. It has been proposed by Stephenson,[176] who has reviewed the chemistry of cellulose and nitrocellulose at length, that the tagging and hence blocking of the hydroxyl groups by TFAA may help unravel some of the questions posed by researchers in this field. †

This work was therefore undertaken as a first step towards that goal. Would, for example, complete trifluoroacetylation of the cellulose take place as was found for the polyvinyl alcohol study, in contrast to the cellulose nitration reaction?

---

† The use of trifluoroacetyl residues as blocking groups in the syntheses of carbohydrates, steroids and polypeptides has been discussed by Tedder in his comprehensive review of the chemistry of trifluoroacetic anhydride.[181]

3.6.2 Experimental

3.6.2a Sample Preparation and Treatment

Two types of cellulose were used in this work, both of which were obtained from Drs F.S. Baker and T.J. Lewis (Ministry of Defence, PERME, Waltham Abbey). Commercially produced linters paper (cellulose type K300) of Shirley fluidity 8.8 and approximate degree of polymerisation 1100, vacuum dried and stored over phosphorous pentoxide was used for the time dependent study of the reaction of TFAA with cellulose. The depth dependence monitoring of the reaction employed cellulose fibres (type 1) which were pressed into discs using a standard Specac press before exposure to TFAA.

Each sample was mounted on a stainless steel probe tip by means of double sided adhesive tape. The samples were exposed to TFAA as described previously (Section 3.2.1) and their ESCA spectra were recorded immediately after exposure. Both ES 200B and ES 300 electron spectrometers were employed in this work, depth profiling being readily achieved utilising the $Mg_{K\alpha}/Ti_{K\alpha}$ dual anode facility of the ES 300 spectrometer. All spectra were recorded in analogue fashion.

3.6.3 Results and Discussion

3.6.3a Reaction of TFAA with cellulose as a function of exposure time

The C_{1s}, O_{1s} and F_{1s} core level spectra of cellulose K300 obtained using the ES 200B $Mg_{K\alpha_{1,2}}$ x-ray source (8kV, 14mA) for the untreated material and after TFAA treatment are displayed in Figure 3.12. The C_{1s} spectrum of the starting material may be

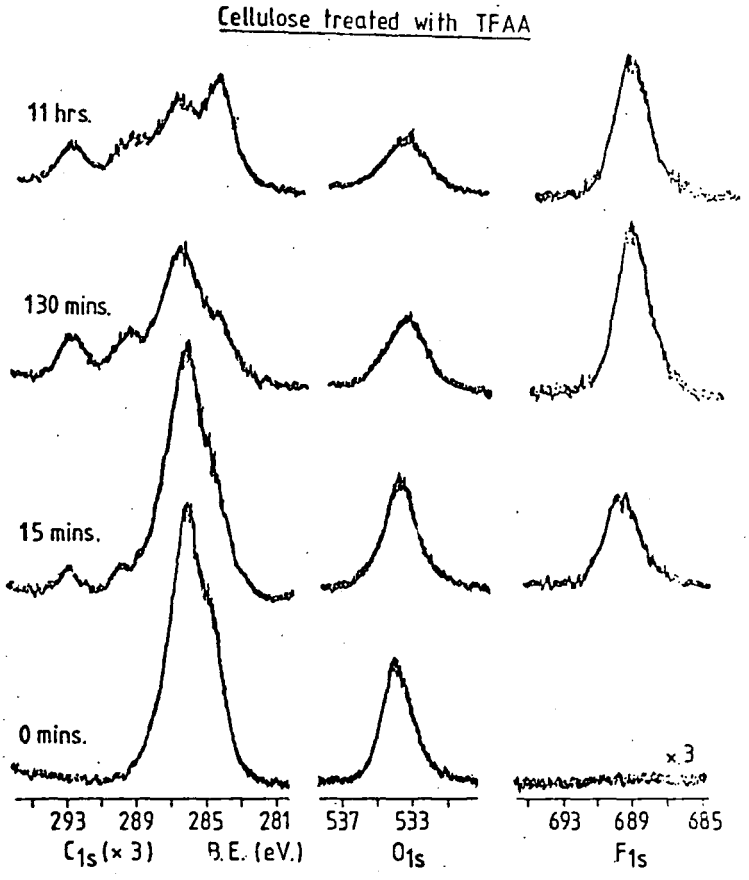

Figure 3.12 $Mg_{K\alpha}$ excited C_{1s}, O_{1s} and F_{1s} core level spectra core level spectra for cellulose linters exposed to TFAA for varying lengths of time.

deconvoluted to reveal three component peaks. The central component at ∿ 286.7eV binding energy arises from the carbon atoms singly bonded to one oxygen atom in cellulose. The carbon atom uniquely attached to two oxygens in the cyclic hemiacetal formulation of the β-D-glucopyranose ring is responsible for a component peak situated

to the higher binding energy side of the main C - O peak. The component at 285eV binding energy arises from extraneous hydrocarbon. In cellulose samples, irrespective of source or type (e.g. linters or staple fibres), the hydrocarbon signal observed is variable but inevitably present. ESCA investigations have shown that this contamination is confined to the very surface of the sample.[160] Consideration of the C_{1s}/O_{1s} intensity ratio, allowing for the C-H contaminant peak, indicates that the cellulose contains little residual water.

On exposure to TFAA vapour for 15 minutes there is clear evidence for trifluoroacetylation as shown by the appearance of a single F_{1s} photoionisation signal, accompanied by the development of CF_3 and $CF_3C(=O)O-$ ester in the C_{1s} envelope at 293.1eV and 290.1eV respectively. The extent of the trifluoroacetylation is considerably less than was found for polyvinyl alcohol after the same exposure time, and for this reason further reactions using extended exposure times (130 minutes and 11 hours) were performed (Figure 3.12). The relative areas of the C_{1s}, O_{1s} and F_{1s} peaks, corrected for hydrocarbon contamination, are tabulated in Table 3.4 and represented graphically in Figure 3.13.

Assessment of the extent of reaction, in terms of the number of hydroxyl groups reacted and the corresponding relative intensity for the trifluoromethyl carbon, reveals that a complete esterification of the available hydroxyl groups is not accomplished even after prolonged exposure time (Figure 3.13).

Table 3.4 TFAA treatment of Cellulose K300. Relative area intensities of core electron signals. Total C_{1s} area, corrected for hydrocarbon contamination, taken as 100 Units.

Exposure time	C_{1s}	O_{1s}	F_{1s}	$\underline{CF}_3$
Untreated	100	139.9	0	0
15 mins.	100	123.8	35.8	6.9
130 mins.	100	122.4	78.3	16.3
11 hours	100	100.0	75.0	15.0

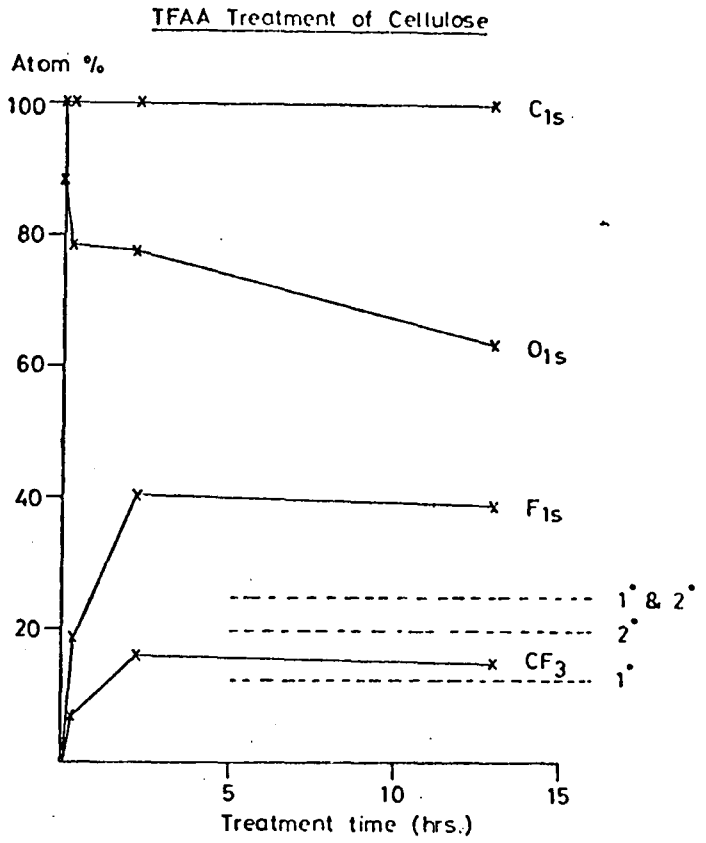

Figure 3.13 Relative surface concentrations (atom percent) of carbon, oxygen, fluorine and $\underline{CF}_3$ groups, corrected for hydrocarbon contamination, for cellulose linters plotted against exposure time to TFAA.

As was found to be the case for polyvinyl alcohol treated with TFAA (Section 3.3.1, Figure 3.7), there is an increase in the magnitude of sample charging on progressive fluorination of the cellulose material (Figure 3.14). It is not surprising that in this case the sample charging is lower, thereby reflecting the lower level of incorporated fluorine.

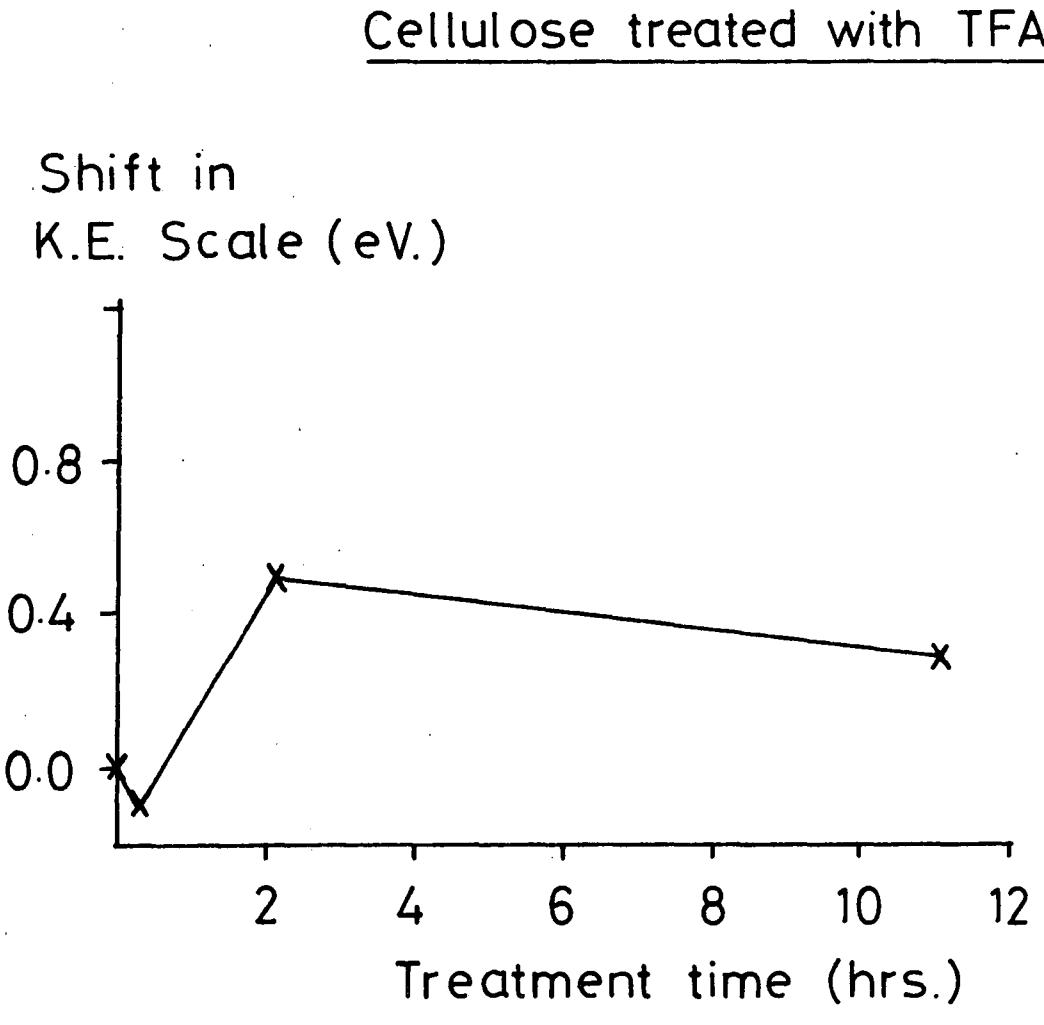

Figure 3.14 The change in surface charging, relative to untreated cellulose, plotted against exposure time to TFAA.

3.6.3b A preliminary depth profiling investigation employing $Ti_{K\alpha}$ x-radiation

In this experiment cellulose Type 1 fibres, pressed and mounted on a spectrometer probe, were exposed to TFAA vapour for 15 minutes. The C_{1s}, O_{1s} and F_{1s} core level spectra of the sample were run using both $Mg_{K\alpha_{1,2}}$ (12kV, 8mA) and $Ti_{K\alpha_{1,2}}$ (13.5kV, 18mA) x-ray sources of the ES300 electron spectrometer.

The relevant spectra are illustrated in Figures 3.15 and 3.16; Table 3.5 lists core level intensity data.

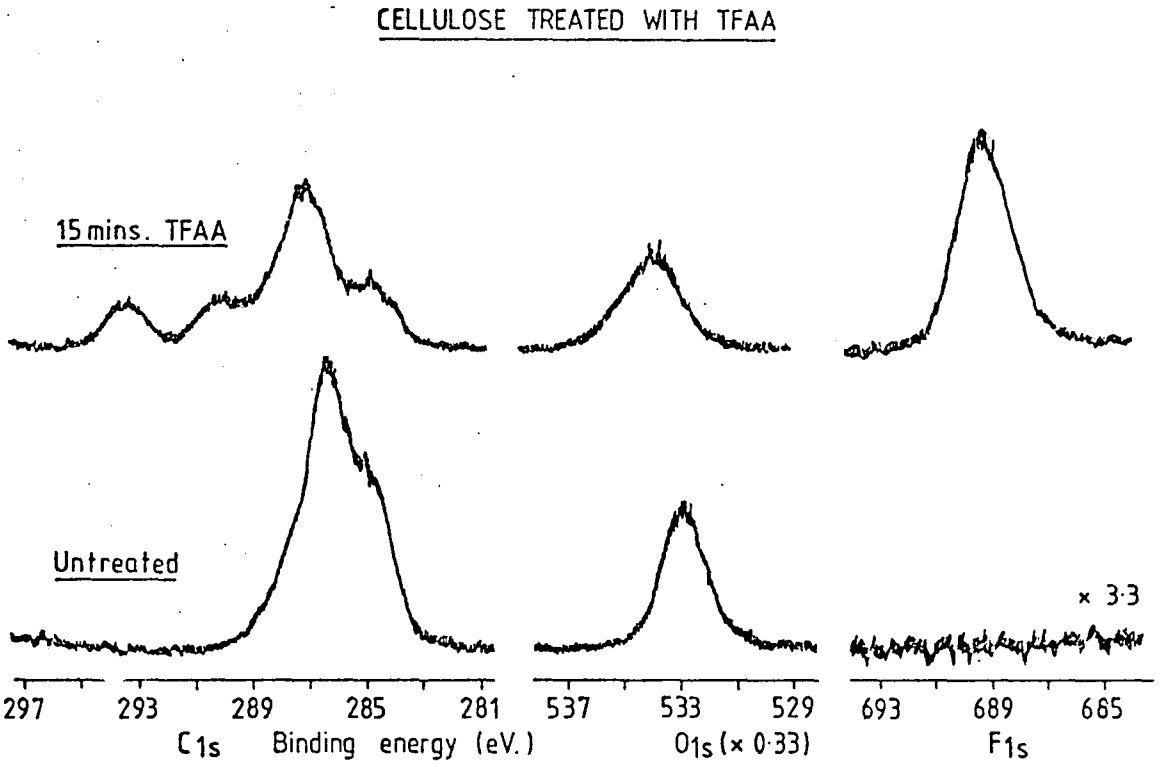

Figure 3.15 $Mg_{K\alpha}$ excited C_{1s}, O_{1s} and F_{1s} core level spectra for cellulose fibres before and after exposure to TFAA vapour for 15 minutes.

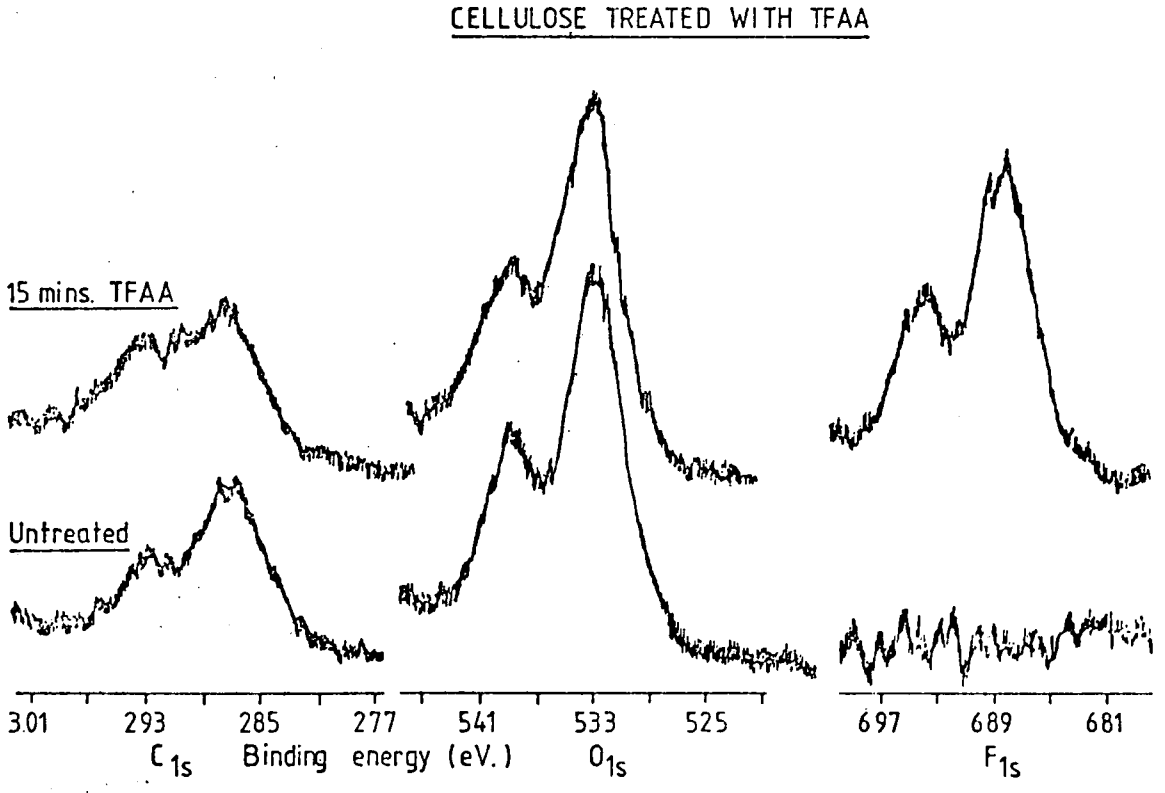

Figure 3.16 $Ti_{K\alpha}$ excited C_{1s}, O_{1s} and F_{1s} core level spectra for cellulose fibres before and after exposure to TFAA vapour for 15 minutes.

Immediately observable in the C_{1s} spectra recorded using the magnesium anode is the shoulder to the low binding energy side of the predominant C - O characteristic of surface hydrocarbon contamination.

Table 3.5 TFAA treatment of cellulose Type 1. Figures indicate atom percent of carbon, oxygen and fluorine detected using $Mg_{K\alpha}$ and $Ti_{K\alpha}$ x-ray sources.

		C_{1s}	O_{1s}	F_{1s}	$\underline{C}F_3$
Untreated	Mg*	100	85.7	0	0
	Ti	100	84.5	49.8	-
15 mins TFAA	Mg*	100	86.5	0	13.9
	Ti	100	66.4	36.9	-

* corrected for hydrocarbon contamination.

The C : O stoichiometry for the untreated cellulose obtained from the titanium anode spectrum shows no evidence for hydrocarbon contamination. This would support the opinion that the contamination is in the form of a surface overlayer.

After exposure to TFAA vapour for 15 minutes pronounced changes are found to occur. The introduction of fluorine into the sample is evidenced by the sharp F_{1s} core level signal and this feature is also seen at the $Ti_{K\alpha}$ sampling depth (Figure 3.16). The shape of the C_{1s} envelope undergoes drastic modification accommodating the trifluoroacetyl group. The functionalisation of this cellulose sample is appreciably more advanced than that for the material used previously (Section 3.6.3a), and may reflect differences in the morphology of the cellulose types.

The depth profiling capabilities of the ESCA experiment (Section 1.6) enable an approximation of the extent of reaction as a function of depth to be made. Figure 3.17 plots the relative

proportion of $\underline{C}F_3$ per 100 carbon atoms against penetration depth, using the $\underline{C}F_3$ and $F_{1s}(Mg_{K\alpha})$, and the F_{1s} $(Ti_{K\alpha})$, arising from the outermost ∿ 45 Å, ∿ 27 Å and ∿ 130 Å respectively. The concentration of CF_3 groups sampled over the outermost ∿ 130 Å corresponds to

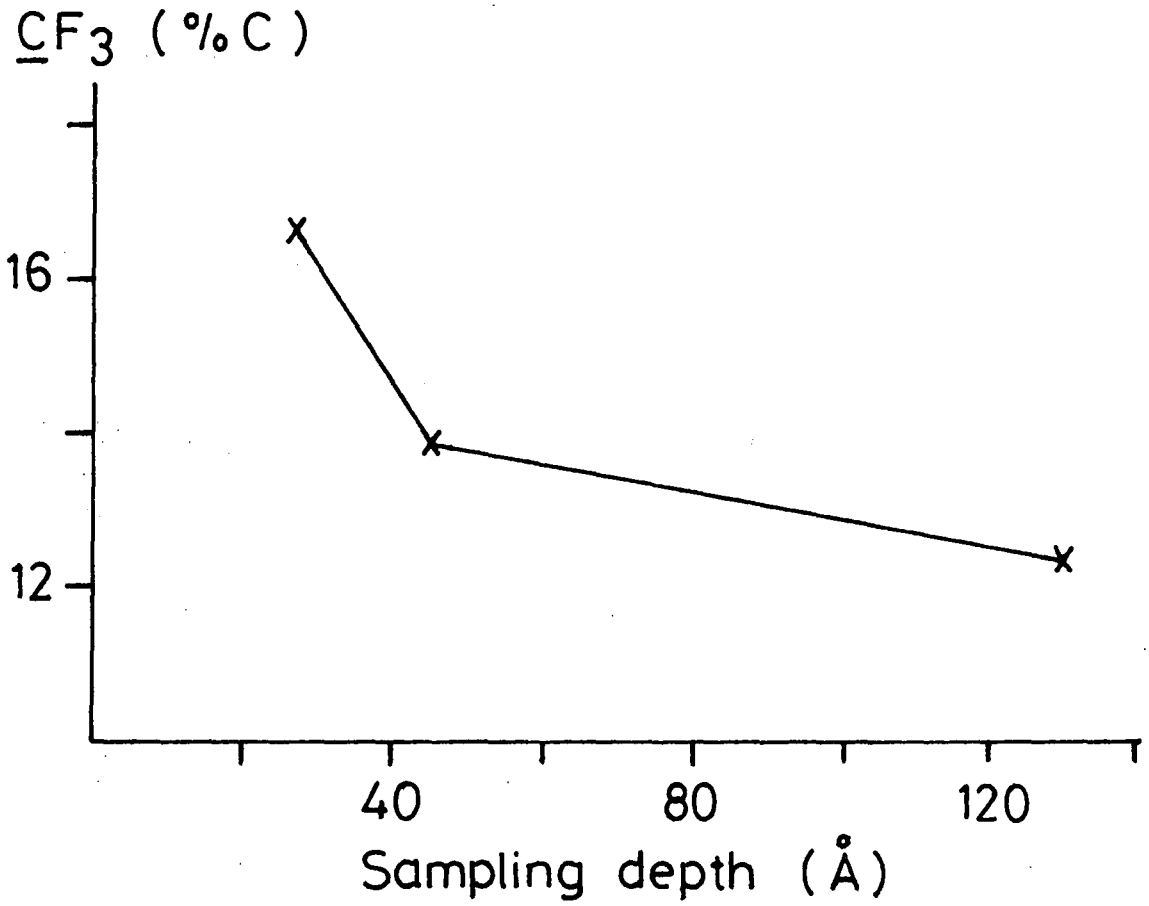

Figure 3.17 TFAA treatment of cellulose Type 1. Variation of trifluoromethyl carbon atom concentration (as percentage of total carbon) with photo-ionisation sampling depth.

esterification of one in three available hydroxyl groups on average. It is not possible to infer from the ESCA data whether or not the labelled hydroxyls are bound solely to primary carbon. It should be noted that the $\underline{CF_3}$ concentration does not bear a linear relationship to the extent of trifluoroacetylation, since for each CF_3 group incorporated, two carbon atoms are added to the cellulose unit.

3.6.4 Conclusions

The results presented in this section have shown that, under the conditions employed, trifluoroacetylation of all the available hydroxyl groups in cellulose is not accomplished, even after the prolonged treatment with TFAA. This is in contrast with the findings for polyvinyl alcohol (Section 3.3). Morphological differences may be responsible. It is also likely that a low level of residual water may have been present within the cellulose material, and hence the hydrolysis of the anhydride to give trifluoroacetic acid would have been favoured. Geddes [180] has reported the interaction of trifluoroacetic acid with cellulose and related compounds at 25°C over a period of some 25 days as studied by infrared spectrophotometry. It was found that, in the presence of water generated in the reaction of cellulose with the acid, equilibrium was attained when about 1.25 -OH groups per glucose residue were esterified. This degree of esterification is in good agreement with that found in this ESCA study (Figure 3.13).

The possible use of TFAA as a blocking agent to study the role of hydroxyl groups in the chemistry of cellulose and nitrocellulose has been discussed (Section 3.6.1). Fowler [182] is currently pursuing this work in the investigation of the role hydroxyl groups play in the x-ray degradation of cellulose nitrates. Early results would seem to demonstrate the usefulness of this approach.

CHAPTER FOUR

ASPECTS OF THE PREPARATION AND SURFACE CHEMISTRY OF POLYACETYLENE WITH SPECIAL REFERENCE TO ITS PASSIFICATION TOWARDS ATMOSPHERIC OXIDATION

CHAPTER FOUR

ASPECTS OF THE PREPARATION AND SURFACE CHEMISTRY OF POLYACETYLENE WITH SPECIAL REFERENCE TO ITS PASSIFICATION TOWARDS ATMOSPHERIC OXIDATION

4.1 Introduction

A major impetus behind research into macromolecular science lies in developing a better understanding of structure- property relationships which, in turn, aid the fabrication of new materials to meet specific economic and social needs. Hence, polymers have been developed which display properties such as strength, elasticity, plasticity, toughness and frictional resistance which are typical of metals.[183] (The oriented polyethylenes developed by Ward,[184] and which have been examined previously,[321] are a recent example of high strength macromolecular materials.)

For several years there has been considerable effort devoted to conducting organic materials with the aim of finding a cheap source that could be tailor-made to conduct electricity.[183,185,186] The significance of developing conducting polymer materials, easily processible according to the standard procedures of the plastics' industry so that they could act as a substitute for metals, provided a fundamental incentive to research in this field.[183]

Highly conjugated polymers, which have an extended π-electron system in their backbone, have received considerable interest in recent years.[183,187] Polyacetylene $(CH)_x$ is the simplest organic polymer with attractive electrical properties, and as such has formed the subject of many investigations. The pure cis polymer is an insulator,

whereas the trans polymer is an intrinsic semiconductor. Both show a dramatic increase in conductivity when doped with either electron acceptor or electron donor species. [183,185] McDiarmid and Heeger have elegantly shown the potential of this material in solid state batteries. [194] Despite the promise exhibited by polyacetylene, the apparent total insolubility and sensitivity to atmospheric oxidation impose considerable practical difficulties and limitations.[188,190,

The synthesis of polyacetylene has been described elsewhere. [183,188,189] The method of preparation of polyacetylene reported by Shirakawa and Ikeda [192,193] serves as the starting point for the majority of investigations into the structure, conductivity, optical and magnetic properties of pure and doped polyacetylene. Termed the 'Shirakawa technique', this procedure involves blowing acetylene onto the quiescent surface of a concentrated solution of a Ziegler catalyst in an inert solvent: the most suitable Ziegler catalyst for this procedure consists of titanium tetrabutoxide and triethylaluminium. A thin layer of polyacetylene forms immediately at the gas/liquid interface, its thickness being controllable between 1μm and several mm, depending upon the quantity of acetylene used. A widely employed variant of this technique involves wetting a glass plate with a capillary film of the catalyst solution. This allows free standing flat films of large area to be prepared. The polyacetylene material so produced appears as a film to the naked eye, but SEM examination reveals that it is in the form of matted fibrils, each fibril of ~ 200Å diameter. [195]

Through the research of Edwards and Feast, [188] a new synthesis of polyacetylene has been achieved, and subsequently refined, [189,196] whereby a soluble, relatively stable and well-characterised polymer

can be converted to polyacetylene where and when required. This synthetic route involves the metathesis ring-opening polymerisation of a suitable monomer, such as 7,8-bis (trifluoromethyl) tricyclo [4,2,2,$0^{2,5}$] deca-3,7,9-triene (I). In this case, the polymer (II) so formed is a fluorinated precursor to polyacetylene which undergoes a thermal transformation reaction with the elimination of 1,2-bis (trifluoromethyl) benzene to yield polyacetylene (III) as outlined in Figure 4.1. The polyacetylene prepared by this route is catalyst-

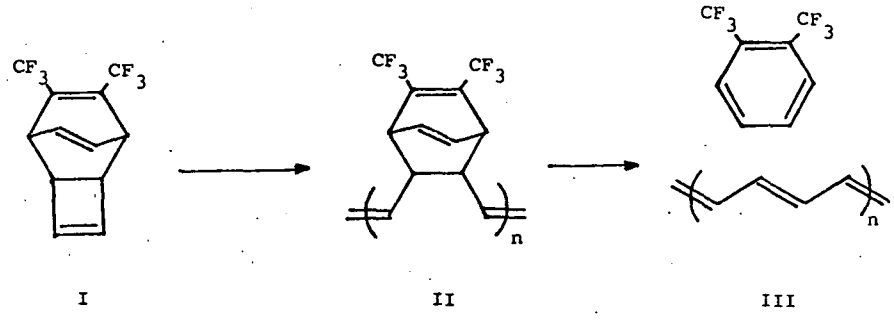

Figure 4.1 A synthetic route to polyacetylene

free and in film form. It is of high density, amorphous and has an essentially trans configuration.[189,196]

The work presented in this chapter sets out to monitor the conversion of the fluorinated precursor polymer to polyacetylene.† The stability of polyacetylene on exposure to the atmosphere is assessed in terms of the material's surface chemistry as revealed by ESCA. The application of a mild surface treatment to the polyacetylene, prior to contact with the air, is explored as a possible means of surface passification. The use and effects of radiofrequency plasmas excited in hydrogen are reported.

---

† The feasibility of studying, using in situ ESCA analysis, the intermediates involved in metathesis ring-opening polymerisations, with special concern for the role of the tungsten hexachloride/tetraphenyl tin catalyst system involved, [188,197] has been considered. This is of interest since the role oxygen plays in such metathesis reactions [197-200] has been the subject of previous experimental [201,202] and theoretical [203,204] investigations. A study of this kind would require a strictly controllable reaction environment, with provision for the total exclusion of oxygen. However, it appeared that tungsten hexachloride suffered oxidative attack under a vacuum of better than 10^{-6} torr prevailing in the ES200B spectrometer source chamber during the analysis. The experimental results of this work have been presented in Section 4.3.1.

4.2 Experimental

4.2.1 Samples and sample preparation

4.2.1a Tungsten hexachloride

In the initial feasibility study to monitor the metathesis polymerisation of the precursor (11), a thin layer of purified tungsten hexachloride (provided by Dr F. Stelzer) was deposited onto a spectrometer probe tip. The tungsten hexachloride was sublimed directly onto the probe tip attached to a liquid nitrogen cold-finger in an inert dry nitrogen atmosphere. The sample was transferred to the ES200B spectrometer for analysis under dry nitrogen (glove bag), avoiding contact with air.

4.2.1b Fluorinated precursor polymer

The precursor polymer (11) was prepared by Dr J.H. Edwards as described elsewhere, and stored under nitrogen at temperatures $< -20^{o}C$. Specimens for ESCA investigation were prepared by dip coating a spectrometer probe tip with a 2% by weight solution of the polymer in acetone under a stream of dry nitrogen. The specimen was transferred immediately under dry nitrogen into a glove bag, flushed with nitrogen and attached to the ES300 spectrometer, for insertion into the spectrometer. Once inside the spectrometer, the sample was cooled to $0^{o}C$ and that temperature was maintained throughout the analysis. The time elapsed from coating the yellow transparent film to ESCA analysis was approximately ten minutes.

4.2.1c Polyacetylene

The formation of polyacetylene was achieved by heating the precursor polymer in vacuo inside the source chamber of the ES300

spectrometer. Thermostatically controlled heating (and cooling) of the sample is achievable from equipment integral to the spectrometer probe itself. A gentle heating of the polymer over a prolonged period of time was known to be preferable for achieving complete elimination of 1,2-bis (trifluoromethyl) benzene, rather than a sudden temperature increase.[205] However, in practice it was difficult to exercise fine control over the conversion temperature during the initial stages of reaction. This was due to the exothermal nature of the elimination reaction[189] rather than any fault associated with the heating equipment. Thus, in a typical conversion and with a spectrometer base pressure of $\sim 2 \times 10^{-9}$ torr (penning gauge), the following observations would be made. Introduction of the sample into the source chamber would cause an increase in pressure to $\sim 2 \times 10^{-8}$ torr. Within seconds of the thermostat, adjusted to $11^{o}C$, being switched on, the probe tip temperature would rise to $\sim$ 110-120^{o}C with an accompanying increase in pressure which would reach $\sim 2 \times 10^{-6}$ torr after $\sim$ 12 minutes heating. After 25 minutes at $120^{o}C$ the pressure would have fallen to $\sim 5 \times 10^{-8}$ torr, and would continue to fall, with heating removed, to a value of $\sim 1.6 \times 10^{-8}$ torr after 60 minutes at $66^{o}C$. Spectra would be recorded after a further hour when the pressure and temperature would have fallen to $\sim 6 \times 10^{-9}$ torr and $\sim 53^{o}C$ respectively.

During the first minute of heating visible changes in the nature of polymer film would be apparent, indicating rapid conversion of the pale yellow precursor polymer into black lustrous polyacetylene, through shades of orange and red.[189]

4.2.2 Hydrogen plasma treatment of polyacetylene

Each sample to be plasma modified was first characterised by ESCA as described in the following section. The polyacetylene

sample was transferred from the spectrometer to a purpose built plasma vessel via a glove bag flushed with dry nitrogen. The plasma vessel comprised a wide cylindrical pyrex (diameter 6cm, height 16cm) tube, sealed at one end and with a greaseless tap, connected to the main vessel by means of a Viton 'O' ring sealed ball and socket joint. Once the polyacetylene sample was inside, the plasma reactor was connected to the main vacuum line to the right hand side of the Pirani gauge marked schematically in Figure 2.1a. A 9 turn 6μH copper plasma coil electrode wound externally was suspended around the vertical plasma reactor.

The vacuum line, with the plasma reactor isolated, was evacuated and flushed with hydrogen gas (supplied by British Oxygen Corporation and used without further purification) and evacuated before opening the valve to the plasma reactor. The same procedure as described in Section 2.2.4a was then adopted before the plasma was initiated. The plasma conditions chosen for this investigation were 0.4W and 10W power for 10 seconds and at 0.2 torr as measured by a Pirani gauge.

After treatment the samples were transferred to the ES300 spectrometer for reanalysis following the reverse of the procedure already described. In this way contact of the sample with air was minimised. Thereafter the samples were stored in air in the dark at ambient temperature in covered petri dishes. The samples were stored in the dark so as to minimise interaction with singlet oxygen.[209] Periodic ESCA analyses on the samples were performed.

4.2.3 ESCA analysis

The preliminary study of tungsten hexachloride was performed on the A.E.I. ES200B spectrometer with a $Mg_{K\alpha_{1,2}}$ X-ray source operated

at 12kV and 15mA, and with a base pressure of $\sim 5 \times 10^{-8}$ torr. Under the conditions employed the gold $4f_{7/2}$ level (at 84eV binding energy), used for calibration purposes, had a FWHM of $\sim$ 1.2eV. Spectra were recorded in analogue fashion. Curve fitting and peak area measurement were performed using a Du Pont 310 analogue curve resolver. [1]

The other investigations were carried out using the Kratos ES300 spectrometer equipped with a Kratos DS300 data system allowing digital acquisition and manipulation of data. Depth profiling was achieved by use of both $Mg_{K\alpha_{1,2}}$ and $Ti_{K\alpha_{1,2}}$ X-ray sources: the chosen operating conditions were 12kV, 8mA for the magnesium anode, and 13.5kV, 18mA for the titanium anode. All spectra were recorded at an electron take off angle of 30^{o}. For this spectrometer and under the conditions employed, the gold $4f_{7/2}$ level had a FWHM of $\sim$ 1.1eV. A detailed ESCA analysis of C_{1s}, F_{1s}, O_{1s} and Si_{2p} core levels together with wide scan (1200eV) and valence band spectra using the magnesium anode took in the order of 2½ hours to complete. A further 40 minutes were allowed for titanium core level spectra to be acquired. The base pressure of the spectrometer was $\sim 2 \times 10^{-9}$ torr and independent studies showed that hydrocarbon contamination was not evident.

4.3 Results and discussion

4.3.1 Chemical stability of tungsten hexachloride during ESCA analysis

It has been mentioned in earlier discussion that one of the initial aims of this work was to design suitable apparatus and procedures to enable polymerisation reactions involving metathesis catalysts to be studied in situ. A necessary prerequisite for

success is the ability to create an oxygen free environment throughout the system. It was also important that the reaction mixture itself would not degrade under x-radiation.

As a first step in this investigation the spectrum of tungsten hexachloride has been monitored as a function of time in the ES200B spectrometer. The W_{4f}, Cl_{2p}, O_{1s} and C_{1s} core level spectra have been studied over a period of 150 minutes, each set taking in the order of 20 minutes to record, and are shown in Figure 4.2:

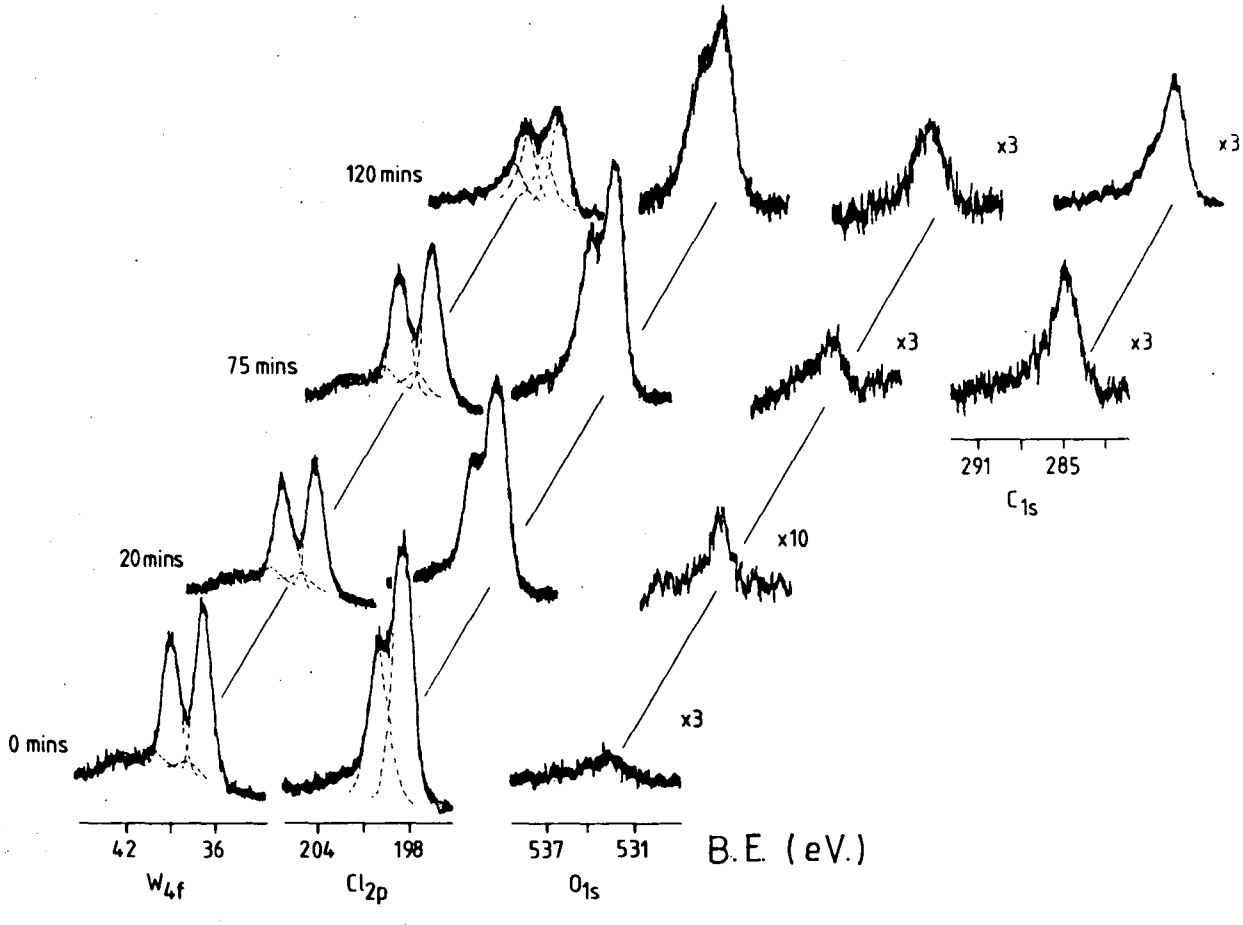

Figure 4.2 W_{4f}, Cl_{2p}, O_{1s} and C_{1s} core level spectra of tungsten hexachloride as a function of time in the ES200B spectrometer ($\sim 10^{-6}$ torr)

the variation of the relative intensities of the core level peaks with time is plotted in Figure 4.3. The graphical representation

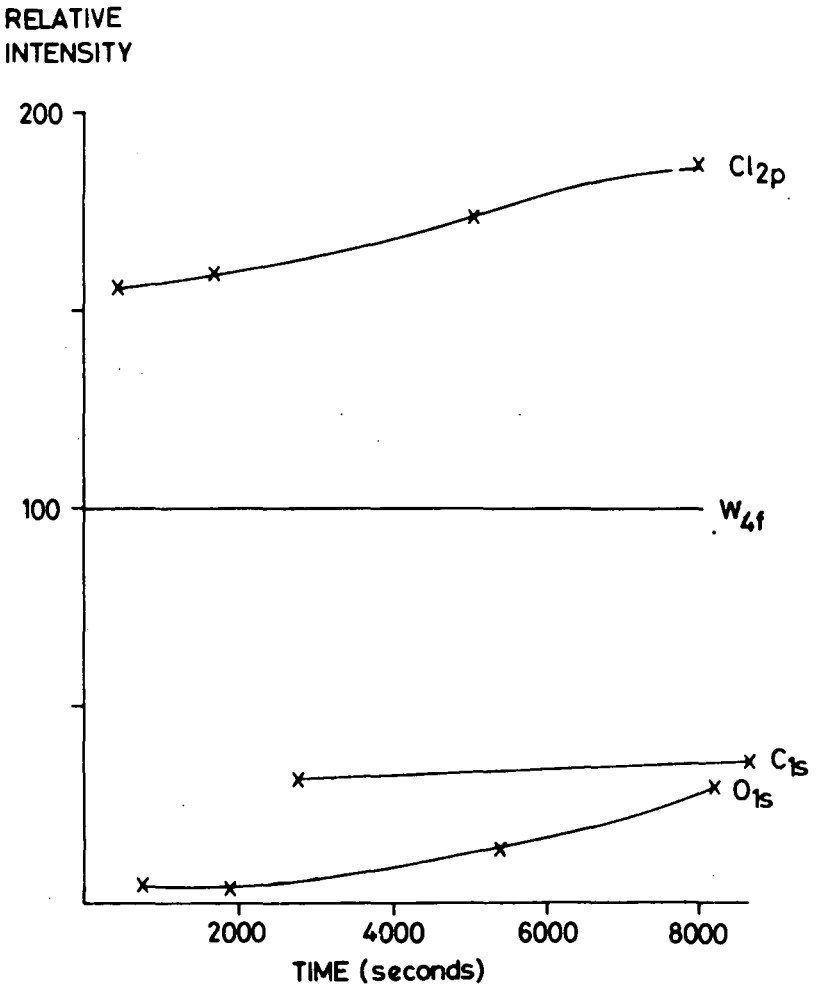

Figure 4.3 The variation of W_{4f}, Cl_{2p}, O_{1s} and C_{1s} core level peak intensities as a function of time in the ES200B spectrometer ($\sim 10^{-6}$ torr).

of the changes in elemental composition, relative to the total signal observed for the tungsten 4f level (Figure 4.3) shows a gradual increase in chlorine levels accompanied by an increase in oxygen levels.

These increases are seen to accelerate with time. Hydrocarbon contamination, as witnessed by the C_{1s} signal, is evident on the 75 minute scan, and the extent of contamination is greater on the final scan. Most probably some level of hydrocarbon exists initially, although no effort was made to monitor C_{1s} levels until the later stages of the experiment. This hydrocarbon component may be inherent in the sample, or be solely a surface deposit from the spectrometer. In any event, all binding energy measurements were made relative to the hydrocarbon peak at 285eV binding energy.

Consideration of the relative intensities of the core level signals and their corresponding photoionisation cross sections permits the calculation of surface stoichiometries. Hence for the first two sets of spectra the W : Cl : O atomic ratios are in reasonable agreement with the expected 1 : 6 : 0 ratios for tungsten hexachloride. Thereafter the ratios show a distinct abundance of oxygen in accordance with the formation of tungsten oxyhalides for example.[206,207] The W_{4f} and Cl_{2p} core level envelopes, both doublets due spin-orbit splitting (Section 1.4.2), exhibit distinct broadening (Figure 4.2). This confirms the formation of new species affecting both tungsten and chlorine electronic environments.

Although the study has provided a somewhat disappointing conclusion, namely the conditions which prevailed in the ES200B spectrometer were not adequate for the intended plan of work, the data is of interest in its own right. To put matters in perspective, an account of the effects of contamination occurring by adsorption of species from the gas phase within the spectrometer has been given by Fuggle.[108] Residual gases including water vapour, hydrocarbons, carbon monoxide and oxygen are present in high vacuum systems

(10^{-5} - 10^{-9} torr). Ultra high vacuum systems, capable of pressures in the 10^{-13} torr range after baking, are under development to facilitate the study of highly reactive surfaces.

4.3.2 The formation of polyacetylene

The effect of heat on the C_{1s} photoionisation signal of the fluorinated precursor polymer (11) is shown in Figure 4.4. The spectra are presented as recorded, with no correction for charging phenomena. The reason for this will become clear in the following discussion. The C_{1s} envelope for the initial precursor polymer, recorded at $0^{o}C$ shows two component peaks, the predominant peak occurring to lower binding energy and representative of carbon not directly bonded to fluorine, and a minor signal corresponding to trifluoromethyl carbon.[210] The separation between these two peaks is 7.6eV. The stoichiometry of the polymer may be obtained from consideration of the contribution of the CF_3 peak to the total C_{1s} signal. In fact two C_{1s} envelopes were recorded during ESCA analysis, the first being acquired within $\sim$ 5 minutes of the sample entering high vacuum, and a second, slower scan was made some 8 minutes after the first. The C_{1s} ^{TOT} : $\underline{CF}_3$ ratios for the two spectra amount to 100 : 17.6 and 100 : 15.5. These figures average to a value of 100 : 16.6, the precise value for the pristine polymer. The corresponding F_{1s} signals, consisting of a single peak in each case, yield values of the fluorine concentration (atom percent, relative to carbon) of 42.4 and 41.0, values that are noticeably lower than the expected figure of 48. These differences would point to a surface depletion of fluorine relative to the bulk over a depth scale of $\sim$ 27 - 45 $\mathring{A}$, the respective sampling depths of the F_{1s} and C_{1s} core levels using a magnesium $K\alpha_{1,2}$ x-ray source.[83]

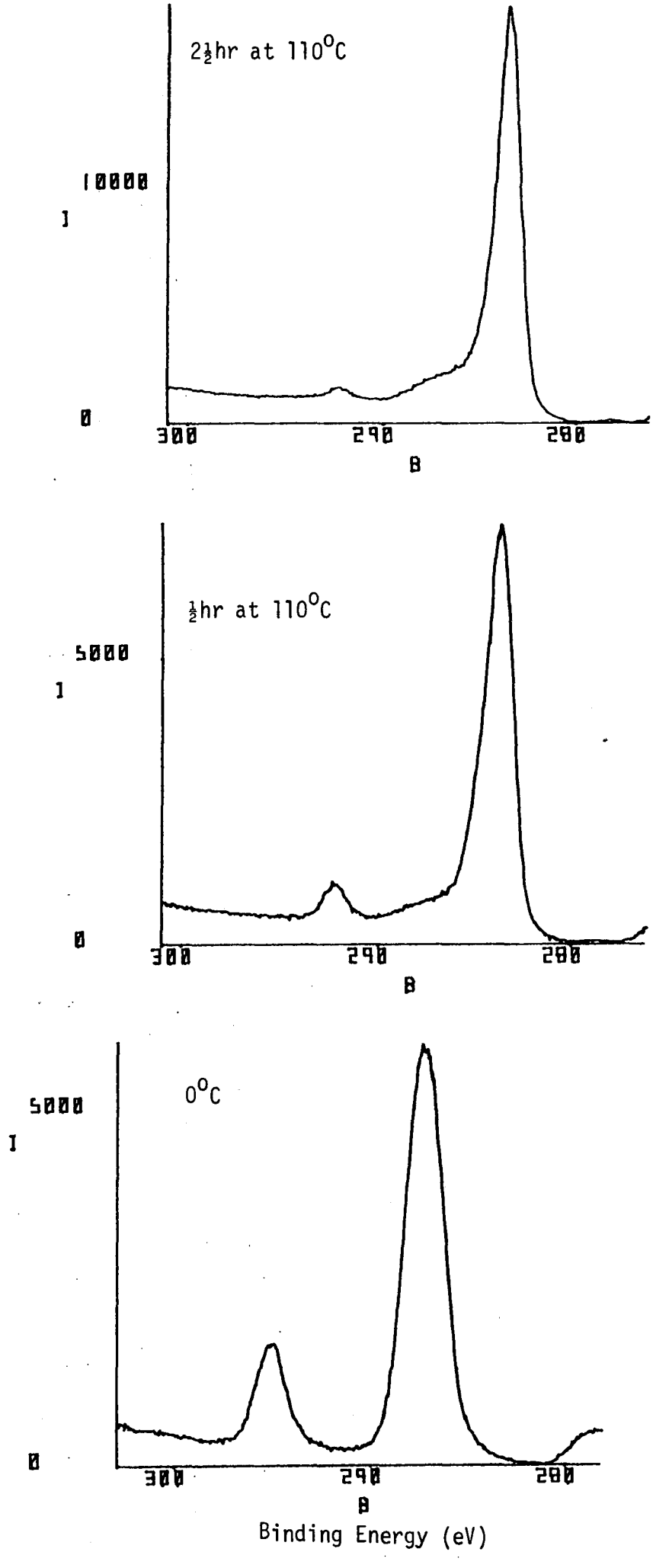

Figure 4.4 The effect of heat (110°C on the $Mg_{K\alpha}$ excited C_{1s} core level envelope of the fluorinated precursor to polyacetylene, without correction for sample charging.

On heating the precursor polymer at 110°C marked changes occur in the C_{1s} core level envelope. After a heating period of 30 minutes the $\underline{C}F_3$ moiety has shrunk to 6.7% of the total C_{1s} intensity. This trend continues, albeit at a slower rate, until after 2½ hours' heating the $\underline{C}F_3$ peak relative intensity amounts to 2.8 (Figure 4.5). This value remains unchanged after leaving the sample in the source chamber overnight without heating. There are also concominant decreases in intensity of the F_{1s} signal.

Polyacetylene is known to be prone to oxidation: its fluorinated precursor is more resistant to oxidation. Oxygen levels were therefore monitored throughout the experiment. A low level of oxygen ($\sim$ 1.3 atom percent relative to carbon), as measured by the O_{1s} signal, was detectable at each stage of ESCA analysis. This extraneous oxygen was accompanied by a weak Si_{2p} core level signal. Both contaminants are constituents of silicon grease, traces of which often remain in glassware even after thorough cleaning, and which is easily detected in the ESCA experiment. The oxygen present in these spectra is thought to arise solely from silicone grease rather than from oxidative attack of the organic system.

Comparison of the nature of the C_{1s} core level spectra for the polymer system before and after heating (Figure 4.4) reveals differences in line shape and peak position. The elimination of 1,2-bis (trifluoromethyl) benzene and its effect on the $\underline{C}F_3$ portion of the C_{1s} signal has already been discussed. There are in addition further consequences which are of value to note.

The shift in position of the total carbon envelope to lower binding energy is evidence in favour of the creation, on heating, of a material which is capable of dissipating the positive charge

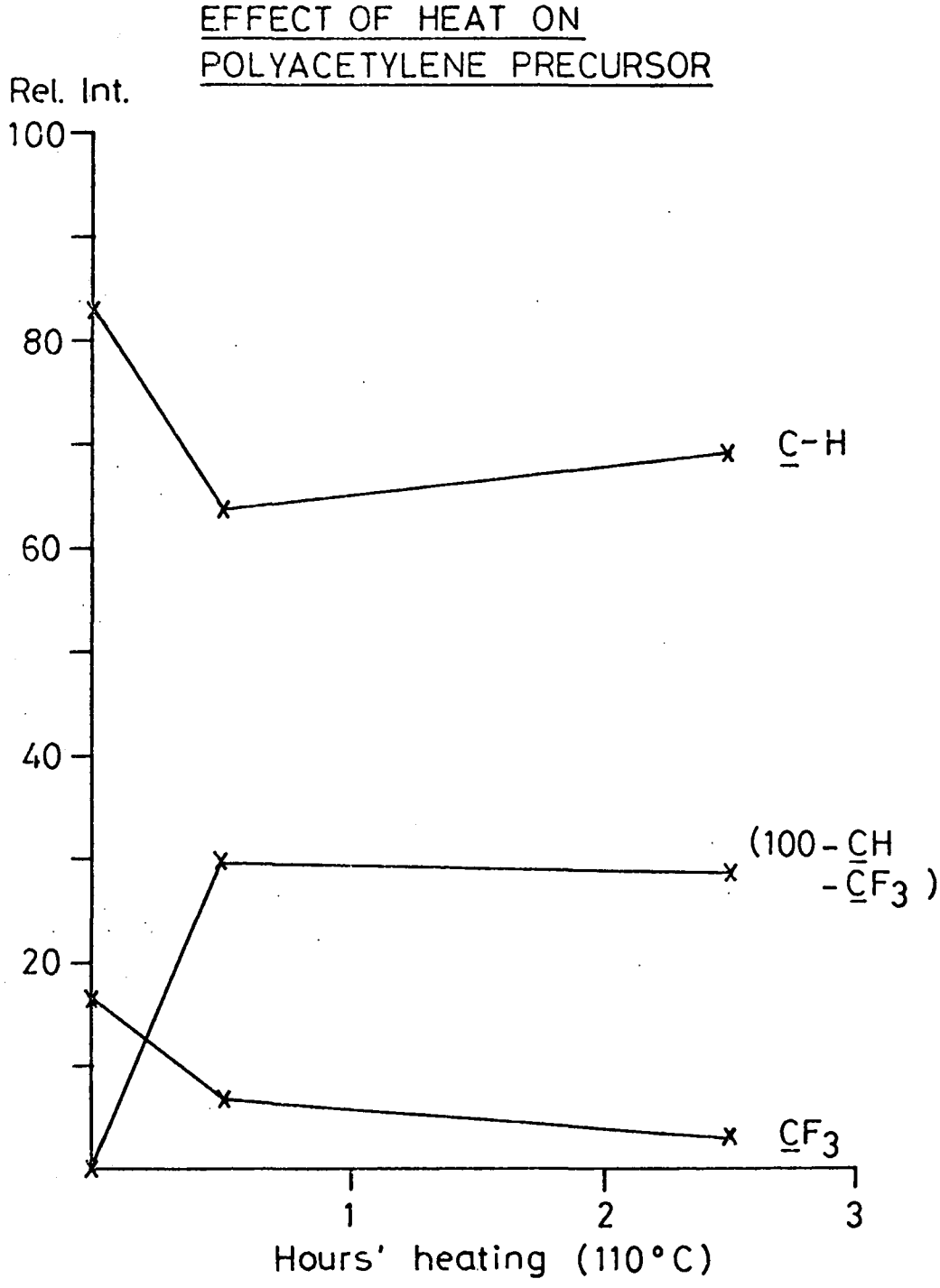

Figure 4.5 The relative intensities of the C_{1s} component peaks for the polyacetylene precursor polymer plotted against heating time ($110^{o}C$). Total C_{1s} envelope intensity is taken as 100 units.

accumulated on the surface during ESCA analysis, that is an electrically conducting material. † Other evidence for the creation of a new type of carbon species comes from inspection of the separation of the predominant carbon component and the trifluoromethyl peak of the C_{1s} envelope. During heating there is a widening of this separation from 7.6eV for the fluorinated precursor polymer, via an intermediate value of 8.5eV after heating for 30 minutes, to a final separation of 8.8eV reached after 2½ hours, at 110°C. The precision to which a peak position may be measured is usually taken as ∿ ± 0.2eV, [133] and hence the observed shift is thought to be real. Indeed the immediate chemical environment of the $\underline{C}F_3$ carbon, and the fluorine atoms, may be considered to remain unperturbed throughout the conversion process, and thus their ESCA spectra should remain unshifted on the binding energy scale, relative to $\underline{C}$ - H functionalities at 285eV. Furthermore, the main photoionisation peak of the fluorinated precursor polymer arising from the hydrocarbon portion of the material will occur at 285eV binding energy as corrected for sample charging. (In fact a third peak would be expected of equal intensity to the $\underline{C}F_3$ peak, shifted slightly to the higher binding energy side of the main $\underline{C}$ - H peak, and arising from $\underline{C}$ - CF_3 environments.) [210] With these factors in mind the binding energy of the polyacetylene carbon species has been calculated as ∿ 284.2eV, relative to hydrocarbon at 285eV.

---

†Whilst pure polyacetylene will behave as an insulator, under the conditions of the ESCA experiment, photoionisation processes will create a deficiency of electrons and hence the conductivity of the polymer will become enhanced.

This is in reasonable agreement with the previous XPS measurements of Shirakawa polyacetylene. [211,212]

Attention may now be paid to the apparent development of a broad high binding energy shoulder to the main C_{1s} photoionisation signal. Two factors are likely to be the major contributors. First, since complete elimination of 1,2-bis (trifluoromethyl) benzene has not been achieved in this experiment, as evidenced by the $\underline{C}F_3$ and F_{1s} peaks, there will be an accompanying signal from the hydrocarbon portion of the remaining precursor polymer fragments. Second, it has been observed by Salaneck et al [211] that the $\pi \rightarrow \pi^*$ transition typical of long chain polyenes appears as a weak shake up peak about 2.5eV removed to higher binding energy side of the main C_{1s} peak. In contrast, Allen and co-workers, [212] in their ion implantation studies of polyacetylene, present a C_{1s} core level spectrum for the pure polymer which shows a shoulder to the higher binding energy side of a single photoionisation peak. This spectrum bears a close resemblance to the spectrum for polyacetylene depicted in Figure 4.4. Oxidation of the polymer surface is not thought to contribute to this shoulder to any significant extent.

The difference in line width between the $\underline{C}F_3$ component and individual hydrocarbon components for the precursor polymer (FWHM $\sim$ 1.8eV), and the carbon-carbon component for the newly created species (FWHM $\sim$ 1.3eV) may be ascribed to differences in the electronic environments of the atoms concerned. [213] This gives further credence to the formation of a conjugated carbon residue.

The polyacetylene produced by the two step synthesis proposed by Edwards and Feast [188] is of high density (ρ = 1.05g.cm^{-3} as measured by flotation). [196] There is evidence to demonstrate the formation of a more closely packed polymer network during the

thermal elimination reaction from the absolute C_{1s} peak intensity measurements of the ESCA experiment. Thus after 30 minutes and 2½ hours at 110°C the absolute intensities of the total C_{1s} signal rise respectively to 102.4% and 104.4% of the C_{1s} absolute intensity for the precursor polymer at 3.3×10^5 counts.

4.3.3 ESCA studies of the atmospheric oxidation of polyacetylene

4.3.3a Introduction

The sensitivity of polyacetylene towards oxidative attack has hindered the development of the potential useage of this material. [188,190,191,214,215] Oxidation of polyacetylene causes deterioration in both its mechanical [191] and electrical properties. [190,209,216,217] Many studies employing a variety of mechanical [191] and electrical procedures [209,217] and analytical tools (infrared [190] and Raman [218] spectrophotometry and electron spin resonance techniques [216,219]) indicate the absolute necessity for an oxygen-free environment to obtain the intrinsic electrical properties of this interesting polymer. Pochan et al. have monitored the effect of oxygen on the conductivity and the kinetics of degradation of polyacetylene films. [190,209,216,217]. They have shown how initial exposure increases the conductivity and then decreases it dramatically with time. It has been shown that the degradation process follows an initial doping that is normally observed for polyacetylene with other electron acceptors. Maximum conductivity was found to occur at 0.14 O_2 molecules per $^-CH = CH-$ unit. [209] Exposure of polyacetylene to oxygen for long time periods is known to cause irreversible chemical changes in the material.

In order to improve the resistivity of polyacetylene towards oxidative degradation several avenues of research continue to receive attention. Four different approaches to resolving this problem have appeared in the literature and are as follows:

i) The synthesis of new conducting polyenes, e.g. poly(1,6-heptadiyne). [220,221]

ii) The synthesis of copolymers polyacetylene with phenylacetylene [222] and methylacetylene [223] for example. It was hoped that while the unchanged structure of the polymer backbone would result in unaltered electrical properties, the side groups would impart better processibility. However the materials did suffer significant decreases in electrical conductivity.

iii) The preparation of polymer blends and composites such as polyacetylene/elastomer blends [215] and polyacetylene/polyethylene composites. [214,224] Varying the composition of the blends allows a range of mechanical and electrical properties to be obtained. Although lasting mechanical properties have been achieved on prolonged exposure to air, there was only a marginal increase in stability of the electrical properties of iodine doped polyacetylene/LDPE composites. [214] This is thought to reflect the poor oxygen barrier properties of polyethylene.

iv) Weber and co-workers [225] have reported that chemical modification of free standing polyacetylene using ion implantation techniques leads to a stabilisation of the polymer.

Oxidation of polyacetylene will occur through the interaction of the solid, via its surface, with the immediate environment. A knowledge of the surface chemistry of polyacetylene is therefore of fundamental importance in the understanding of the oxidative degradation process. It is surprising to find that comparatively few studies of the chemical reactivity of oxygen towards polyacetylene have been reported, [190,218] considerably more attention being given to physical effects. Recently, Gibson and Pochan [190] have used weight uptake, infrared and elemental analyses to monitor the kinetics of oxidation of polyacetylene fibrils by air. Two reaction conditions were used, ambient air under fluorescent room lighting, and dry air in the absence of ultraviolet light at 25°C. Their results pointed to initial rapid 'surface' oxidation followed by a slower 'bulk' oxidation process. Surface sensitive analytical tools were not applied. Hence it is particularly timely that this present ESCA investigation using polyacetylene film should have been undertaken.

In addition results will also be shown of the effects of surface specific hydrogen plasma treatments on the surface chemistry of polyacetylene, and on the subsequent stability of the treated polymer towards the atmosphere. Hydrogen plasma treatment was chosen for investigation since previous work in Durham [174] together with the results presented in Chapter Two of this thesis indicate the reductive nature of the hydrogen plasma. Specifically it was the aim of this work to test whether hydrogen plasma treatment would produce an overlayer of saturated polyethylene-type material, possibly cross-linked, which would be resistant to oxidative attack. Plasma treatments in general produce effects which are uniform and continuous over the substrates enveloped in the discharge. [133] Hopefully an even, pinhole free overlayer would be produced which would act as an effective barrier to the atmosphere and so prevent polyacetylene oxidation.

4.3.3b Results

Due to the high comparative element of this investigation it is convenient to present spectra showing the effects of atmospheric oxidation on unmodified polyacetylene and then to consider the effect of plasma modification. The presentation of results is complicated by the effect of the electrical properties of polyacetylene on energy referencing and hence on deconvolution of the ESCA core level signals. The method of energy referencing most often used for hydrocarbon containing polymers (i.e. referencing to the 'hydrocarbon' peak at 285eV binding energy) is not applicable. Instead the photoionisation signals have been referenced to the low level fluorine peak which is invariably present. The binding energy of the F_{1s} peak in the fluorinated polymer precursor, that is 688.7eV (relative to the hydrocarbon present at 285eV), has been adopted for reference. There is good evidence to support this methodology arising from analysis of the deconvoluted C_{1s} spectra of the oxidised materials. This will be discussed in detail at a later stage. ESCA spectra have been recorded using magnesium and titanium x-ray sources. Hence non-destructive analytical depth profiling may be accomplished. For the initial discussion, results obtained using the magnesium anode ($h\nu$ = 1253.7eV), sampling the outermost $\sim$ 50Å of the solid, will be used. Then these findings will be compared with ESCA data from the more deeply probing titanium anode ($h\nu$ = 4510eV) of sampling depth $\sim$ 130Å.

Figure 4.6 shows the effects of exposure to air at ambient temperature ($\sim$19^{o}C) in the dark for 5½ days and 36 days on the $Mg_{K\alpha}$ excited C_{1s} core level spectrum of polyacetylene film. The polyacetylene samples for this, and the hydrogen plasma treatment studies, were prepared as described in Section 4.2.1c. Complete defluorination

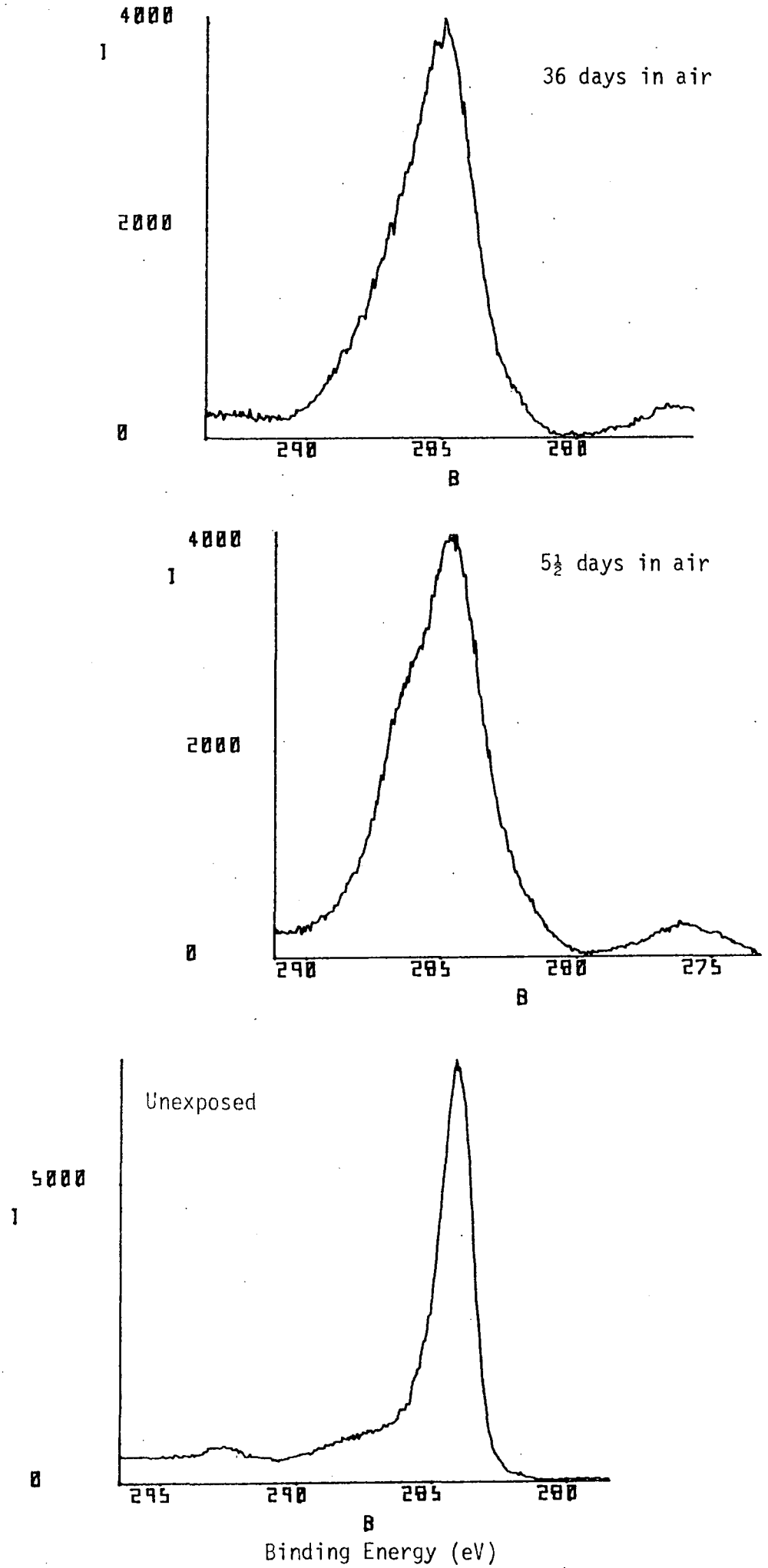

Figure 4.6 The effect of exposure to air at ambient temperature (~19°C) in the dark on the $Mg_{K\alpha}$ - excited C_{1s} core level spectrum of polyacetylene film.

of the precursor polymer was not achieved, as evidenced by weak $\underline{CF}_3$ and F_{1s} photoionisation signals. Nonetheless the thermal elimination reaction yielded polyacetylene materials with average carbon chain lengths of at least $\sim$ 40 atoms. There is evidence to suppose that the conjugated chain length may be somewhat reduced due to electronic defects.[195] Quantitative aspects of the nature of the residual fluorine, and also of extraneous silicon, will be presented later, only gross features of the C_{1s} envelopes will receive initial attention.

After 5½ days' exposure to air in the dark there are dramatic changes in the shape and position of the C_{1s} envelope. There is comparatively little further change for the 36 day exposure C_{1s} spectrum. The development of the pronounced shoulder to the higher binding energy side of the C_{1s} maxima for these spectra indicates extensive surface oxidation. The C_{1s} envelope shifts to higher binding energy (referenced to F_{1s} at 688eV binding energy), such that the major carbon component is positioned at $\sim$ 285eV. There is also a broadening of the component C_{1s} signals, and evidence for sample charging. These observations point to changes in the electrical and chemical nature of the carbon framework of the polymer, and to the formation of a non-conducting surface. The oxygen content of the film rose dramatically and after 5½ days' and 36 days' exposure to air; the respective C : O atomic ratios, as obtained from O_{1s} core level data, were 100 : 41.3 and 100 : 43.4.

It is of interest to compare these findings with those for polyacetylene film stored in contact with the air in a sealed pyrex tube for approximately 4 months. During this time part of the film had become bleached and was a pale yellow colour. Both bleached and unbleached specimens were examined by ESCA, and an infrared spectrum of the bleached film was run. The relevant spectra are shown in Figures 4.7 and 4.8.

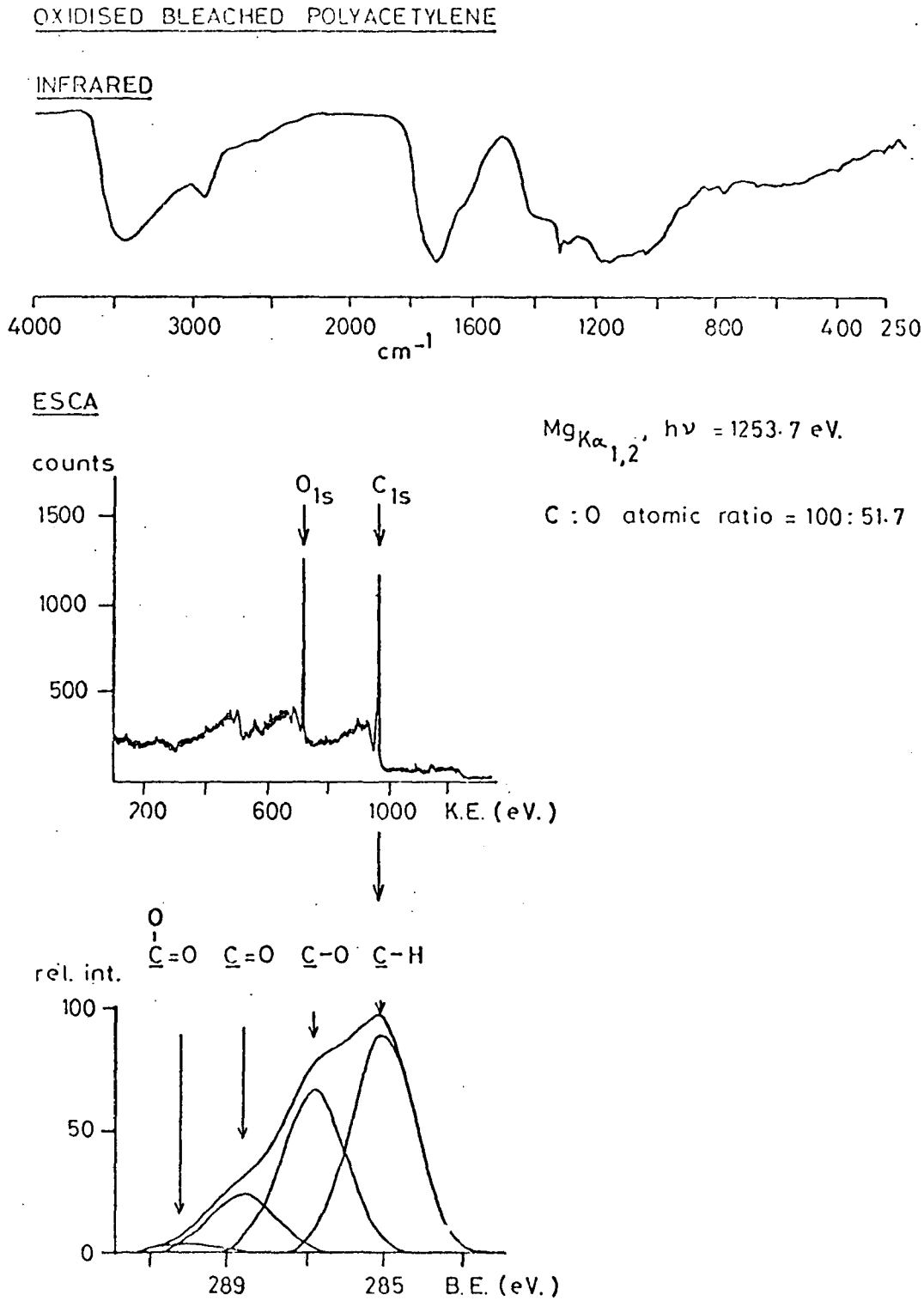

Figure 4.7 The infrared spectrum (Perkin Elmer 457 spectrophotometer), ESCA $Mg_{K\alpha}$ wide scan (1200eV) spectrum and deconvoluted C_{1s} core level spectrum of bleached oxidised polyacetylene film.

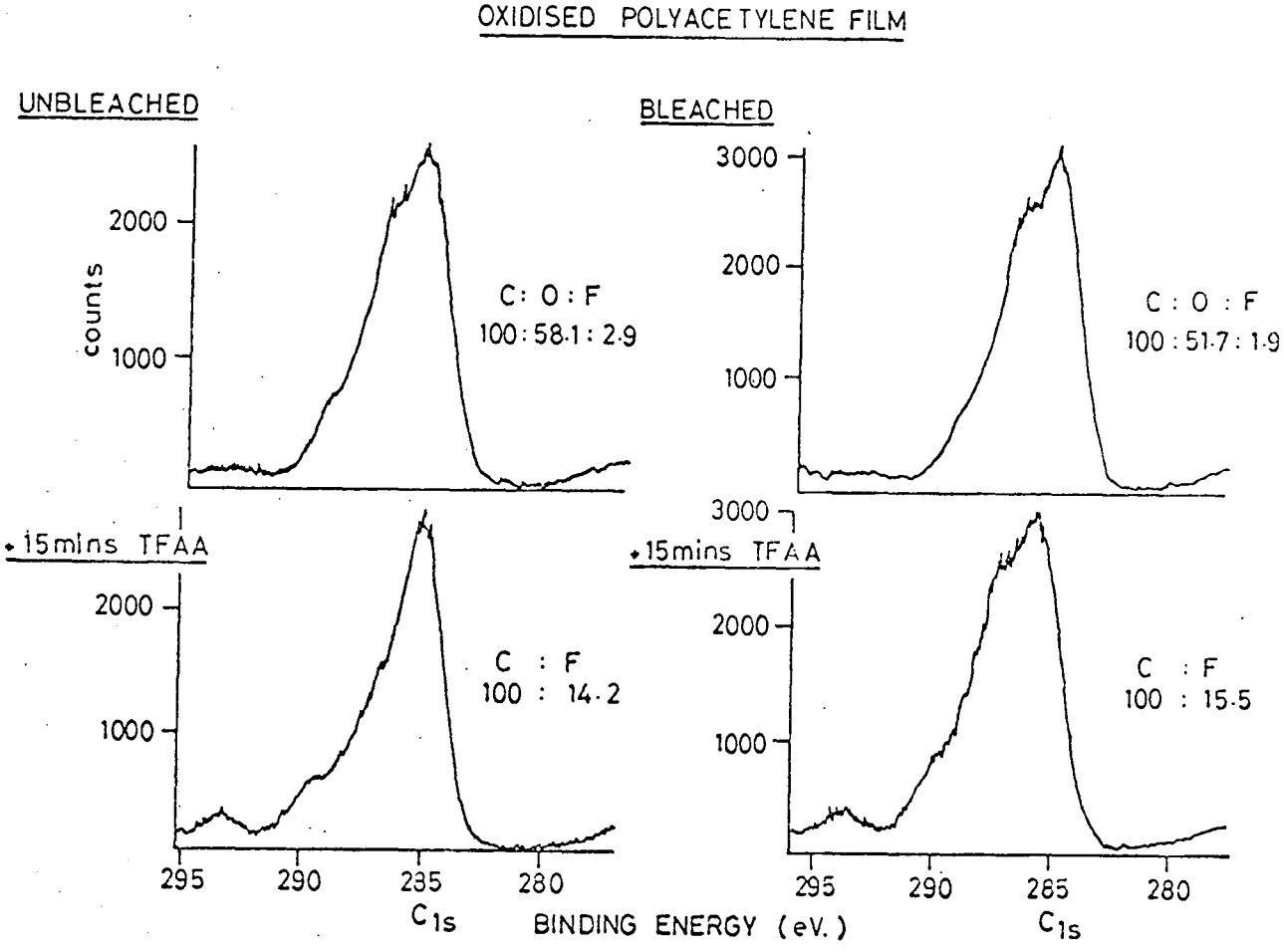

Figure 4.8 C_{1s} core level spectra of oxidised polyacetylene film, both bleached and unbleached, before and after exposure to TFAA vapour for 15 minutes. Carbon : oxygen : fluorine atomic ratios are also shown.

The infrared spectrum (Figure 4.7) bears close resemblance to the spectrum of oxidised polyacetylene published by Gibson and Pochan.[190] The broad band at 1720cm^{-1} may be assigned to carbonyl groups, and the absorption at 3450cm^{-1} to hydroperoxy and/or hydroxyl moieties. A peak at 1140cm^{-1} corresponding to C - O stretching would contribute to the broad absorption in this region.

The wide scan spectrum of the oxidised polyacetylene shows two prominent photoionisation peaks corresponding to carbon and oxygen. There is little difference in the surface compositions for the bleached and unbleached samples, the C : O atomic ratios being 100 : 51.7 and 100 : 58.1 respectively. Curve resolution of the C_{1s} envelopes indicates the presence of carbon singly bonded to oxygen species and carbonyl functionalities with the possibility of a low level of carboxyl carbon (Figure 4.7). The bleached and unbleached samples have similar distributions of oxidised carbon functional groups. Both samples show more extensive surface oxidation than does the polyacetylene exposed to the air for 36 days. As before, the shifted peak positions, sample charging phenomena and line broadening of C_{1s} components for the oxidised polyacetylene spectra reflect a loss of electrical conductivity.

Figure 4.8 shows that the oxidised films do show a small incorporation of the trifluoroacetate label on exposure to trifluoroacetic anhydride vapour for 15 minutes. This would indicate a low level of surface hydroxyl groups in the oxidised polyacetylene films. (A full account of this method of surface hydroxyl identification is given in Chapter Three of this thesis).

The effects of hydrogen plasma will now receive consideration. A detailed semi-quantitative analysis of the ESCA results will be left until a later discussion. Figures 4.9 and 4.10 present the

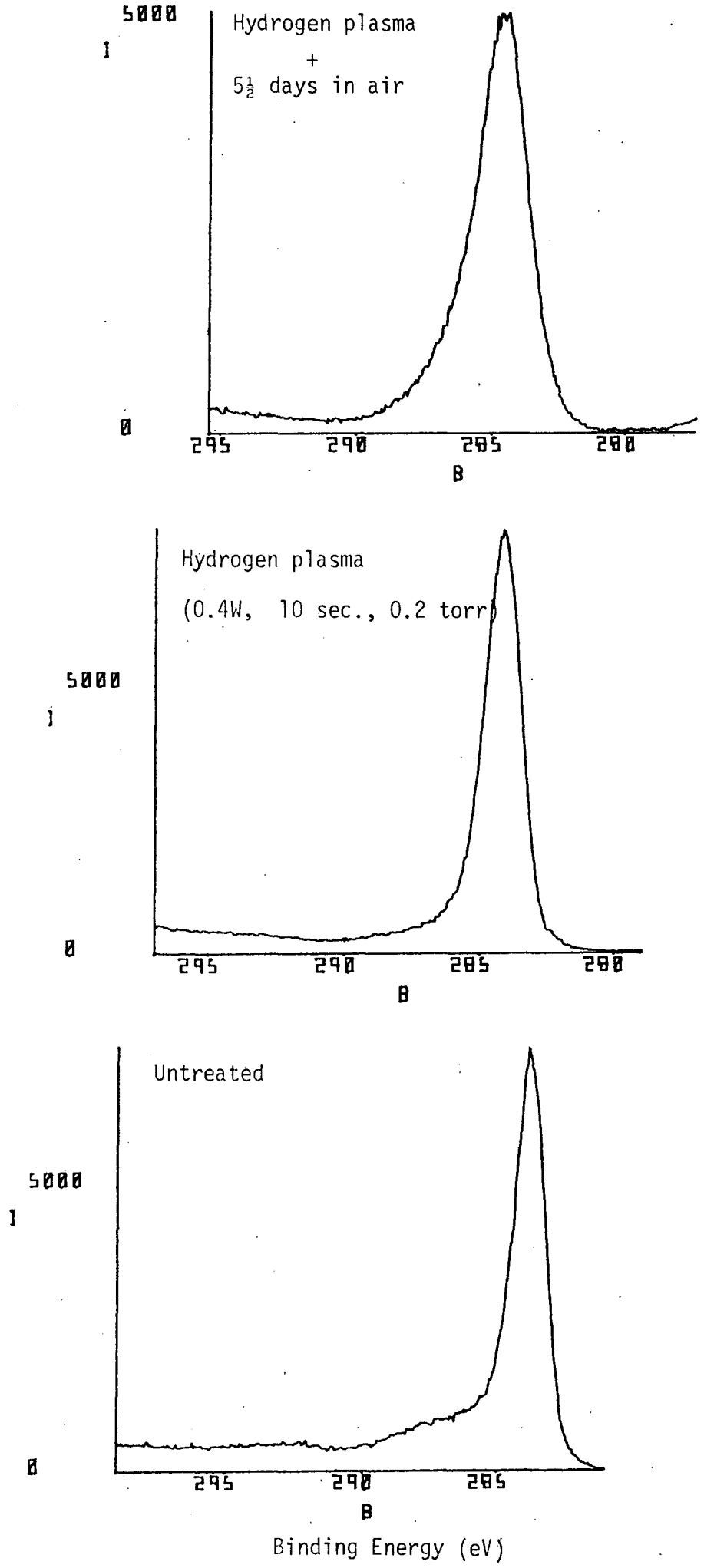

Figure 4.9 $Mg_{K\alpha}$ C_{1s} core level spectra of polyacetylene, untreated, after hydrogen plasma treatment (0.4W, 10 secs., 0.2 torr), and the plasma modified sample after 5½ days in the air (~19°C, dark).

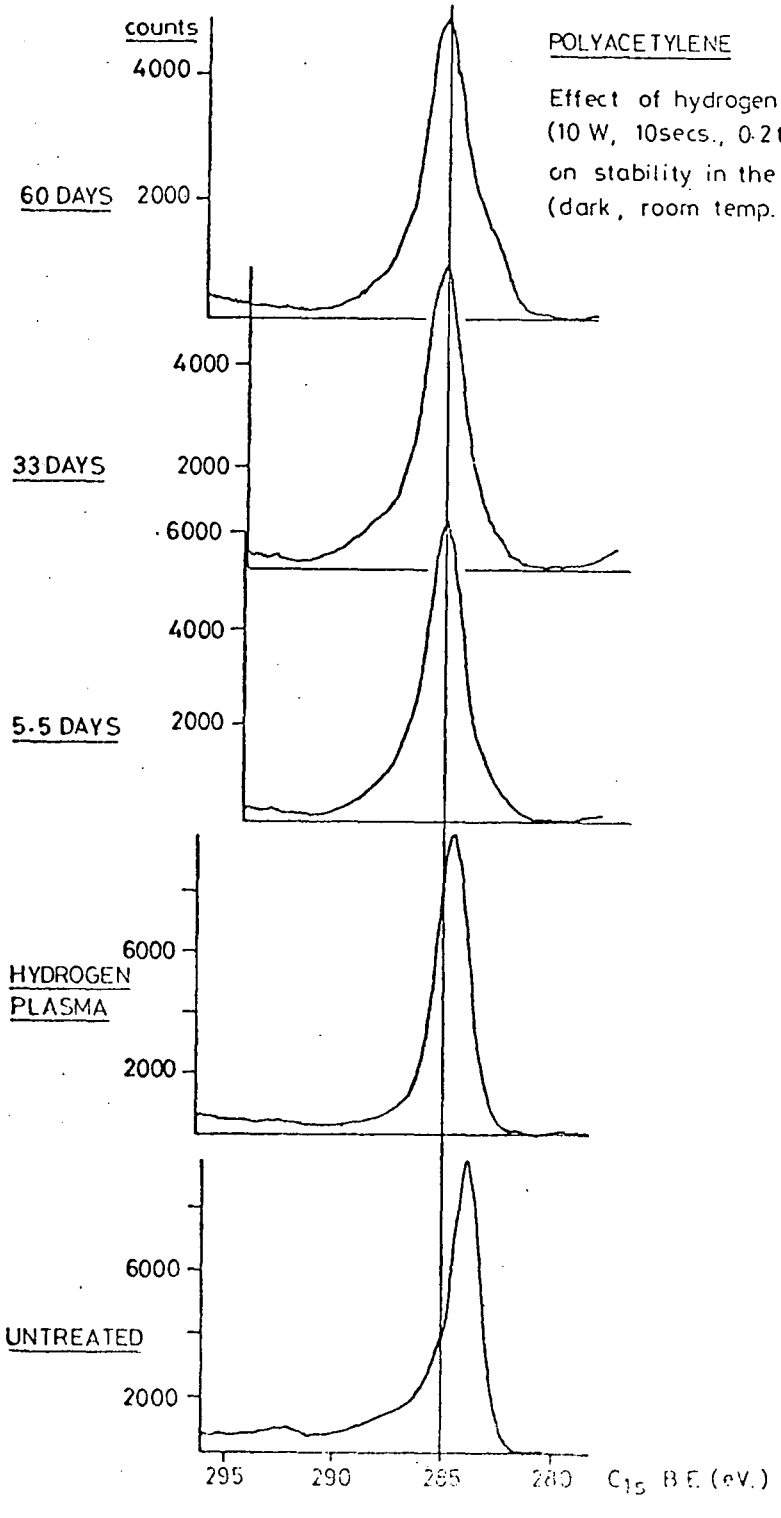

Figure 4.10 $Mg_{K\alpha}$ C_{1s} core level spectra of polyacetylene, untreated, after hydrocarbon plasma treatment (10W, 10 secs., 0.2 torr), and the plasma modified sample after $5\frac{1}{2}$ days, 33 days and 60 days in the air (~19°C, dark).

C_{1s} core level spectra of polyacetylene showing the effects of the plasma treatments and the subsequent interaction of the treated films with air.

Similar changes in the C_{1s} core level spectrum of polyacetylene are brought about by plasma treatments of 0.4W and 10W power, each for a period of 10 seconds and at 0.2 torr pressure as set by a Pirani gauge head. The C_{1s} peak is seen to broaden and shift to higher binding energy. The shoulder associated with $\pi \rightarrow \pi^*$ transitions is seen to diminish in intensity on hydrogen plasma treatment and this occurs to a slightly greater extent for the stronger plasma power. Although there is evidence for a low level of oxygen incorporation after the polyacetylene has been plasma treated, the resultant C_{1s} envelopes remain dominated by a single peak. The effect of the hydrogen plasma is to modify the polyacetylene film so as to produce an essentially hydrocarbon material over the ESCA sampling depth amenable to study using $Mg_{K\alpha}$ radiation. For the C_{1s} core level this would be $\sim$ 45Å. The modified polyacetylene gives an $Mg_{K\alpha}$ C_{1s} ESCA spectrum which shows certain similarities with that for a polyethylene type material.

ESCA valence band spectra may provide valuable information related to the electronic structure of polymers.[226,227] Valence band spectra of untreated polyacetylene, hydrogen plasma treated polyacetylene and oxidised polyacetylene film are compared in Figure 4.11. Even very mild plasma treatment (0.4W) produces noticeable changes in the C - C band region of the $Mg_{K\alpha}$ excited valence band spectrum (1235 - 1245eV kinetic energy). There is a marked increase in oxygen content for the oxidised sample, as revealed by the O_{2s} peak at 1230eV kinetic energy. The oxidation also causes a broadening

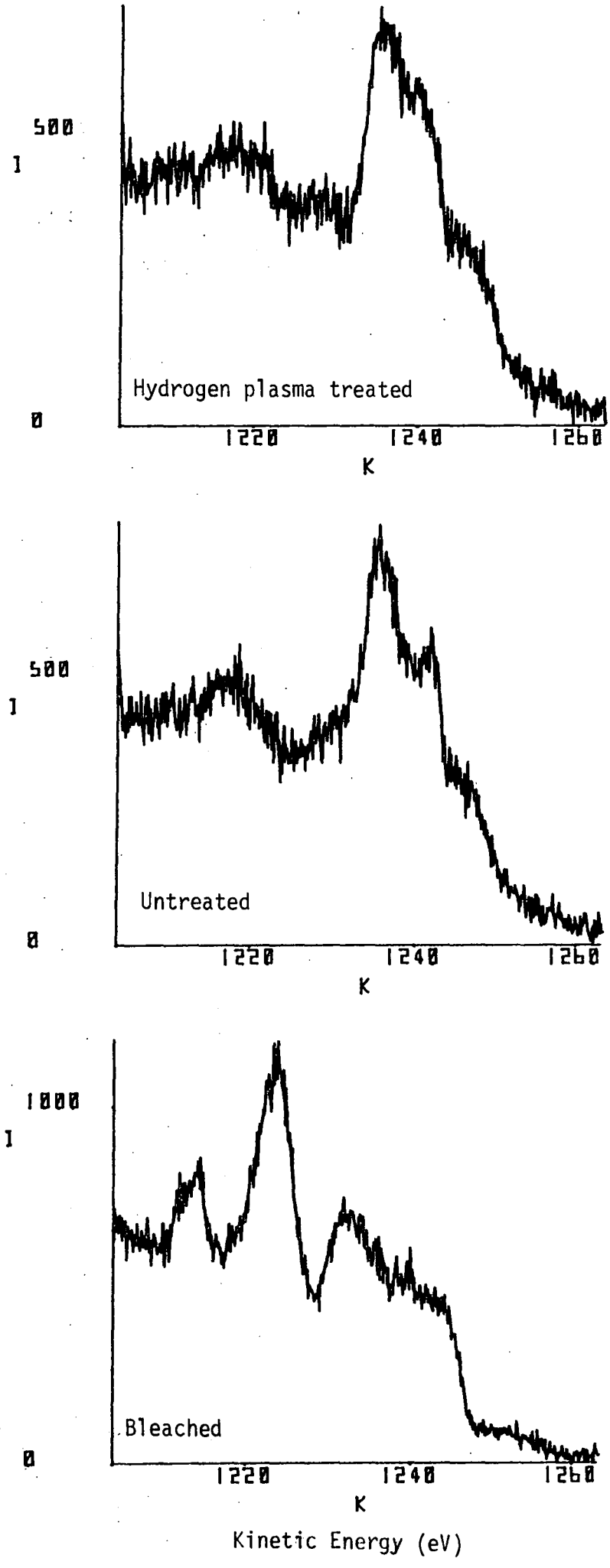

Figure 4.11 Valence band spectra of untreated polyacetylene, hydrogen plasma treated (0.4W, 10 secs., 0.2 torr) polyacetylene and oxidised bleached polyacetylene film.

and loss of fine structure of the carbon band. The oxidised polyacetylene sample shows a more predominant F_{2s} peak ($\sim$ 1210eV kinetic energy).

The appearance to the human eye of the hydrocarbon plasma treated films is no different from the untreated polyacetylene.

The modification brought about by hydrogen plasma has a profound effect on the subsequent interaction of the treated polyacetylene films with the atmosphere. Consideration of the $Mg_{K\alpha}$ C_{1s} line shapes of the exposed treated films, as shown in Figures 4.9 and 4.10, reveals that, although there is some development of oxidised carbon functionalities, the extent of this oxidative attack is markedly less than if the films had been exposed without hydrogen plasma pretreatment. Confirmation is provided by O_{1s} core level data of the $Mg_{K\alpha}$ ESCA experiment. This 'passification' remains even after 60 days' exposure.

The semi-quantitative analyses of the ESCA spectra of the polyacetylene samples examined are presented in tabular form (Tables 4.1 and 4.2). The intensities of the individual components of the C_{1s} envelopes are shown in Table 4.1. The curve fitting procedure, as described by Clark [1] and shown schematically in Table 1.5, used as a binding energy scale reference marker the F_{1s} signal at 688.7eV binding energy. Oxidation of the polyacetylene surface, whether plasma treated or not, leads to the formation of carbon singly bonded to oxygen and carbonyl functionalities, the former being consistently the most predominant of the oxidised species. There appears to be a low level of carboxyl functionality present on the surface of the polyacetylene film exposed to the atmosphere for $\sim$ 4 months.

Table 4.1 Relative intensities of C_{1s} core level peak components (Mg anode) for the polyacetylene samples studied. Figures in brackets indicate binding energies (eV).

Treatment/ Exposure to air	<u>C</u> - H	<u>C</u> - O	> <u>C</u> = O	<u>C</u>(=O)-O	<u>C</u>F_3	Tot C_{1s} - <u>C</u>-H - <u>C</u>F_3	FWHM (eV)	
	(284.1)				(292.7)		(<u>C</u>-H)	(<u>C</u>F_3)
Untreated	71.7	-	-	-	3.1	25.2	1.4	1.6
	(282.7) (284.6)	(286.4)	(288.0)					
+ 5.5 days	11.3 51.7	29.4	7.7	-	-	-	1.9	
	(283.1) (284.9)	(286.7)	(288.4)					
+ 36 days	11.3 54.9	25.0	8.8	-	-	-	1.9	

continued overleaf.....

Table 4.1 (continued)

	C - H	C - O	> C = O	O C O	CF_3	Tot C_{1s} - $CH-CF_3$	FWHM (eV) (C-H)	FWHM (eV) (CF_3)
Oxidised film	(284.8)	(286.5)	(288.3)	(289.6)				
Unbleached	47.7	36.6	13.0	2.7	-	-	1.9	
+ 15 mins TFAA					(293.7) 2.2			
Oxidised film	(284.9)	(286.6)	(288.4)	(289.8)				
Bleached	48.6	36.4	13.2	1.8	-	-	1.9	
+ 15 mins TFAA					(293.8) 2.4			

continued overleaf....

Table 4.1 (continued)

	C - H	C - O	> C = O	O C O	CF_3	Tot. C_{1s} - C-H - CF_3	FWHM (eV) (C-H)	FWHM (eV) (CF_3)
	(284.1)				(292.8)			
Untreated	71.7	-	-	-	3.1	25.2	1.4,	1.6
H. Plasma	(284.6)							
0.4W	89.1	-	-	-	-	10.9	1.6	
	(283.0) (284.6)	(286.2)	(287.8)					
5.5 Days	5.2 71.5	18.2	5.2	-	-	-	1.9	

continued overleaf.....

Table 4.1 (continued)

	C - H	C - O	> C = O	O=C-O	CF_3	Tot. C_{1s}- C-H - CF_3	FWHM (eV) (C-H)	FWHM (eV) (CF_3)
	(283.9)				(292.6)			
Untreated	61.8				2.4	35.8	1.4,	1.6
H. Plasma	(284.6)	(286.2)	(287.8)					
10W	86.5	11.3	2.2	-	-	-	1.6	
	(283.2) (285.0)	(286.7)	(288.3)				1.9	
+ 5.5 Days	8.8 70.4	14.8	5.9					
	(283.4) (285.2)	(286.9)	(288.6)				1.9	
+ 33 Days	10.4 68.7	13.7	7.2					
	(283.3) (285.3)	(287.0)	(288.7)				1.9	
+ 60 Days	19.1 64.0	12.8	4.1					

Table 4.2 Carbon, oxygen and fluorine atomic ratios at $Mg_{K\alpha}$ and $Ti_{K\alpha}$ sampling depths for the polyacetylene samples studied. Oxygen concentrations as derived from deconvoluted $Mg_{K\alpha}$ C_{1s} envelopes (see text) and absolute $Mg_{K\alpha}$ C_{1s} peak intensities are shown.

Treatment/ Exposure	Tot.	$Mg_{K\alpha}$		$Ti_{K\alpha}$		[Oxygen]	[Oxygen]	Abs.
	C_{1s}	O_{1s}	F_{1s}	O_{1s}	F_{1s}	C-O as -OH	C-O as C-O-C	C_{1s}
Untreated	100	3.0	5.3	6.3	9.9	-	-	100
5.5 Days	100	41.3	5.0	45.0	5.7	37.1	22.4	106.7
36 Days	100	43.4	3.6	41.9	4.5	33.8	21.3	97.7

continued overleaf.....

Table 4.2 (continued)

Treatment/ Exposure	Tot.	$Mg_{K\alpha}$		$Ti_{K\alpha}$		[Oxygen]	[Oxygen]	Abs.
	C_{1s}	O_{1s}	F_{1s}	O_{1s}	F_{1s}	C-O as -OH	C-O as C-O-C	C_{1s}
Oxidised film Unbleached	100	58.1	2.9	53.5	3.6	55.0	34.0	-
+15 mins TFAA	100	46.4	14.2	30.2	6.6	-	-	-
Oxidised film Bleached	100	51.7	1.9	57.0	0.9	53.2	33.0	-
+15 mins TFAA	100	55.9	15.5	36.4	7.2	-	-	-

continued overleaf.....

Table 4.2 (continued)

Treatment/ Exposure	Tot.	$Mg_{K\alpha}$		$Ti_{K\alpha}$		[Oxygen]	[Oxygen]	Abs.
	C_{1s}	O_{1s}	F_{1s}	O_{1s}	F_{1s}	C-O as -OH	C-O as C-O-C	C_{1s}
Untreated	100	2.2	1.7	-	-	-	-	100
H. Plasma 0.4W	100	4.4	1.1	3.4	3.3	-	-	100.6
5.5 Days	100	17.7	1.4	27.9	1.9	23.4	14.3	92.6

continued overleaf.....

Table4 .2 (continued)

Treatment/ Exposure	Tot.	$Mg_{K\alpha}$		$Ti_{K\alpha}$		[Oxygen]	[Oxygen]	Abs.
	C_{1s}	O_{1s}	F_{1s}	O_{1s}	F_{1s}	C-O as -OH	C-O as C-O-C	C_{1s}
Untreated	100	2.5	3.8	4.0	4.6	-	-	100
H Plasma 10W	100	8.9	3.9	5.3	4.7	13.5	7.9	93.6
5.5 Days	100	22.6	2.6	35.6	3.1	20.7	13.3	79.5
33 Days	100	27.6	2.4	35.0	4.9	20.9	14.1	75.7
60 Days	100	24.2	2.9	39.1	4.3	16.9	10.5	69.0

The validity of the method of energy referencing may now be assessed by consideration of carbon/oxygen stoichiometry data for the samples examined. Oxygen concentrations in the polyacetylene samples may be measured using two independent means. The most obvious route is via the O_{1s} core level itself, converting relative intensity into a carbon : oxygen atomic ratio using the appropriate sensitivity factor. Such data are given for both $Mg_{K\alpha}$ and $Ti_{K\alpha}$ x-ray sources in Table 4.2. The second approach is from analysis of the C_{1s} envelope alone. Two specific cases have been tabulated (Table 4.2), namely one where all the carbon singly bonded to oxygen takes the form of $\underline{C}$ - OH carbon, and the other which considers the $\underline{C}$ - O groups as ether (C - O - C) linkages. Comparison of the C_{1s} derived oxygen concentrations with those from the O_{1s} core level values would indicate a reasonably close correspondence between the data sets, taking $\underline{C}$ - O as $\underline{C}$ - OH. The presence of hydroperoxide carbon functional groups ($\underline{C}$ - OOH) would increase the C_{1s} derived oxygen concentration. A mixture of ether, alcohol and hydroperoxide functionalities may well be present. Thus the analyses lend some credence to the method of energy referencing adopted for this study.

Gibson and Pochan [190] propose that the air oxidation of polyacetylene at room temperature and in the absence of ultraviolet light involves the interaction of triplet oxygen with existing free radicals:

$$O_2 + R^{\bullet} \rightarrow ROO^{\bullet} \qquad (4.2a)$$

$$ROO^{\bullet} + RH \rightarrow ROOH + R^{\bullet} \qquad (4.2b)$$

$$ROOH \rightarrow >C{=}O + >CH(OH) \qquad (4.2c)$$

This reaction pathway would account for the observed transformations of the ESCA C_{1s} line shape.

Absolute intensity measurements of the $Mg_{K\alpha}C_{1s}$ envelopes indicate that the carbon atoms of polyacetylene become less closely packed on air oxidation in the surface regions at least (Table 4.1). The same is true for hydrogen plasma treatment of the freshly produced polyacetylene.

Alternative insights into the changes under consideration here come from the analysis of core levels other than C_{1s}, and from comparison of the $Mg_{K\alpha}$ and $Ti_{K\alpha}$ derived elemental analyses.

Low levels of fluorine and silicon were detected for each sample. The variation in intensity of these elements as measured by the F_{1s} and Si_{2p} core level spectra are shown in Figures 4.12 and 4.13 respectively. The level of fluorine as recorded by the more deeply probing titanium x-ray spectra is consistently slightly higher than is found nearer the surface using magnesium x-radiation. These findings suggest that the fluorine originates from within the bulk polymer itself rather than from external sources. This is quite reasonable. Figure 4.13 plots the Si_{2p} relative intensity data for $Mg_{K\alpha}$ spectra and shows how the silicon concentration increases with exposure time to the atmosphere. The 10W hydrogen plasma treated sample shows less surface silicon than the untreated polyacetylene upon contact with the air. The silicon concentration remains low throughout the experiment, reaching $\sim$3 atom percent relative to carbon even after prolonged exposure. These observations are consistent with a low level of sample contamination by silicone grease.

The variation of oxygen concentration with plasma treatment and contact with the atmosphere as monitored by $Mg_{K\alpha}$ and $Ti_{K\alpha}$ ESCA spectra are shown in graphical form in Figure 4.14. This provides a convenient means of assessing the depth to which oxidative attack occurs. A feature common to each sample, for both $Mg_{K\alpha}$ and $Ti_{K\alpha}$ spectra,

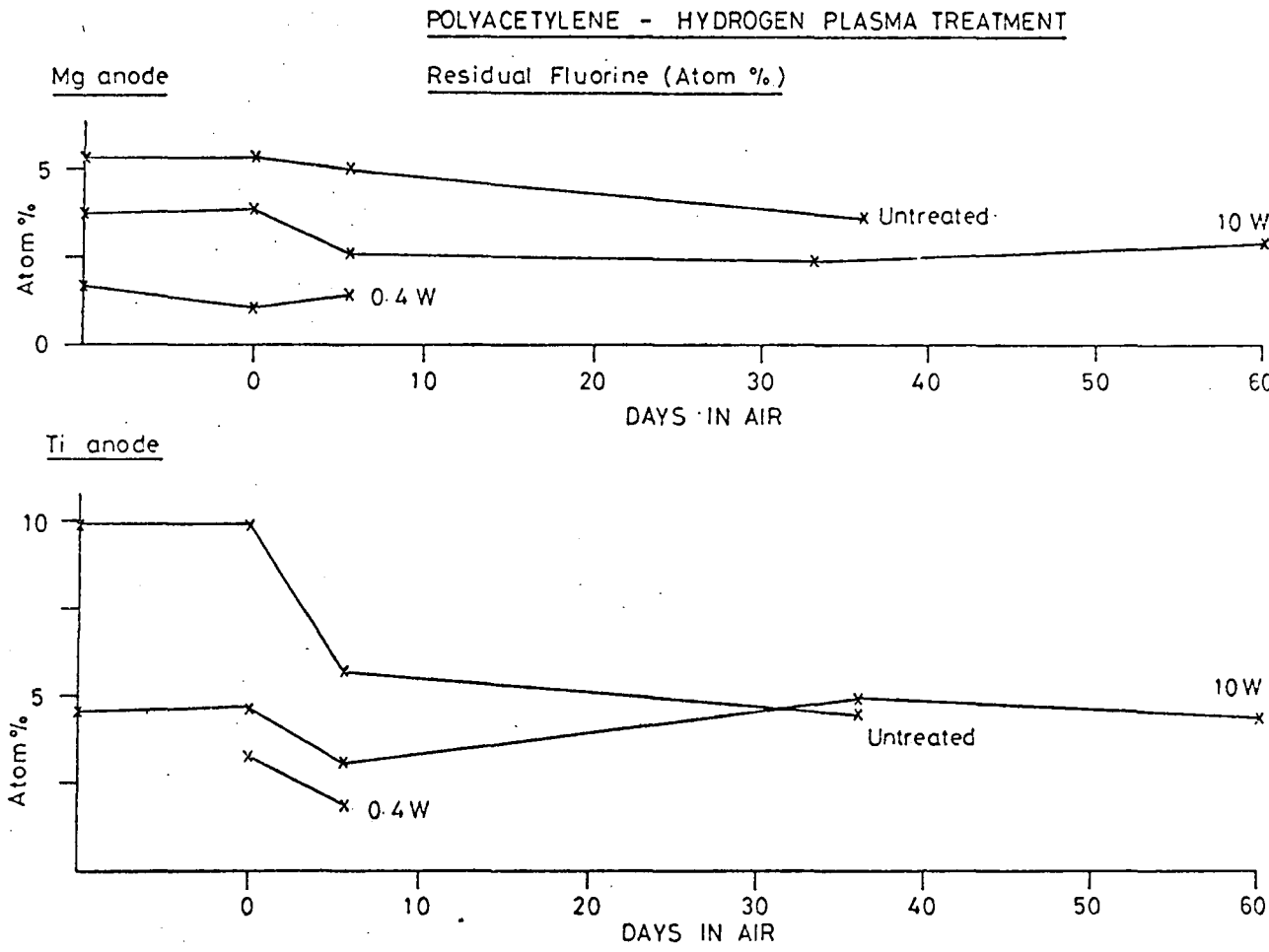

Figure 4.12 Fluorine concentrations (atom percent, relative to carbon) for the polyacetylene samples examined at both $Mg_{K\alpha}$ and $Ti_{K\alpha}$ sampling depths, ~45Å and ~130Å respectively.

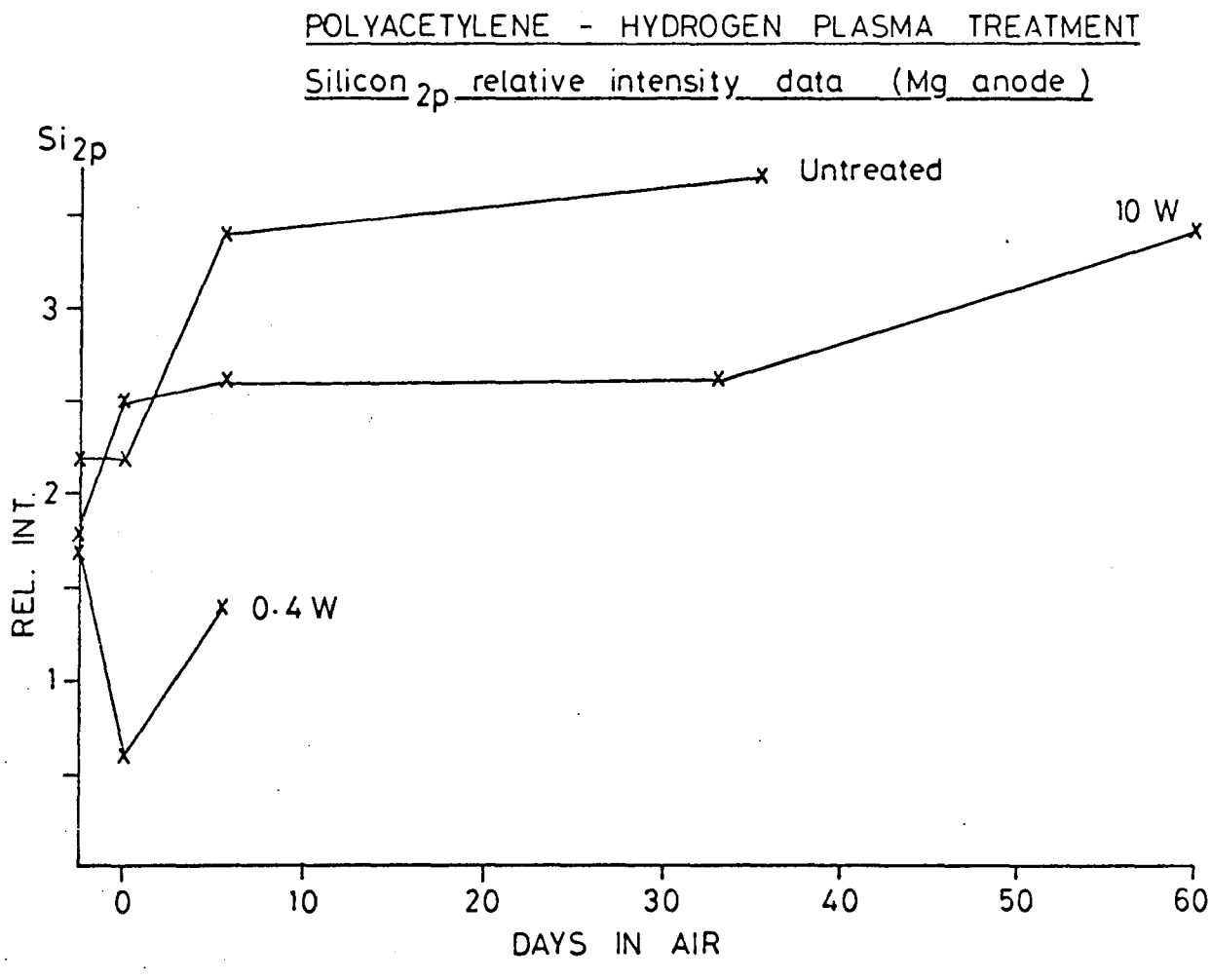

Figure 4.13 Silicon 2p relative intensity data (total C_{1s} taken as 100 units) for the polyacetylene samples examined using $Mg_{K\alpha}$ x-radiation.

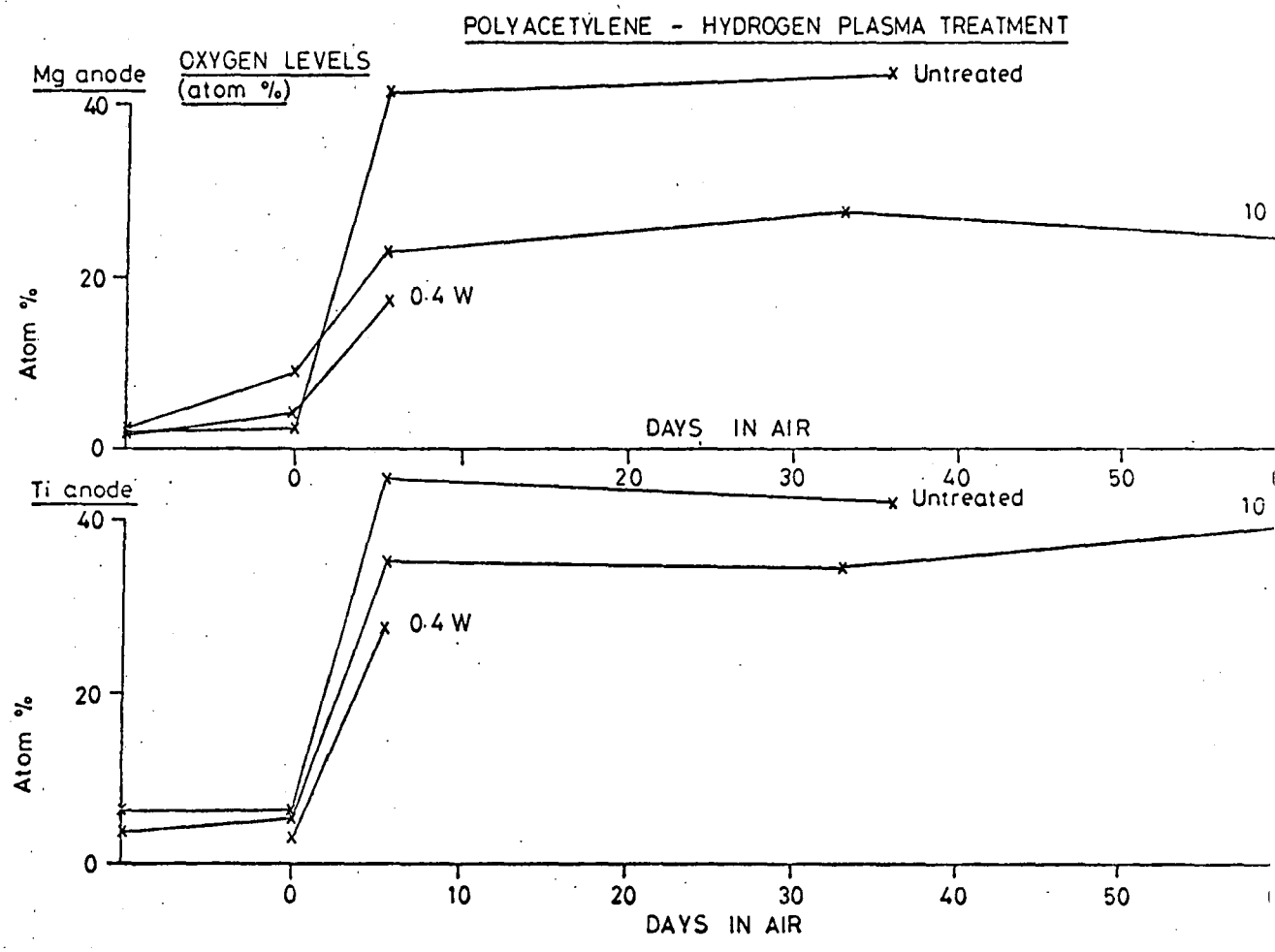

Figure 4.14 Oxygen concentrations (atom percent, relative to carbon) for the polyacetylene samples examined at both $Mg_{K\alpha}$ and $Ti_{K\alpha}$ sampling depths, ~45Å and ~130Å respectively.

regardless of whether hydrogen plasma pretreatment has been applied or not, is that the sample oxidation approaches an equilibrium concentration after 5½ days in the air. The effect of hydrogen plasma on the outermost ∿50Å of material, as followed by the $Mg_{K\alpha}$ spectra, is to render the polyacetylene less susceptible to oxidative attack. Hence for the pretreated sample the equilibrium C : O atomic ratio is ∿100 : 25, whilst the C : O atomic ratio for the exposed untreated polyacetylene is ∿100 : 43. The corresponding values for film exposed for ∿4 months average to ∿100 : 55. As a rough approximation therefore the hydrogen plasma pretreatment reduces subsequent oxidation by a factor of 2 at the $Mg_{K\alpha}$ sampling depth. The homogeneity of the oxidation of untreated polyacetylene is demonstrated by sampling the outermost ∿130Å of the film using the titanium x-ray source. For the plasma treated sample a different situation exists. The $Ti_{K\alpha}$ spectra reveal more extensive oxidation than was found for the more surface sensitive $Mg_{K\alpha}$ spectra. The level of oxidation at the $Ti_{K\alpha}$ sampling depth is nonetheless lower than for the untreated film.

A measure of the surface/bulk composition of polyacetylene film, untreated and exposed to air, and hydrogen plasma treated and exposed to air is displayed in Figure 4.15. The initial polyacetylene samples have a bulk (titanium) oxygen content higher than for the surface (magnesium). It must be realised that the figures plotted in Figure 4.15 are ratios of oxygen concentrations and are independent of the absolute magnitude of oxidation. There is an increase in the level of surface oxygen, relative to the bulk on hydrogen plasma treatment. This is most likely to arise from traces of oxygen present when the discharge is initiated. Upon contact with the air the plasma treated sample shows greater oxidation in the bulk than in the surface.

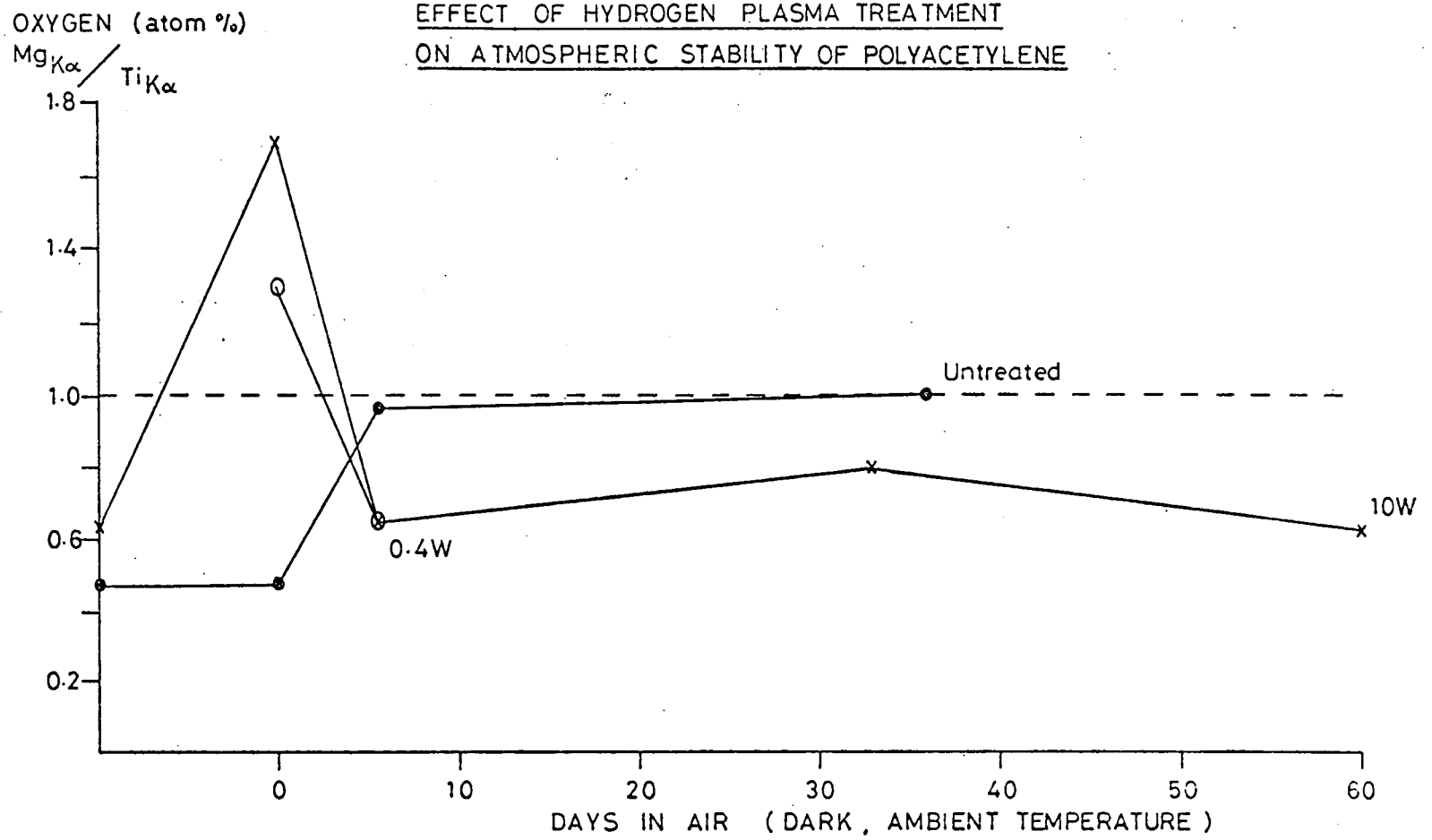

Figure 4.15 A measure of the surface/bulk composition of polyacetylene film, untreated and exposed to air, and hydrogen plasma treated and exposed to air.

N.B. Oxygen (atom %) Mg/Ti.

Value = 1 indicates surface and bulk composition the same
> 1 indicates higher surface oxygen concentration
< 1 indicates higher bulk oxygen concentration

This contrasts with the homogeneous oxidation of the untreated sample at least to the sampling depth of the ESCA experiment.

These results indicate that hydrogen plasma creates a thin surface overlayer of polyacetylene modified material which is more resistant to atmospheric attack than the untreated polyacetylene. The thickness of this overlayer is only in the region of a few tens of angstroms. Two possible explanations may account for the bulk oxidation phenomenon. Plasma treatments are recognised as effecting uniform continuous modifications. It is possible that handling of the polyacetylene coated probe tips using metal tweezers may have created flaws in the modified overlayers. Oxygen would then be able to penetrate the passive overlayer. Alternatively, the modified overlayer, although relatively unreactive towards oxidation itself, may have poor barrier characteristics towards oxygen. The passage of oxygen through the overlayer to the unmodified polyacetylene would be inhibited but not totally prevented and oxidation of the bulk would then be possible. The latter explanation receives some support from the literature. Galvin and Wnek, [214] in their studies of polyacetylene/polyethylene composites, report that the increase in stability of iodine-doped composites is marginal at best. This they ascribe to the poor oxygen barrier properties of polyethylene.

The plasma polymerisation of a suitable monomer to a controlled thickness, using the polyacetylene film as a substrate, may prove to be a valuable alternative.

4.4 Conclusions

The need for ultra-high vacuum conditions, certainly better than 10^{-6} - 10^{-7} torr, for the ESCA study of the role of oxygen in metathesis reactions has been demonstrated.

The in vacuo formation of polyacetylene film via the route of Edwards and Feast [188] has been monitored from a surface chemistry viewpoint.

The depth profiling ESCA investigation has confirmed that polyacetylene is prone to atmospheric oxidation. The oxidation of polyacetylene is homogeneous over the sampling depth of $\sim$ 130Å of the ESCA experiment employing titanium x-radiation. Oxidation leads to the formation of carbon singly bonded to oxygen and carbonyl surface functionalities. Carboxyl groups were detected at low concentration for polyacetylene exposed to air for a prolonged period ($\sim$ 4 months). These surface sensitive measurements agree with, and complement, previous findings from infrared spectrophotometry, [190] a bulk analytical technique.

The application of a mild surface treatment to polyacetylene film, prior to contact with the air, has been explored as a possible means of passification. The use of radiofrequency hydrogen plasma discharges has been reported. It has been shown that hydrogen plasma treatment does modify the surface of polyacetylene to produce an essentially hydrocarbon-like overlayer, possibly of a polyethylenic character. This overlayer is more resistant to atmospheric oxidation than the untreated polyacetylene. Oxidation of the material beneath the overlayer does occur. This may be due to poor oxygen barrier properties of the overlayer.

It is proposed that plasma polymerisation of a suitable monomer to a controlled thickness using the polyacetylene film as a substrate may produce a coating of a material with enhanced barrier properties.

Finally, this piece of work provides an excellent example of the analytical capabilities of the various information levels available in the ESCA experiment.

CHAPTER FIVE

ASPECTS OF THE SURFACE CHEMISTRY OF SOME NATURALLY OCCURRING CARBONACEOUS MATERIALS

CHAPTER FIVE

ASPECTS OF THE SURFACE CHEMISTRY OF SOME NATURALLY OCCURRING CARBONACEOUS MATERIALS

5.1 Introduction

Previous chapters in this thesis have concentrated on the surface chemistry of organic polymer systems of well characterised composition. In contrast the present chapter focusses on the ESCA analysis of naturally occurring carbonaceous materials, with a particular emphasis being placed on the study of coal.

Recent years have witnessed a surge in research endeavours towards a better understanding of structure/reactivity relationships of fossil fuels in general.[228,229] Special interest is being paid to the potential of coal and oil shale as workable alternatives to the oil and natural gas fossil fuels, today's major energy sources.

Coal, an inhomogeneous organic rock, is a complex substance.[230] As described by Hunt,[231] coal is 'a readily combustible rock containing more than 50 percent by weight, and more than 70 percent by volume of organic material formed from the compaction or induration of variously altered plant remains.' As such it has an organic and an inorganic structure. It is also a porous rock and has an associated physical structure. Both the chemical and physical characteristics of coal are therefore factors which determine the reactivity of coal and hence its suitability as feedstock for combustion, carbonification, pyrolysis, gasification and liquefaction processes.[230]

The very nature of coal poses difficulties for the analyst. Over the last few years considerable advances in analytical, and especially spectroscopic, techniques have been made, and there is now

an armoury of sophisticated instrumental probes [232] available to the coal scientist in addition to wet chemical approaches. [229] Particular interest is being received by those techniques which are capable of providing structural information on the material as studied in its solid state, with minimal sample preparation requirements. Rouxhet et al. [233] have reviewed the use of infrared spectroscopy to study solid coals, kerogens and humic substances, whilst Kuehn et al. [234] have applied Fourier transform infrared techniques, as described by Painter and Coleman [235] in coal characterisation studies. The development of solid state magnetic resonance techniques holds considerable promise for the analysis of fossil fuel energy problems. [229,236]

The availability of these modern analytical tools does not in itself lead to a better understanding of structure/property relationships applicable to coal utilisation. Standardised methods of coal sampling, handling and storage are being adopted, and the availability of 'standard' reference coal samples through coal banks will facilitate the comparison of experimental results from different laboratories. [239] The analysis of individual components of a whole coal sample, obtainable from coal maceral separation techniques, [240] adds a further dimension to coal characterisation.

Recent reports [230,239] into basic coal sciences research present critical surveys of the present-day philosophy and methodology used in the elucidation of the structure and characteristics of coals and coal-related materials, including oil shales. Gorbaty [230] has emphasised the scope of modern surface characterisation techniques in the investigation of the mechanism(s) involved in gasification, and in the catalysis of coal liquefaction and hydrocarbon synthesis.

This is entirely reasonable in view of the fundamental role which the interaction of the solid coal with the immediate environment does play in aspects of coal utilisation. [241]

Since the introduction of commercially available instrumentation in the early 1970s ESCA has become recognised by both academia and industry as a powerful analytical tool for the investigation of the surface structure, bonding and reactivity of solid materials. However, comparatively few ESCA studies have been reported relating to geochemical samples, [169,242-252] and to coal science [169,246-252] in particular. Previous work has been reviewed by Wilson [169] and by Perry and Grint. [253] Early studies concentrated on the analysis of organic oxygen and organic sulphur. [246] Difficulties were encountered due to the presence of mineral matter which contributed to both the total oxygen (e.g. silicates) and total sulphur (e.g. inorganic sulphates and iron pyrites, FeS_2) photoionisation line shapes. Furthermore the need for energy referencing to allow for sample charging effects (especially manifest in spectra of insulating samples, see Section 1.5) was not always recognised.

Other ESCA studies have focussed on coal carbonisation, [253] analysis of coal ash [254] and airborne particulates. [246]

More recently the nature of nitrogen and sulphur species present in coal, [249] and the changes in surface oxygen on carbonisation and thermal oxidation in air, relative to the untreated coals, have been the subjects of ESCA investigations. [250-2]

Brown and co-workers [247] analysed four North American coals and their ash, the main emphasis being a comparison of trace element analysis by ESCA and by spark source mass spectrometry.

Cheung [255] has discussed the effect of the polynuclear aromatic ring content of coals on the C_{1s} lineshape. It is claimed

that a simple C_{1s} lineshape analysis provides a measure of the fraction of carbon present in polynuclear aromatic rings. However, no allowance has been made for the contribution of oxygen bonded to carbon functionalities to the overall C_{1s} envelope.

Previous research by Clark and co-workers has provided a wealth of information on the characterisation and reactivity of organic, biological and polymeric systems.[1,132,140,143,160,256-8] Wilson[169,248] has recently applied this expertise to the analysis of materials of interest to the organic geochemist. The aims of these initial investigations of a set of geochemical materials, which comprised brown coal, kerogens and bitumens, were: first, to probe the nature of the chemical bonding within the solid network (would ESCA be able to detect differences in functional group distribution for these related complex materials, for example?); and second, to relate ESCA-derived surface elemental stoichiometric data with bulk elemental analysis using standard microanalytical techniques.

The results of these preliminary investigations have prompted further research, and it is these latest findings which will be presented here. The material to be reported will illustrate the suitability of ESCA to study coal, kerogen and bitumen, not only in their unaltered form, but also after modification, either naturally occurring, as effected through thermal alteration and by weathering processes, or artificially induced, as exemplified by ultraviolet light oxidation reactions. Where appropriate the ESCA results will be supplemented by results from other analytical techniques.

No attempt has been made to review the voluminous literature of coal science. An introduction to the organic geochemistry of coal, bitumen and kerogen has been given by Wilson.[169] Throughout this work reference has been made to several of the texts on the science and technology of coal and related materials.[231,233,259-264]

5.2 Experimental

5.2.1 Samples

The origins of the materials examined in this chapter are as follows:

1) Specimens of torbanite (Bathgate, Lothian, U.K.), vitrinite Babbington, Nottingham, U.K.), Kimmeridge kerogen (Kimmeridge Bay, Dorset, U.K., a type II kerogen) and brown coal (Miocene Age, Indonesia) were donated by Dr A.G. Douglas, University of Newcastle-upon-Tyne, U.K.).

2) Naturally occurring bitumens, Gilsonite (Eocene, Uinta Basin, Utah, U.S.A.), Grahamite (Sardis, Oklaham, U.S.A.) and Wurtzilite (Ranger Station Mine, U.S.A.) were received from Dr J.M. Hunt, Woods Hole Oceanographic Institution, Woods Hole, Massachusetts, U.S.A. Gilsonite 'selects' (a commercial grade originating from the interior of a Gilsonite vein) was provided by Morris Ashby, U.S.A.

3) A series of coal samples from the Lower Kittanning seam in Ohio and Pennsylvania, U.S.A. were obtained in sealed, dark glass sample bottles direct from Professor P.H. Given, Pennsylvania State University, P.A., U.S.A. Table 5.1 lists the origins of these coals together with some details of their characteristics. A full description of the nature, collection and storage of these samples is to be found elsewhere. Elemental analyses were performed at Pennsylvania State University according to the following standard methods [306,318]: carbon and hydrogen, ASTM D-3178; nitrogen, ASTM D-3179; sulphur, ASTM D-2492

Table 5.1 Lower Kittanning Seam coal. Origin carbon, sulphur, mineral matter (MM) and FeS_2 content and vitrinite reflectance - mean max. ($\bar{R}_{max}$).

PSOC No.	County	%C (dmmf)†	%C (dry)	%S (dry)	%MM (% FeS_2)	$\bar{R}_{max}$.
308*	Vinton	80.2	69.4	4.3 (4.1)/	13.5 (6.0)	0.47
322	Somerset	84.6	70.2	1.5 (1.9)	14.8 (6.1)	1.34
755*	Tuscarawas	82.4	70.2	5.7 (5.9)	14.8 (6.1)	0.58
1010	Fayette	87.9	70.2	3.3 (5.2)	20.1 (4.6)	1.11
1011	Jefferson	86.9	68.4	2.5 (3.3)	21.3 (3.2)	0.92
1017	Armstrong	84.5	69.1	3.7 (3.5)	18.2 (3.7)	0.79
1024	Centre	88.9	76.7	0.9 (1.1)	13.8 (0.1)	1.31
1025	Centre	89.3	75.8	3.9 (5.7)	15.2 (5.6)	1.23
1133	Cambria	90.7	70.5	1.5 (1.2)	22.3 (2.3)	1.55

† dmmf = dry mineral matter free basis
* denotes coal from Ohio, otherwise Pennsylvania is the State of origin.
/ figure in bracket denotes % S as analysed in Durham [327]

(total sulphur using a Leco induction furnace); oxygen, by difference (cf. ASTM D-3176).

4) Anthracite, Pumpquart Vein, Cynheidre Colliery, South Wales, and Oxfordshire coal (NCB No. 88205, depth of burial 952m), of Westphalian 'D' age (Tenuis Chronozone) were supplied by Mr G.J. Liposits, National Coal Board, Denaby Main, Doncaster, South Yorkshire, U.K.

5) Heat altered coal was collected by permission of the National Coal Board from Togston open cast site, Northumberland, U.K.

6) Oriented graphite (basal plane and prismatic edge) was purchased from Union Carbide.

7) Manufacturers/suppliers of the polymer samples used here are as follows: Nylon-6,6 and polydiphenyl siloxane, Cellomer Associates; polyethylene terephthalate, 'Mylar' film, Dr T. Kent, Home Office (PSDB); polyphenylene sulphide, 'Ryton', Phillips Chemical Company.

8) The ferrous sulphide used was of a technical grade.

9) Illinois No. 6 and Rawhide coal samples were provided by Dr M.L. Gorbaty, Exxon Research and Engineering Company, Linden, New Jersey, U.S.A.

A key to the location of results for each particular material is provided in Table 5.2.

Table 5.2 Location of results for each material

Material	Section															
	531	532a	532b	533	534	535	536	537b	537c	537d	537e	537f	538a	538b	538c	539
Acklington Dyke Coal							X									X
Anthracite					X	X				X	X				X	X
Brown Coal	X	X	X		X	X			X		X					X
Ferrous Sulphide												X				
Gilsonite	X	X						X								
Grahamite	X															
Graphite					X	X				X						
Illinois No. 6 Coal													X	X	X	
Kimmeridge Kerogen	X											X				
Lower Kittanning Coal				X	X	X										X
Nylon-6,6			X													
Oxfordshire Coal									X		X					
Polydiphenyl Siloxane			X													
Polyethylene Terephthalate			X													
Polyphenylene Sulphide												X				
Rawhide Coal													X	X	X	
Torbanite	X															
Vitrinite	X															
Wurtzilite	X															

5.2.2 Sample Preparation

The samples were prepared for ESCA analysis by grinding a portion of the material to a fine powder using a pestle and mortar. The freshly powdered sample was mounted on the spectrometer probe tip by means of double-sided adhesive Scotch insulating tape.

In the case of the analysis of bitumen fracture surfaces the solid samples were cleaved using a scalpel blade and mounted on the spectrometer probe tip in the usual way.

5.2.3 UV Irradiation

A Rayonet preparative photochemical reactor, Model RPR-208, total output 120 watts 254 nm ultra-violet energy, was used for the irradiation of the geochemical samples. All irradiations were performed in an air environment. A freshly powdered sample, mounted on a spectrometer probe tip, was suspended on thread in the centre of the reaction chamber. A cooling fan, integral to the reactor, established an equilibrium reaction temperature of $\sim 30^{o}C$ within the first 30 minutes of irradiation. Each sample was analysed for changes in surface composition immediately after treatment.

5.2.4 Natural Weathering

Freshly prepared samples, as described above, were placed outdoors in a south facing aspect at $\sim 60^{o}$ to the horizontal, and allowed to weather for one week in Durham during the periods 6th - 13th August 1983, and 19th - 26th October 1983. Records of the climatic conditions prevailing during these time intervals have been made available by Dr Ray Harris, Department of Geography, University of Durham. These details are to be presented in the discussion section of this chapter.

5.2.5 ESCA Analysis

The ESCA spectra were recorded using either an AEI ES200B or Kratos ES300 spectrometer operating at typically 12kV and 15mA, and 12kV and 11mA respectively using $Mg_{K\alpha_{1,2}}$ x-radiation and with a base pressure of $\sim 5 \times 10^{-8}$ torr. Under the experimental conditions employed for the magnesium anode, the gold $4f_{7/2}$ level (at 84eV binding energy) used for calibration purposes had a full width at half maximum height (FWHM) of $\sim$ 1.15eV. The ES300 has a higher energy photon source ($Ti_{K\alpha_{1,2}}$, $h\nu$ = 4510eV) which typically samples the outermost $\sim$ 130 Å of a solid (compared with $\sim$ 50 Å for the $Mg_{K\alpha_{1,2}}$ x-rays), thereby allowing a means of non-destructive depth profiling. The titanium anode was operated at 13.5kV and 18mA.

A complete ESCA analysis took in the region of 2 - 3 hours to complete; the core level spectra of the elements carbon, oxygen, nitrogen and sulphur were recorded in typically one hour, depending on the intensity of the respective photoionisation signals. Radiation damage to the sample from long-term exposure to the X-ray beam was not evident.

Deconvolution and area ratios were determined, in the case of the ES200B spectra, using a Dupont 310 analogue curve resolver as described by Clark[1]; the ES300 spectrometer is equipped with a Kratos DS300 data acquisition/manipulation system. The accuracy of measurement is of the order of $\sim$ 5%.

5.2.6 Elemental Analysis

Except where stated otherwise, the elemental analyses of the coal samples involved in this work have been performed by the specialist laboratories of the following organisations:- Pennsylvania State University, U.S.A. (Lower Kittanning Seam coal); National Coal Board,

U.K. (Acklington Dyke heat altered coal); Linden, New Jersey, U.S.A. (Illinois No. 6 and Rawhide coals).

5.2.7 Optical Microscopy [263,286]

5.2.7a Sample Preparation

Samples were mounted as particulate blocks in synthetic resin. The blocks were prepared for reflectance measurements by a widely used and standard procedure, namely grinding on a diamond lap to produce a flat, then grinding on two grades (200 and 400) of wet silicon carbide paper until the surface was matt, but scratch free, followed by successive polishing stages with three grades of alumina (5/20, 3/50, and 'gamma') dispersed on wet, Selvyt-covered, brass laps.

5.2.7b Optical Measurements

Reflectance measurements were made at 546nm using a Zeiss standard universal reflected light microscope, attached to either an EMI 6094b or EMI9844b photomultiplier. Samples were measured using a Berek prism and oil immersion(oil, $n_{546nm} \sim 1.520$), at magnification x 500. An aperture size of $\sim$ 10μm was used. Measurements were recorded on Philips PM8220 or PM8251 single pen chart recorders possessing 10-mV full-scale deflection. The reflectance measurements were determined by comparison against standards of known optical properties. In the case of unaltered coal an isotropic glass standard (reflectance (oil, 546nm) = 0.4532%), whereas a diamond standard(reflectance (oil, 546nm) = 5.233%) was used for reflectance measurements of the natural coke samples. Further details are to be found elsewhere.[263,286]

5.2.8 X-ray Diffraction

Each sample (72μm mesh) was prepared using a smear mount technique, mounting the sample onto a glass slide with acetone. Charts were recorded using a Philips PW1130 3 kilowatt generator/diffractometer assembly using $Co_{K\alpha}$ radiation. The goniometer scan speed was 1^{o} of 2θ/min and chart speed of 100mm/min. Goniometer slits were set at 2^{o}, 0.2^{o}, 2^{o}.

5.2.9 Solid-state ^{13}C n.m.r.

Samples of coal and natural coke from the Togston open cast site, Northumberland, U.K. have been analysed by Dr P.J. Stephenson in the laboratories of Professor C.A. Fife (Guelph-Waterloo Centre for Graduate Work in Chemistry, University of Guelph, Ontario, Canada). The solid-state ^{13}C spectra were obtained at 22.6MHz on a Bruker CXP-100 spectrometer, described elsewhere.[319] The techniques of magic angle spinning (MAS), which is used to remove chemical shift anistropy, and high-power dipolar decoupling, which removes the ^{13}C-^{1}H dipolar interactions, were employed. Chemical shifts were referenced as parts per million (ppm) from external hexamethyldisiloxane (HMDS) whose chemical shift is assumed to be -2.1 ppm from tetramethylsilane (TMS).

5.2.10 Incoherent Inelastic Neutron Scattering (IINS) Spectroscopy

The IINS spectra presented in this chapter have been recorded by Ms J. Nichol (University of Durham) using a beryllium filter spectrometer of the neutron beam facility at Harwell.

5.3 Results and Discussion

5.3.1 Core level Spectra

As an introduction to the nature of the information levels in the ESCA experiment applied to geochemical materials, it is worthwhile reviewing some of the earlier work by Wilson.[169,248] Figure 5.1 shows the core level signals for the C_{1s}, O_{1s}, N_{1s} and S_{2p} levels for Gilsonite 'selects', Kimmeridge kerogen, vitrinite and brown coal. Visual inspection reveals the striking differences in surface chemistry in respect of nitrogen, oxygen and sulphur functionalities.

Perhaps the most striking feature arises from the comparatively high concentration of sulphur in Kimmeridge kerogen. Here ESCA distinguishes between sulphur present in at least two oxidation states, as identified by their absolute binding energies as sulphur in +2 and +6 oxidation states, the latter component occurring at higher binding energy.[207] This contrasts with the case for vitrinite concentrate where the sulphur level is much lower and exists almost exclusively in an unoxidised form as organic sulphide. Sulphur was not detected in the ESCA spectrum of brown coal.

Recently the ESCA spectra of two naturally occurring bitumens, Grahamite and Wurtzilite have been run (supplementary to the earlier study of Gilsonites).[169,248] The results for the Grahamite sample will be presented later in this section. All three types of bitumen show essentially hydrocarbon-like C_{1s} line shapes (cf. Figure 5.1). Differences do exist for the S_{2p} envelopes as shown in Figures 5.1 and 5.2, and these reflect differences in the distribution of sulphur functionalities for the three bitumens. The sample of Gilsonite 'selects' has the lowest sulphur content, the carbon to sulphur atomic ratio being 100 : 0.2, whilst the respective values for Grahamite and

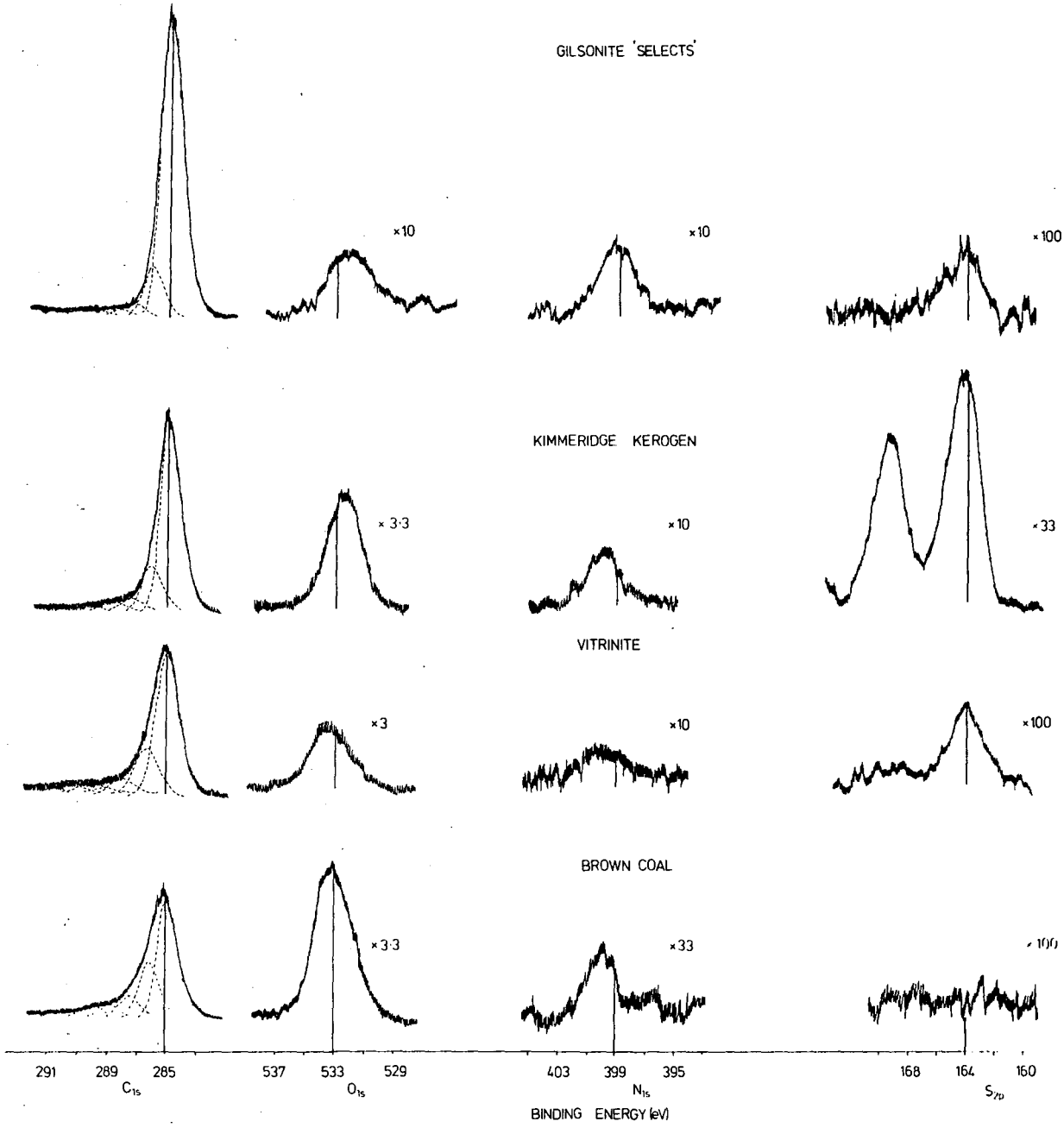

Figure 5.1 C_{1s}, O_{1s}, N_{1s} and S_{2p} core level signals for 'Gilsonite' selects, Kimmeridge kerogen, vitrinite and brown coal.

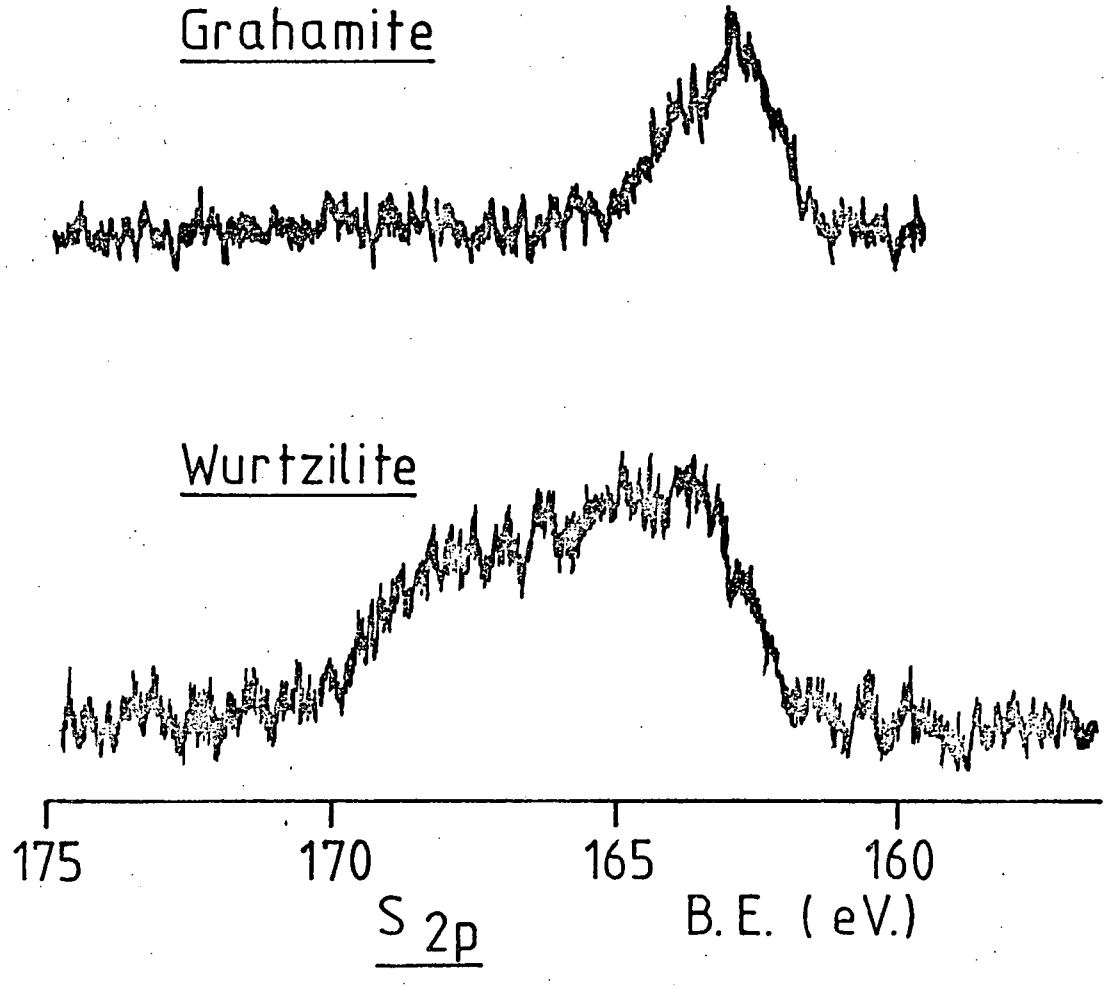

Figure 5 .2 S_{2p} core level signals for Wurtzilite and Grahamite.

Wurtzilite are 100 : 0.6 and 100 : 1.7. Both Gilsonite and Grahamite S_{2p} envelopes show that sulphur exists primarily in the unoxidised form. Wurtzilite however gives a markedly different S_{2p} envelope which is much broader than has been observed in previous (or indeed present) ESCA studies of geochemical materials performed in Durham . Stretching from ∿ 163 -∿170 eV binding energy, the peak is thought to arise from sulphur in several chemical environments,[207] such as sulphide, oxidised sulphur types and elemental sulphur. [231]

Deconvolution of the C_{1s} photoionisation envelopes reveals component peaks to the high binding energy side of a predominant hydrocarbon component at 285 eV binding energy. These peaks are characteristic of functionalised carbon, and from extensive characterisation of simple model compounds [58,59] the following assignments can be made: C-N 286.0 eV, C-O 286.6 eV, C=O 288.0 eV and $\underline{C}^{=O}_{-O}$ 289.2 eV. There may also be a contribution to this high binding energy shoulder arising from shake-up satellites associated with conjugated structures. [143]

Relative area ratios may be used to quantify surface chemistry. Whilst the O_{1s} core level signal will consist of contributions from both the organic and mineral phases, [207] it is possible to derive ESCA organic oxygen concentrations. A method adopted previously [169,252] is to subtract mineral oxygen away from the total oxygen, taking the mineral oxygen to be bound with silicon and aluminium as SiO_2 and Al_2O_3 respectively. This method does not take into account inorganic oxygen bound in the form of sulphate for example.

The ability of ESCA to monitor demineralisation procedures, such as are commonly employed in kerogen isolation from sediments,[304] is illustrated in Figure 5.3 which shows wide scan (1200 eV) spectra of torbanite, before and after wet chemical demineralisation. The untreated torbanite spectrum is dominated by the O_{1s} photoelectron signal.

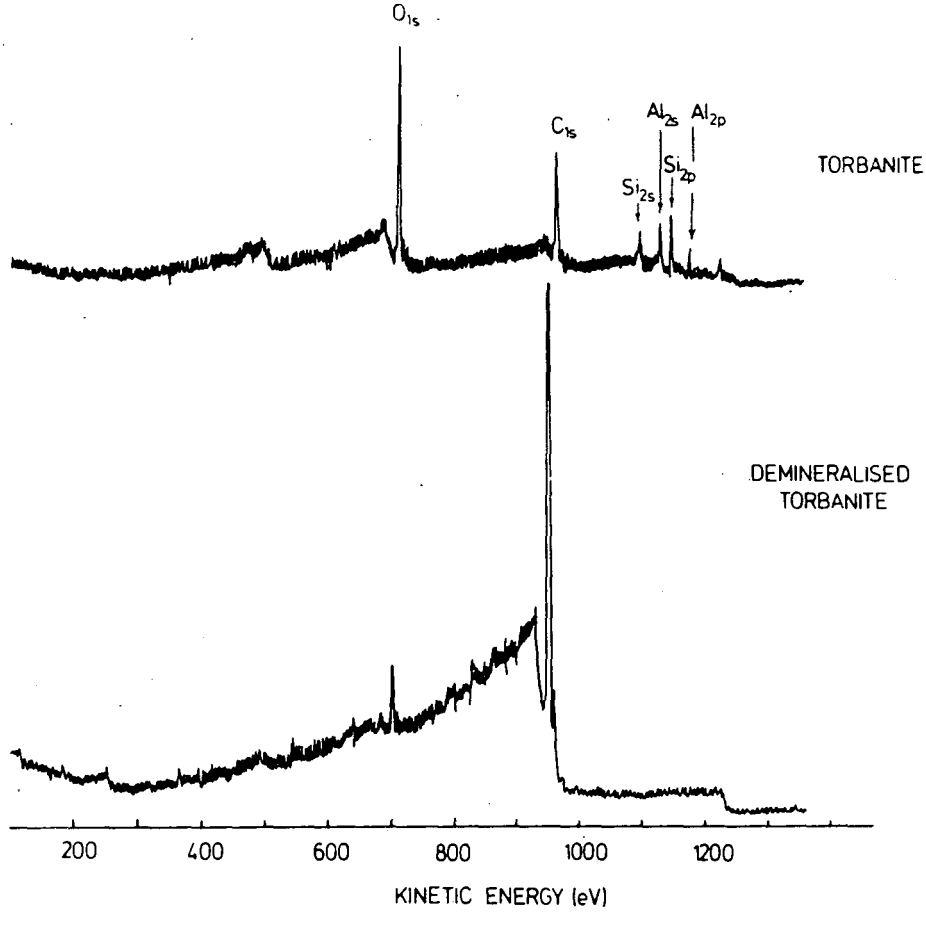

Figure 5.3 ESCA wide scan spectra of untreated and demineralised torbanite

Contributions from the silicon and aluminium component of the mineral matrix are clearly evident. This is in contrast to the spectrum for demineralised torbanite in which the C_{1s} peak predominates over a greatly reduced O_{1s} component, corresponding almost exclusively to organic oxygen: the silicon and aluminium are not visible at the sensitivity at which the spectrum was recorded.

The surface sensitivity of ESCA is such that the fracture surface composition of cleaved Grahamite bitumen has been studied. Hence low levels of silicon (Si_{2p} 104.8eV) and aluminium (Al_{2p} 76.3eV) were clearly discernible whereas the ESCA spectrum of the powdered Grahamite detected no mineral content. The elemental composition of the fracture surface, as determined by ESCA, is $C_{100}\ N_{1.3}\ O_{5.5}\ S_{0.6}\ Si_{0.3}\ Al_{0.3}$, and this shows an expected enrichment of surface (mineral) oxygen over the composition of $C_{100}\ N_{1.3}\ O_{4.6}\ S_{0.6}$ for the powdered (bulk) material.

5.3.2 Semiquantitative ESCA analysis

5.3.2a Previous work [248]

Consideration of the relative intensities of the individual photoionisation peaks for the elements carbon, nitrogen, oxygen and sulphur allows elemental stoichiometric data to be acquired. Hence an insight into the overall elemental composition at the ESCA sampling depth may be ascertained. This is an area which has received attention by Wilson and comparison has been made of ESCA derived elemental stoichiometries with figures derived from conventional analytical techniques. Although good agreement between the different analytical methods was found in the case of a series of Gilsonite samples, there were some discrepancies for the other materials examined. This was particularly true for the brown coal analyses.

It was thought likely that differences in the homogeneity of the samples would be a contributing factor, the naturally occurring bitumen samples being more homogeneous than brown coal. A more detailed investigation has since been performed and appears in the literature. [248] To put perspective on this recent assessment, the previous analyses are reproduced in Tables 5.3 to 5.5.

Table 5.3 Elemental analyses and overall stoichiometric data for a series of Gilsonite samples. [248]

Material	Elemental analyses (wt.%)					Overall stoichiometry				
	C	H	N	O	S	C	H	N	O	S
Gilsonite "selects"	(84.25)	(12.38)	(2.84)	—	(0.61)	(100)	(176.3)	(2.89)	—	(0.27)
ES *200*	82.57	—	2.75	1.99	0.38	100	—	2.86	1.74	0.17
ES *300*	82.13	—	2.47	2.46	0.55	100	—	2.58	2.25	0.25
Chepeta vein	(82.98)	(11.09)	(2.38)	(3.05)	0.50	(100)	(160.4)	(2.46)	(2.76)	(0.23)
	82.23	—	1.72	4.5	0.46	100	—	1.79	4.10	0.21
Cowboy vein	(83.24)	(11.21)	(1.00)	(3.7)	(0.85)	(100)	(161.6)	(1.03)	(3.33)	(0.38)
	82.59	—	1.42	3.94	0.84	100	—	1.47	3.58	0.38
Neil vein	(83.09)	(11.11)	(1.93)	(3.35)	(0.52)	(100)	(160.5)	(1.99)	(3.02)	(0.23)
	80.31	—	2.99	5.67	—	100	—	3.19	5.30	—
Hard gilsonite*	(81.39)	(11.07)	(2.47)	(4.53)	(0.54)	(100)	(163.2)	(2.60)	(4.17)	(0.25)
	79.01	—	3.75	5.59	0.58	100	—	4.07	5.31	0.27
Gusher vein	(86.02)	(11.29)	(2.23)	—	(0.49)	(100)	(157.5)	(2.22)	—	(0.21)
(Weathered gilsonite)	81.10	—	2.78	4.09	0.74	100	—	2.94	3.78	0.34

N.B. ESCA results were obtained using the ES *200* instrumentation unless otherwise specified.
Microanalytical results in parentheses.
*Details relating to the precise origin of this sample are not available.

Table 5.4 Elemental analyses and overal stoichiometric data for a series of geochemical samples (microanalytical results in parentheses).[248]

Material	Elemental analysis (wt.%)					Overall stoichiometry				
	C	H	N	O	S	C	H	N	O	S
Untreated torbanite*[1]	(56.02) 39.80	(7.86) —	(1.55) 0.58	(34.06) 51.76	(0.51) —	(100) 100	(168.4) —	(2.37) 1.26	(45.60) 97.56	(0.34) —
Demineralised torbanite*[1]	(81.87) 79.13	(11.25) —	(1.41) 1.62	(4.64) 7.22	(0.83) 0.78	(100) 100	(164.90) —	(1.43) 1.76	(4.25) 6.84	(0.38) 0.37
Kimmeridge kerogen*[1]	(57.09) 72.46	(6.37) —	(1.85) 2.20	(23.49) 9.33	(11.2) 9.63.	(100) 100	(133.89) —	(2.78) 2.60	(30.86) 9.66	(7.34) 4.98
Vitrinite*[1]	(74.0) 79.06	(5.2) —	(1.6) 2.32	(18.6) 12.52	(0.64) 0.89	(100) 100	(84.32) —	(1.85) 2.52	(18.85) 11.88	(0.32) 0.42
Brown coal*[2]	(53.59) 69.41	(5.29) —	(0.88) 1.02	(40.24) 25.83	(0.42) —	(100) 100	(118.93) —	(1.40) 1.26	(56.43) 27.9	(0.33) —
ES *300*	69.17	—	0.96	29.87	—	100	—	1.19	32.39	—

N.B. ES *200* spectrometer used for all ESCA measurements, except where stated otherwise. Mineral components not taken into consideration.

*[1] No residual ash detected upon combustion.

*[2] Denotes averaged value

Table 5.5 Microanalysis of Gilsonite 'selects'

Analysis centre	Elemental composition (wt.%)					Overall stoichiometry				
	C	H	N	S*[1]	O	C	H	N	S	O
Durham	82.68	12.72	3.51	(0.62)	0.48	100	184.60	3.64	(0.28)	0.44
	83.35	12.61	2.45	(0.59)	0.98	100	181.55	2.52	(0.27)	0.88
	82.51	13.26	2.84		0.78	100	192.85	2.95		0.71
	84.20	12.20	3.06		0.54	100	173.87	3.12		0.48
	84.18	12.75	2.80		-0.34	100	173.91	2.88		
	83.98	12.92	2.58		-0.09	100	184.60	2.63		
	84.08	12.61	2.72		-0.02	100	179.97	2.77		
	83.10	12.47	2.60		1.22	100	180.07	2.68		1.10
	84.90	13.10	2.73		-1.34	100	185.16	2.76		
	84.65	12.63	2.56		-0.45	100	179.04	2.59		
*[2]	85.32	11.71	3.02		-0.66	100	164.70	3.03		
*[2]	85.06	12.00	3.20		-0.87	100	169.29	3.22		
Bristol	86.16	11.09	2.88		-0.74	100	154.46	2.87		
	85.34	11.22	2.81		0.02	100	157.77	2.82		0.02
Mean, $\bar{x}$	84.25	12.38	2.84	(0.61)		100	175.85	2.89		0.61
Standard deviation, σ	1.07	0.66	0.28				10.97	0.29		0.38
σ as % of $\bar{x}$	1.27	5.33	9.86				6.24	10.16		62.58

*[1] Sulphur analysis performed on two samples only. Averaged value included in calculation of oxygen by difference.

*[2] Measurements recorded prior to refurbishing of elemental analyser instrumentation.

5.3.2b Comparison of brown coal elemental analytical data

In order to check the reproducibility of the ESCA-derived atomic ratios, comparison has been made of relative and absolute peak area measurement using two homogeneous polymeric materials in thin film form (Nylon 6,6 and polyethylene terephthalate (PET)) of well defined surface composition, together with brown coal. Powdered polydiphenyl siloxane has also been included as an intermediate homogeneous powdered material. The ES300 spectrometer, equipped with DS300 data system, was used for this work.

Two independent factors which are likely to affect the reproducibility of ESCA results have been considered, namely sample-to-sample variation due to inhomogeneity, and the reproducibility with which the photoionisation signal can be distinguished from the background count rate. Estimation of the likely contributions made by these distinct factors has been carried out: first, by analysing ten samples of each material; and second, by performing ten peak area measurements per core level for one particular set of ESCA results, chosen at random, for each of the four materials. The results shown in Table 5.6 give the average relative peak areas, $\bar{x}$, of the core level peak (the total C_{1s} peak area being taken as 100 units), the standard deviation, σ, and the standard deviation expressed as a percentage of the mean value.

Comparison of the data for sample-to-sample variation for brown coal with the figures for the polymer samples would suggest that the scatter of the data points for brown coal arises primarily from sample inhomogeneity. Upon consideration of the variation due to peak area measurement, this is indeed found to be the case for the O_{1s} and Si_{2p} core level signals. For the N_{1s} peak however, the scatter in data points can be attributed, almost exclusively, to errors involved

Table 5.6 Reproducibility of ESCA relative intensity measurements.

(ES300 spectrometer equipped with DS300 data system)

	Polyethylene terephthalate film (C_{100} O_{40}).			
	Relative Intensity		Absolute Intensity	
	C_{1s}	O_{1s}	C_{1s}	O_{1s}
Sample-to-sample variation				
$\bar{x}$	(100)	57.24	547127	313353
σ		1.29	70113	42156
σ as % of $\bar{x}$		2.25	12.8	13.5
Variation in peak area measurement				
$\bar{x}$	(100)	57.48	458234	263312
σ		1.36	5919	3639
σ as % of $\bar{x}$		2.37	1.3	1.4

continued overleaf.....

Table 5.6 (continued)

Nylon - 6,6 film (C_{100} $O_{16.7}$ $N_{16.7}$)

	Relative Intensity			Absolute Intensity		
	C_{1s}	O_{1s}	N_{1s}	C_{1s}	O_{1s}	N_{1s}
Sample-to-sample variation						
$\bar{x}$	(100)	26.99	18.42	622239	140964	96524
σ		1.07	1.21	60391	17248	15490
σ as % of $\bar{x}$		3.97	6.59	11.6	12.2	16.0
Variation in peak area measurement						
$\bar{x}$	(100)	27.45	17.39	472354	130108	83085
σ		1.54	2.27	3190	2882	3366
σ as % of $\bar{x}$		5.60	13.07	0.7	2.2	4.1

continued overleaf.....

Table 5.6 (continued)

Polydiphenyl siloxane powder (C_{100} $O_{8.3}$ $Si_{8.3}$)

	Relative Intensity			Absolute Intensity		
	C_{1s}	O_{1s}	Si_{2p}	C_{1s}	O_{1s}	Si_{2p}
Sample-to-sample variation						
$\bar{x}$	(100)	16.98	11.34	154429	26361	17372
σ		1.11	0.71	32627	6469	3111
σ as % of $\bar{x}$		6.51	6.30	21.1	24.5	17.9
Variation in peak area measurement						
$\bar{x}$	(100)	18.09	11.02	185886	33834	20492
σ		0.77	0.45	1901	1381	846
σ as % of $\bar{x}$		4.26	4.12	1.0	4.1	4.1

continued overleaf.....

Table 5.6 (continued)

Brown coal powder (C_{100} $O_{32.4}$ $N_{1.4}$ $Si_{5.4}$)

	Relative Intensity				Absolute Intensity†			
	C_{1s}	O_{1s}	N_{1s}	Si_{2p}	C_{1s}	O_{1s}	N_{1s}	Si_{2p}
Sample-to-sample variation								
$\bar{x}$	(100)	51.09	1.66	6.59	182655	174259	13052	31269
σ		7.71	0.46	2.66	57913	50553	5658	8622
σ as % of $\bar{x}$		15.09	28.09	40.44	31.7	29.01	43.3	27.6
Variation in peak area measurement								
$\bar{x}$	(100)	41.92	1.27	3.62	270418	226717	17239	29398
σ		0.40	0.38	0.19	2385	2461	5279	1486
σ as % of $\bar{x}$		0.95	30.14	5.23	0.9	1.1	30.6	5.1

† Counts for brown coal involve multiple sweeps of core level signals as follows:

O_{1s}, 2 sweeps; N_{1s}, 5 sweeps; Si_{2p}, 3 sweeps.

with peak area measurement. This arises from the low intensity and broad nature of the N_{1s} signal (Figure 5.1). A similar problem has been discussed by Frost et al.[246] for elements present in trace amounts. Repeated scanning and computer averaging would obviate this effect but at the increased risk of hydrocarbon overlayer build-up, leading to further error in the ESCA analysis. An alternative approach might be to increase the x-ray flux, with the increased risk of sample degradation.

To complement the picture, Table 5.7 examines the error in C_{1s}/X intensity ratios arising from signal-noise considerations assuming that the noise will bear a square root dependence on the signal intensity, and where X is the core level, other than carbon 1s, which is in question. The table shows that the error will be minimised by increasing the intensities of the respective peaks.

The physical form of the sample is seen to affect the absolute intensity of the ESCA spectrum and the sample-to-sample variation in the absolute intensity measurements (Table 5.6). Hence the C_{1s} core level spectra of the powdered polydiphenyl siloxane are of lower absolute intensity than for either of the polymer films (PET or Nylon-6,6). These differences will also be apparent when comparing the ESCA spectra powdered coal samples with those of samples analysed in the form of thin films.

Ten analyses of brown coal using standard microanalytical techniques were performed over two days and the results are tabulated in Table 5.8. It may be concluded that instrumental factors give a day-to-day variation which is most apparent for the hydrogen analyses. Overall there is less scatter in these analyses than has been found for the ESCA results. It is important to note, however, that residual ash was detected upon combustion for three samples only during the standard microanalytical procedures, whereas the ESCA spectra showed the presence

Table 5.7 Error in measurement of simple ratios associated with absolute signal intensity and background noise

Two signals from C_{1s} and X core levels

Respective intensities N_C and N_X

Signal noise $\pm (N_C)^{\frac{1}{2}}$ and $\pm (N_X)^{\frac{1}{2}}$

Error in $\frac{N_C}{N_X} = \pm \frac{N_C}{N_X} \left(\frac{1}{N_C} + \frac{1}{N_X} \right)^{\frac{1}{2}}$

$\frac{N_C}{N_X} = 1000$						
N_C	10	10^2	10^3	10^4	10^5	10^6
N_X			1	10	10^2	10^3
error			$\pm 10^3$	± 316	$\pm 10^2$	± 31.6
error as % of $\frac{N_C}{N_X}$			100	32	10	3.2

$\frac{N_C}{N_X} = 100$						
N_C	10	10^2	10^3	10^4	10^5	10^6
N_X		1	10	10^2	10^3	10^4
error		± 100	± 32	± 10	± 3.2	± 1
error as % of $\frac{N_C}{N_X}$		± 100	± 32	± 10	± 3.2	± 1

$\frac{N_C}{N_X} = 10$						
N_C	10	10^2	10^3	10^4	10^5	10^6
N_X	1	10	10^2	10^3	10^4	10^5
error	± 10	± 3.3	± 1	± 0.33	± 0.11	± 0.033
error as % of $\frac{N_C}{N_X}$	± 100	± 33	± 10	± 3.3	± 1.1	± 0.33

continued overleaf.....

Table 5.7 (continued)

$\frac{N_C}{N_X} = 1$						
N_C	10	10^2	10^3	10^4	10^5	10^6
N_X	10	10^2	10^3	10^4	10^5	10^6
error	±0.45	±0.14	±0.045	±0.014	±0.0045	±0.0014
error as % of $\frac{N_C}{N_X}$	±45	±14	±4.5	±1.4	±0.45	±0.14

Table 5.8 Microanalysis of brown coal. [248]

	Elemental composition (wt.%)				Overall stoichiometry			
	C	H	N	O	C	H	N	O
Day *1*	53.20	5.96	0.86	39.98	100	135.25	1.39	56.36
	53.03	6.01	0.87	40.09	100	136.00	1.41	56.70
	52.76	6.29	0.92	40.03	100	143.06	1.49	56.90
	52.55	6.27	0.92	40.26	100	143.18	1.50	57.46
	52.43	6.25	0.97	40.35	100	143.05	1.59	57.72
Day *2*	53.61	4.47	0.86	41.06	100	100.06	1.38	57.74
	54.09	4.49	0.76	40.66*[2]	100	99.61	1.20	56.38
	54.30	4.26	0.90	40.54*[2]	100	94.14	1.42	55.99
	57.54	4.55	0.84	37.07	100	94.89	1.25	48.32
	52.39	4.37	0.85	42.39*[2]	100	100.10	1.39	60.68
$\bar{x}$	53.59	5.29	0.88	40.24	100	118.93	1.40	56.43
σ	1.54	0.92	0.07	1.32		22.57	0.11	3.14
σ as % of $\bar{x}$	2.87	17.39	7.95	3.28		18.98	8.14	5.56

All analyses performed at Durham.
*[2] Trace amount of residual ash detected upon combustion.

of Si, at varying levels, for each sample analysed. Furthermore, a linear relationship is found to exist between the relative area measurements for the O_{1s} and Si_{2p} photoionisation signals (Figure 5.4). No such relationship is found to hold for the N_{1s} and Si_{2p} peaks.

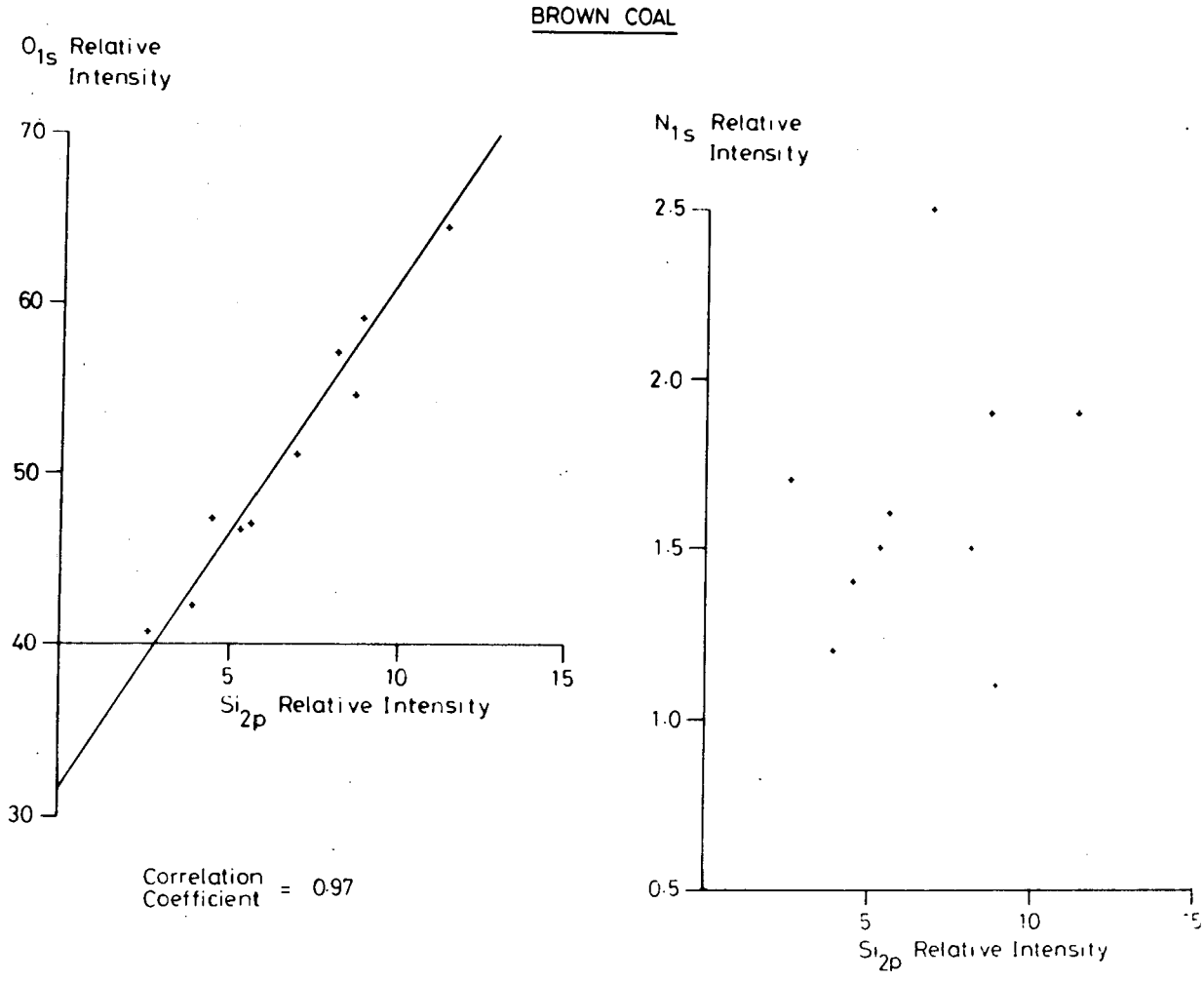

Figure 5.4 Relationships between O_{1s} and Si_{2p}, and N_{1s} and Si_{2p} relative peak areas from the analyses of brown coal. (Total C_{1s} peak intensity taken as 100 units.)

O_{1s} Rel. Int. = $3Si_{2p}$ Rel. Int. + 31.6

5.3.3 Lower Kittanning seam coal

5.3.3a Introduction

The preliminary investigation of the characterisation of kerogens, brown coal and Gilsonite by means of ESCA illustrated the promise of the applicability of ESCA to study of naturally occurring carbonaceous materials. Further studies of coal samples of more precisely defined origin were therefore sought. To this end a series of coals have been examined from the Lower Kittanning seam in Pennsylvania and Ohio, USA.

The Lower Kittanning coal seam has been the subject of a number of detailed investigations from both geological and physico-chemical standpoints:[263,306-313] recently, Fourier transform infrared spectroscopic [234] and solid state ^{13}C nuclear magnetic resonance analyses [305] have been published in the literature. As stated by Davis, [306] 'a set of samples from a coal seam is especially valuable in affording a suite of materials differing in some respects (degree of metamorphism and depositional environments) but being similar in others (age, palaeoclimates, vegetation).' The Lower Kittanning seam in the northern Appalachian Trough is an excellent example. The seam is of very large areal extent, stretching over the states of Ohio, Pennsylvania and West Virginia. The coal-bearing strata in western Pennsylvania and eastern Ohio are Pennsylvanian in age. The Lower Kittanning seam is part of the Kittanning formation, the central portion of the Allegheny group. Described as the most persistent coal bed of the Allegheny group, the seam varies in thickness, averaging from 2 to 4 feet.[306]

Interest in the Lower Kittanning seam coals stems from the considerable lateral variation of rank which increases from west to east

(high volatile C to low volatile bituminous),[306,307,312] and also sulphur content.[306,310,312] Further, the seam was deposited in a relatively narrow range of geological time from much of the same type of vegetational communities.[306] The depositional environment however did vary regionally in salinity from marine to freshwater.[306,308,309,311] This variation has been studied and mapped based on studies of fossil and trace element assemblages of the shales overlying the Lower Kittanning coal seam in relation to the underlying coal; petrographic studies and studies of spore and pollen assemblages have been performed and all are reviewed by Davis.[306]

Williams and Keith[310] have shown that the sulphur distribution in the Lower Kittanning seam coal is related to the environmental character of the immediately overlying rocks. Areas of relatively high sulphur content occur where the overlying rocks are marine, and areas of low sulphur where the overlying rocks are continental. The high sulphur content of coals overlain by marine beds is thought to have been caused by the increased availability of sulphate ions in sea water.[310] Anaerobic bacteria then reduced the sulphate to disulphides and hydrogen sulphide, which was subsequently incorporated into the peat.† [263]

---

† Sulphur in coal is recognised as existing in three forms:[318] inorganic sulphates, inorganic sulphides (e.g. iron pyrites, FeS_2) and organic sulphur compounds. The sulphur present in peat swamps originates from plant and animal protein, largely from bacterial protein, or it has been brought in from outside areas as sulphate ions through streams and/or sea water.[263] The transformation of sulphur groups and the incorporation of sulphur during coalification follows complex pathways,[263,314] and these are discussed elsewhere.

5.3.3b Qualitative ESCA analysis

The ESCA analyses of the Lower Kittanning coal seam samples will be discussed before comparison is made of the ESCA 'surface' elemental analyses and the corresponding analyses using standard microanalytical (bulk) techniques.

Relative intensity data for the ESCA spectra are presented in Table 5.9 and 5.10. Table 5.9 reveals differences in elemental composition between the coal samples at the ESCA sampling depth. As expected the C_{1s} photoionisation signal dominates the spectrum of each coal, the second most intense signal being due to oxygen. Each O_{1s} core level envelope will be composed of peaks arising from both organic oxygen and inorganic oxygen from the mineral matter portion of the coal. Each coal shows evidence of a silicon and aluminium containing mineral matter component, although there is a wide variation in $^{Si}2p/Al_{2p}$ ratio for the coal samples analysed. At first consideration this may be thought to reflect changes in the silicon : aluminium ratio for coals from different locations: this is probably not the case for reasons to be discussed at a later stage. For the coal samples under investigation here, the tendency is for the coals of higher rank (as measured by %C, dmmf and vitrinite reflectance (Table 5.1)) to exhibit a lower intensity total O_{1s} signal.

A low level of nitrogen is found in each sample. There is a small variation in nitrogen concentration from mine to mine, and this is in agreement with an earlier study by Stadnichenko. [307] The broad nature of the N_{1s} core level signal for each coal which is centred at $\sim$ 400.6 eV binding energy is indicative of there being several carbon bonded to nitrogen environments, including aliphatic and aromatic amines, and heterocyclic nitrogen functionalities such as

Table 5.9 Lower Kittanning Seam Coal. Relative Areas of C_{1s}, O_{1s}, N_{1s}, S_{2p}, Si_{2p} and Al_{2p} core level signals. Figures in brackets indicate binding energies (eV).

PSOC No.	C_{1s}	O_{1s}	N_{1s}	S_{2p}(Tot.)	S_{2p}(ox)	S_{2p}(unox)	Si_{2p}	Al_{2p}	Si_{2p}/Al_{2p}
308	100	(534.0) 48.1	(400.7) 2.1	3.1	(169.9) 2.0	(164.0) 1.1	(104.0) 3.3	(75.6) 2.3	1.43
322	100	(534.4) 56.2	(400.6) 2.3	1.9	(170.0) 1.4	(164.6) 0.5	(104.4) 6.5	(76.1) 3.8	1.71
755	100	(534.2) 37.6	(401.0) 1.7	3.8	(170.0) 2.1	(164.3) 1.7	(104.4) 3.4	(75.8) 1.5	2.37
1010	100	(534.1) 21.7	(400.6) 1.3	1.4	(169.5) 0.8	(164.3) 0.6	(103.8) 2.0	(75.6) 1.1	1.82
1011	100	(534.2) 29.3	(400.5) 1.8	1.3	(169.7) 0.6	(163.9) 0.7	(103.9) 3.1	(75.5) 1.6	1.94
1017	100	(534.1) 32.7	(400.6) 1.6	2.9	(170.0) 1.8	(164.3) 1.1	(104.0) 4.4	(75.6) 1.8	2.44
1024	100	(533.9) 12.0	(400.4) 1.4	0.9	(169.6) 0.3	(164.5) 0.6	(103.7) 2.2	(75.4) 0.5	4.4
1025		(534.0) 14.1	(400.8) 1.3	1.8	(169.7) 1.0	(166.5) 0.8	(103.9) 1.5	(75.6) 0.6	2.5
1133	100	(534.0) 15.0	(400.1) 1.6	0.6	(169.4) 0.3	(164.0) 0.3	(103.8) 1.6	(75.6) 0.9	1.8

Table 5.10 Lower Kittanning Seam Coal. Relative Areas of C_{1s} component peaks.
(Total C_{1s} taken as 100 units. Figures in brackets indicate binding energies (eV)).

PSOC No.	C-H	C-O	C=O	O ‖ C-O			Sample Charging (eV)
308	55.2	(286.4) 30.4	(288.0) 6.6	(289.3) 3.9	(290.6) 3.9	-	4.2
322	56.2	(286.4) 27.5	(288.1) 7.9	(289.2) 4.5	(290.7) 3.9	-	3.7
755	57.8	(286.3) 25.8	(287.9) 6.2	(289.1) 4.5	(290.4) 4.5	-	3.7
1010	65.8	(286.5) 19.1	(288.1) 4.6	(289.5) 4.6	(290.8) 3.9	(292.3) 2.0	3.8
1011	68.0	(286.4) 21.8	(287.9) 4.1	(289.3) 2.7	(290.4) 2.0	(292.2) 1.4	3.9
1017	60.1	(286.4) 24.2	(288.0) 4.9	(289.3) 3.6	(290.4) 4.2	(292.1) 2.4	4.2
1024	69.0	(286.4) 18.6	(287.8) 3.5	(289.3) 3.5	(290.4) 3.5	(292.0) 2.1	3.4

continued overleaf.....

Table 5.10 (continued)

PSOC No.	C-H	C-O	C=O	O ‖ C-O			Sampling Charging (eV)
		(286.4)	(288.2)	(289.3)	(290.5)	(292.1)	
1025	69.9	17.2	3.5	2.8	4.1	2.1	3.4
		(286.3)	(288.0)	(289.2)	(290.4)	(291.6)	
1133	71.4	17.9	3.6	2.9	2.9	1.5	3.3

pyrrolic nitrogen.[105] The low absolute intensity of the N_{1s} envelope did not permit curve resolution of the signal as has been described by Jones et al.[249] Under the conditions prevailing at the time of analysis the acquisition of a suitably intense N_{1s} spectrum was not of the highest priority. No evidence was found for the presence of oxidised nitrogen species such as nitrate ester linkages which would occur to higher binding energy of the amine type N_{1s} peak, in the 407 eV region.[105] There is no evidence for inorganic nitrogen.

The sulphur content of each coal is indicated by the presence of a S_{2p} (and S_{2s}) photoionisation envelope which takes the form of a well separated doublet. The two component peaks correspond to oxidised and unoxidised sulphur moieties and are centred at $\sim$ 169.8 eV and $\sim$ 164.5 eV binding energy respectively.[105] Although unequivocal assignment of a particular species to each component cannot be made, a study of model compounds is helpful when analysing spectra of materials of unknown composition. For example, the spectra of ferrous sulphide, polyphenylene sulphide and bisphenol-A polysulphone have been reported[169] (see also Figures 5.38, 39). Inorganic sulphide, as in FeS_2, is found at a binding energy of $\sim$ 162 eV, whereas the polyphenyl sulphide organic sulphide peak occurs at $\sim$ 163 eV: the S_{2p} sulphone $(- \overset{\overset{O}{\|}}{\underset{\underset{O}{\|}}{S}} -)$ peak of bisphenol-A polysulphone is centred at 168 eV binding energy. In addition, reference tables are available in the literature.[105,246]

Although the coal samples were known to contain FeS_2 (Table 5.1), no attempt was made to analyse for iron in the ESCA experiment.

Table 5.10 shows the relative areas and peak positions of the deconvoluted C_{1s} components. The components occurring at $\sim$ 290.4 eV and $\sim$ 292.1 eV may be atrributed to $\pi \rightarrow \pi^*$ shake-up satellites arising

from conjugated species (e.g. aromatic ring systems).[143] Carbonate groups, if present, would contribute to the peak at ∿ 290.4 eV. Over the range of coals, the C_{1s} ESCA spectra show a higher proportion of carbon singly bonded to oxygen functionality than either $\underline{C}$ = O or $\underline{C}$ - O. The contribution of the functionalised carbon components to the total C_{1s} peak intensity is found to decrease with increasing coal rank. It should be remembered that the peak assigned to $\underline{C}$ - O functionalities will also include some contribution from organic carbon-nitrogen and carbon-sulphur linkages (Section 5.3.1) and that the presence of these groups may become more significant as the rank of the coal increases.

Figure 5.5 shows C_{1s} spectra and also spectra spanning the 0 - 250 eV binding energy range illustrating signals from sulphur, silicon, aluminium and oxygen. Further discussion of the valence band spectra of the Lower Kittanning seam coals and of the C_{1s} line shapes will take place in Sections 5.3.4 and 5.3.5 respectively.

5.3.3c Semi-quantitative analyses

Comparison of the ESCA elemental analyses with the corresponding data on the bulk coal composition, previously determined at Pennsylvania State University coal research centre, will now receive attention. The methods of bulk analysis have already been cited in Section 5.2. The elements to be considered are nitrogen, sulphur, silicon, aluminium and oxygen.

For nitrogen (Figure 5.6) there is a clear trend between the ESCA and bulk analyses. The least squares line of best fit through the data points passes through the origin. Figure 5.6 also shows the data for total sulphur content. The wide range of sulphur contents

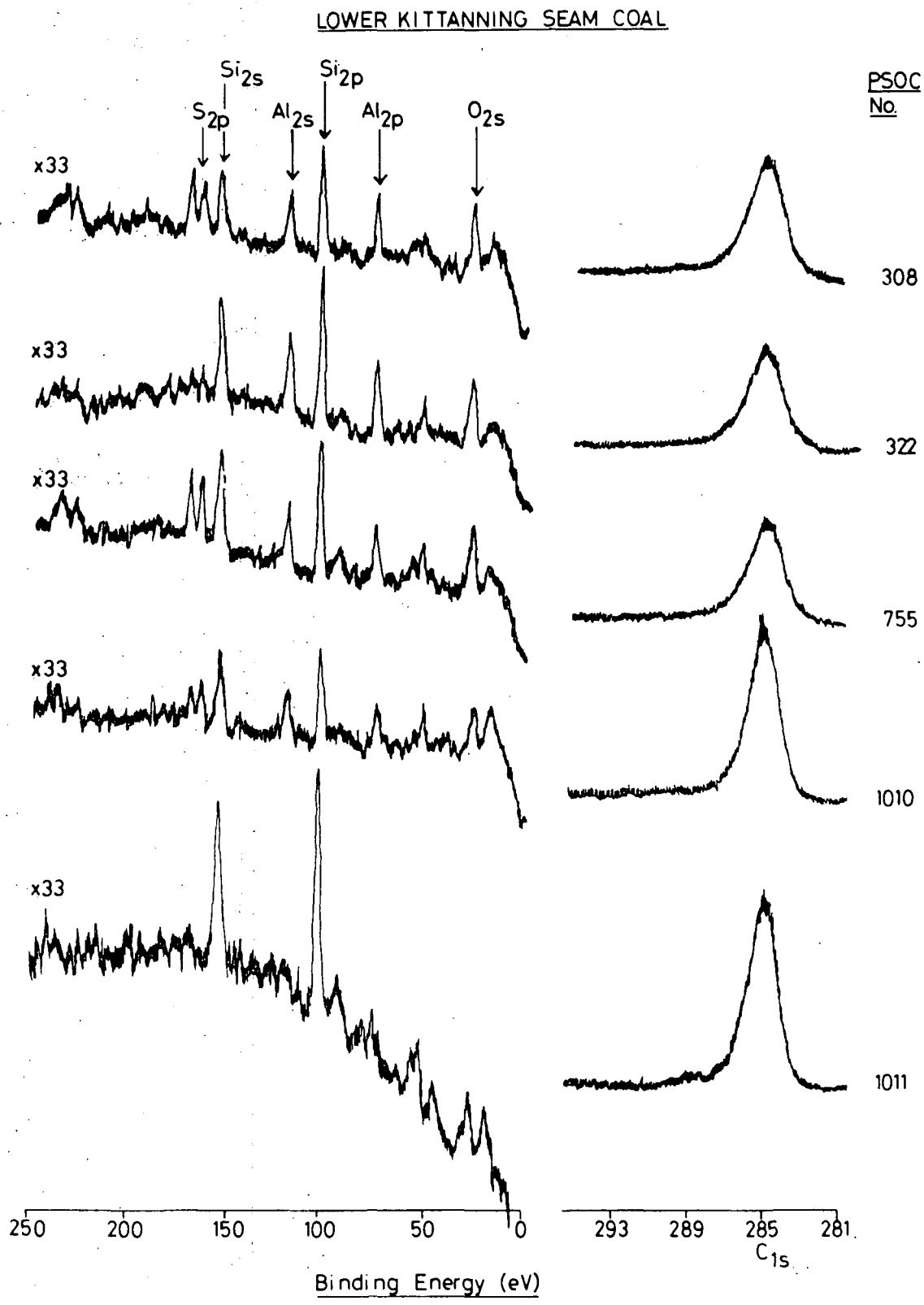

Figure 5.5 Lower Kittanning seam coal, C_{1s} core levels and 0-250eV binding energy scans.

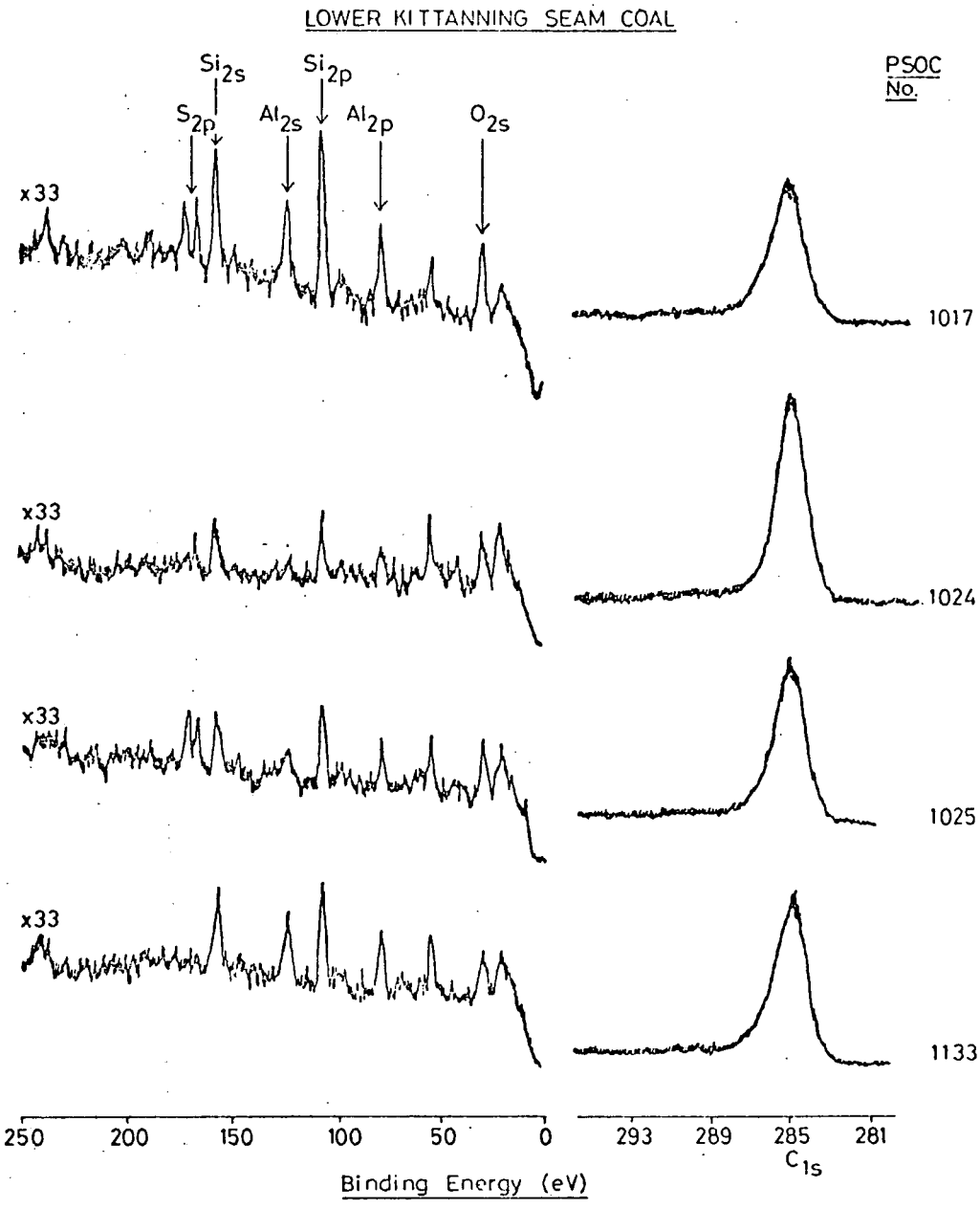

Figure 5.5 (continued)

for these coal samples reflects the lateral environmental differences of the Lower Kittanning seam.[306] There is more scatter in the data points, although the line of best fit is found to pass close to the origin. These results indicate that the ESCA derived atomic ratios are lower than bulk measurements. This may be due to surface/bulk effects. An alternative explanation may involve a real decrease in

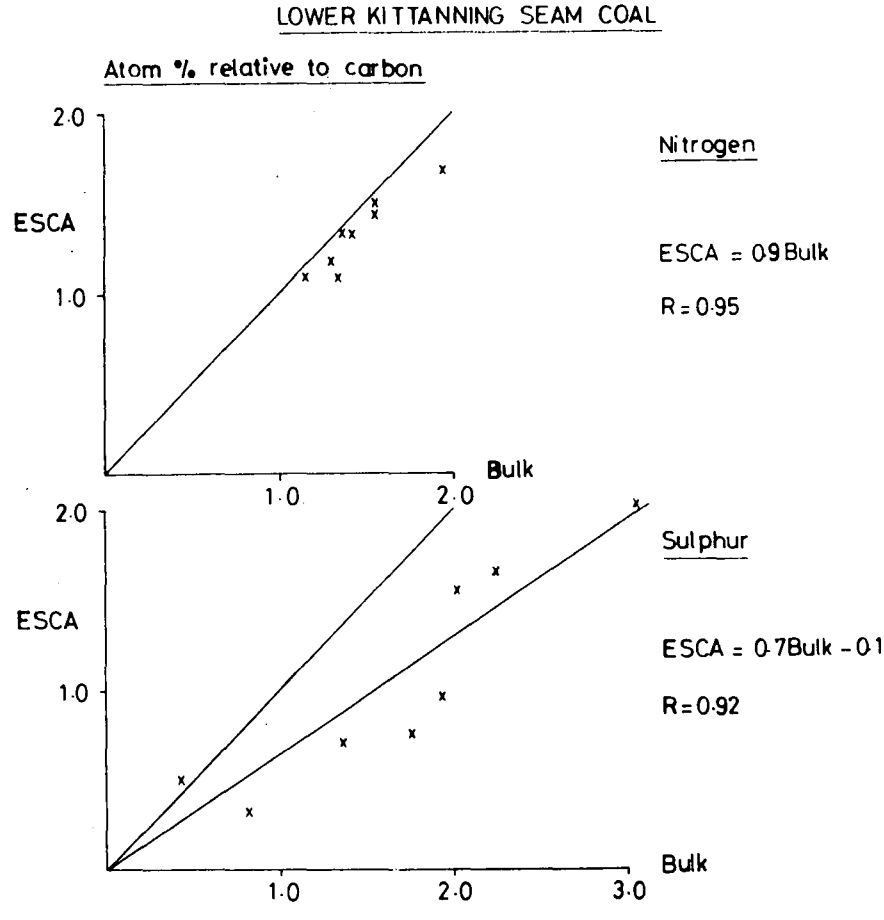

Figure 5.6 The relationships between ESCA- and bulk-derived atomic ratio measurements for nitrogen and total sulphur for Lower Kittanning seam coal.

sulphur on storage.[315] Analysis of the sulphur levels in the coal samples, performed in Durham, would suggest that this is not the case (Table 5.1). Far more variation is found to exist between ESCA and bulk measurements for silicon and aluminium (Figure 5.7). Grint and Perry[251] have reported similar observations for a rank range of British coals which they attribute to the coal fracture mechanism on grinding.

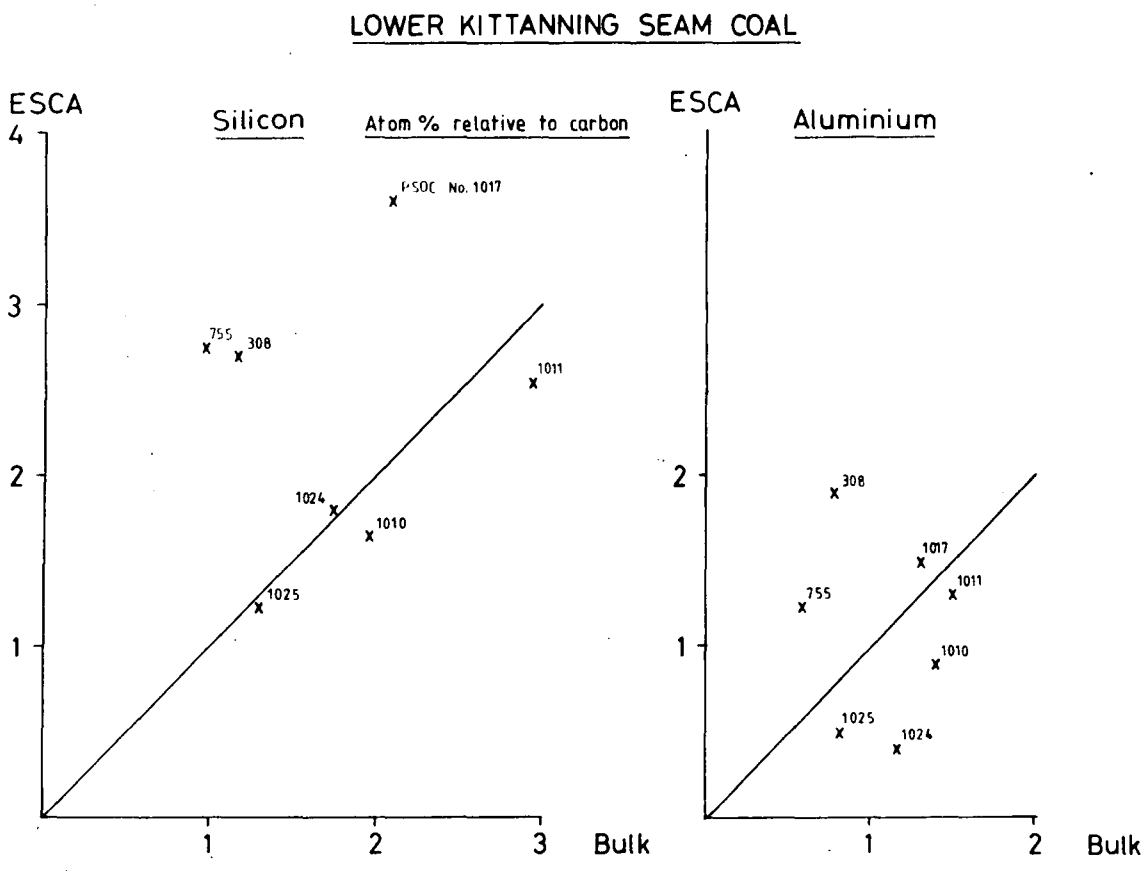

Figure 5.7 The relationships between ESCA- and bulk-derived atomic ratio measurements for silicon and aluminium for Lower Kittanning seam coal.

Figure 5.8 pertains to the organic oxygen concentrations, expressed as atomic percent relative to carbon for the ESCA experiment and the bulk analyses by difference. The ESCA organic oxygen values were found by subtracting mineral oxygen away from the total oxygen, taking the mineral oxygen to be bound with silicon and aluminium as SiO_2 and Al_2O_3 respectively. The trend which emerges is that the organic oxygen atomic concentration as determined by ESCA is higher than the Pennsylvania State University Coal Bank data suggest. The line of best fit through the data points cuts the 'ESCA axis' at a value of 2.9 atom percent. A similar situation was found to exist for the rank range of British coals, prepared for analysis by ESCA by grinding under heptane reported earlier.[251] It has been suggested that this may reflect the presence of oxygen as a terminating functional group at the coal fracture surface. It is of interest to note the rank-related trend in the data set, coal of lowest rank showing the most deviation from the one to one, ESCA bulk relationship which might be expected to hold. A number of factors should not be ruled out in accounting for the enhanced ESCA organic oxygen content, relative to the bulk measurement, namely, surface oxidation arising from sample preparation, moisture content, pore size which will affect the surface/volume ratio,[263] and sample storage.[306] Coal is known to undergo rapid deterioration attributable to oxidation even when stored under strictly controlled conditions.[306] Since the coal samples were mined (and presumably analysed) between 1974 and 1978,[316] oxidation of the whole coal on storage may be the most significant factor.

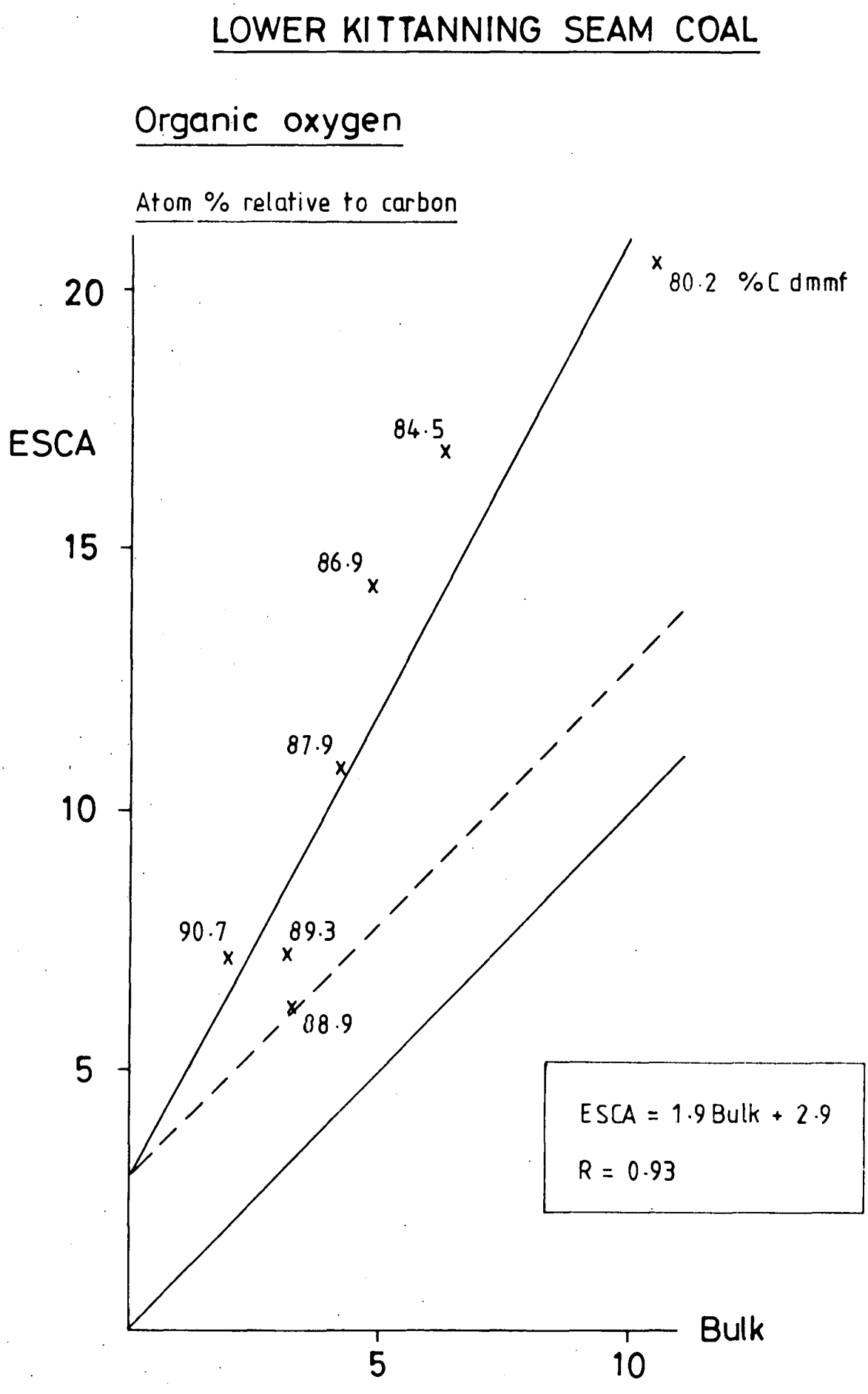

Figure 5.8 The relationship between ESCA- and bulk-derived atomic ratio measurements for organic oxygen for Lower Kittanning seam coal.

5.3.3d A note on sample preparation

Perry and Grint [252] in parallel studies on the application of x-ray photoelectron spectroscopy (XPS)† to coal characterisation have emphasised the need to minimise exposure to the atmosphere during sample handling. They advocate the preparation of coal samples for analysis by grinding under heptane in a vibratory ball mill. This method of preparation produces coal surfaces with oxygen concentrations which correlate well over the whole rank range with the bulk oxygen concentrations.

In contrast however, Jones and co-workers [249] in their studies of nitrogen and sulphur in coal using XPS state: 'By sample grinding immediately before study, surface oxidation is minimised and the XPS spectra appear characteristic of the bulk substance.' No further details on their sample grinding procedures are given.

Whilst the possibility of surface oxidation during grinding in air cannot be ruled out (and indeed Solomon and Mains [317] have demonstrated the oxidative effects of grinding coal in air, in a ball mill, using ESCA), it is this method of preparation which has been chosen for the work presented in this thesis. The reasons are as follows: grinding using a pestle and mortar is simple; compared with the use of a ball mill, it is far less harsh; the introduction of an 'inert' solvent such as heptane, it is thought, may well interact with the coal in some physical or chemical way and hence may affect the coal's characteristics; and finally, the samples of coal prepared in this

---

† Although the terms x-ray photoelectron spectroscopy (XPS) and electron spectroscopy for chemical application (ESCA) are synonymous, some authors express a strong preference for the use of one or other of them.

manner are likely to bear closer similarities with coal as found in industrial environments.

The question of the oxidation of coal on exposure to the atmosphere will receive further consideration in a following section of this chapter (Section 5.3.8).

5.3.4 Valence Band Signals

Little attention has been paid to the study of ESCA valence band spectra, despite their ability to depict directly the bonding within molecules.[227] The valence band region (0 - 50 eV binding energy) has been shown to be of particular value for distinguishing between skeletally isomeric polymer systems which exhibit similar overall core-level band profiles.[226] The valence energy levels are able to provide a 'fingerprint' for a given polymeric structure which may then be compared with appropriate model compounds.

This methodology has been applied to the study of a rank range of coals, from brown coal to anthracite. The relevant spectra are displayed in Figure 5.9: the valence band spectrum of graphite is included for the sake of comparison. Each valence level takes the form of an unresolved band profile since there are a large number of occupied levels compressed into a narrow range. Even so, there is a clear rank-dependent trend in the coal valence band traces. The O_{2s} band centred at $\sim$ 28 eV binding energy diminishes in intensity with increasing rank. The structure to the lower binding energy side of the O_{2s} signal will reflect the environments of the carbon valence electrons. Clearly evident from the form of the valence bands displayed in Figure 5.9 is the progressive extension of the occupied levels towards the Fermi edge in going from brown coal to graphite. The valence band profiles of anthracite and anthracene are closely similar.

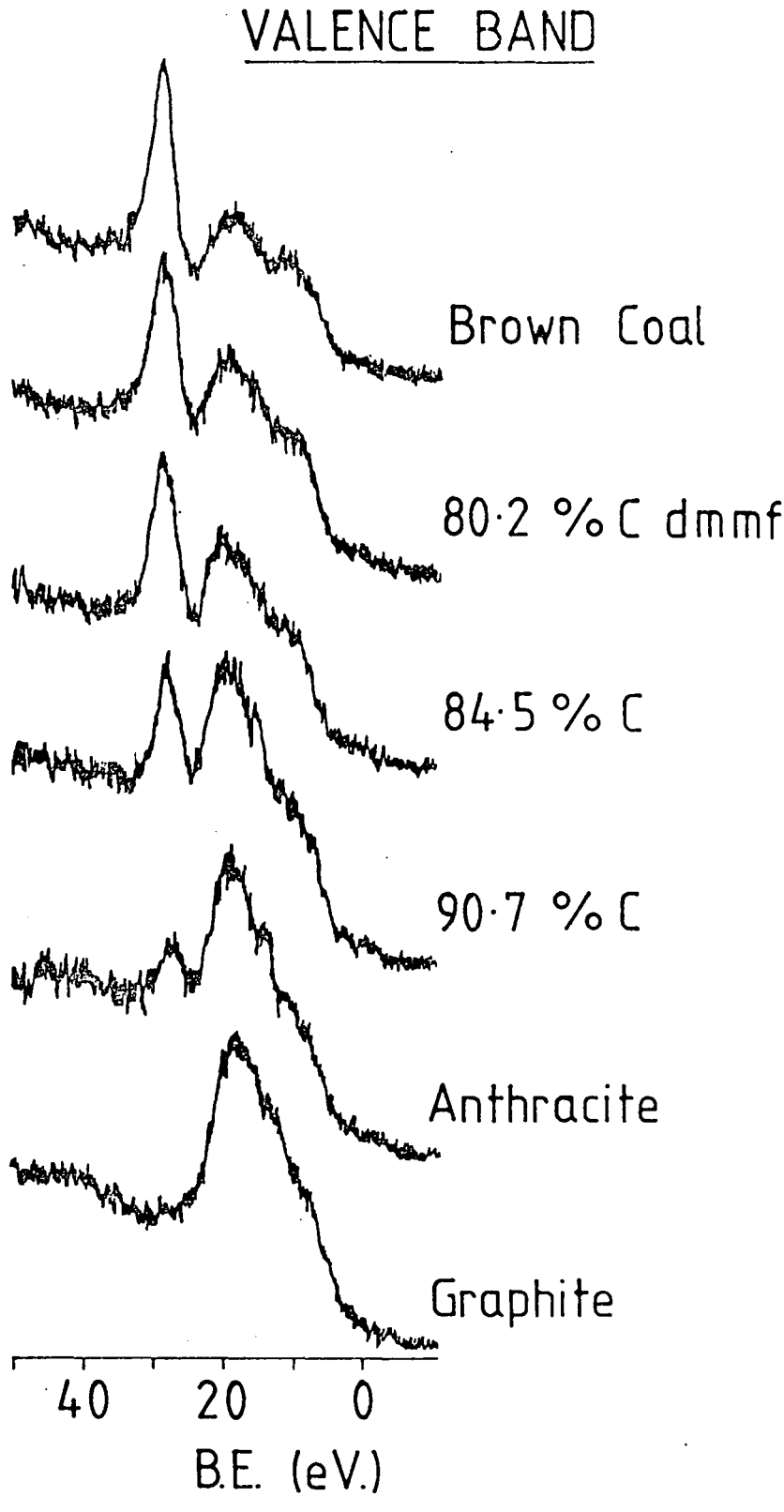

Figure 5.9 $Mg_{K\alpha}$ excited valence band spectra of a rank-range of coals: the valence band spectrum of graphite is included for comparison.

5.3.5 C_{1s} photoionisation signals

It is of interest to note that the line width of the individual photoionisation peaks of the C_{1s} core level envelopes show a narrowing as coal rank increases. Hence the FWHM of brown coal is $\sim$ 2.1 eV, whilst for the 84.5%C (dmmf) coal from the Lower Kittanning seam (PSOC No. 1017) and for anthracite the corresponding values are $\sim$ 1.8 eV and $\sim$ 1.5 eV respectively. The graphite C_{1s} core level peak has a FWHM of $\sim$ 1.2 eV.† There are also concomitant decreases in sample charging during analysis, a feature associated with insulating materials, [226] and in the absolute binding energy of the predominant C_{1s} signal. These factors may be attributable to the increase in electrical conductivity of coal with increasing coal rank.[259] Similar trends in line width and sample charging are observed for the rank-range of coals from the Lower Kittanning seam (Figure 5.5 and Table 5.10.

These trends also exist for the ESCA spectra of naturally occurring heat altered coal, the subject for discussion in the following section.

---

† These values were obtained for spectra recorded on the ES300 spectrometer with a $Mg_{K\alpha}$ x-ray source. The relevant spectra are shown in Figure 5.10.

Figure 5.10 Mg_{K_α} excited C_{1s} core level spectra of a rank-range of coals : the C_{1s} spectrum of graphite is included for comparison.

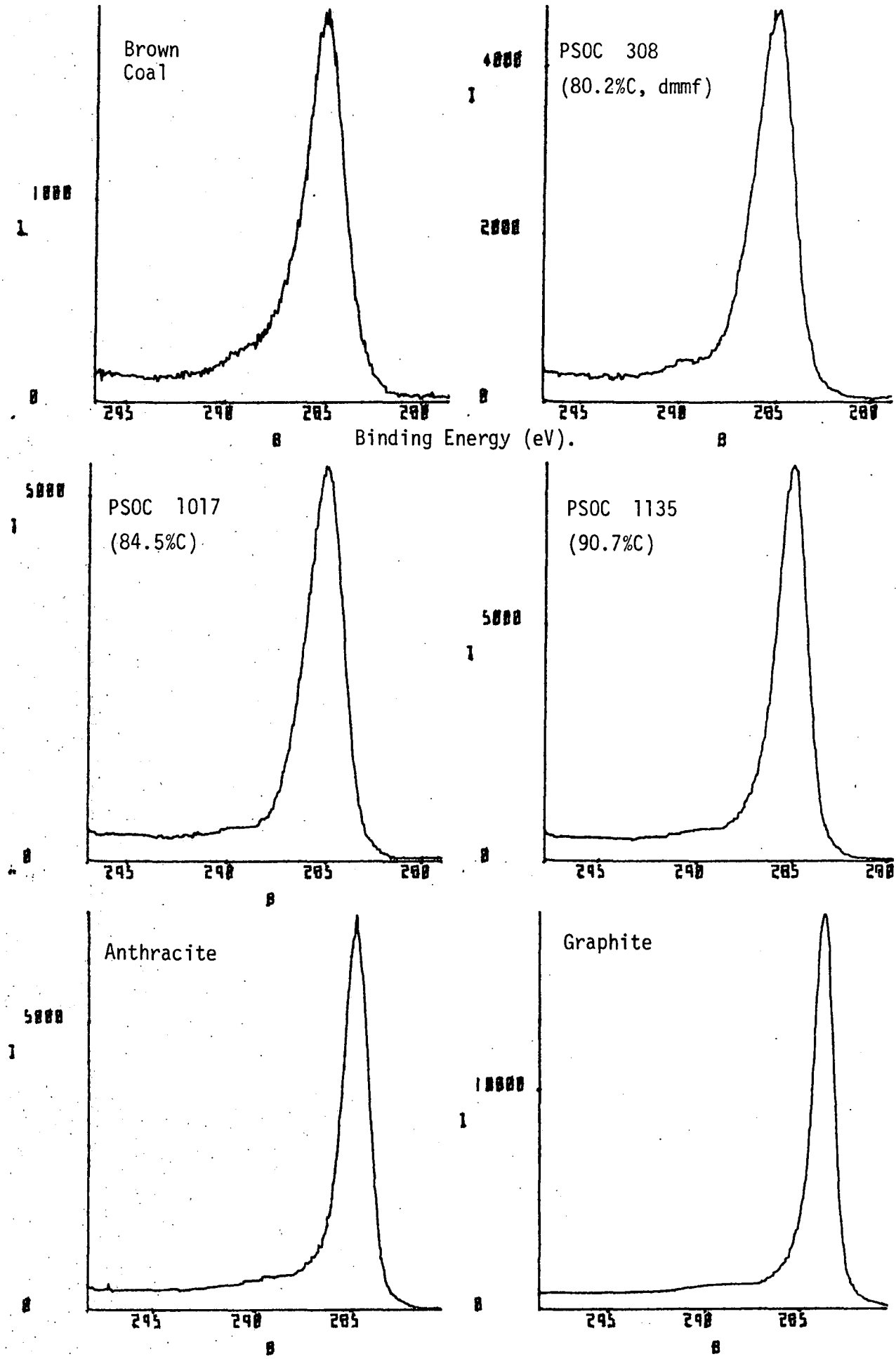

5.3.6 Naturally occurring heat altered coal

5.3.6a Introduction

The formation of coke from coal is an area of appreciable industrial importance. [241,263] As such it continues to be the subject of a strong research effort aimed at the better understanding of carbonisation processes so as to aid the production of coke for specific purposes.

Carbonisation, the heating of coal in the absence of air, [241] thereby removing volatile matter, has been investigated by chemical, physical and optical means, and has been found to be a complex phenomenon. [241,259,263,264] The possibility of producing a good coke from a given coal will depend not only on the chemical physico-chemical properties inherent in the coal, but also on external factors such as coal preparation, rate of coking and on the nature of additives, such as pitch or bitumen, which may be mixed with the coal prior to coking. [263] Of the texts which discuss the carbonisation of coal, those of Grainger and Gibson, [241] and Francis and Peters [264] provide sound introductions to industrial considerations.

Coke formation is not confined to the laboratory/commercial situation. Where coalfields have been invaded by dykes, sills and other types of igneous intrusion, the heat from such intrusions causes changes to occur in the coal. [263,265] In such cases the formation of thermally affected coal † will depend on the properties of both the intruding and intruded rock. Thus analysis of the intruded rock may provide information on the igneous mass at the time of intrusion. Stach et al. [263] provide

---

† Also known as natural coke, geological coke, burnt coal, cinder coal, jhama and thermally metamorphosed coal.

a full review of naturally occurring cokes and their formation with particular emphasis on petrological studies. Raistrick and Marshall's oft-cited account of the igneous alteration of coal seams [265] concentrates on results from proximate analyses.

A related area of research examines the effects of igneous instrusions into organic-rich sedimentary accumulations. [231,266-270] The aims of these studies of the effect of heat stress on organic matter are to examine thermally induced changes in the chemical structure of the organic matter and to derive a better understanding of coal and petroleum development. This is an area where the application of newly developed analytical techniques, such as solid state ^{13}C nuclear magnetic resonance spectroscopy [269] and fluorescent light microscopy, [263] is proving to be of considerable value to the organic geochemist.

Here the usefulness of ESCA in the study of a suite of naturally occurring heat altered coal samples is examined. The findings of the ESCA experiment are put in perspective by first considering data from standard analytical procedures for coals and cokes involving proximate and ultimate analyses, and optical microscopy.

5.3.3b Coals and cokes examined

The author is fortunate to live in an area having an abundance of coalfields, some of which have been affected by igneous intrusions. Descriptions of the Northumberland and Durham coalfields are available in the literature, [265, 271-8] and geological surveys of the area provide useful background information. [279-282] The coal for this investigation is from the National Coal Board open cast site at Togston, Northumberland, U.K. The coal field at Togston has been penetrated by the Acklington Dyke, the most northerly of a series of basic (tholeiite) dykes which trend west-north-west to east-south-east in the north of England. [279,281-3]

The Acklington Dyke forms part of a dyke-swarm radiating from the Tertiary igneous centre on the Isle of Mull and has been studied petrographically and chemically. [282,283]

Coal samples were taken from a recently exposed coal seam at different distances along a straight line at right angles to a spur of the main dyke formation. Samples are numbered 1 to 9 and distances are referenced to sample 1, closest to the intrusion. Sample 1 was estimated to be ∿ 2.5m from the spur and ∿ 16m north of the main dyke formation. [284] Samples were taken at different depths from the roof of the coal seam so as to explore possible vertical variations in coal characteristics. A sample of coal (sample 9), thought to be representative of unaffected coal, was collected from the same coal seam at a position ∿ 245m north of the main dyke. [284] Sample locations are tabulated in Table 5.11.

Table 5.11 Coals and Cokes examined

Sample No.	Lateral Distance from sample 1 (cm)	Depth range sampled (cm)
1	0	0 - 18
2	0	18 - 30
3	0	30 - 43
4	23	0 - 15
5	23	15 - 30
6	85	0 - 15
7	85	15 - 30
8	245	0 - 15
9	Block bottom leaf 245m north of dyke	0 - 15

Grid references: Samples 1 - 8, 425658 602173

Sample 9, 425765 602403

Samples 1 - 7 resembled natural coke whilst samples 8 and 9 exhibited the lustre and banded structure of unaffected coal.

5.3.6c N.C.B. Analyses

Analyses of the coal samples as performed in N.C.B. laboratories are presented in Table 5.12; ash analyses on selected samples are given in Table 5.13.

Table 5.12 NCB analyses of Acklington Dyke coal (wt %, -72 BS mesh)

	Coal Sample								
	1	2	3	4	5	6	7	8	9
Air Dried Basis									
Moisture	2.9	3.3	2.8	2.8	2.3	2.4	2.1	3.5	6.2
Volatile Matter	5.9	7.4	7.8	6.4	8.2	7.0	9.8	33.5	33.3
Fixed Carbon	85.2	41.1	55.1	83.1	79.7	83.4	78.2	59.1	54.0
Ash	6.0	48.2	34.3	7.7	9.8	7.2	9.9	3.9	6.5
Mineral Matter	7.2	53.4	38.1	9.8	12.5	8.3	12.5	4.9	8.3

continued overleaf

Table 5.12 (continued)

Air Dried Basis	Coal Sample 1	2	3	4	5	6	7	8	9
Sulphate S	0.17	0.14	0.14	0.12	0.17	0.04	0.08	0.06	0.07
Pyritic S	0.80	0.76	0.66	2.62	2.20	0.67	1.78	0.64	0.58
Organic S	0.63	0.46	0.54	0.38	0.42	0.47	0.64	0.74	0.55
Total S	1.60	1.36	1.34	3.12	2.79	1.18	2.30	1.44	1.20
Chlorine	0.09	0.06	0.06	0.08	0.07	0.10	0.12	0.06	0.04
CO_2	0.12	0.08	0.08	0.08	0.78	0.11	1.03	0.29	1.24
Carbon	84.5	41.4	55.3	81.4	79.7	83.1	79.8	76.7	71.3
Hydrogen	2.4	1.8	2.2	2.5	2.8	3.0	3.0	5.0	4.6
Nitrogen	1.11	0.77	1.05	1.19	1.47	1.58	1.53	1.73	1.65

continued overleaf

Table 5.12 (continued)

	Coal Sample								
	1	2*	3*	4	5	6	7	8	9
Dry Ash Free									
Volatile Matter	6.5	15.2	12.4	7.2	9.3	7.7	11.1	36.2	38.1
Dry Mineral Matter Free									
Volatile Matter	5.5	-	-	5.7	7.2	6.7	8.9	35.8	37.0
Carbon	94.0	-	-	93.1	93.3	93.0	93.1	83.6	83.0
Hydrogen	2.7	-	-	2.9	3.3	3.4	3.5	5.4	5.4
Nitrogen	1.2	-	-	1.4	1.7	1.8	1.8	1.9	1.9
Caking Test									
Swelling No. (British Standards)	0	0	0	0	0	0	0	3	1.5

* Please refer to the notes which follow on the standard N.C.B. presentation of coal analyses, point 8

Table 5.13 N.C.B. analyses of Acklington Dyke coal

Ash Analyses (wt %)

	Coal Sample			
	1	4	8	9
Ash % (Air Dried)	6.0	7.7	3.9	6.5
SiO_2	32.0	22.7	27.6	32.5
Al_2O_3	25.0	17.2	20.4	20.3
Fe_2O_3	27.3	48.8	28.7	17.5
CaO	4.5	2.6	8.1	14.9
MgO	4.2	2.6	4.1	8.6
TiO_2	0.9	0.6	0.9	1.1
Na_2O	1.3	0.9	0.5	0.3
K_2O	0.8	0.5	0.5	0.3
SO_3	3.1	1.9	6.2	4.5
P_2O_5	0.3	0.3	0.2	0.2
Mn_3O_4	0.1	< 0.1	0.2	0.3

The Standard N.C.B. Presentation of Coal Analyses

1. Analysis is carried out on the air dried (ad) sample and for the dry ash-free basis, the effects of moisture and ash are taken out

$$\frac{100 - (M_{ad} + A_{ad})}{100}$$

2. The dry mineral matter-free basis is a calculated one, taking account of the chemical changes that take place in the mineral matter during the ashing process. The main changes are:-

   (i) liberation of carbon dioxide from carbonates

   (ii) liberation of water from silicates

   (iii) conversion of iron pyrites to iron oxide

   (iv) liberation of chlorine from chlorides

   (v) fixation of sulphur gases by basic oxides.

3. The determination of mineral matter is rather laborious and an inaccurate process, thus in the U.K. a formula is used and it was devised by the British Coal Utilisation Research Association (B.C.U.R.A.):-

$$\text{Mineral Matter}_{ad} = 1.10\ \text{Ash}_{ad} + 0.53\ \text{Total sulphur}_{ad} + 0.74\ CO_{2,ad} - 0.36$$

   The conversion to 'dmmf' basis is $\dfrac{100}{100 - (\text{Moisture}_{ad} + MM_{ad})}$

4. When carbon is reported by the N.C.B. on the 'dmmf' basis, it is in reality 'organic carbon' (Co). The determined carbon figure is corrected for the carbon present in coal as carbonate by the formula:-

$$Co = C_{ad} - 0.273\ CO_{2,ad}$$

5. Total hydrogen is corrected for the hydrogen in the water of constitution of silicates (shale in the mineral matter, hence the pyrite and carbonate factors).

$$H = H_{Total,ad} - 0.014\ Ash_{ad} + 0.02\ S_{pyrite,ad} + 0.02\ CO_{2,ad}$$

T_{Total} excludes hydrogen from moisture in coal.

6. Nitrogen and organic sulphur need not be corrected, but they still have to be converted from air dried to 'dmmf' basis.
7. The above notes are given in detail with the derivations in British Standards Institution 1980/81. Methods for analysis and testing of coal and coke. BS1016, part 16. Methods for reporting results.
8. Acklington Dyke sample Nos. 2 and 3 are very high in ash and in this case the B.C.U.R.A. formula is not valid. When the elements are converted to 'dmmf' basis, the errors are such that the oxygen value, arrived at by difference, is meaningless.

The variations in the coal analyses (Table 5.12) are thought to reflect real differences in the nature of the coal. The contact between the igneous intrusive and the coal may be sharp and planar, or it may be diffuse and irregular. Zones of more severely altered coal may form therefore within the coal seam. [284,285] The data in Table 6.12 reveal a marked change in the characteristics of the coal seam (viz. volatile matter, fixed carbon, carbon content (dmmf) and hydrogen content) [265] between sample positions 6 and 8. Coal from position 8 shows only slight signs of being heat affected and bears a far stronger resemblance to coal sample 9 than it does to the cinder coal at position 6. The collection of additional samples at intermediate positions between samples 6 and 8 was not possible since the coal seam was mined shortly after the author's visit.

5.3.6d Optical Microscopy

During carbonisation, coking coals soften on heating, swell on decomposition and resolidify during continued degasification. [259,286]

Changes in the state of the coal and coke, both naturally occurring and laboratory controlled, have been monitored using optical microscopy. microscopy. [263,278,285-7] (Scanning electron microscopy has also been used in studies of morphological changes occurring during carbonisation and gasification of coals and pitches. [287])

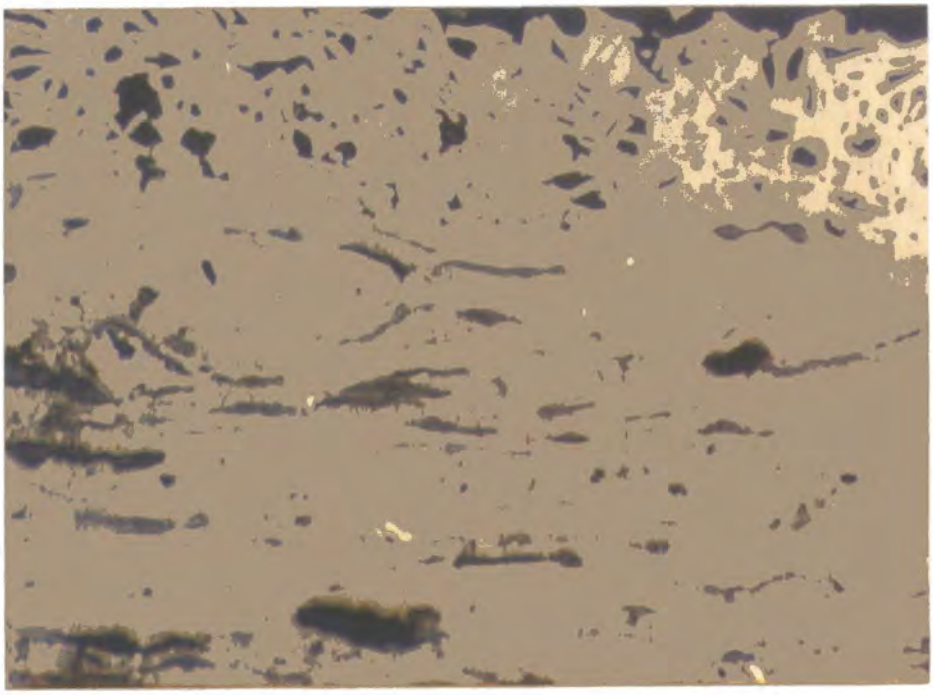

Figure 5.11a

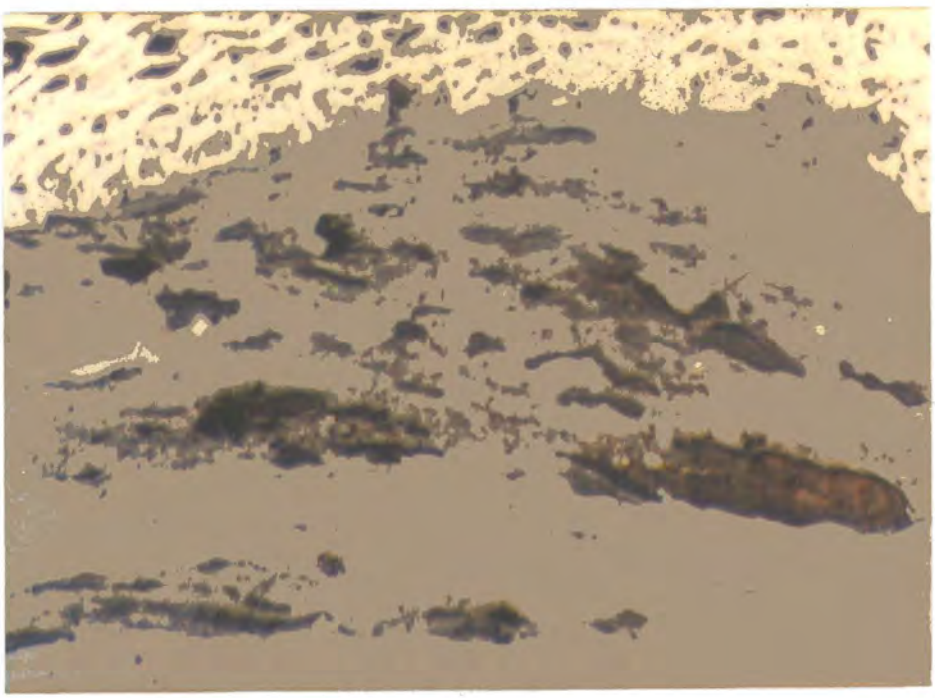

Figure 5.11b

Acklington Dyke coal. Photomicrographs of coal and natural coke from the Togston open cast site, Northumberland, x 296. See text for details.

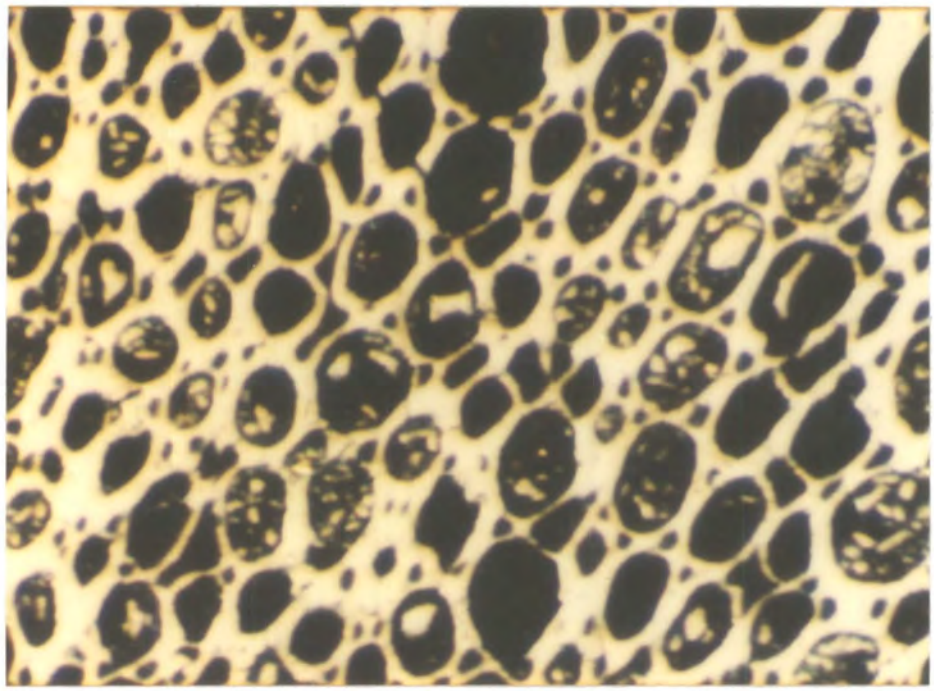

Figure 5.11c

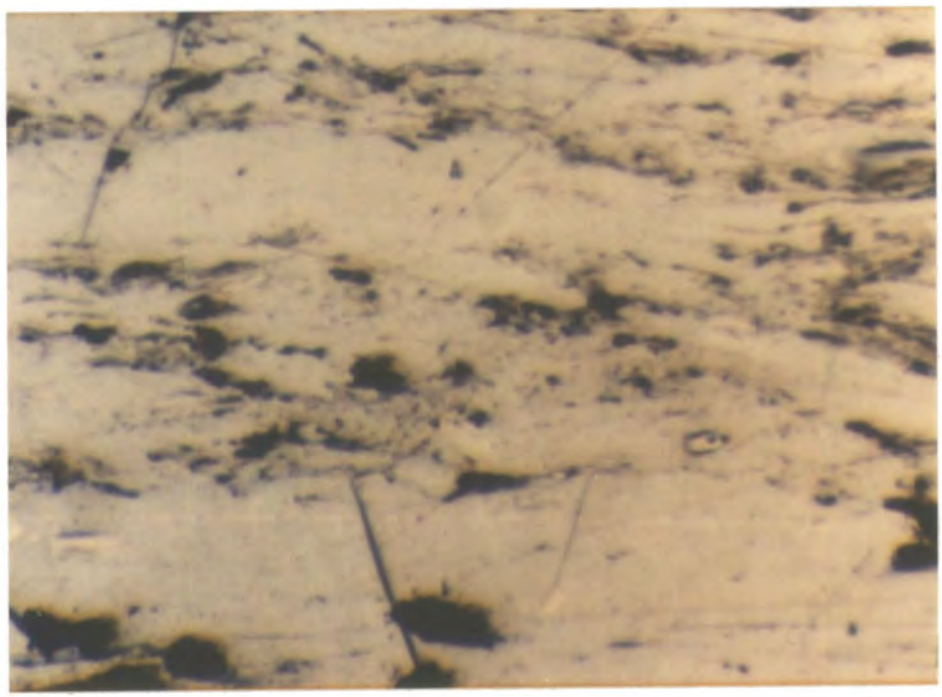

Figure 5.11d

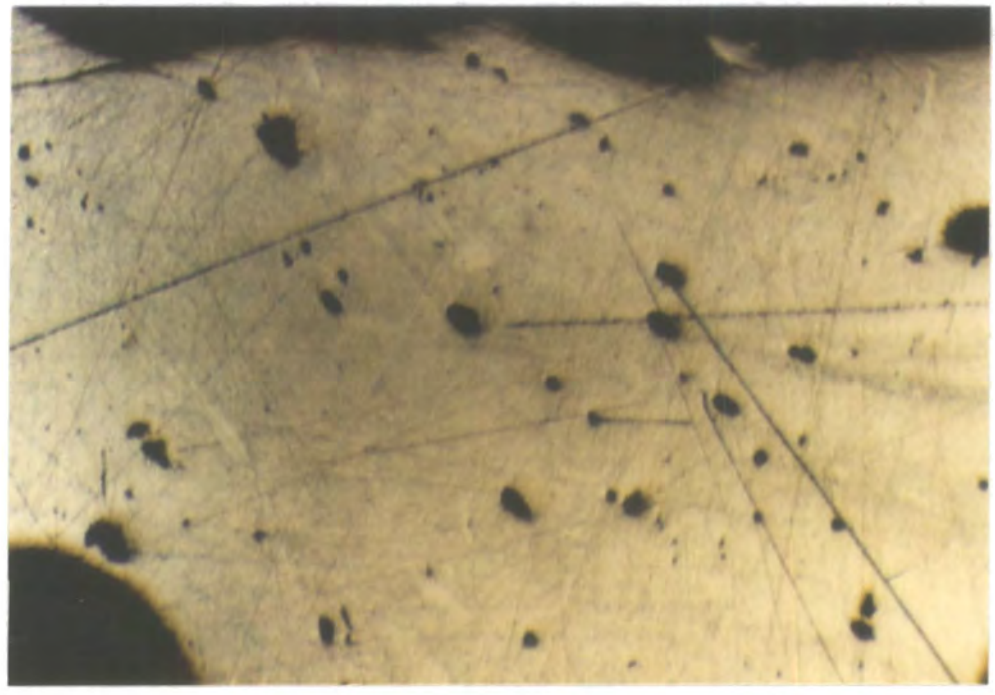

Figure 5.11e

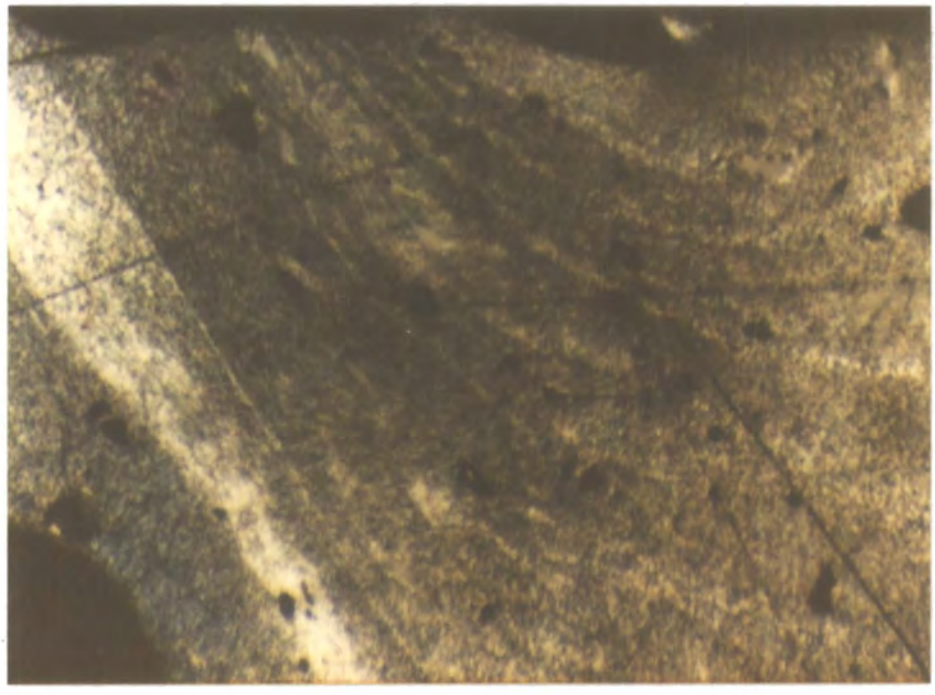

Figure 5.11f

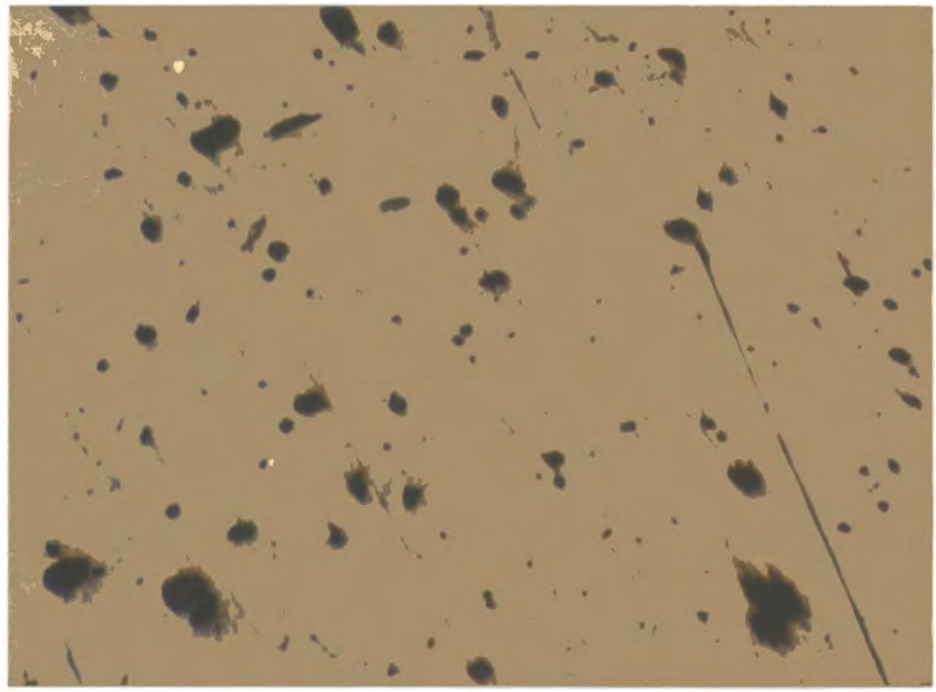

Figure 5.11g

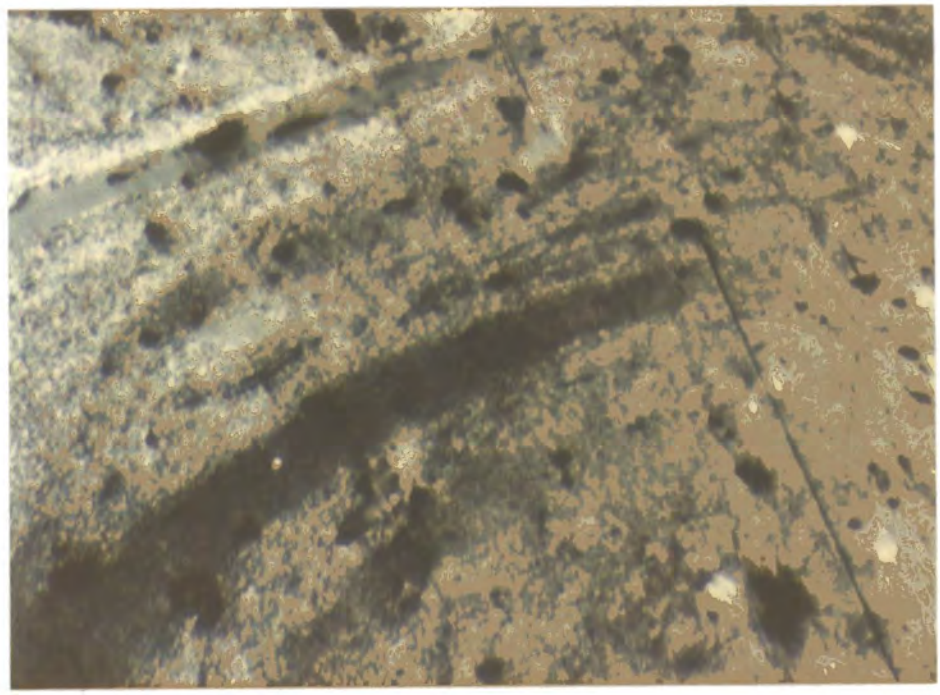

Figure 5.11h

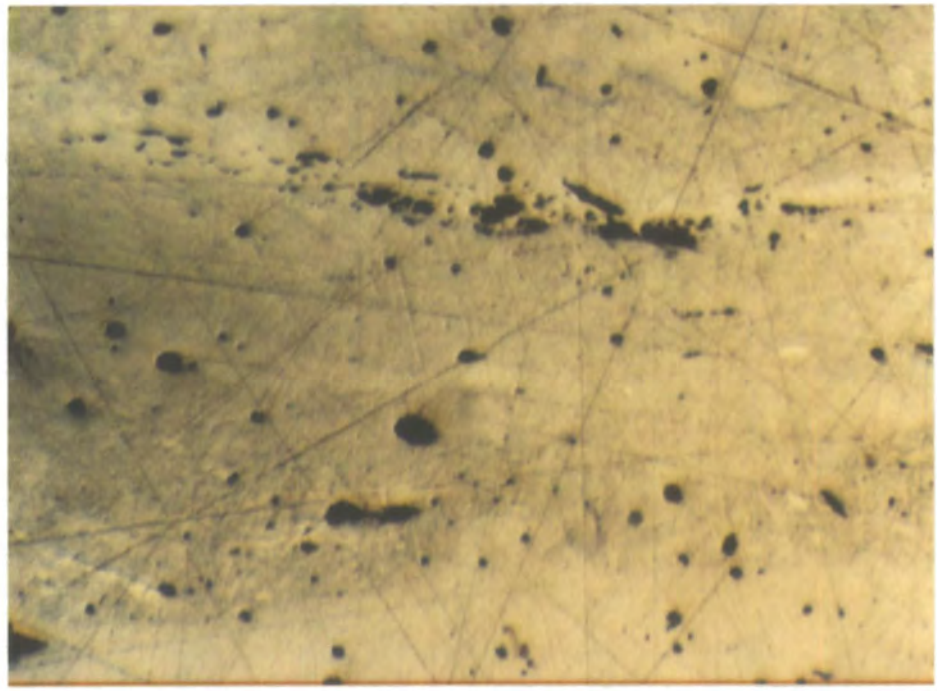

Figure 5.11i

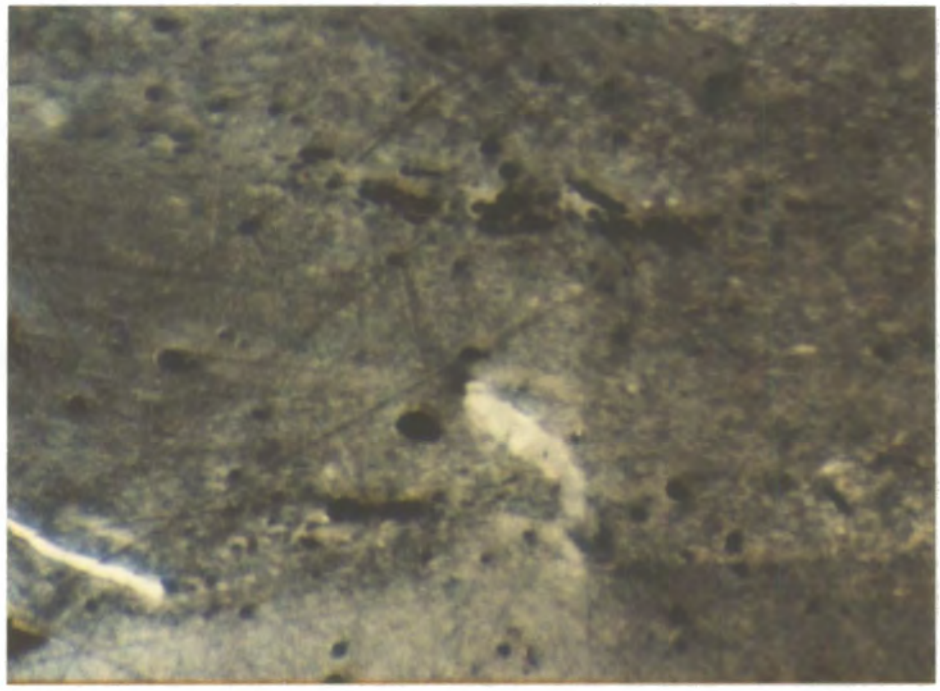

Figure 5.11j

The photomicrographs shown in Figure 5.11 are illustrative of the petrological changes accompanying carbonisation, [263,278,285] and have been taken on polished surfaces under oil immersion using plane-polarised white light. Since the petrology of thermally metamorphosed bituminous coals is complex, the interested reader is referred to accounts given by those expert in the field. [263,278,286]

Figure 5.11a reveals the inhomogeneous nature of coal. Under the microscope the components of coal may be differentiated by their morphology. [263] Macerals, as they were termed by Stopes, [288] are analogous to the minerals of inorganic rocks but differ in having less uniform chemical composition and physical properties. All macerals have the suffix 'inite', and are classified in three groups : [262]

1) Vitrinite, originating from wood or bark, and is the most abundant maceral group (appearing light grey in Figures 5.11a and 5.11b);
2) Exinite (or lipinite), formed from the remains of spores (e.g. the dark grey/orange area in Figure 5.11b), resins, algae and cuticles (appearing dark grey in Figures 5.11a and 5.11b);
3) Inertinite, named for its relatively inert behaviour on coking, comes from the same type of plant components as vitrinite, although this material was strongly affected by oxygen during the early stages of coalification. The characteristic optical property of inertinite macerals is their high reflectance. [263] Hence the inertinite components in the photomicrographs of the coals in Figures 5.11a and 5.11b appear off-white against the vitrinite background. Figure 5.11c shows fusinite, a member of the inertinite maceral group, from heat altered coal (sample 4). Here the cellular structure of the plant remains have been well preserved. The term 'screen' or 'sieve' structure has been used to describe such structure. [263]

In many cases the walls of the empty cells have been fractured and pushed into one another, resulting in 'bogen' or 'star' structure (e.g. top of Figures 5.11a and 5.11b). [263]

Where the temperature has been comparatively low, say less than 300°C, the bedding of the coal becomes distorted resulting from the high local pressure during intrusion [263] (cf. Figures 5.11a and 5.11b). Figure 5.11d shows some vesiculation of the heat altered coal due to the evolution of volatile carbonaceous matter. [278] Figures 5.11e-j show photomicrographs of natural coke. The full degree of the true textural complexity of the field of view becomes apparent only when the microscope analyser is placed in the optical train (cf. Figures 5.11e,g,i and Figures 5.11f,h,j). [286] The formation of coke with mosaic structure suggests that the product formed at ∿ 500°C and above. [289] The mosaic units have higher reflectance than that of the unaltered maceral and have a characteristic anisotropy. The optical anisotropy is brought about by the formation of highly imperfect crystals of graphite within the coke structure. [286,287] Both maximum reflectance and anisotropy increase with temperature of alteration. [263,278,286]

The examination of the polished surfaces of the coal and coke samples did reveal the presence of a low level of finely dispersed mineral matter (quartz and iron sulphide for example). This mineral matter may have been inherent in the matrix of the coal, or it may originate from the intrusive action of the dyke. [263,285]

5.3.6e Reflectance Measurements

Reflectance, which is related to the temperature of carbonisation and also to the chemical composition of the thermally affected coal, is an important parameter in the assessment of carbonisation processes. [263,286]

Individual reflectance measurements for the vitrinite of samples 9 and 8 and for the natural coke samples (nos. 7 - 1) are plotted in histogram form in Figure 5.12. Statistical data is provided in Table 5.14. The mean reflectivities are plotted as a function of their relative positions in Figure 5.13.

Table 5.14 Acklington Dyke Coal

The measurement of the reflectance of vitrinite

Sample No.	$\bar{r}$ (%)	σ	N
1	3.54	0.36	92
2	3.40	0.31	52
3	2.75	0.44	73
4	2.95	0.32	78
5	2.70	0.38	62
6	2.72	0.21	60
7	2.66	0.24	55
8	0.82	0.05	60
9	0.67	0.05	58

N.B.

$\bar{r}$ = average of measured reflectance values.

For samples nos. 8 and 9, $\bar{r} = \bar{R}$

σ = standard deviation of reflectance values.

N = number of measurements per sample.

The reflectivity measurements are seen to increase on approaching the igneous intrusion. This increase stems from the development of graphitic-like domains within the coke. The development of optical

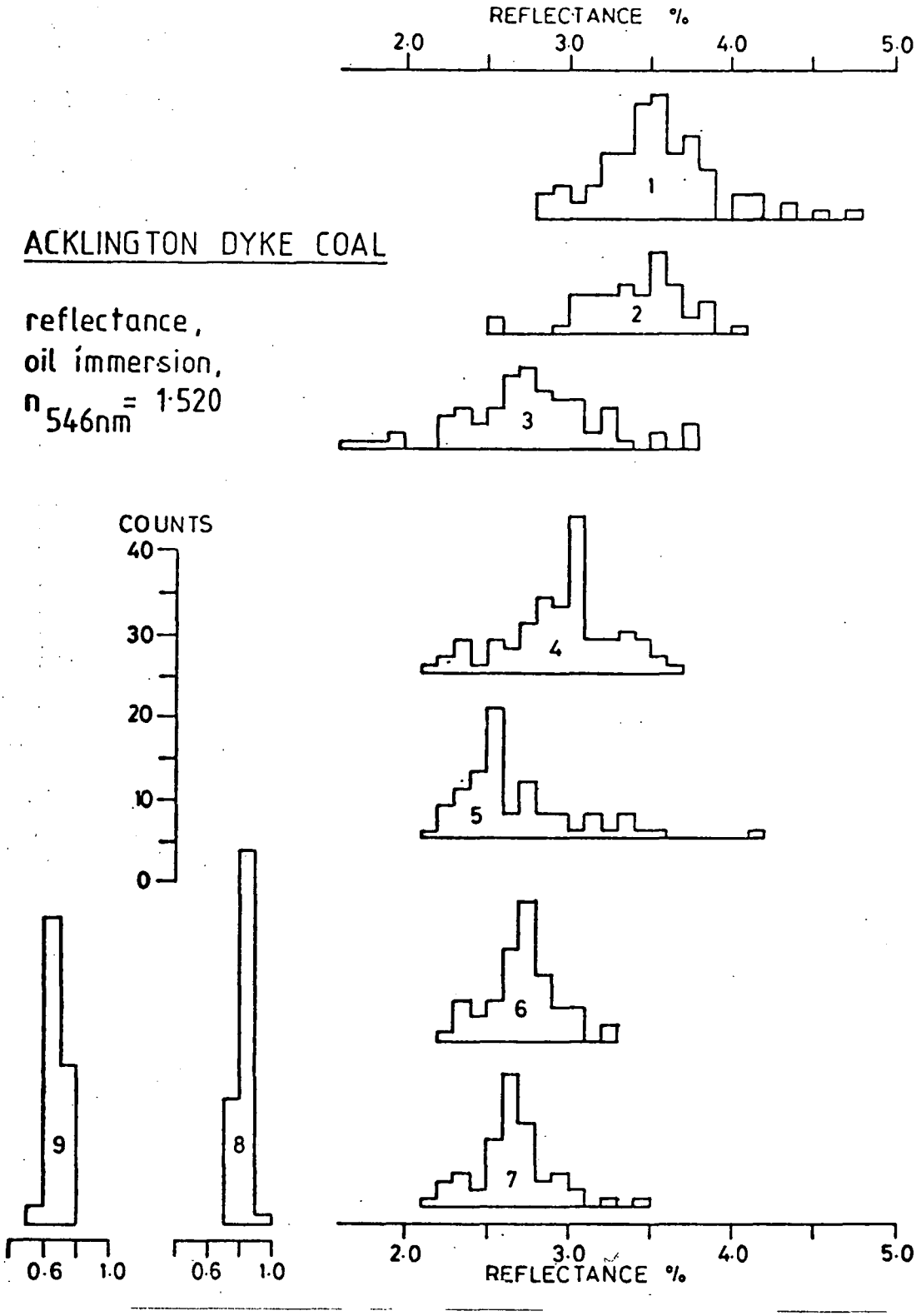

Figure 5.12 Acklington Dyke coal. Histogram representation of reflectance measurements.

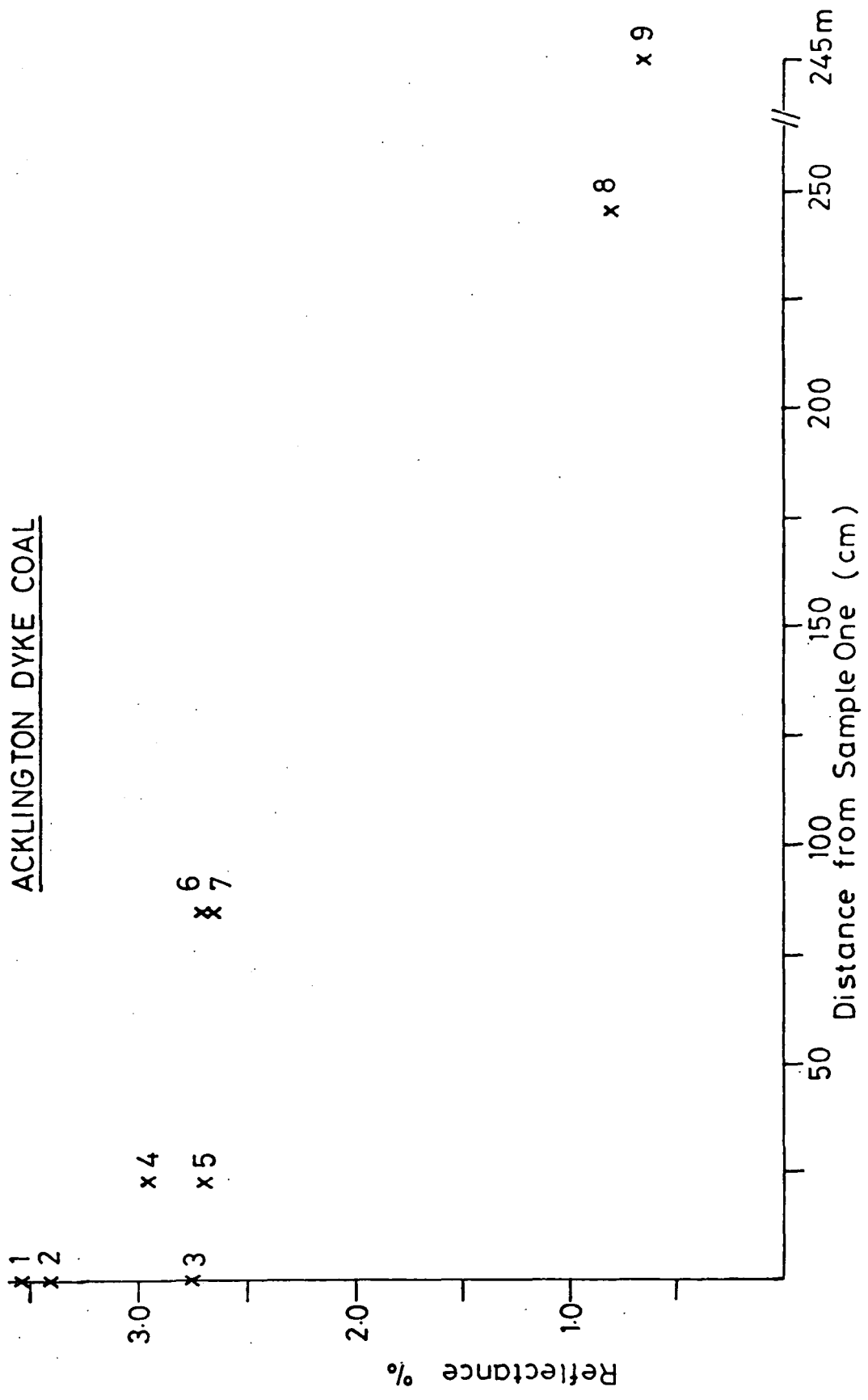

Figure 5.13 Acklington Dyke coal. Mean reflectivities of coal samples plotted in relation to their relative sample locations.

anisotropy on carbonisation is apparent from the increased scatter in reflectivity measurements for the heat altered coal. [286,289] (It should be remembered that all reflectance measurements were made without rotation of the microscope stage. Maximum reflectance values therefore are not available.) There will be other factors which may contribute to the variation in reflectance measurements, some of which may become increasingly more significant for heat altered coals.[286,287,289]

There is a tendency for the samples taken from nearer the roof of the coal seam to exhibit a greater reflectance than samples taken at the same location at increased depth.

The author has been advised [289] that the reflectance of the natural coke from position 1 suggests that the coke was situated $\sim$ 3m from contact with the dyke. In addition, the coal sample 9 ($\bar{R}_{oil}$ = 0.67) is thought to have undergone some thermally induced changes. The vitrinite reflectance of unaltered coal, taken from the same site, was found to be slightly lower ($\bar{R}_{oil} \sim 0.4 - 0.5$).

5.3.6f X-ray Diffraction and Solid State ^{13}C nmr Spectroscopy

The previous sections have made reference to the development of graphitic character within the carbon matrix on coal carbonisation. Two techniques have been used to probe such a change, namely x-ray diffraction [259,290,291] and solid state ^{13}C nmr spectroscopy. [269]

Figure 5.14 presents the x-ray diffraction curves for coal sample 9 and for the natural coke from position 1. Structural differences between the two materials are revealed, in addition to information on the mineral matter contents.

Coal sample 9 shows the x-ray pattern of a typical coal, a very broad amorphous peak band $\sim 19^{o}2\theta - 32^{o}2\theta$ on which are the peaks of typical 'cleat' minerals (minerals found in cracks and cleavages) associated with coal. [263,285] These minerals are kaolinite

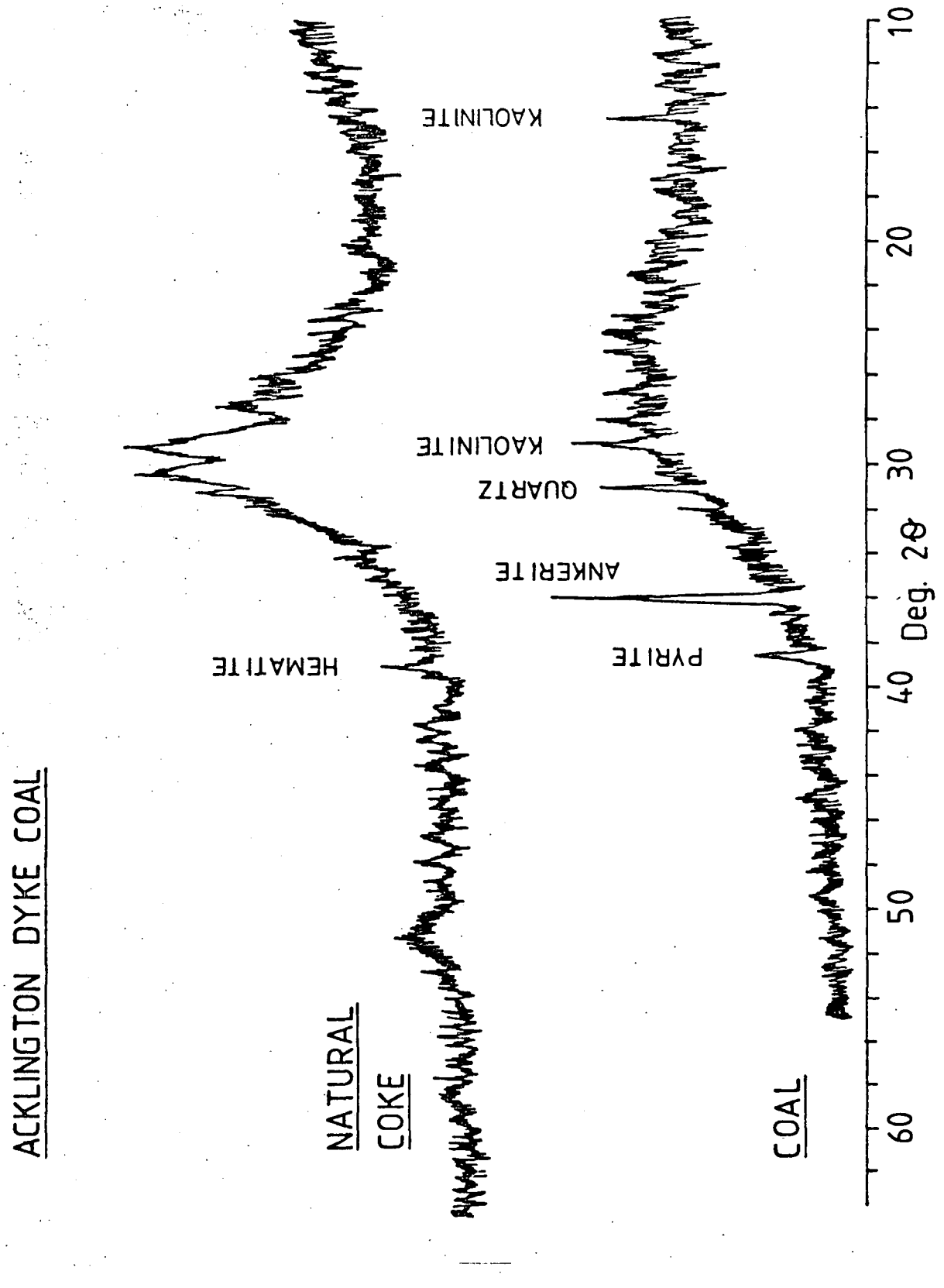

Figure 5.14 Acklington Dyke coal, X-ray diffraction curves for natural coke and unaltered coal.

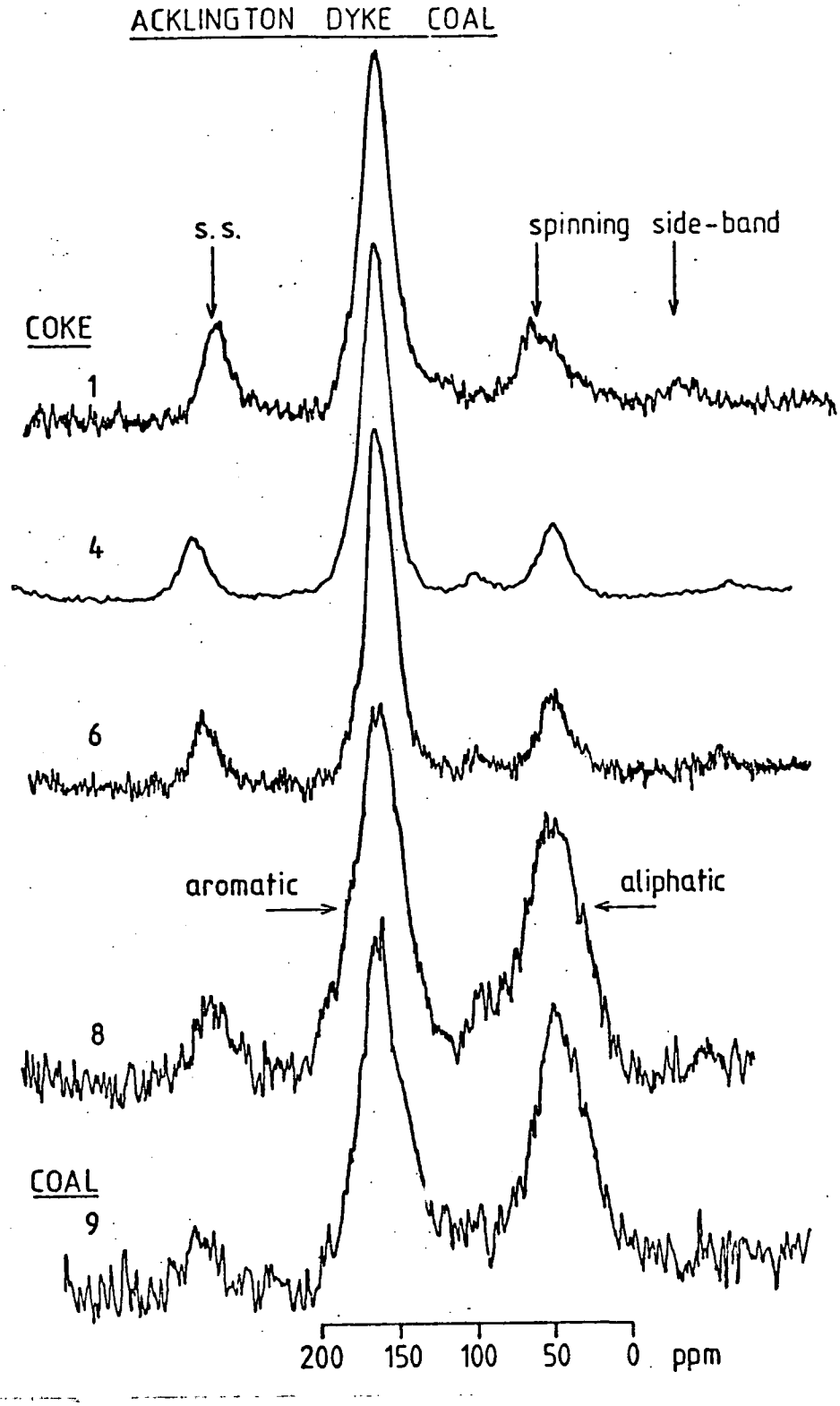

Figure 5.15 Acklington Dyke coal. Solid state ^{13}C nmr spectra.

(Al_4 Si_4 O_{10} $(OH)_8$), pyrite and ankerite (a calcium, magnesium and iron carbonate mineral). [292]

In contrast, the natural coke shows a structurally more ordered pattern with a major peak at ~ 3.46Å. On the extended chart of this sample a less prominent peak was noted at ~ 2.03Å. This is very similar to the x-ray pattern of graphite which has peaks at 3.36Å and 2.08Å. [293] Also found on the extended chart was evidence of the mineral hematite (Fe_2O_3), most probably produced through the action of heat on pyrite. [263]

The solid state ^{13}C nmr spectra of the coal and coke samples, obtained using the technique of magic angle spinning, indicate an increase in the apparent aromaticity of the coal on coking, the change in apparent aromatic : aliphatic carbon ratio being the greatest on going from sample positions 8 to 6 (Figure 5.15).

5.3.6g ESCA analyses

ESCA analyses of the coal and coke have been carried out on freshly powdered samples (those used for the N.C.B. analyses), and the relative area measurements of the C_{1s}, O_{1s}, N_{1s}, S_{2p}, Si_{2p} and Al_{2p} core level spectra are tabulated in Table 5.15. Scans of the 0 - 250eV binding energy region of $Mg_{K\alpha}$ excited spectra of specimens from each sampling position are displayed in Figure 5.16. As was the case for the coals of the Lower Kittanning seam (Section 5.3.3), the relative areas of the Si_{2p} and Al_{2p} photoionisation peaks may not reflect the bulk composition of the whole coal.

Figure 5.16 indicates a surface chemistry of the coked coals enriched in silicon and aluminium compared with the coal collected well away from the intrusive body (Sample 9). ESCA analyses of the silicon and aluminium levels of different samples, each taken from the same

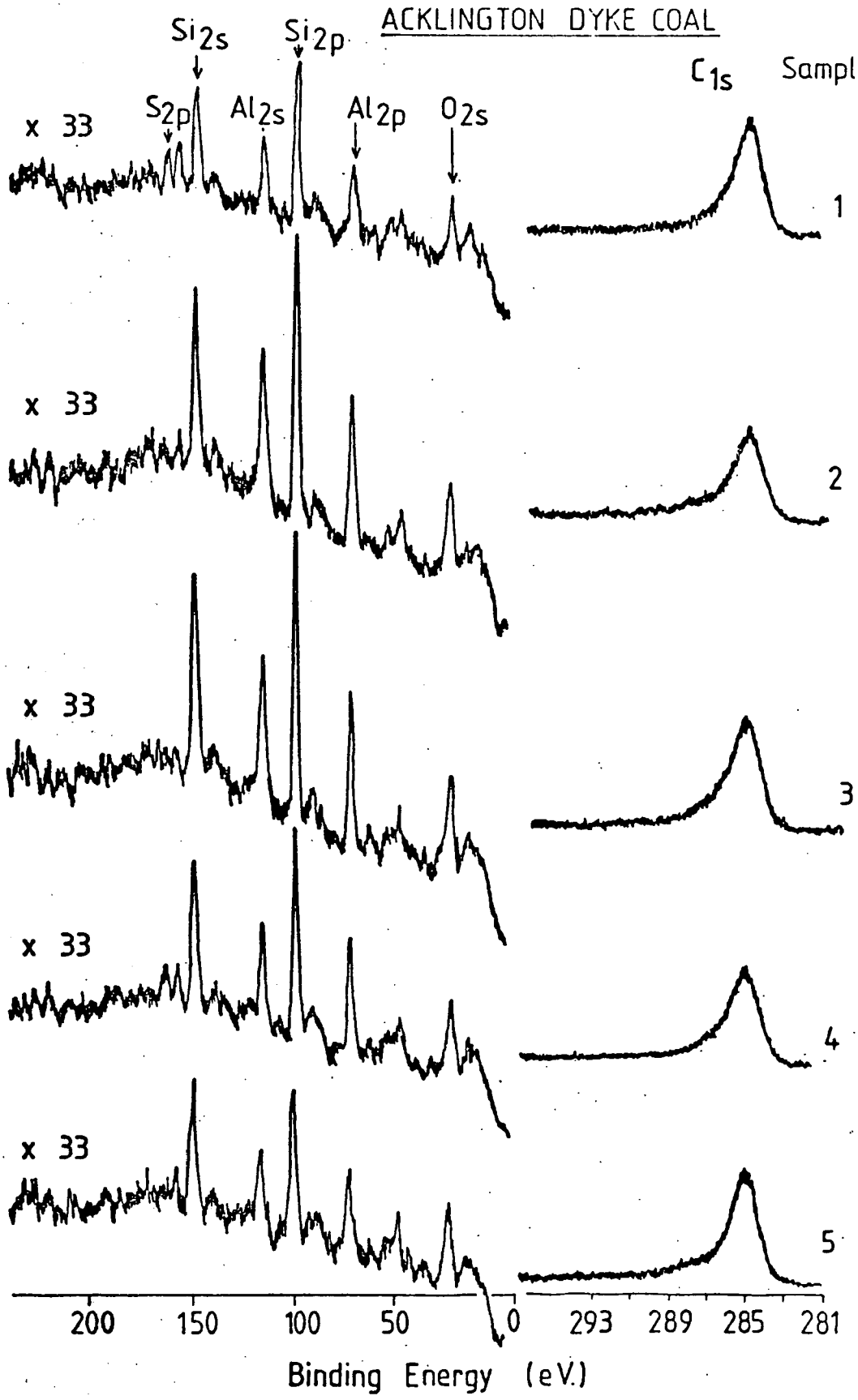

Figure 5.16 Acklington Dyke coal. C_{1s} core level spectra and 0 - 250eV binding energy scans.

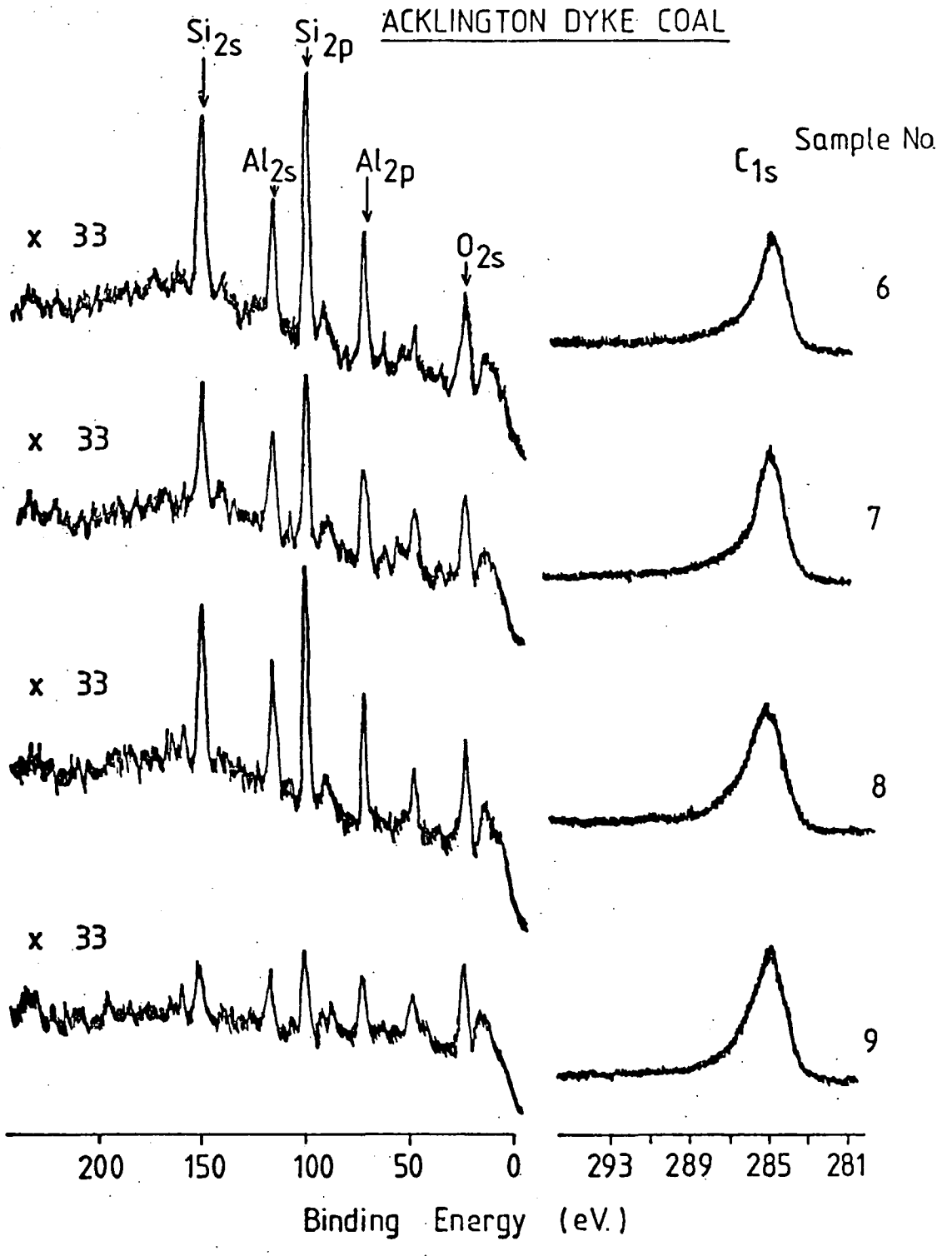

Figure 5.16 (continued)

Table 5.15 Acklington Dyke coal

ESCA relative peak area measurements

Sample no.	C_{1s}	O_{1s}	N_{1s}	S_{2p}	$S_{2p}(ox)^{\dagger}$	Si_{2p}	Al_{2p}
1	100	31.1	0.59	1.64	63.4	1.29	0.33
4	100	23.6	1.05	0.61	57.0	0.62	0.31
5	100	29.0	0.43	1.42	59.3	1.0	0.41
6	100	33.8	1.53	0.58	52.7	1.1	0.62
7	100	30.2	1.28	0.70	51.0	2.34	0.66
8	100	28.9	0.86	0.80	45.0	0.57	0.21
9	100	30.4	1.68	0.60	37.1	0.64	0.37

† Percentage of total S_{2p} envelope as oxidised sulphur.

sampling position, have been plotted against the corresponding oxygen level, all levels expressed relative to carbon. Sampling positions 1 (natural coke) and 9 (uncoked coal) have been considered and the results are shown in Figure 5.17. Similarly plots of the silicon levels versus aluminium levels are shown in Figure 5.18. The raw data and linear regression analyses for these plots are given in Table 5.16. It is seen that linear relationships exist between O_{1s} and Si_{2p}, O_{1s} and Al_{2p} (and Si_{2p} and Al_{2p}) ESCA relative peak area measurements. This data demonstrates the inhomogeneous nature of the samples as far as the distribution of silicon and aluminium containing minerals are concerned (see also Section 5.3.3c). For the particular samples examined here, the ESCA analyses show the coked coal to have markedly higher silicon and aluminium surface concentrations than the uncoked coal. This observation is not apparent from either the N.C.B. data (Table 5.12) or the ESCA analysis of the powdered coals (Table 5.15).

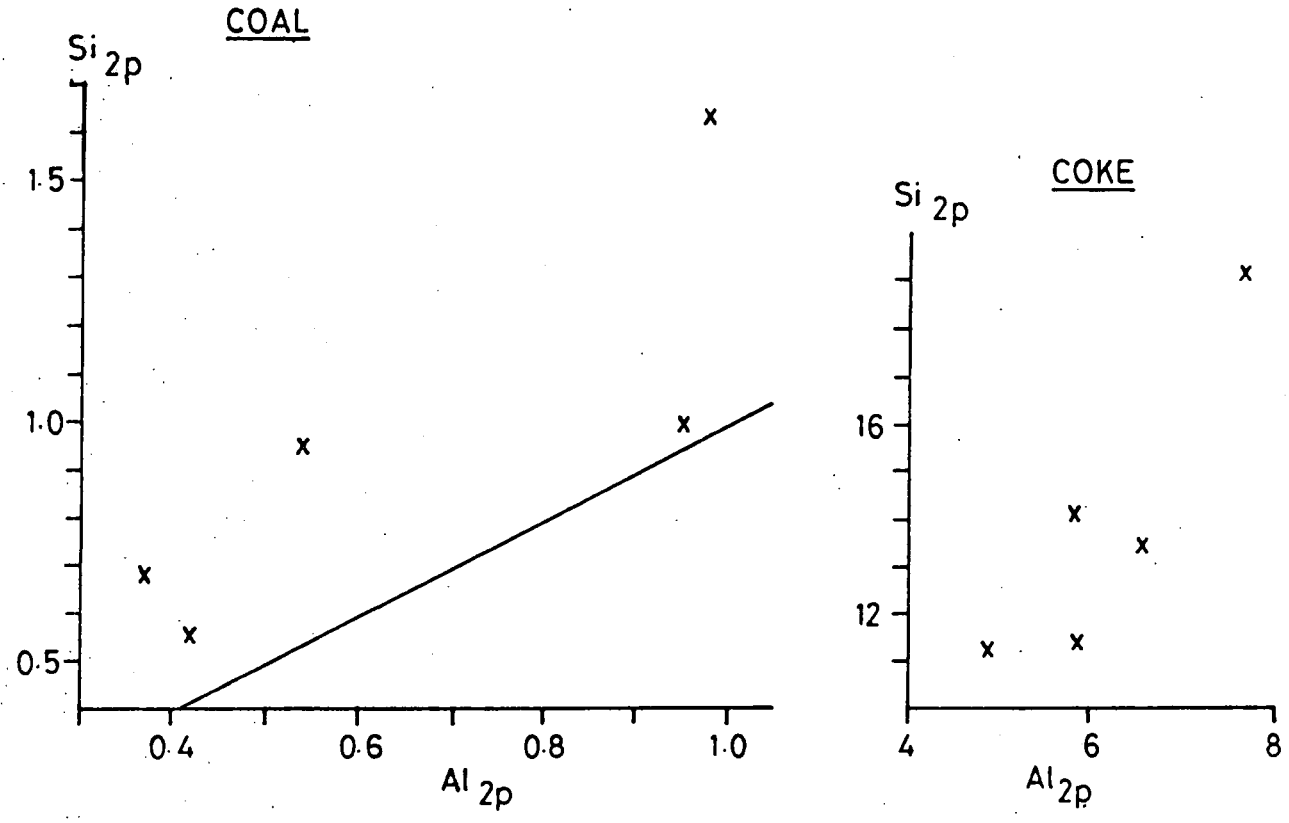

Figure 5.17 Acklington Dyke coal. Relationships between O_{1s} and Si_{2p}, and O_{1s} and Al_{2p} relative peaks from the analyses of unaltered coal and natural coke. (Total C_{1s} peak intensity taken as 100 units.)

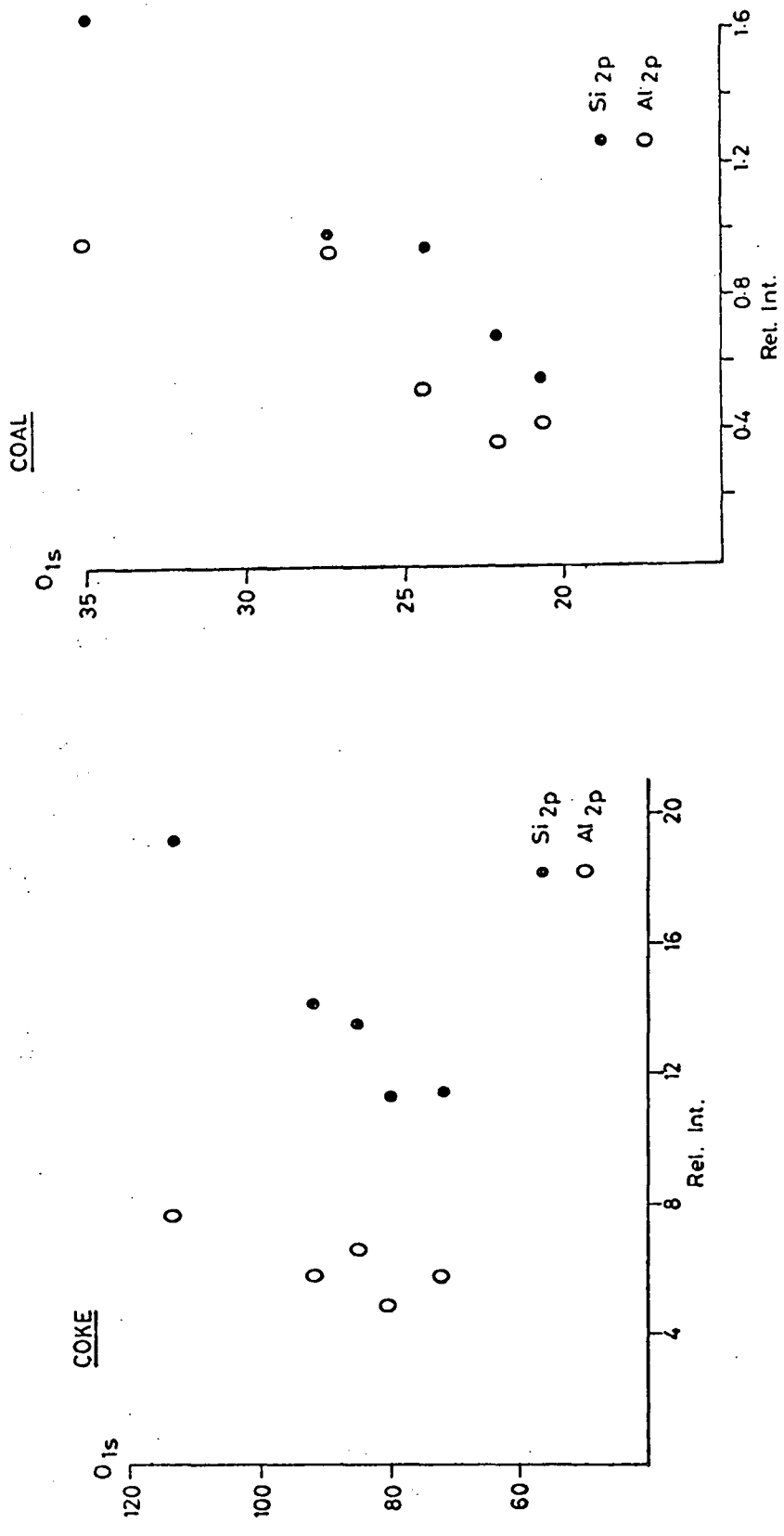

Figure 5.18 Acklington Dyke coal. Relationship between Si_{2p} and Al_{2p} relative peak areas from the analyses of unaltered coal and natural coke. (Total C_{1s} peak intensity taken as 100 units.)

Table 5.16 Acklington Dyke coal

O_{1s}, Si_{2p} and Al_{2p} relative area measurements for coked and uncoked coal.
Total C_{1s} peak area taken as 100 units.

Natural Coke (Sample 1)			Uncoked Coal (Sample 9)		
O_{1s}	Si_{2p}	Al_{2p}	O_{1s}	Si_{2p}	Al_{2p}
91.64	14.10	5.76	24.44	0.953	0.536
84.89	13.43	6.53	20.64	0.554	0.414
113.27	19.15	7.63	27.41	0.998	0.945
72.00	11.37	5.81	35.16	1.640	0.974
80.49	11.30	4.85	22.09	0.684	0.363

Continued overleaf

Table 5.16 (continued)

$O_{1s} = 4.76\ Si_{2p} + 22.48$	$O_{1s} = 13.55\ Si_{2p} + 12.86$
$(r = 0.976)$	$(r = 0.989)$
$O_{1s} = 11.68\ Al_{2p} + 17.01$	$O_{1s} = 17.34\ Al_{2p} + 14.74$
$(r = 0.775)$	$(r = 0.883)$
$Si_{2p} = 2.74\ Al_{2p} - 2.89$	$Si_{2p} = 1.19\ Al_{2p} + 0.20$
$(r = 0.886)$	$(r = 0.829)$

N.B. The numerical data presented here are 'raw' figures and are not indicative of the precision of measurement (see Section 5.3.2b). r = correlation coefficient.

The data in Table 5.16 would indicate that, for each sampling location, silicon and aluminium are constituents common to a particular mineral type, kaolinite for example, or are associated with more than one mineral, the relative concentrations of which remain constant at that location. The ESCA derived surface Si : Al atomic ratio is seen to increase by a factor of 2.3 on going from the uncoked coal to the natural coke. This is indicative of an enrichment in silicon, as detected by ESCA, for the heat altered coal.

The results of sulphur analyses using ESCA (Table 5.15) and standard N.C.B. methods (Table 5.12) show sulphur levels are highest for the heat altered coal. This increase is quite reasonable and arises from the interaction of the intrusive mass with the coal bed. [263] Figure 5.19 illustrates S_{2p} core level signals of four coals from different sampling positions. The contribution of oxidised sulphur species to the overall S_{2p} envelope becomes increasingly more significant as the intrusion is approached.

The $Mg_{K\alpha}$ excited C_{1s} spectra of the coked and uncoked coal (Figure 5.20) possess essentially non-functionalised carbon character. There are two important differences : first, the C_{1s} line shape is narrower for the coked sample than for the uncoked coal, the respective FWHMs being $\sim$ 1.7eV and $\sim$ 2.1eV[†] (the FWHM of sample 8 is intermediate between the two); and second, the C_{1s} peak for the coked coal is positioned at $\sim$ 284.8eV binding energy, whereas the peak for the uncoked coal is centred at $\sim$ 285eV binding energy. These observations are indicative of an increase in the electrical conductivity of the carbon network, [294,295] and of the development of a certain graphite character on carbonisation. As would be expected, the changes in the carbon network are also reflected in the structure of the valence band spectra (Figure 5.21).

[†] These values were obtained for spectra recorded using ES300 instrumentation.

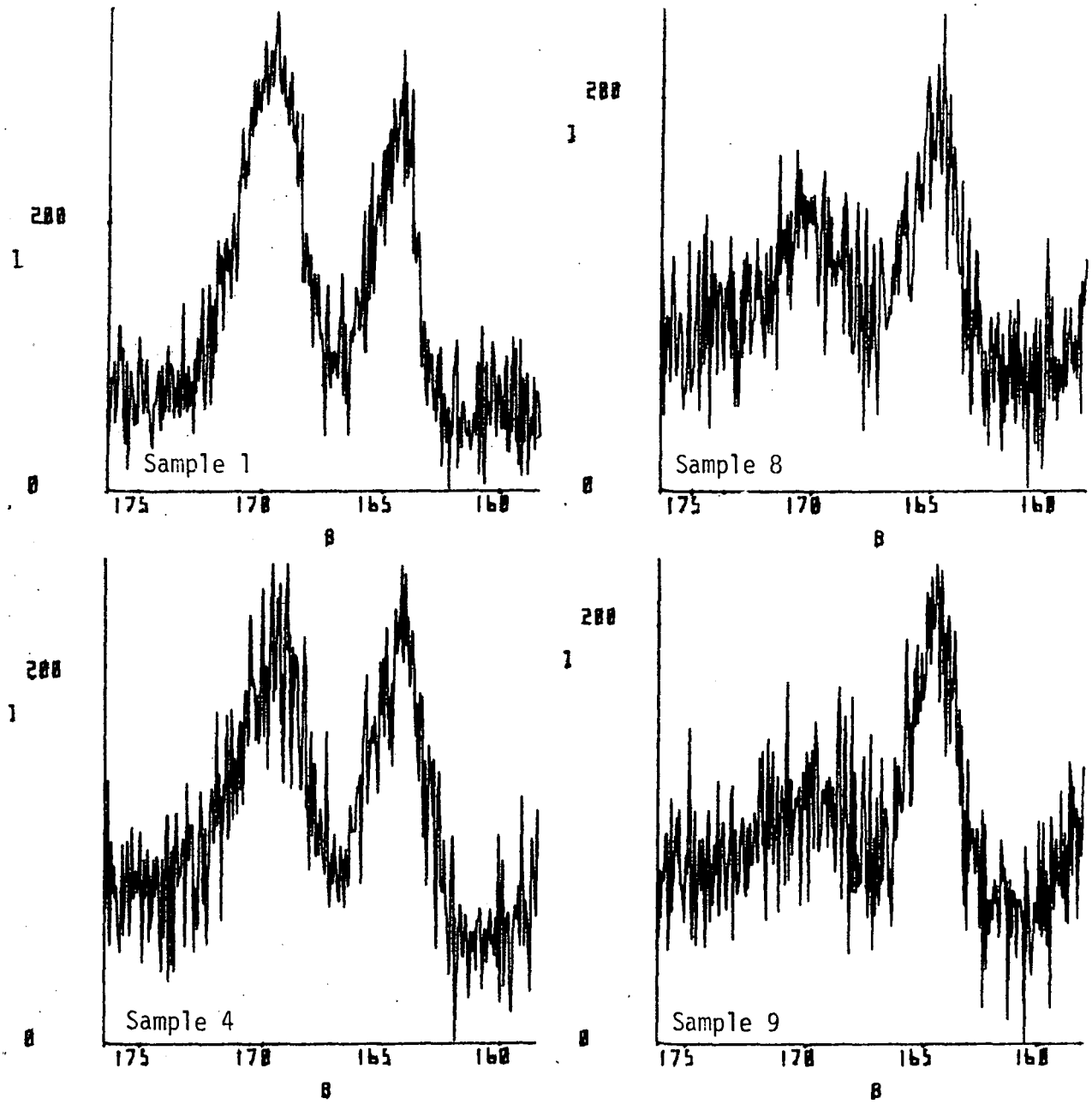

Figure 5.19 Acklington Dyke coal. S_{2p} core level envelopes for coal and coke samples from different locations.

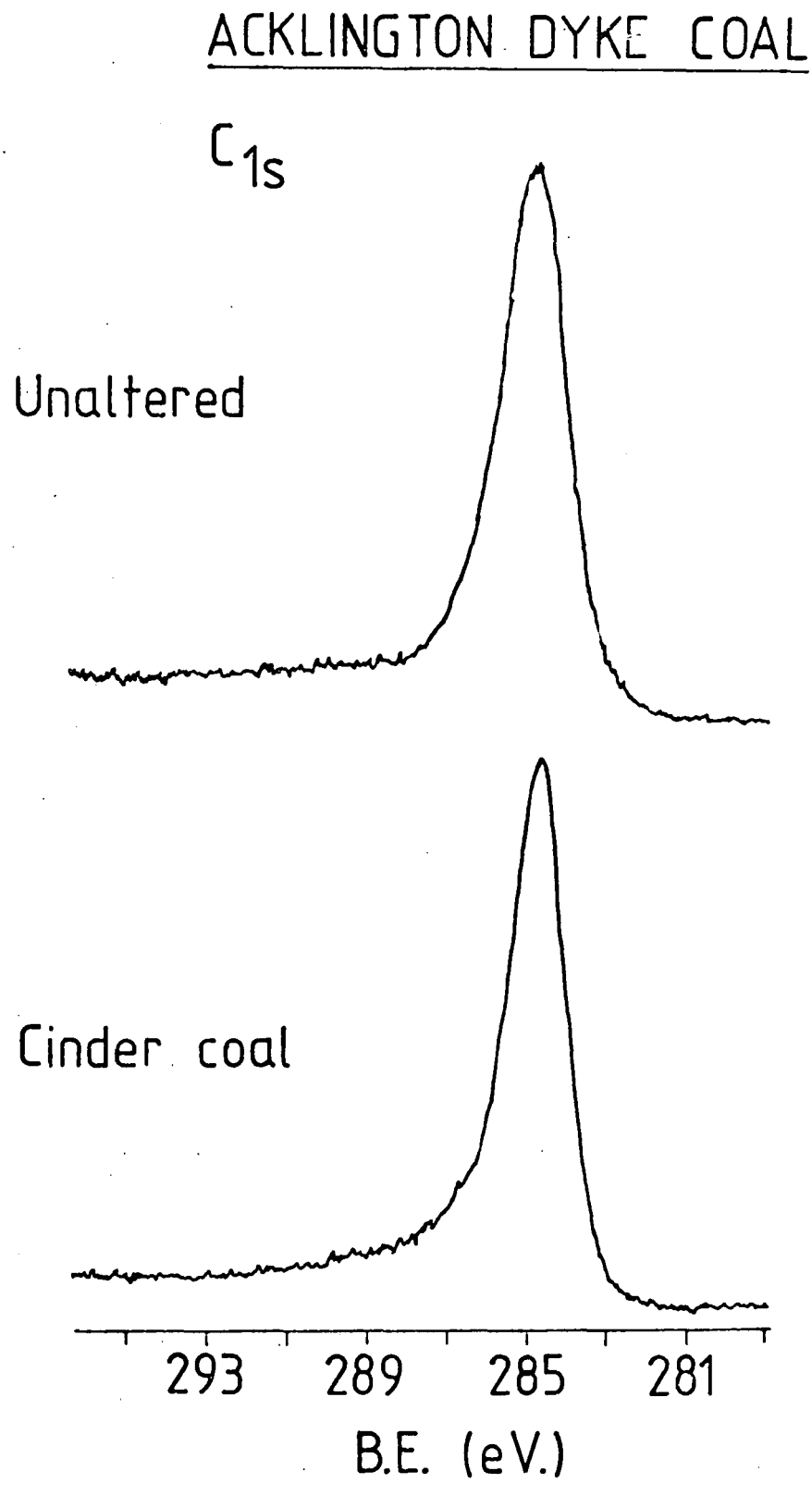

Figure 5.20 Acklington Dyke coal. C_{1s} core level spectra for unaltered coal and natural coke.

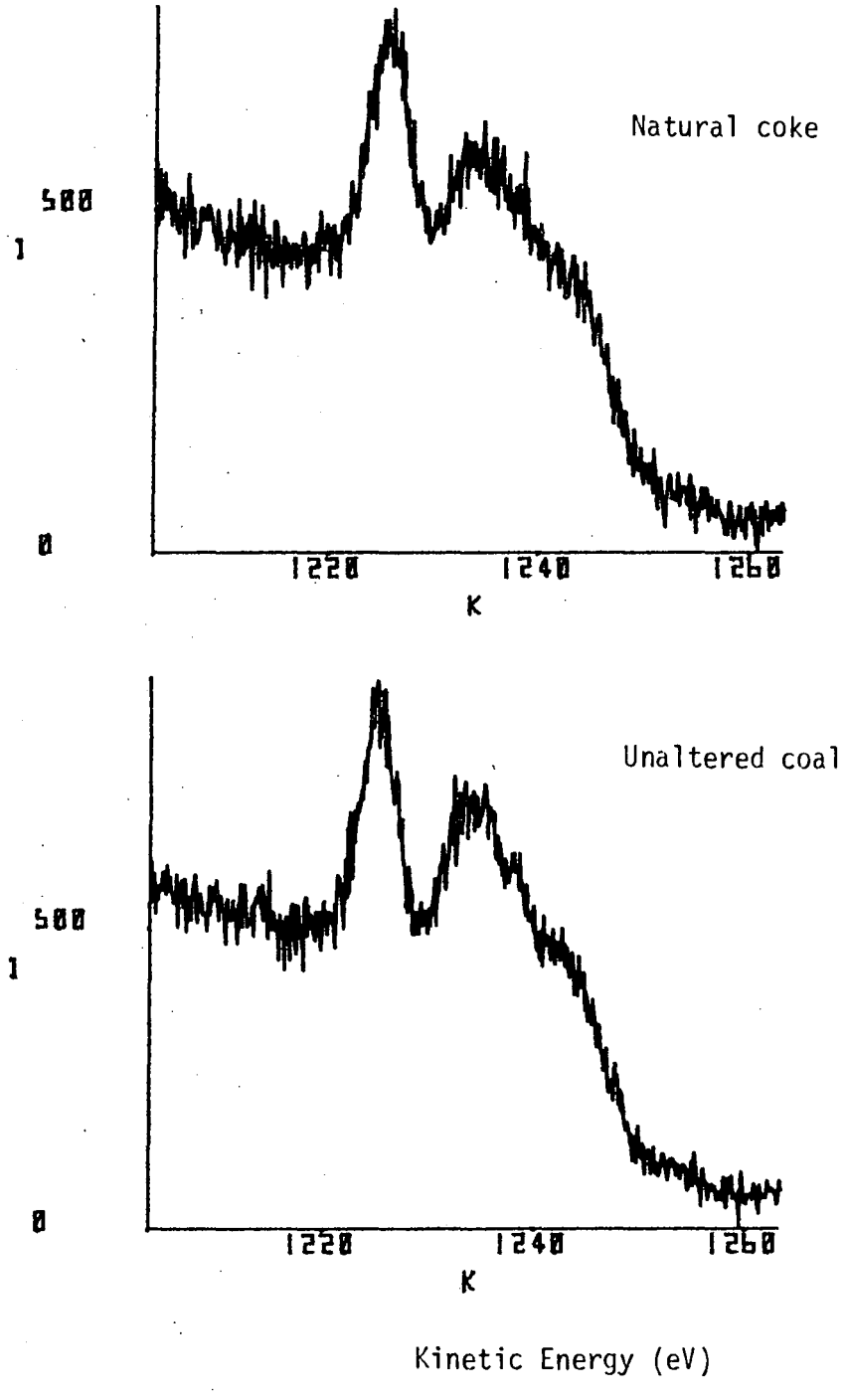

Figure 5.21 Acklington Dyke coal. $Mg_{K\alpha}$ excited valence band spectra for unaltered coal and natural coke.

5.3.7 UV oxidation of some carbonaceous materials

5.3.7a Introduction

The atmospheric oxidation of coals is known to result in the deterioration of their subsequent coking properties [259,263,264,296,297] and liquefaction properties [298] and this poses serious problems to the industrialist : spontaneous combustion of coals on storage is also non-trivial. [263,264,297] Concern is reflected in the voluminous literature pertaining to coal oxidation, the emphasis being placed on the study of thermally oxidised coals. A variety of physical and chemical methods have been employed as research tools. [250,251,259,263,264,296,297] It is clear from this work that low level oxidation is all that is required to cause serious deterioration in the desirable industrial properties of the coal. Analytical techniques capable of monitoring these low level oxidation reactions of coals are therefore in high demand. [297]

This thesis has demonstrated the wealth of information which may be acquired pertaining to surface oxidation phenomena from the ESCA experiment. ESCA is able to detect low level surface functionalisation where bulk analytical techniques would detect no change, relative to the bulk. Hence the application of ESCA to the study of coal oxidation is particularly apposite.

As a natural extension of the laboratory's interest in surface oxidation phenomena, studies on the oxidation of 'geopolymers' have been undertaken. Previous work[169] has investigated the extent to which a series of geochemical materials undergo changes in functionality, as detected by ESCA, when subjected to low power inductively coupled radiofrequency plasmas, excited principally in oxygen. The interaction of geochemical materials in their solid state with ultra-violet light has now received attention. This appears to be an area for which no previous literature

data is available. Here the interaction of Gilsonite pitch with ultra-violet light (254nm) in air will be discussed in some detail. Thereafter results will be presented relating to other carbonaceous materials.

5.3.7b Gilsonite 'selects'

The C_{1s}, O_{1s}, N_{1s} and S_{2p} core level spectra for untreated Gilsonite pitch and Gilsonite exposed to ultra-violet radiation (254nm) in air for exposure times of up to 18 hours are displayed in Figure 5.22. The relative areas of the O_{1s}, N_{1s} and S_{2p} photoionisation signals, plotted as a function of exposure time, are shown in Figure 5.23 and Table 5.17. Visual inspection of the spectra reveals the extensive oxidative features evolved during this mild treatment. The C_{1s} core level spectrum for the Gilsonite pitch used in this study demonstrates the predominant hydrocarbon nature of Gilsonite as is evident by the major component of the C_{1s} envelope at 285eV binding energy. A slight shoulder to the higher binding energy side of the main hydrocarbon peak is characteristic of carbon singly bonded to oxygen or C-N environments. Evidence for such functionalities is given by the presence of low intensity O_{1s} and N_{1s} photoionisation peaks. There is also evident in the spectrum a very low level of sulphur functionality. The S_{2p} core level peak (Figure 5.22) is broad in nature, being dominated by components centred at $\sim$ 163.5eV, corresponding to unoxidised sulphur moieties.

Photo-induced oxidation of both carbon and sulphur species is apparent even after 30 minutes irradiation. The C_{1s} signal shows the development of oxidised carbon species which bring about the growth of the high binding energy shoulder. The component at 285.0eV arises from carbon in the Gilsonite which has not been a site of oxidative attack.

Figure 5.22 C_{1s}, O_{1s}, N_{1s} and S_{2p} core level spectra for Gilsonite 'selects' as a function of exposure time to U.V. irradiation (254nm) in air at ~ 30°C.

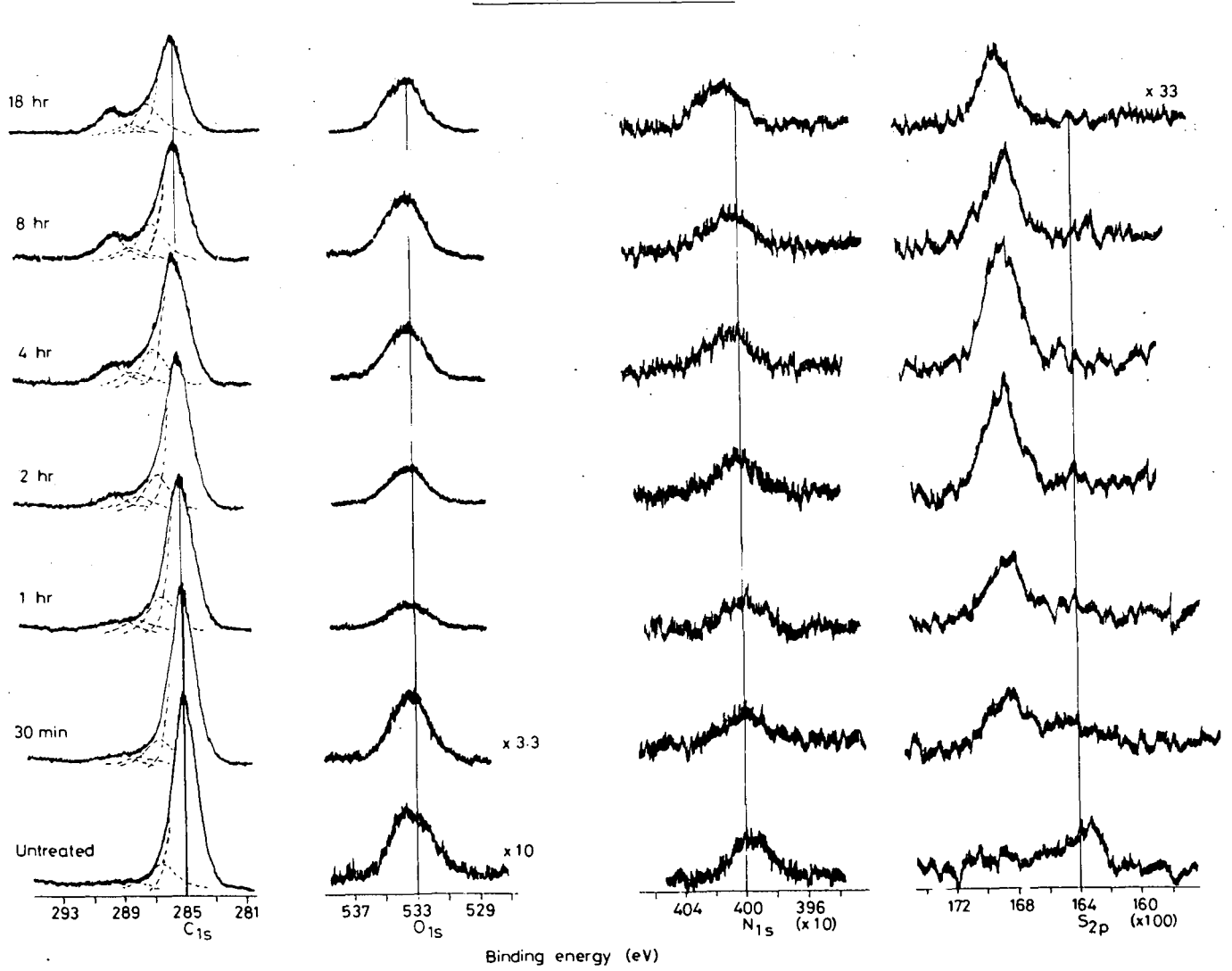

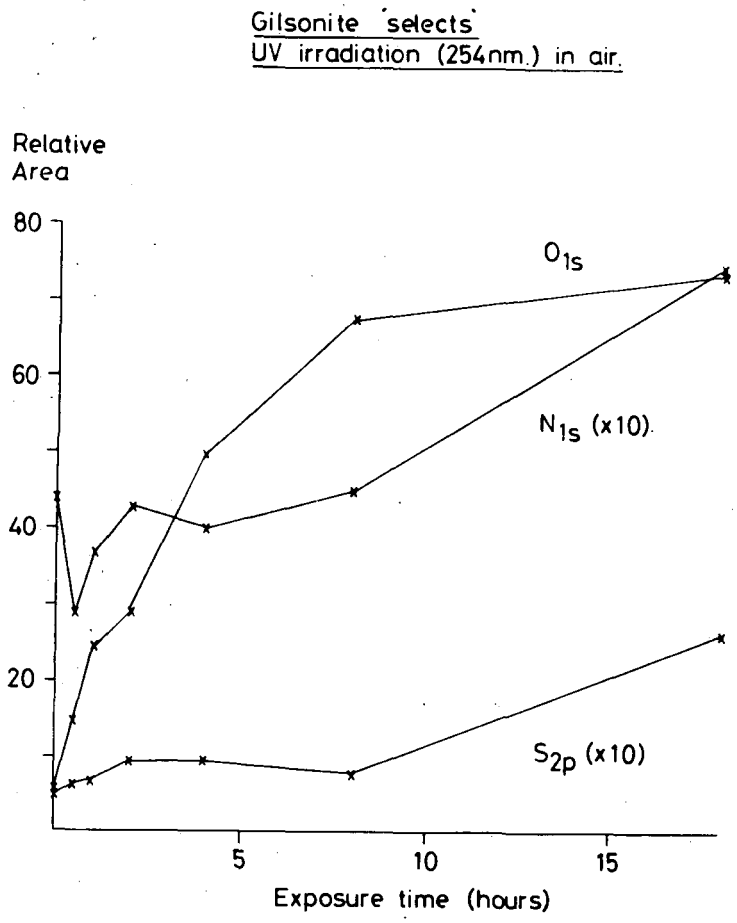

Figure 5.23 Relative areas of the O_{1s}, N_{1s} and S_{2p} photoionisation signals (expressed as per cent of total C_{1s} band intensity) for Gilsonite 'selects' as a function of exposure time to U.V. irradiation (254nm) in air at $\sim 30^{o}C$.

It should be noted that the ESCA experiment is unable to distinguish between aliphatic and aromatic C-H, or between carbon in primary, secondary or tertiary environments. Carbons in hydroxyl, ether, peroxide and hydroperoxide groups can contribute to the peak centred at 286.5eV, whilst that at 287.8eV can originate from aldehydic and ketone carbons. Acids, esters, peroxyacids and peroxyester species

Table 5.17 U.V. irradiation of Gilsonite 'selects' (254nm in air, ~ 30°C)

Relative peak area measurements (Total C_{1s} peak area taken as 100 units. Figures in brackets indicate binding energies (eV).)

Irradiation time (hrs)	C - H	C - O	C = O	O ‖ C - O	O_{1s}	N_{1s}	Total S_{2p}	Charging (eV)
0	85.5	(286.5) 10.3	(287.8) 1.7	(289.2) 2.6	(533.3) 6.0	(399.8) 4.4	0.49	4.7
½	81.3	(286.5) 10.6	(287.8) 2.4	(289.3) 4.1	(533.2) 15.6	(400.0) 2.9	0.65	4.6
1	72.7	(286.4) 16.7	(287.7) 4.9	(289.1) 5.7	(533.2) 24.4	(400.1) 3.7	0.73	5.0
2	71.9	(286.5) 16.4	(287.7) 5.0	(289.3) 6.4	(533.3) 29.1	(400.5) 4.3	0.96	5.0
4	66.7	(286.6) 18.0	(287.9) 5.7	(289.3) 10.6	(533.3) 49.6	(400.6) 4.0	0.96	5.2
8	62.9	(286.5) 18.9	(287.9) 5.7	(289.1) 14.9	(533.2) 67.4	(400.6) 4.5	0.81	5.1
18	60.6	(286.7) 19.4	(287.9) 5.7	(289.0) 17.7	(533.1) 73.1	(400.1) 7.4	2.64	5.1

will give rise to the peak at 289.2eV. Oxidation of sulphur species is also initiated and, after 30 minutes irradiation, conversion of sulphur functionality of oxidation state +2 into oxidised sulphur (oxidation state +6) and occurring at 168.4eV binding energy in the S_{2p} spectrum is well advanced. A concomitant increase in surface oxygen is evident from consideration of the O_{1s} core level signal. The range of binding energies covered by the O_{1s} core levels is much smaller than that for the C_{1s} levels. Although the O_{1s} binding energies potentially contain considerable information regarding the nature of the oxidised surface species, [58] the limited resolution and small range of binding energies preclude the extraction of this information by a unique deconvolution of the O_{1s} envelopes.

Prolonged exposure to ultra-violet (U.V.) light causes more extensive oxidation as revealed by ESCA. After 4 hours irradiation the C_{1s} high binding energy shoulder has become dominated by $\underline{C}$ - O and $\underline{C}\begin{matrix}\diagup\!\!\!=\!O\\ \diagdown\!O\end{matrix}$ functionalities: the S_{2p} core level envelope is comprised almost exclusively of oxidised sulphur.

The rapid initial uptake of oxygen into the surface of Gilsonite 'selects' is most clearly depicted in Figure 5.23. After 8 hours exposure an equilibrium situation is reached where the rate of desorption of low molecular weight oxidised carbon species approximates to the rate of oxidation of freshly exposed unoxidised surface carbon. At equilibrium the carbon to oxygen atomic ratio is 100 : 42, and this reflects extensive surface oxidation in the outermost 50Å of the solid as sampled by ESCA. The relative areas of the N_{1s} and S_{2p} photoionisation peaks (Figure 5.23) show little change during the first 8 hours of irradiation. The nitrogen and sulphur surface concentrations are found to increase after 18 hours irradiation. These increases are thought to be real, and may be explained in terms of loss of nitrogen and sulphur

species proceeding at a slower rate than the desorption of low molecular weight oxygen containing fragments: reaction of external nitrogen and sulphur sources at the gas/solid interface is thought unlikely. Grint and Perry [299] have found a similar increase in surface sulphur concentration of bituminous coal upon thermal oxidation treatment.

Throughout the treatment the nature of the nitrogen remains unoxidised, there being no evidence for the formation of oxidised nitrogen functionalities.

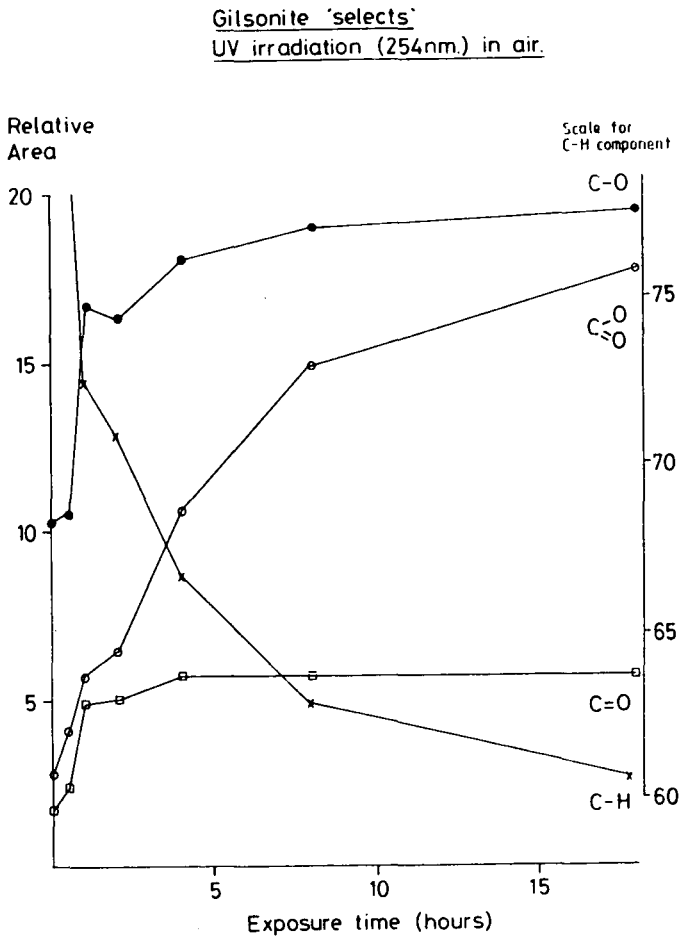

Figure 5.24 Relative areas of the individual C_{1s} component peaks (expressed as per cent of total C_{1s} band intensity) for Gilsonite 'selects' as a function of exposure time to U.V. irradiation (254nm) in air at $\sim 30^{o}C$. N.B. 'C-H' refers to the unoxidised carbon component of the C_{1s} envelope.

Figure 5.24 offers a graphical representation of the component peak analysis of the C_{1s} envelope as a function of exposure time. The initial rapid decrease in unoxidised carbon (depicted as 'C-H' in Figure 5.24) is accompanied by the development of extensive oxidised carbon functionalities in the form of carbon singly bonded to oxygen, carbonyl and carboxyl groups. The development of these functional groups has been found to occur in the thermal oxidation of coal.[252,259] The low level of carbonyl functionality reaches an equilibrium value of $\sim$ 5% of the total C_{1s} envelope in the first hour of irradiation. This contrasts with the situation for both C-O and $\underline{C}(=O)-O$, which continue to grow in intensity to respective values of 19.4% and 17.7% after 18 hours irradiation. Consideration of the corresponding C:O atomic ratio as derived from the C_{1s} and O_{1s} core level signals leads to the supposition that the carbon singly bonded to oxygen and carboxyl C_{1s} components arise, at least in part, from ether and ester surface functionalities, rather than being solely attributable to free hydroxyl and acid groups for example.

5.3.7c Brown coal and Oxfordshire coal

The interaction of U.V. light (254nm) with brown coal and Oxfordshire coal under the same conditions as for the Gilsonite 'selects' experiment has been explored. The results for each material have been tabulated (Table 5.18 and 5.19), and graphical representations are also offered (Figures 5.25 - 5.28).

Both coal types show surface oxidation on irradiation with U.V. light. After prolonged exposure (18 hours) these materials exhibit similar levels of surface organic oxygen content to that found for Gilsonite 'selects'.[259] Van Krevelen has observed that, during the oxidation of coal by gaseous oxygen, coals of very different rank yield

end products of approximately identical compositions. In the initial stages of reaction it would appear that oxygen uptake is more rapid for material with the lower inherent oxygen content. The tendency for the N_{1s} and S_{2p} photoionisation peaks to show a slight intensity increase after continued exposure to U.V. light, as was found for Gilsonite 'selects', is also apparent in the case of the Oxfordshire coal (Figure 5.27).

Figures 5.24, 26, 28 reveal differences in the development of carbon-oxygen functionality as given by deconvolution of the C_{1s} peak envelopes. The C_{1s} spectra for Gilsonite 'selects', brown coal and Oxfordshire coal are to be found in Figures 5.22, 29, 30 respectively. All three materials show $\underline{C}$ - O, $\underline{C}$ = O and $\underline{C}(=O)$ - O functionalities on their oxidised surfaces. Carbonyl groups form the minor C_{1s} component for exposure times in excess of $\sim$ 5 hours, carboxyl and carbon singly bonded to oxygen groups dominating the high binding energy shoulder of the C_{1s} envelope. In each case the unfunctionalised carbon component remains the predominant carbon peak overall. For the time scale of these experiments, the $\underline{C}$ - O functionality develops essentially within the first five hours of irradiation. In contrast however, the development of carboxyl continues throughout the duration of the experiment. The $\underline{C}(=O)$ - O component of the C_{1s} envelope for the Oxfordshire coal becomes of greater intensity than the $\underline{C}$ - O component after $\sim$ 13½ hours' irradiation time.

These results exemplify the observations of other research workers whose thermal oxidation studies reveal different findings for different coals.[302]

Table 5.18 U.V. irradiation of Brown Coal. (254nm in air, ~ 30°C)

Relative peak area measurements. (Total C_{1s} peak area taken as 100 units).

Irradiation time (hrs)	C - H	C - O	>C = O	O ‖ C - O	O_{1s}
0	76.0	(286.8) 14.1	(288.1) 5.2	(289.4) 4.8	35.9
½	72.6	(286.8) 17.1	(288.1) 5.9	(289.3) 4.5	37.3
1	70.2	(286.6) 17.3	(288.0) 6.6	(289.5) 5.8	40.7
2	68.0	(286.8) 18.2	(288.0) 7.3	(289.4) 6.5	50.9
4	67.3	(286.7) 15.9	(288.1) 8.6	(289.4) 8.3	55.7
8	65.9	(286.8) 16.6	(288.2) 7.7	(289.5) 9.8	66.1
18	65.5	(286.9) 16.8	(288.0) 6.2	(289.5) 11.5	76.4

Table 5.19 U.V. irradiation of Oxfordshire coal (254nm in air, ~ 30°C)

Relative peak area measurements. (Total C_{1s} peak area taken as 100 units.)

Irradiation time (hrs)	C - H	C - O	> C = 0	O || C - O	O_{1s}	N_{1s}	Total S_{2p}	Si_{2p}	Al_{2p}
		(286.6)	(287.9)	(289.3)					
0	83.1	8.7	4.3	2.2	25.9	0.8	0.7	0.8	0.5
		(286.7)	(288.0)	(289.5)					
½	83.4	8.5	5.8	2.3	30.0	1.6	1.6	2.4	1.5
		(286.7)	(288.0)	(289.5)					
1	86.7	7.9	3.1	2.3	35.8	-	0.2	2.3	1.5
		(286.6)	(288.0)	(289.4)					
2	73.0	14.1	6.2	6.7	43.6	1.7	1.4	2.7	1.6
		(286.6)	(288.0)	(289.4)					
4	74.0	13.6	6.0	6.4	53.9	3.2	1.4	2.9	1.6
		(286.7)	(288.0)	(289.3)					
8	73.0	12.7	5.2	9.2	60.1	1.3	0.5	2.2	0.4
		(286.7)	(288.0)	(289.3)					
12	69.4	12.3	7.2	11.2	69.7	3.1	1.9	2.4	1.1
		(286.7)	(287.7)	(289.1)					
18	67.8	12.2	3.5	16.5	77.2	4.2	2.7	1.8	1.8

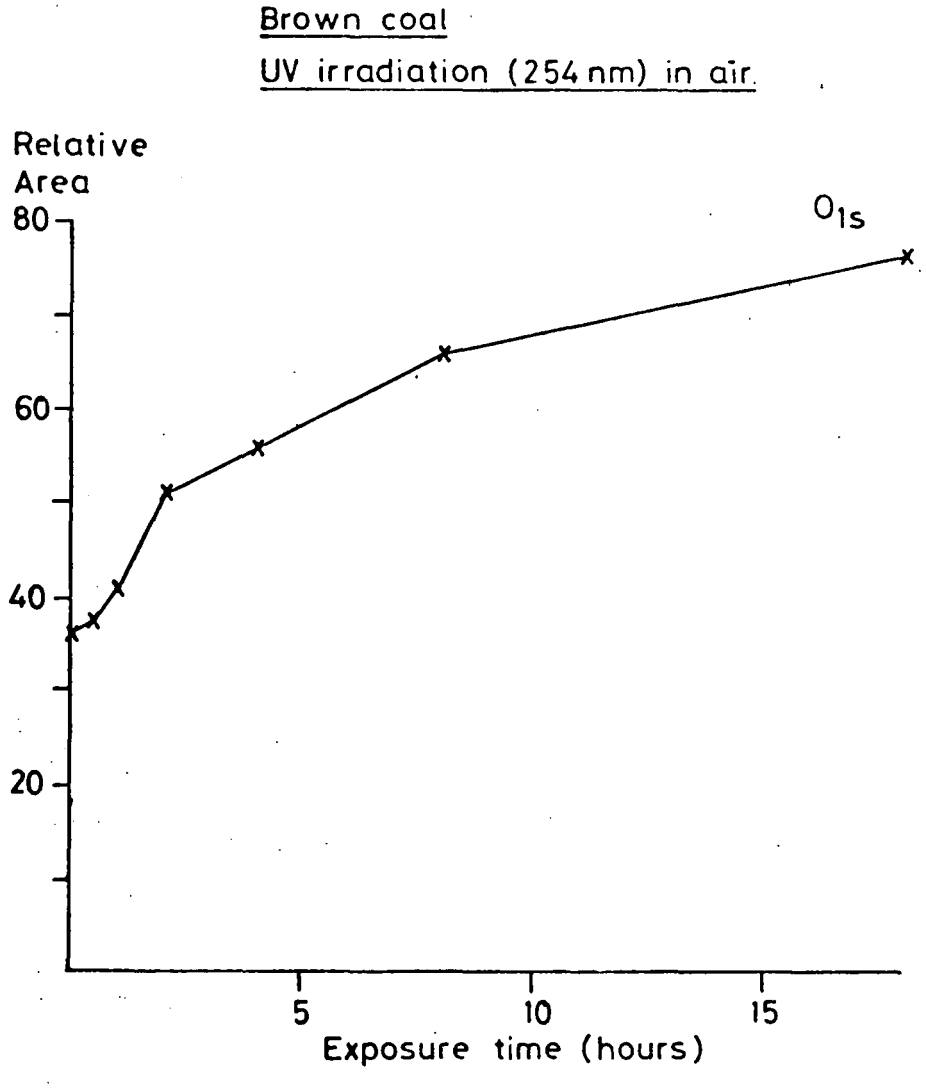

Figure 5.25 Relative area of the O_{1s} core level signal (expressed as per cent of total C_{1s} band intensity) for brown coal as a function of exposure time to U.V. irradiation (254nm) in air at $\sim 30^{o}C$.

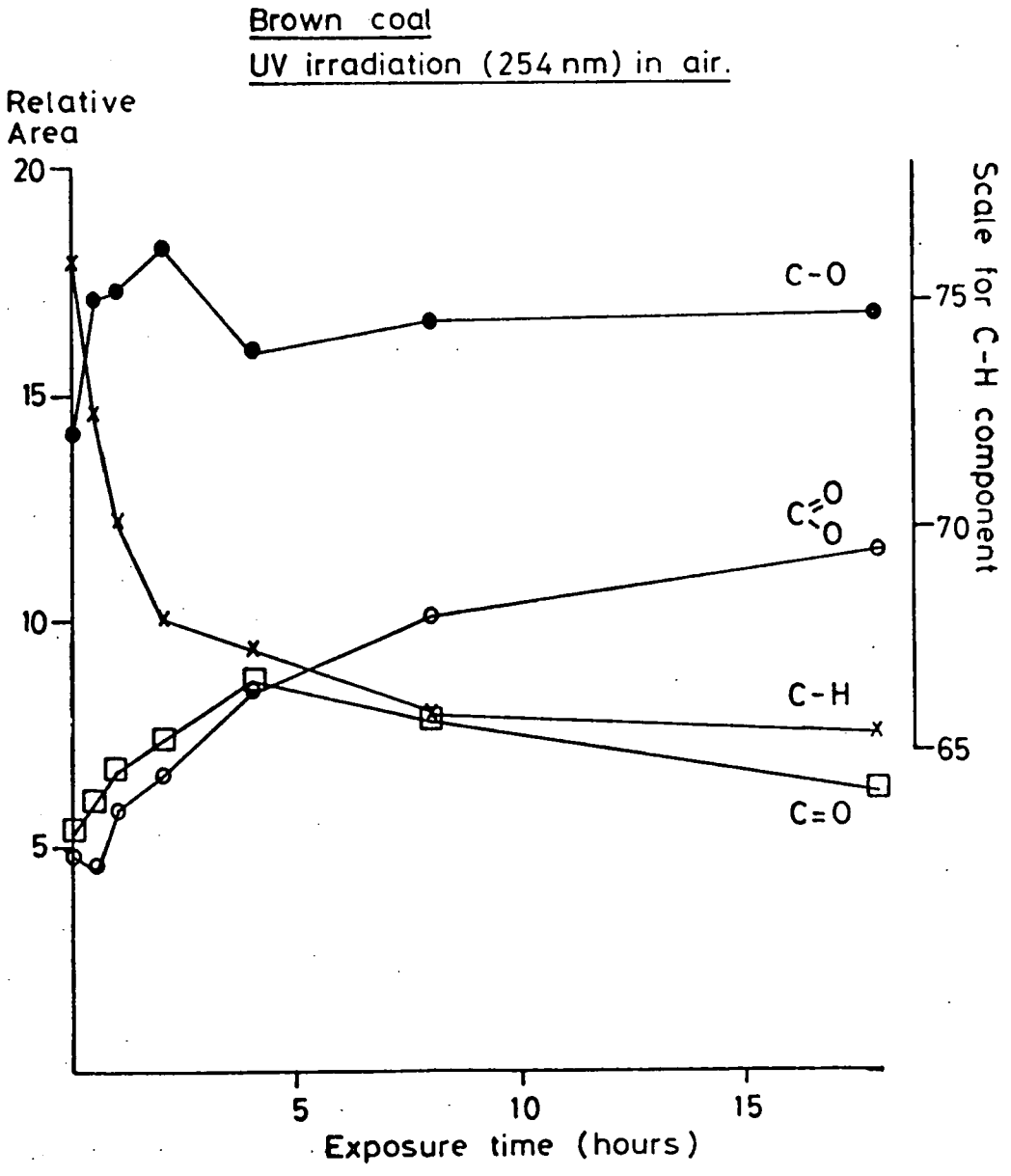

Figure 5.26 Relative areas of the individual C_{1s} component peaks (expressed as per cent of total C_{1s} band intensity) for brown coal as a function of exposure time to U.V. irradiation (254nm) in air at $\sim 30^{o}C$.

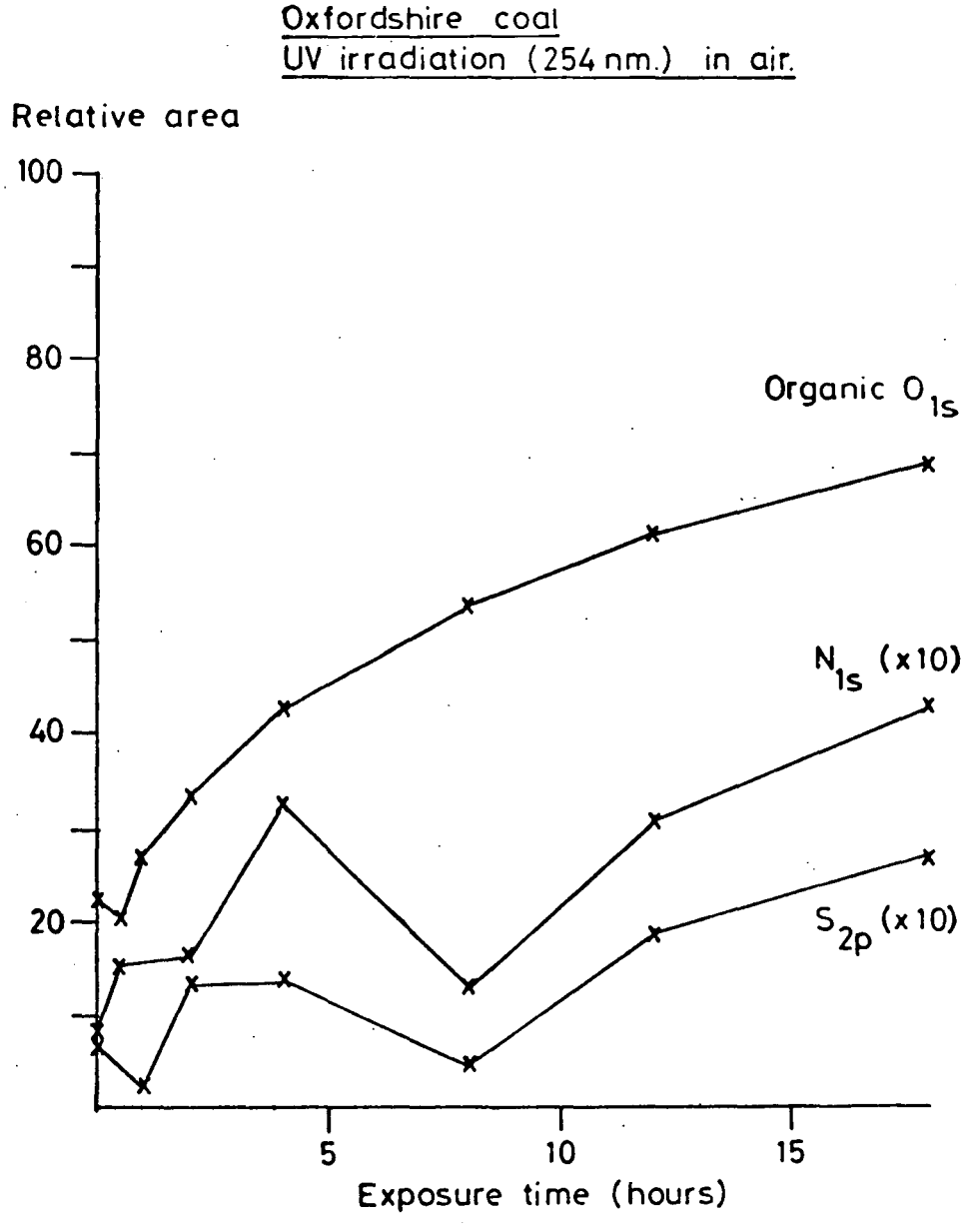

Figure 5.27 Relative areas of the O_{1s}, N_{1s} and S_{2p} photoionisation signals (expressed as per cent of total C_{1s} band intensity) for Oxfordshire coal as a function of exposure time to U.V. irradiation (254nm) in air at $\sim 30^{o}C$.

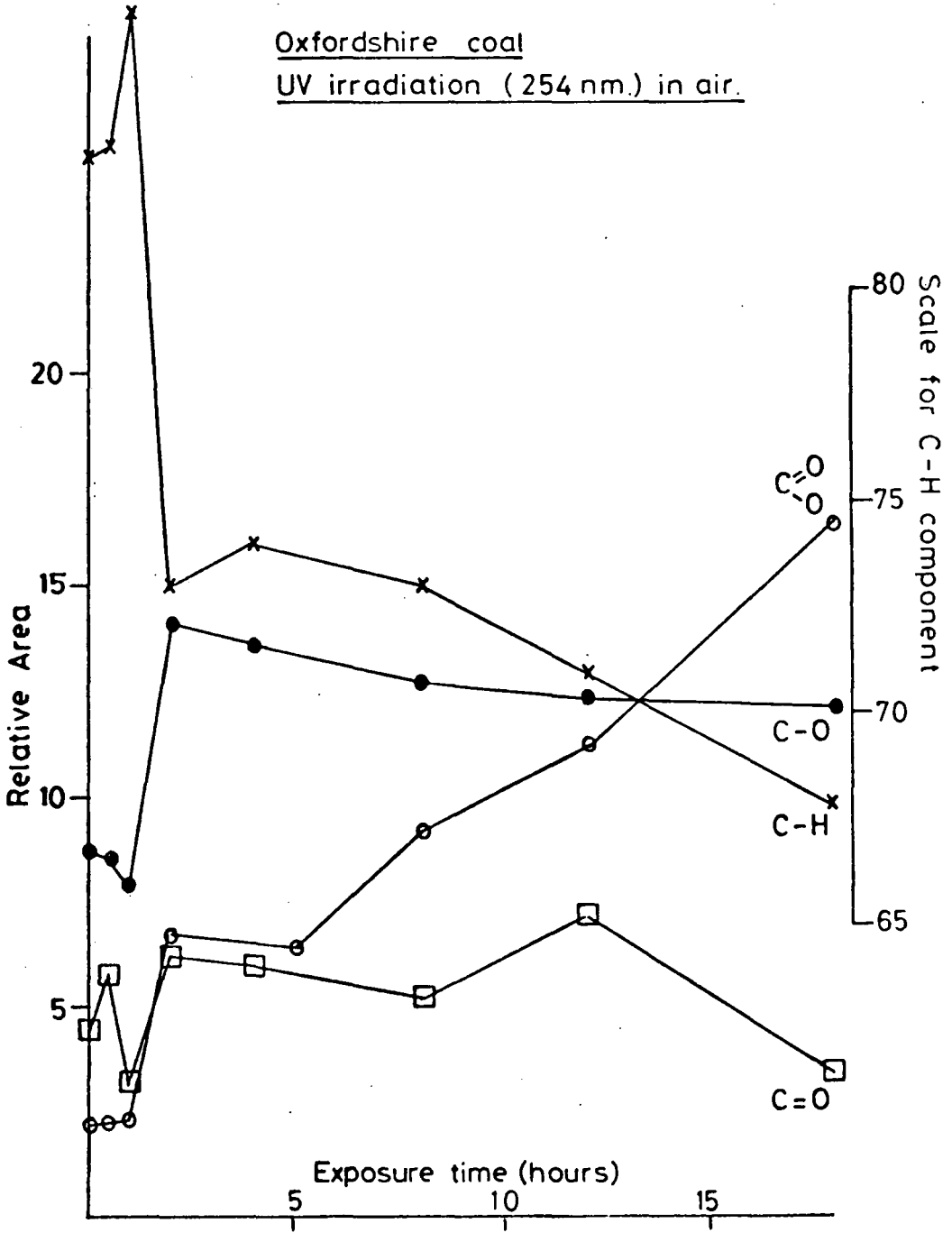

Figure 5.28 Relative areas of the individual C_{1s} component peaks (expressed as per cent of total C_{1s} band intensity) for Oxfordshire coal as a function of exposure time to U.V. irradiation (254nm) in air at $\sim 30^{o}C$.

Figure 5.29 The C_{1s} core level spectrum for brown coal as a function of exposure time to U.V. irradiation (254nm) in air at ~ 30°C.

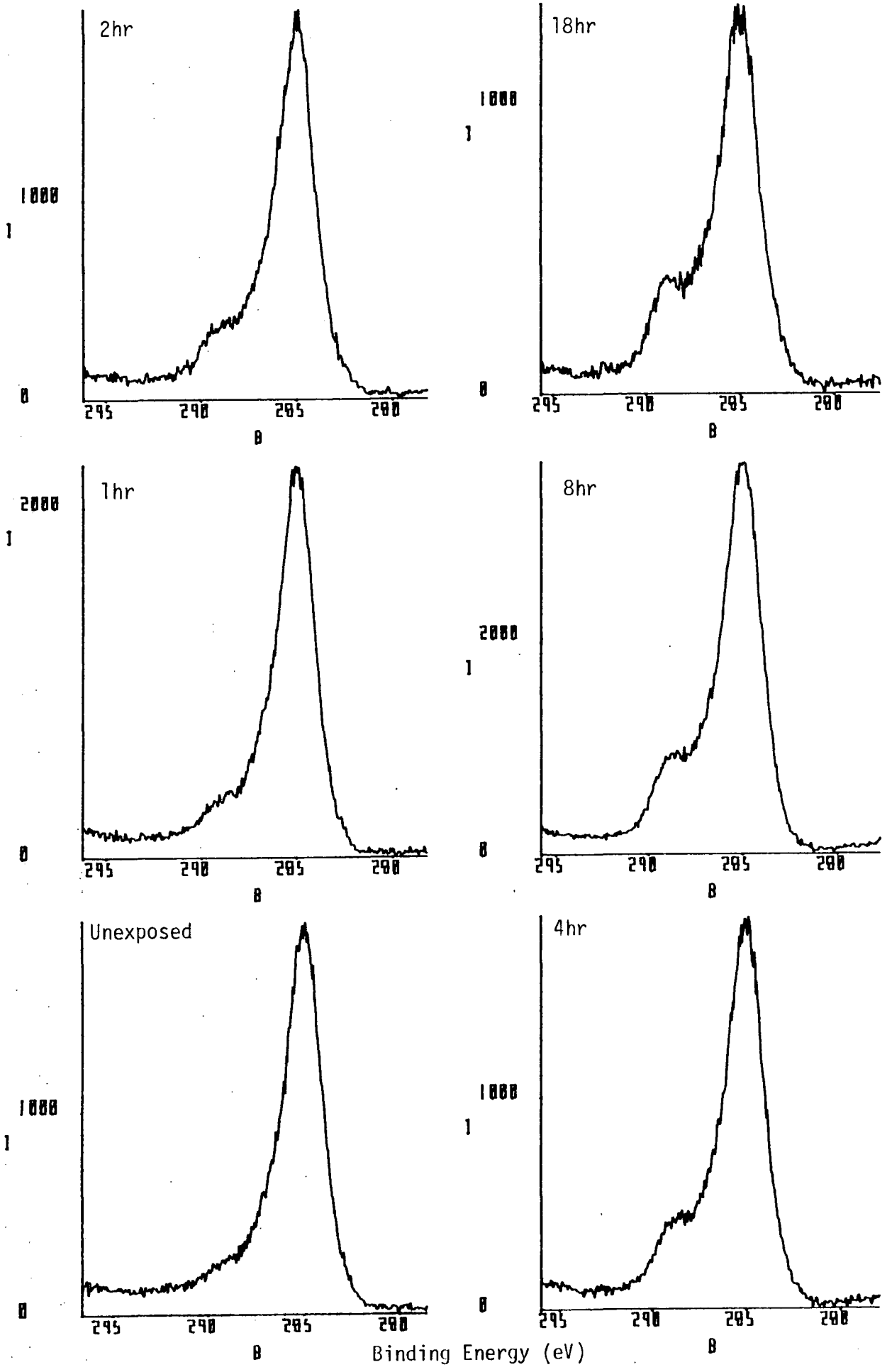

Figure 5.30 The C_{1s} core level spectrum for Oxfordshire coal as a function of exposure time to U.V. irradiation (254nm) in air at ~ 30°C.

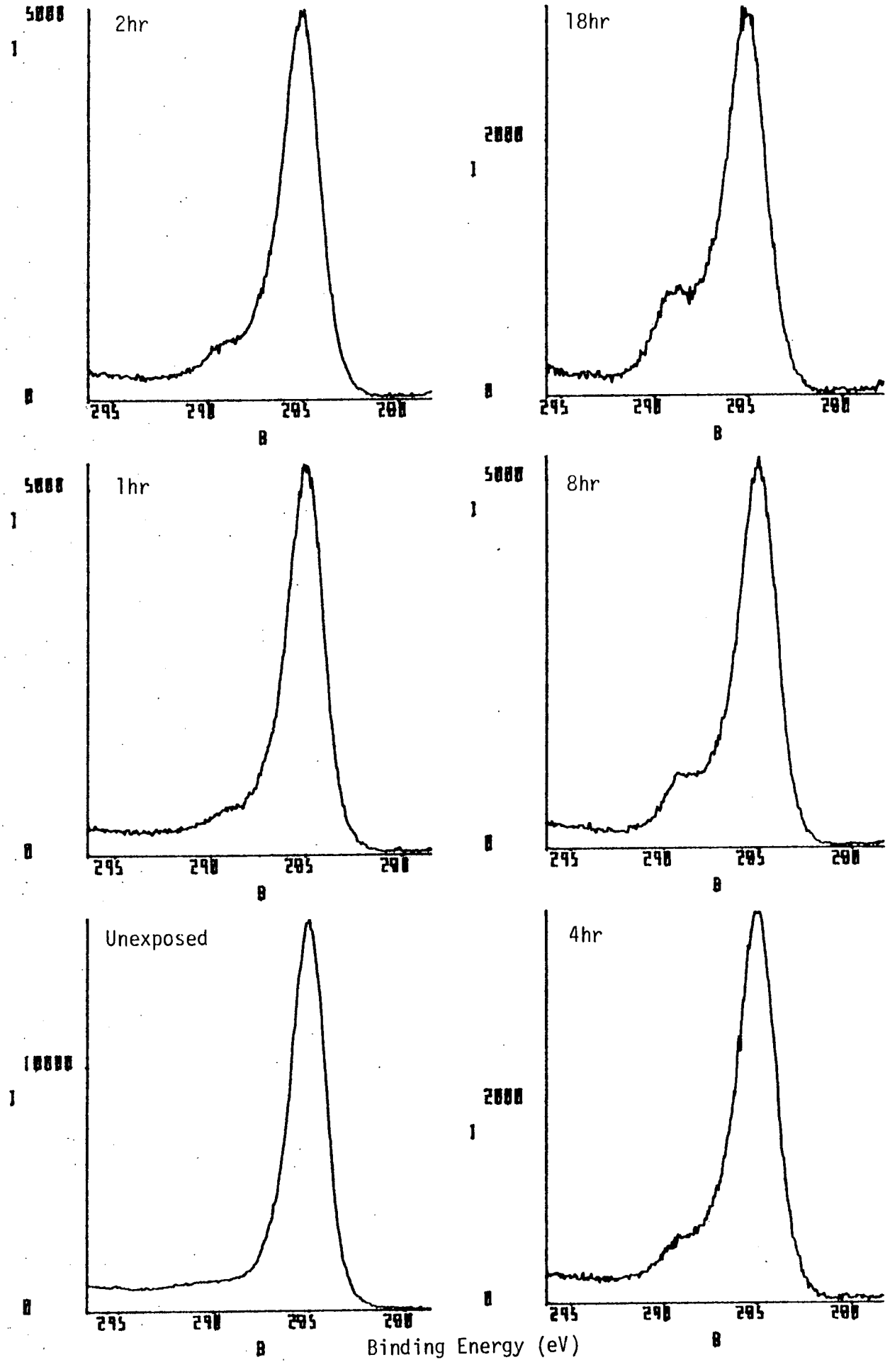

5.3.7d Anthracite and Graphite

Investigation of the U.V. irradiation of Cynheidre anthracite reveals only a slight absolute increase in surface oxygen content, the C : O atomic ratio changing from 100 : 5 to 100 : 7 after four hours' exposure time. Analysis of the C_{1s} envelope of the U.V. oxidised anthracite gives a carbon distribution as follows:-

$\underline{C}$ - H	$\underline{C}$ - O	$\underline{C}$ = O	$\underline{C}$ - O (O: =O)
(284.8)	(286.6)	(288.2)	(289.7)
79.8	12.2	4.5	3.5

Figure 5.31 shows the C_{1s} profiles of the oxidised and unexposed anthracite samples. The difference spectrum (oxidised - unexposed), obtained using the normalisation and subtraction facilities of the DS300 data manipulation package, helps accentuate the development of oxidised functionality. (The C_{1s}, O_{1s}, N_{1s}, S_{2p}, Si_{2p} and Al_{2p} core level spectra of anthracite are discussed in a later section (Section 5.3.8c).)

The interaction of U.V. light (254nm in air at 30^{o}, 4 hours) with samples of oriented graphite (both basal and prismatic edge planes) have also been considered. Low levels of oxygen were found on the surfaces of the unexposed graphites, the respective atomic C : O ratios for basal and prismatic edge planes being 100 : 0.7 and 100 : 1.8. Slight oxygen uptake is all that is observed for either material; the edge plane appears to undergo the most surface oxygen enrichment (Figure 5.32). Accordingly there is little change in the valence band spectra of these materials (Figure 5.33).

Comparison of the results for the surface oxidation of brown coal, Oxfordshire coal and anthracite upon four hours' exposure to U.V. light, under the particular conditions of this study, would indicate a decrease in reactivity towards photo-oxidation with increasing coal rank.

Figure 5.31 C_{1s} profiles of anthracite, before and after 4 hrs' exposure to U.V. light (254nm) in air at ~ 30°C : the C_{1s} difference spectrum (exposed - unexposed) is also shown.

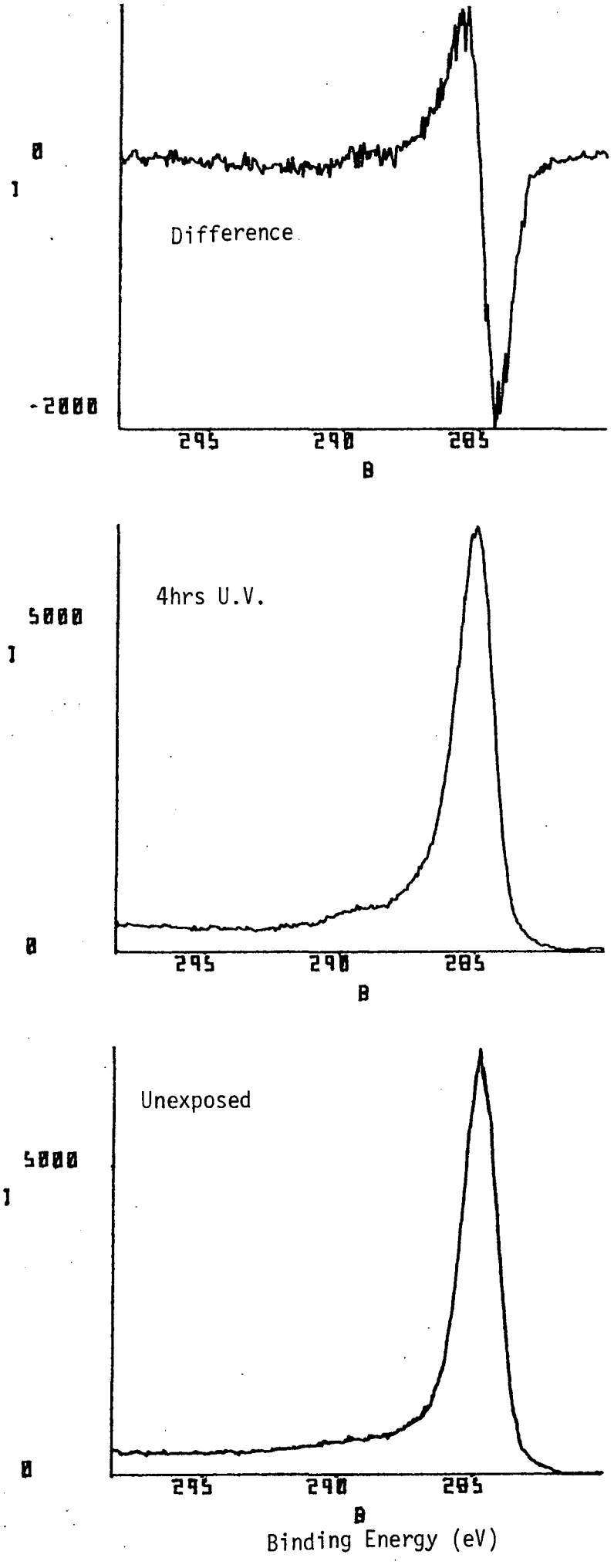

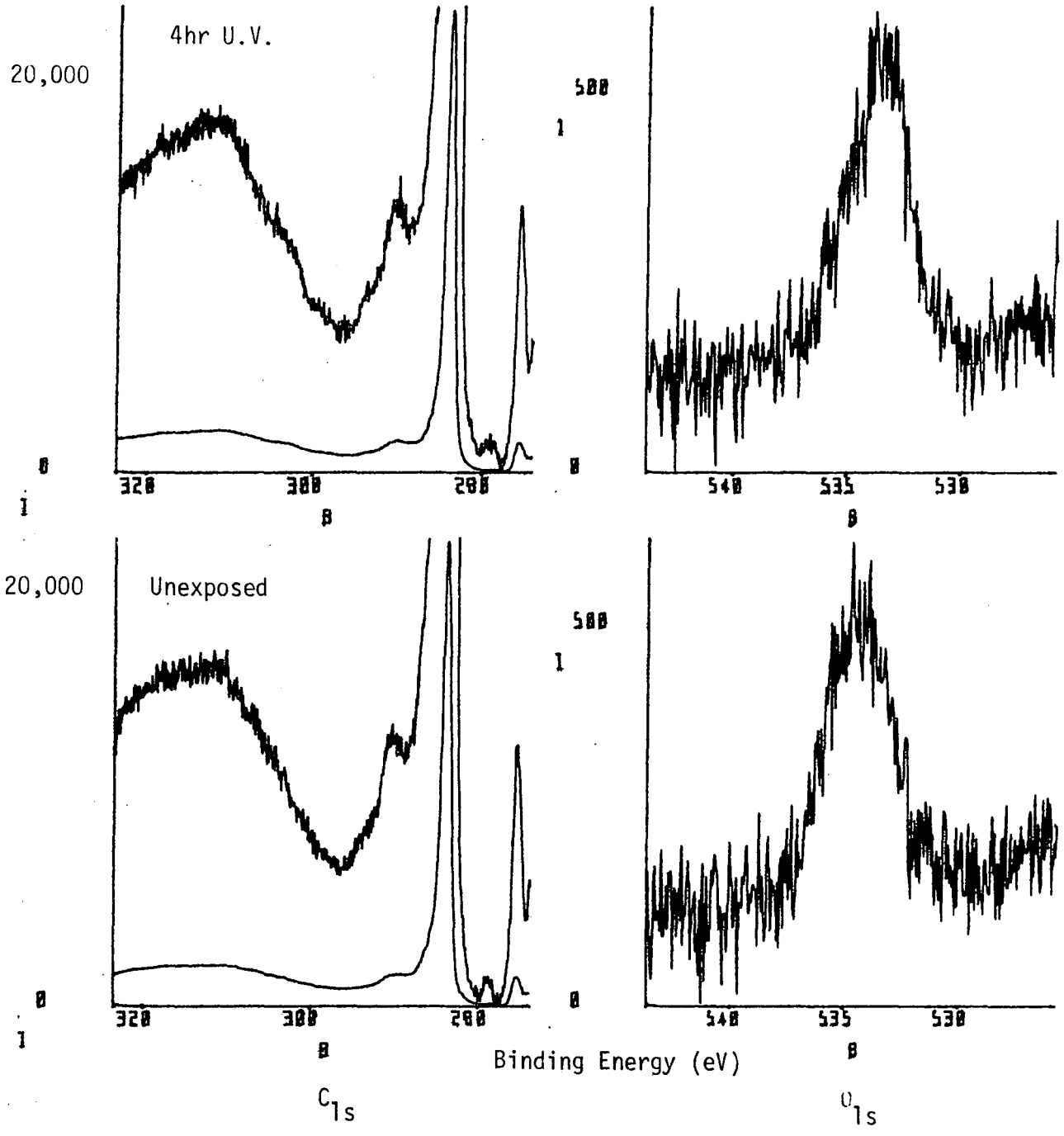

Figure 5.32a Oriented graphite, basal plane. C_{1s} and O_{1s} core level spectra before and after 4 hours' exposure to U.V. light (254nm) in air at $\sim 30^{o}C$.

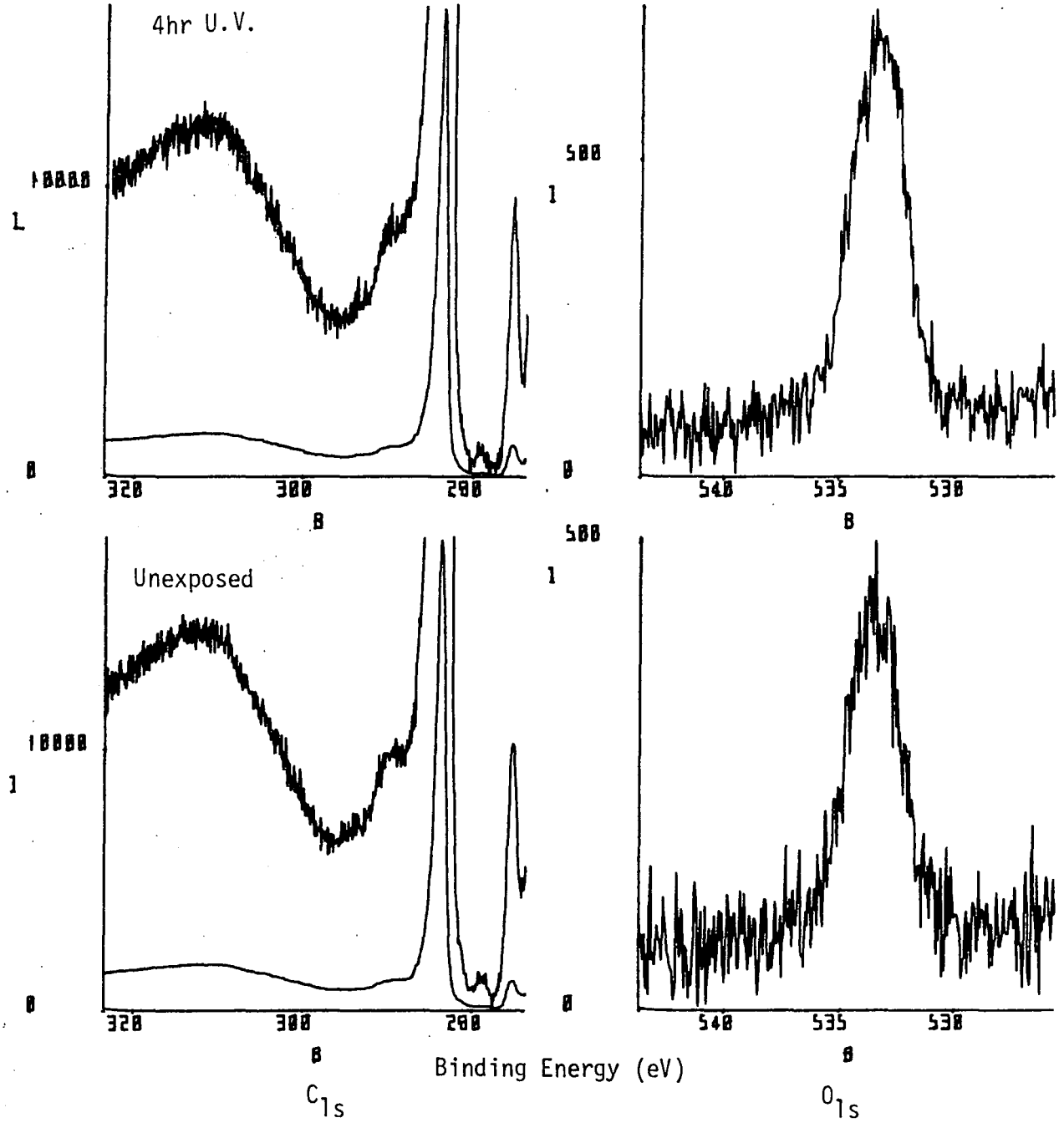

Figure 5.32b Oriented graphite, prismatic edge. C_{1s} and O_{1s} core level spectra before and after 4 hours' exposure to U.V. light (254nm) in air at $\sim 30^{o}C$.

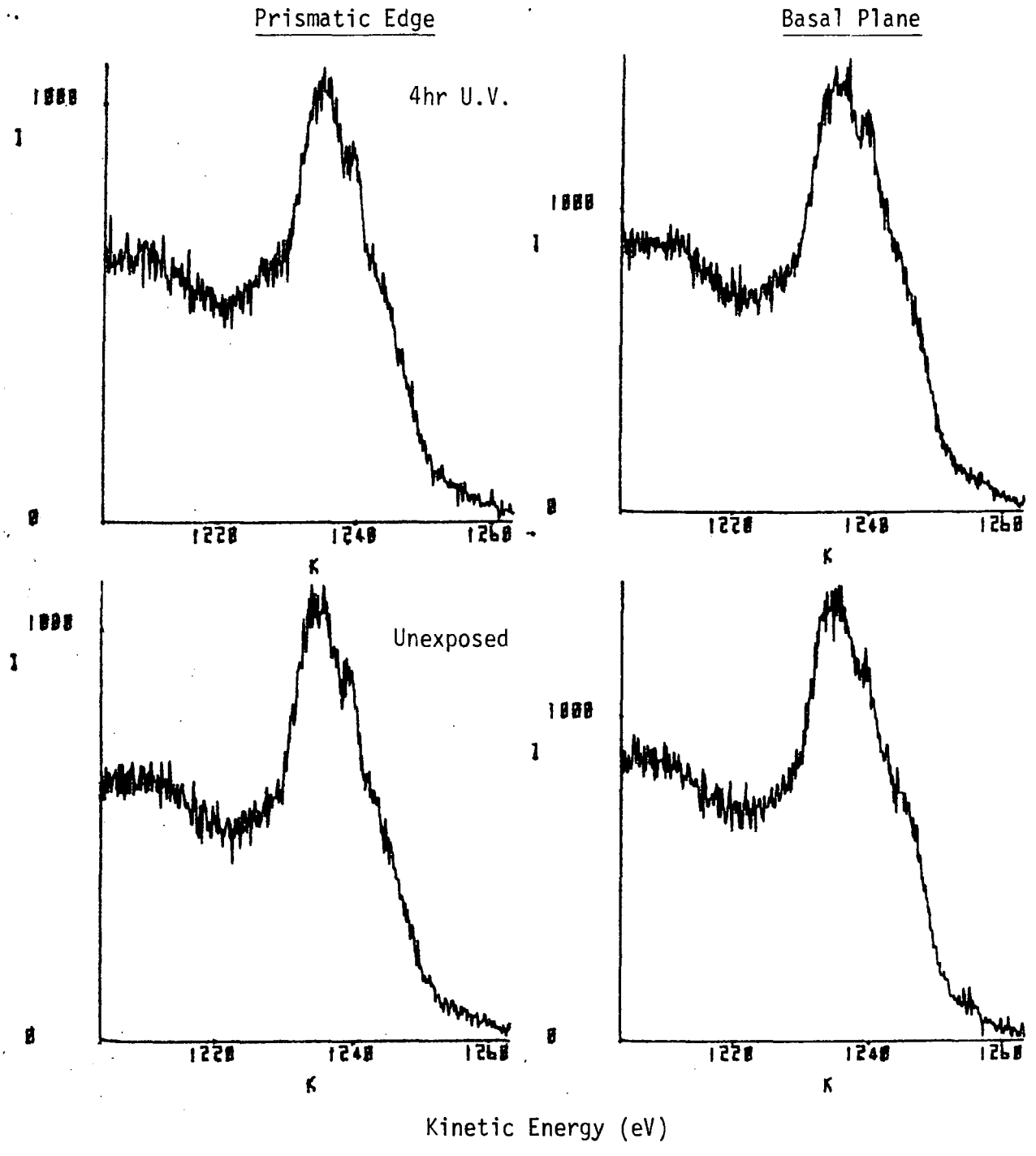

Figure 5.33 Valence band spectra of oriented graphite (basal plane and prismatic edge) before and after 4 hours' exposure to U.V. light (254nm) in air at $\sim 30^{o}C$.

It is of interest to note that Carpenter and Sergeant [303] state, in their investigations of the initial stages of the oxidation of coal with molecular oxygen, that there is a 'pronounced increase in oxygen reactivity with decrease in coal rank from 94 to 87 per cent carbon'.

5.3.7e Interaction with Trifluoroacetic Anhydride

The oxygen functional group distributions of unoxidised and oxidised coals have been the subject of research effort. [229, 300-302] This is geared towards a better understanding of the deterioration of the desirable fluidity and dilation properties of bituminous coals upon oxidation. It would appear that it is the development of a more highly cross-linked coal structure upon oxidation which is responsible for the destruction of the plastic properties of bituminous coal. [302]

The ESCA experiment is unable to give a direct measure of the C - O - C cross-link surface concentration for a material, such as an oxidised coal, which may also contain other carbon singly bonded to oxygen functionalities, C - OH or C - OOH for example. (Jones and Townend [300] showed that formation of hydroperoxides is an important step in the very early stages of coal weathering; at room temperature the concentration builds up and then decays.)

Derivatisation techniques are sometimes able to provide a further dimension to ESCA functional group distribution analyses. Here the interaction of trifluoroacetic anhydride (TFAA) vapour with samples of coal, before and after exposure to U.V. light, has been studied. The aim of these experiments was to monitor changes in concentration of surface C - OH groups upon oxidation. Preliminary studies on the interaction of TFAA vapour with brown coal suggest that a treatment time of 15 minutes is sufficient for reaction to occur, at least as far as the ESCA $Mg_{K\alpha}$ sampling depth ($\sim$ 50Å) is concerned.

No attempt has been made in these initial experiments to evaluate the effects of differences in the physical characteristics (e.g. porosites, internal surface area, moisture content) associated with coals of different rank.

Figures 5.34 - 36 show the C_{1s}, F_{1s} and O_{1s} core level spectra for brown coal, Oxfordshire coal and anthracite, unexposed and U.V. irradiated (4 hours), after 15 minutes reaction with TFAA vapour. Relative area measurements are tabulated in Table 5.20. All samples show fluorine incorporated into their surface regions. There are however differences in the extent of trifluoromethyl acetylation, reflecting not only changes in reactivity upon photo-oxidation, but also varying reactivity for different coal types. The surface fluorine concentration calculations suggest evidence for a degree of surface specificity. Chapter Three discusses the depth profiling capabilities of the ESCA experiment with reference to TFAA derivatisation reactions in some detail.

Scrutiny of Table 5.20 leads to the supposition that the reaction of brown coal with TFAA is enhanced at the very surface. The interaction of brown coal with U.V. light reduces the extent of the subsequent TFAA derivatisation reaction. The increase in the intensity of the carbon singly bonded to oxygen C_{1s} peak component upon irradiation may therefore arise from the formation of ether cross-links. The TFAA derivatisable C - OH groups do appear to take part in the photo-induced oxidation of brown coal.

This situation is contrasted by the results for the Oxfordshire coal. Figures of the fluorine atom concentration would indicate a homogeneous reaction over the ESCA sampling depth. Little difference in surface TFAA incorporation is found between the unexposed and the irradiated coal samples. This is despite the fact that the C_{1s} envelope

Figure 5.34 C_{1s}, F_{1s} and O_{1s} core level spectra for brown coal, unexposed and U.V. irradiated (4hrs, 254nm in air at $\sim 30^{o}C$), after 15 minutes' reaction with TFAA vapour.

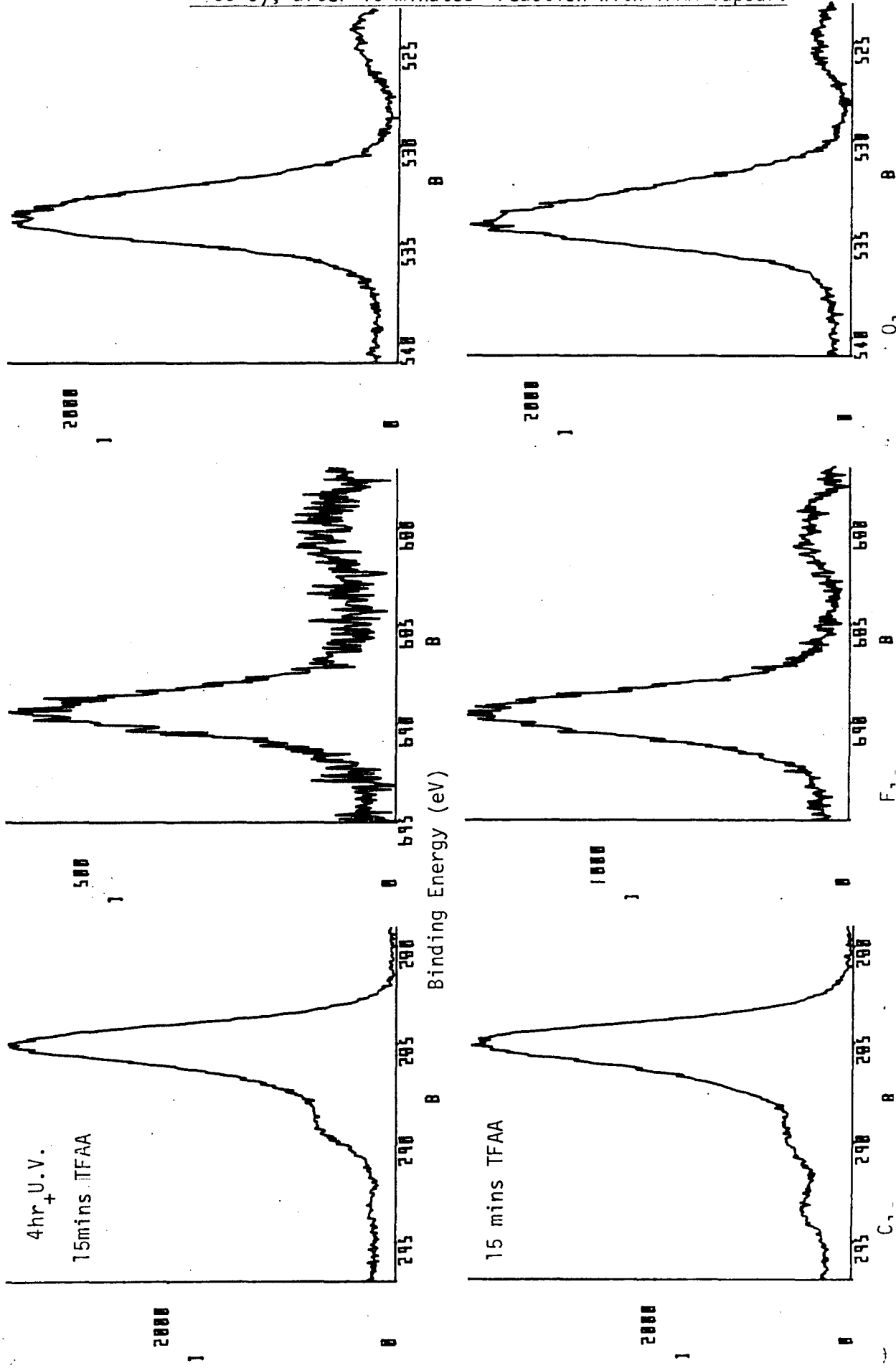

Figure 5.35 C_{1s}, F_{1s} and O_{1s} core level spectra for Oxfordshire coal, unexposed and U.V. irradiated (4hrs, 254nm in air at ~ 30°C), after 15 minutes' reaction with TFAA vapour.

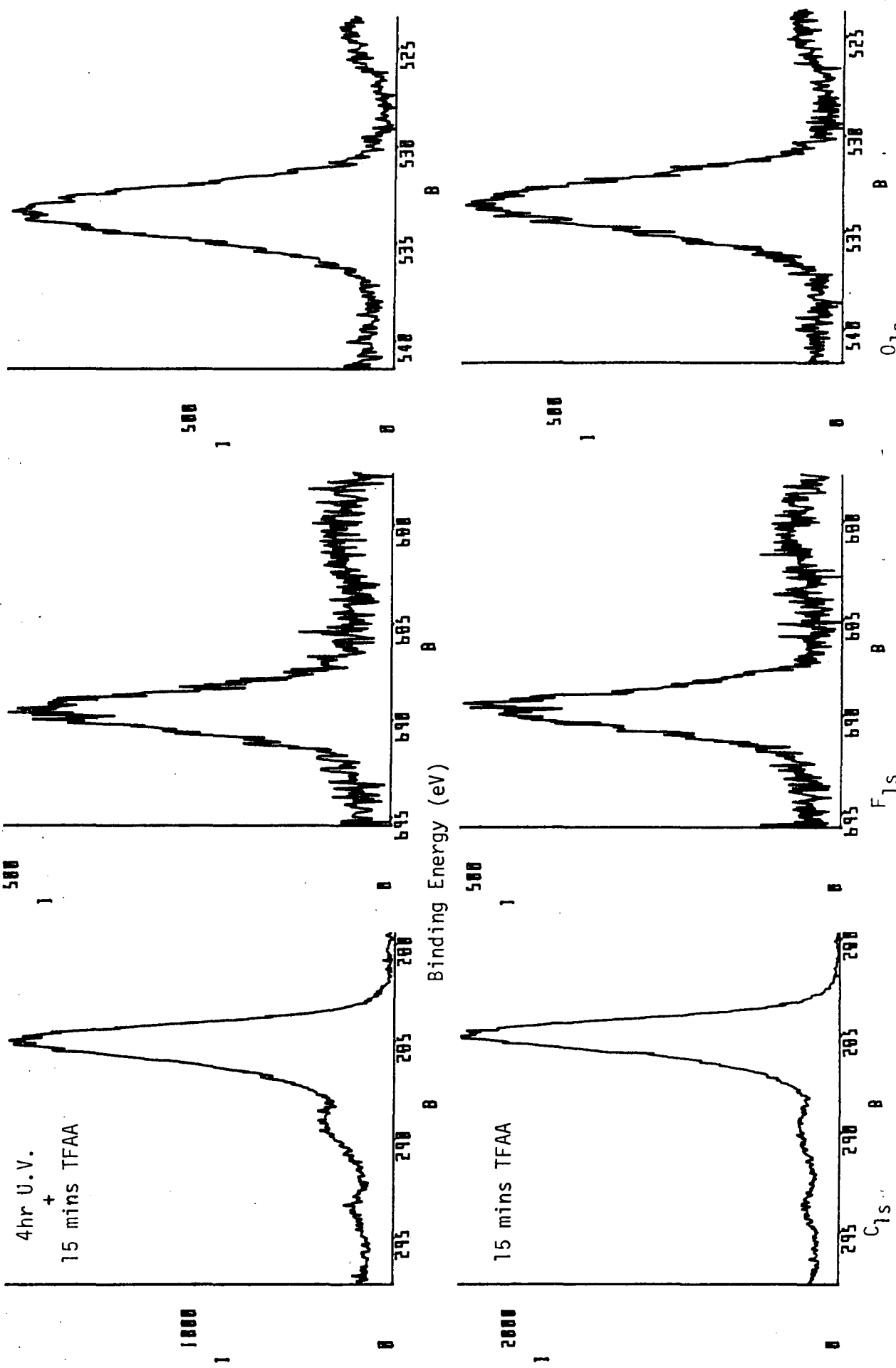

Figure 5.36 C_{1s}, F_{1s} and O_{1s} core level spectra for anthracite, unexposed and U.V. irradiated (4hrs, 254nm in air at ~ 30°C), after 15 minutes' reaction with TFAA vapour.

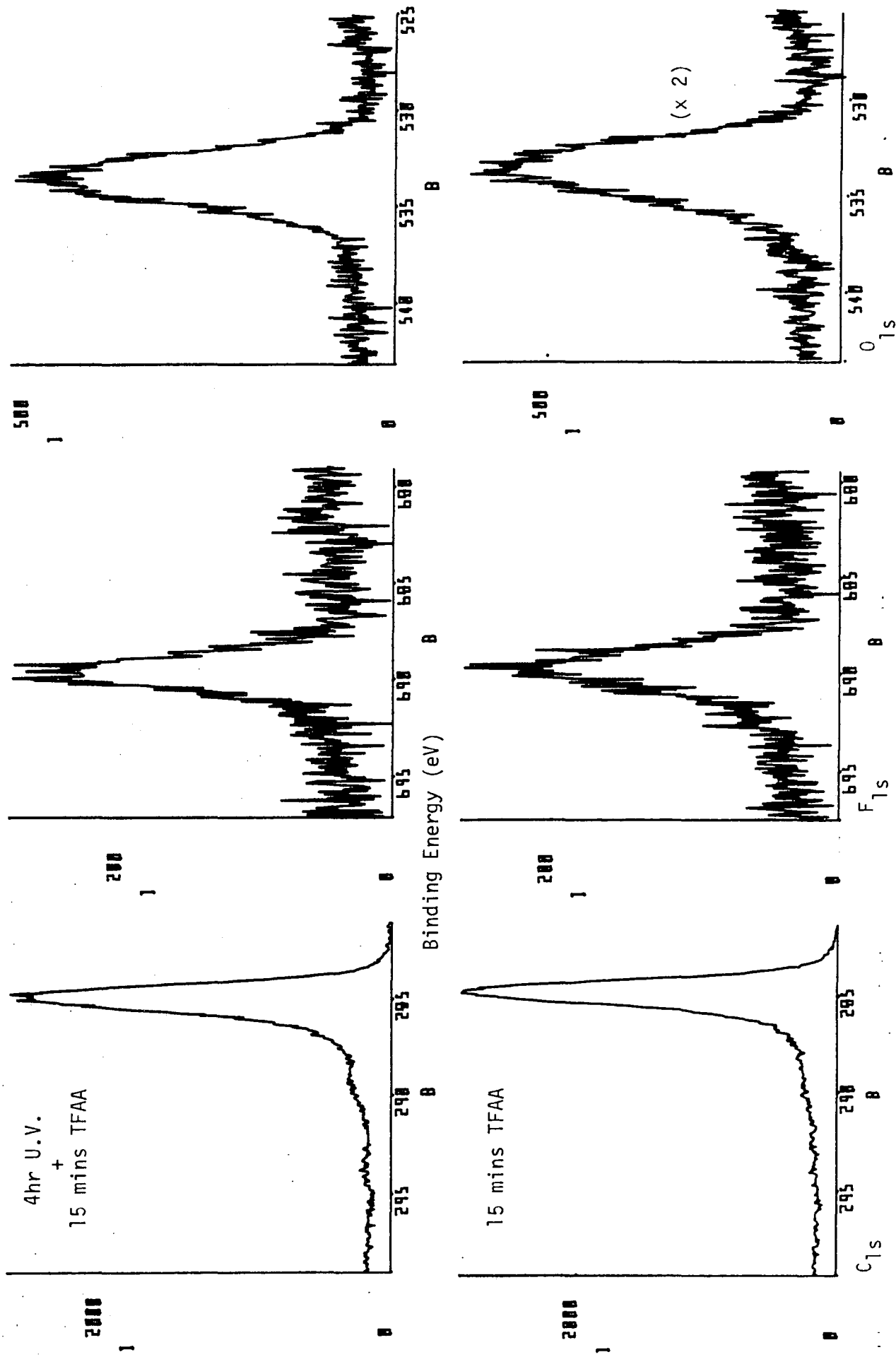

Table 5.20 Interaction of TFAA vapour (15 mins) with coal samples, unexposed and irradiated (4hrs, 254nm in air ~ 30°C.).

	Relative area measurements				Fluorine atom concentration*		Estimated no. of derivatised C-O groups per 100 carbon atoms†		
Brown Coal	C_{1s}	$\underline{C}F_3$	F_{1s}	O_{1s}	$\underline{C}F_3$	F_{1s}	Total ǂ C - O	TFAA labelled C - O	Total C - O − TFAA labelled
Unexposed	100	3.9	35.2	57.7	11.7	18.3	14.1	4.6	9.5
4hrs irradiation	100	0.5	13.9	72.3	1.5	7.2	15.9	0.5	15.4
Oxfordshire Coal									
Unexposed	100	3.9	18.1	34.8	11.7	9.4	8.7	4.6	4.1
4hrs irradiation	100	3.3	17.7	51.3	9.9	9.2	13.6	3.8	9.8
Anthracite									
Unexposed	100	-	8.5	14.3	-	4.4	-	-	-
4hrs irradiation	100	2.6	7.1	22.2	7.8	3.7	12.2	2.9	9.3

* Depth profiling of the reaction is made possible by the consideration of the fluorine atom concentration values which may be derived from the trifluoromethyl carbon signal and from the F_{1s} signal itself. For $Mg_{K\alpha}$ excited spectra, the $\underline{C}F_3$ signal will sample the outermost ~45Å of the sample, whilst the F_{1s} signal will be slightly more surface specific and will probe the outermost ~27Å (Section 3.3.1).

† Based on $\underline{C}F_3$ peak area measurements.

ǂ Figures from Tables 5.17 - 19.

of the irradiated coal shows a C - O component ∿ 1.6 times the intensity of the C - O portion for the unexposed coal. The TFAA derivatisable C - OH groups are not seen to be involved with the oxidation processes of the Oxfordshire coal. Nonetheless, development of C - O functionality occurs.

In the case of anthracite, it is difficult to draw conclusions from the deconvoluted envelopes as far as the development of C - O functionality. This is due to the assymetry of the C_{1s} envelope for the unexposed anthracite, associated with the skeletal arrangement of the carbon network. The ESCA difference spectrum of anthracite (U.V. irradiated - unexposed), shown in Figure 5.31, and the data presented in Table 5.20, suggest that the C - O portion of the C_{1s} envelope does become more predominant after U.V. irradiation of the sample.

5.3.7f Oxidation of Sulphide Moieties

The results presented in this account of the artificially induced oxidation of naturally occurring carbonaceous materials have shown that, when present, the sulphide type sulphur functionalities are prone to oxidation (e.g. Figure 5.22). Another example of this phenomenon is presented in Figure 5.37 and Table 5.21, which show the effects of 2 hours' U.V. irradiation on the C_{1s}, S_{2p}, O_{1s} and N_{1s} spectra of Kimmeridge kerogen.

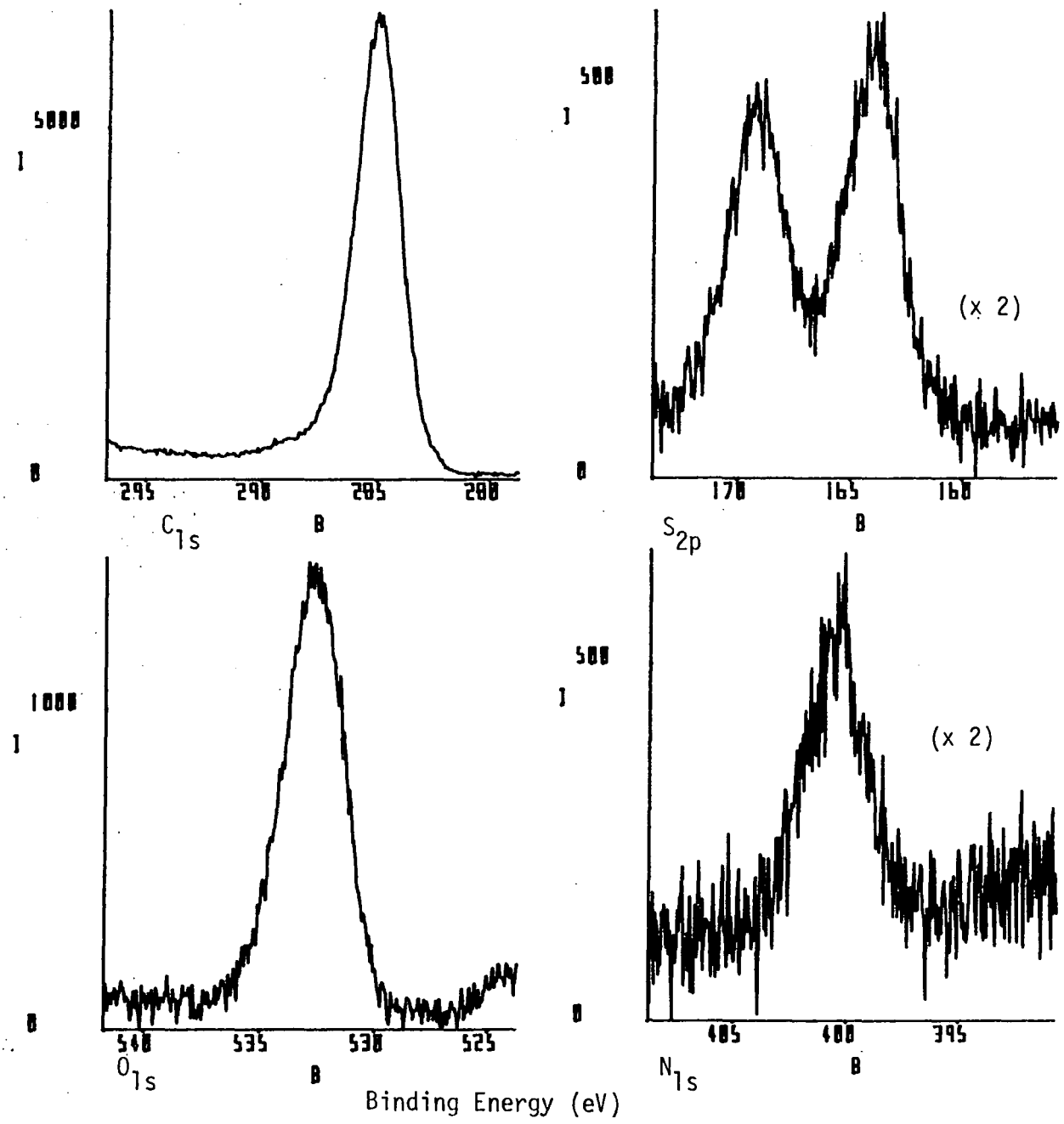

Figure 5.37a C_{1s}, S_{2p}, O_{1s} and N_{1s} core level spectra of Kimmeridge (a) untreated, (b) after 2 hours' U.V. irradiation (254nm in air at $\sim 30^{o}C$).

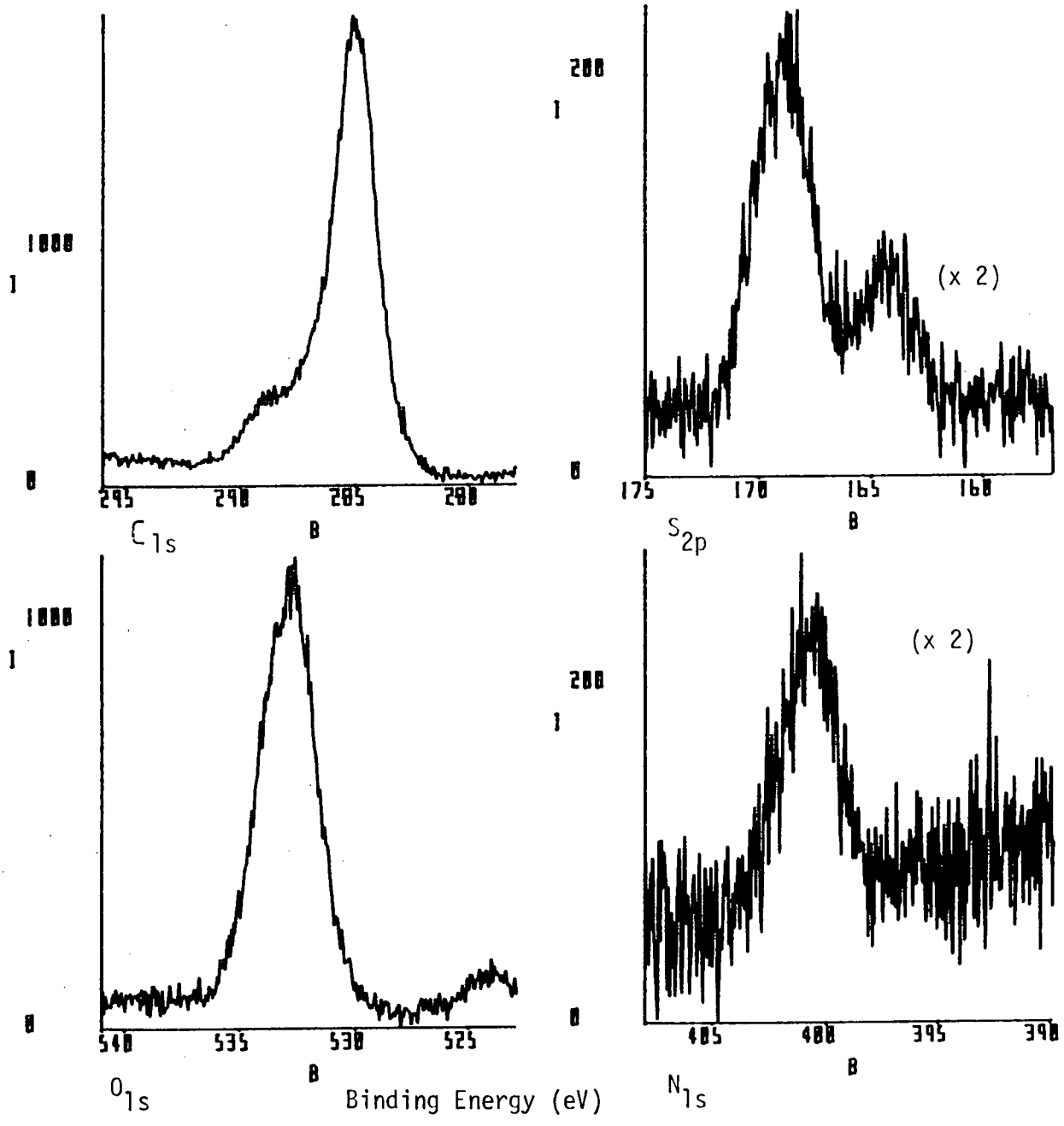

Figure 5.37b Kimmeridge kerogen, 2hr U.V.

Table 5.21 Kimmeridge Kerogen. Effect of exposure to U.V. light (2hrs, 254nm, in air ~30°C) on the relative peak areas of the core level signals

	C_{1s}	O_{1s}	N_{1s}	S_{2p}	$S_{unox.}$ *
unexposed	100	26.1	4.7	7.1	53.8
2hrs U.V.	100	57.3	3.4	7.3	30.3

* Unoxidised sulphur as a percentage of total sulphur.

U.V. irradiation leads to the formation of oxidised carbon functionalities and the development of a high binding energy shoulder to the C_{1s} envelope; the conversion of sulphide type sulphur to sulphate sulphur also occurs.

The behaviour of sulphur in coals and other fossil fuels is of particular interest to the industrialist since sulphur, even if present in low concentrations, can cause detrimental effects on coal usage, and also poses environmental problems.

The work to be discussed here concerns the relative reactivity of organic and inorganic sulphide towards U.V. oxidation. Polyphenylene sulphide film and freshly powdered ferrous sulphide (technical grade) have been examined, before and after exposure to U.V. light. Core level spectra of the polyphenylene sulphide and ferrous sulphide are shown in Figures 5.38 and 5.39 respectively; relative area measurements of the spectra are given in Table 5.22.

The spectra for the untreated polyphenylene sulphide show the presence of a relatively low level of oxygen. An Si_{2p} peak also present suggests slight contamination of the surface regions of the polymer film.

Fig. 5.38a C_{1s}, S_{2p} and O_{1s} core level spectra of polyphenylene sulphide film, (a) untreated and after ½ hour's U.V. irradiation, (b) untreated and after 2 hours' U.V. irradiation (254nm in air at ≈ 30°C).

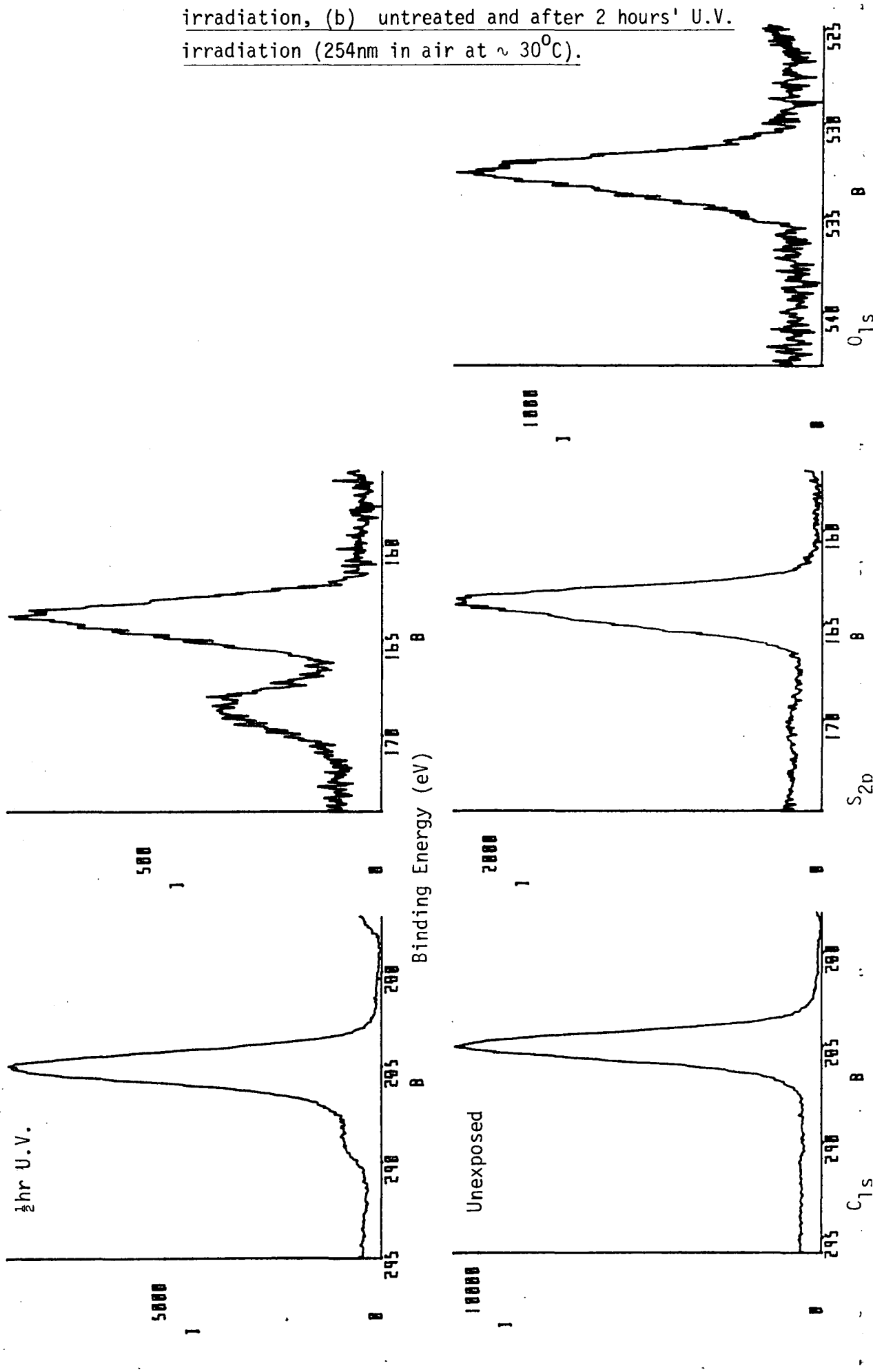

Figure 5.38b Polyphenylene sulphide

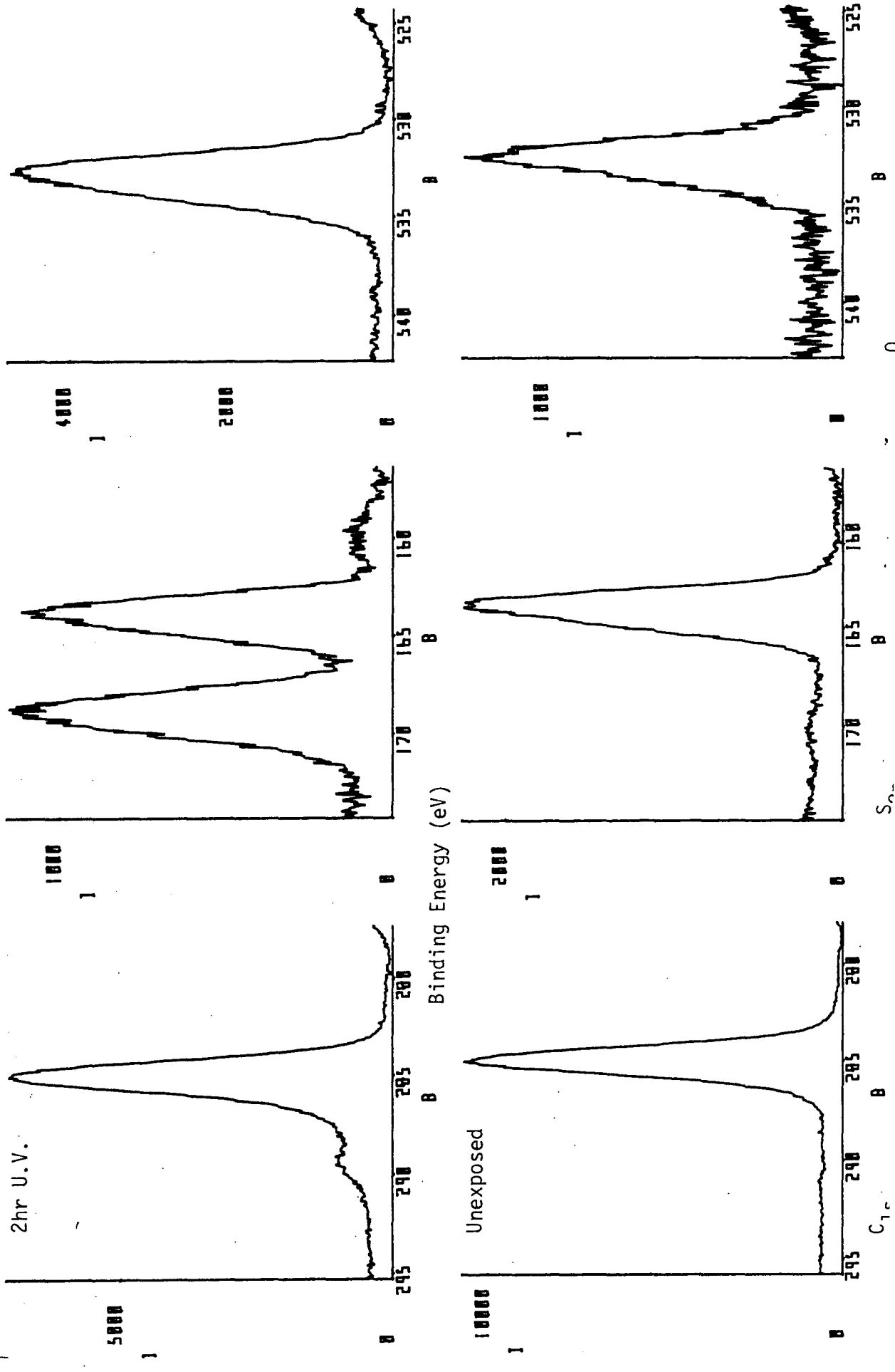

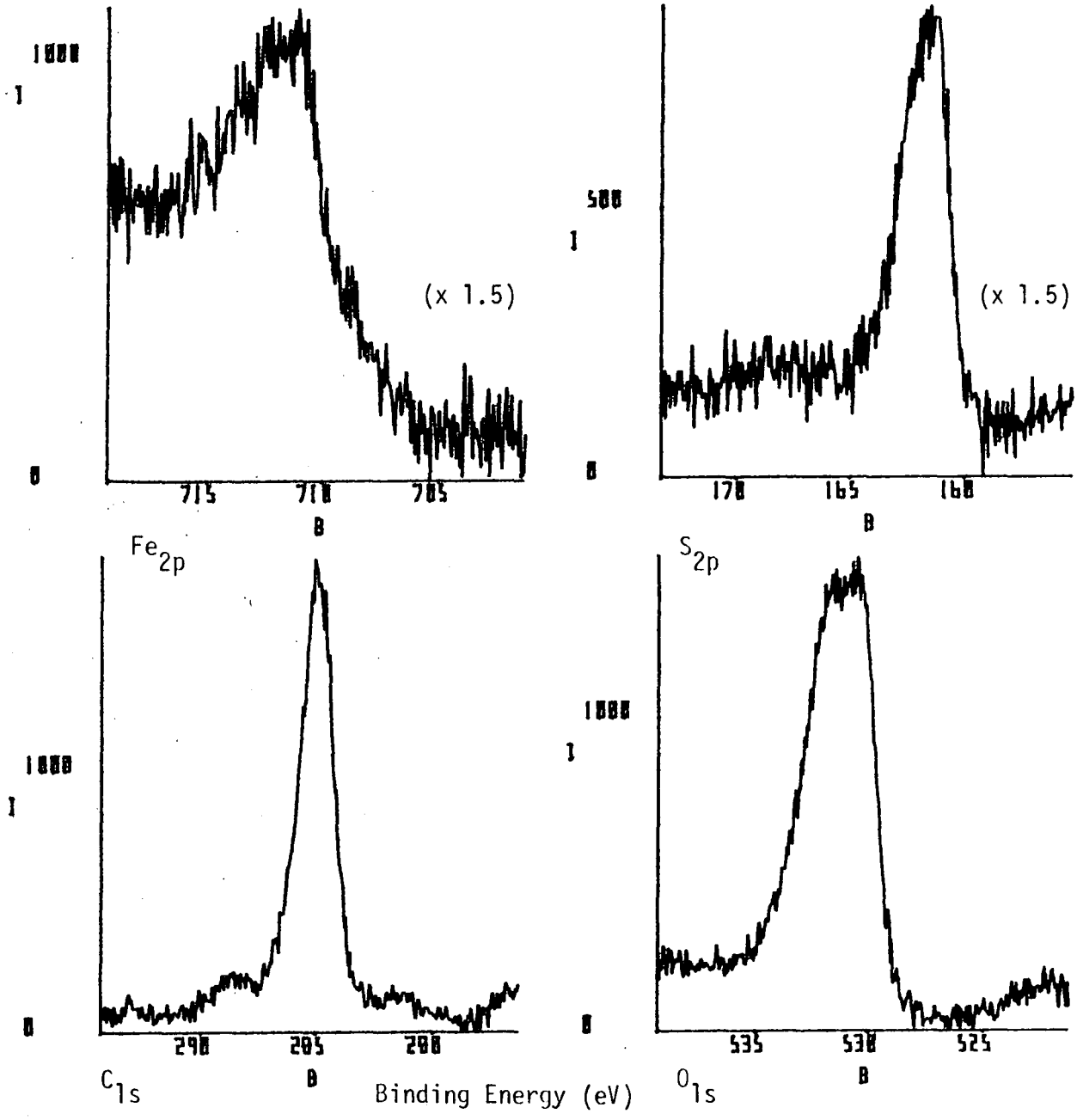

Figure 5.39a Fe_{2p}, S_{2p}, C_{1s} and O_{1s} core level spectra of ferrous sulphide, (a) as received, (b) after 2 hours' U.V. irradiation, (c) after 18 hours' U.V. irradiation (254nm in air at $\sim 30^{o}C$).

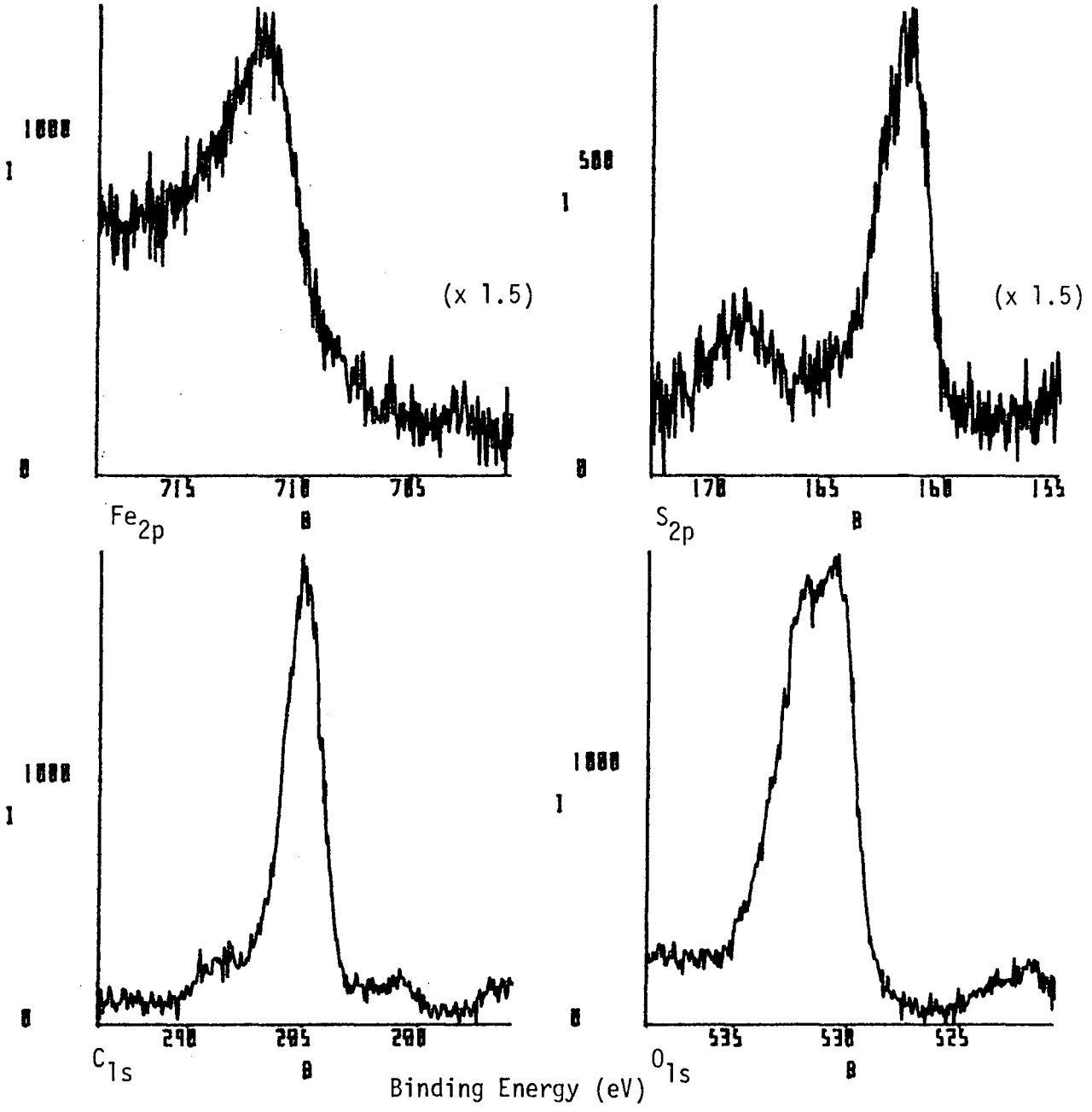

Figure 5.39b Ferrous sulphide, 2hr U.V.

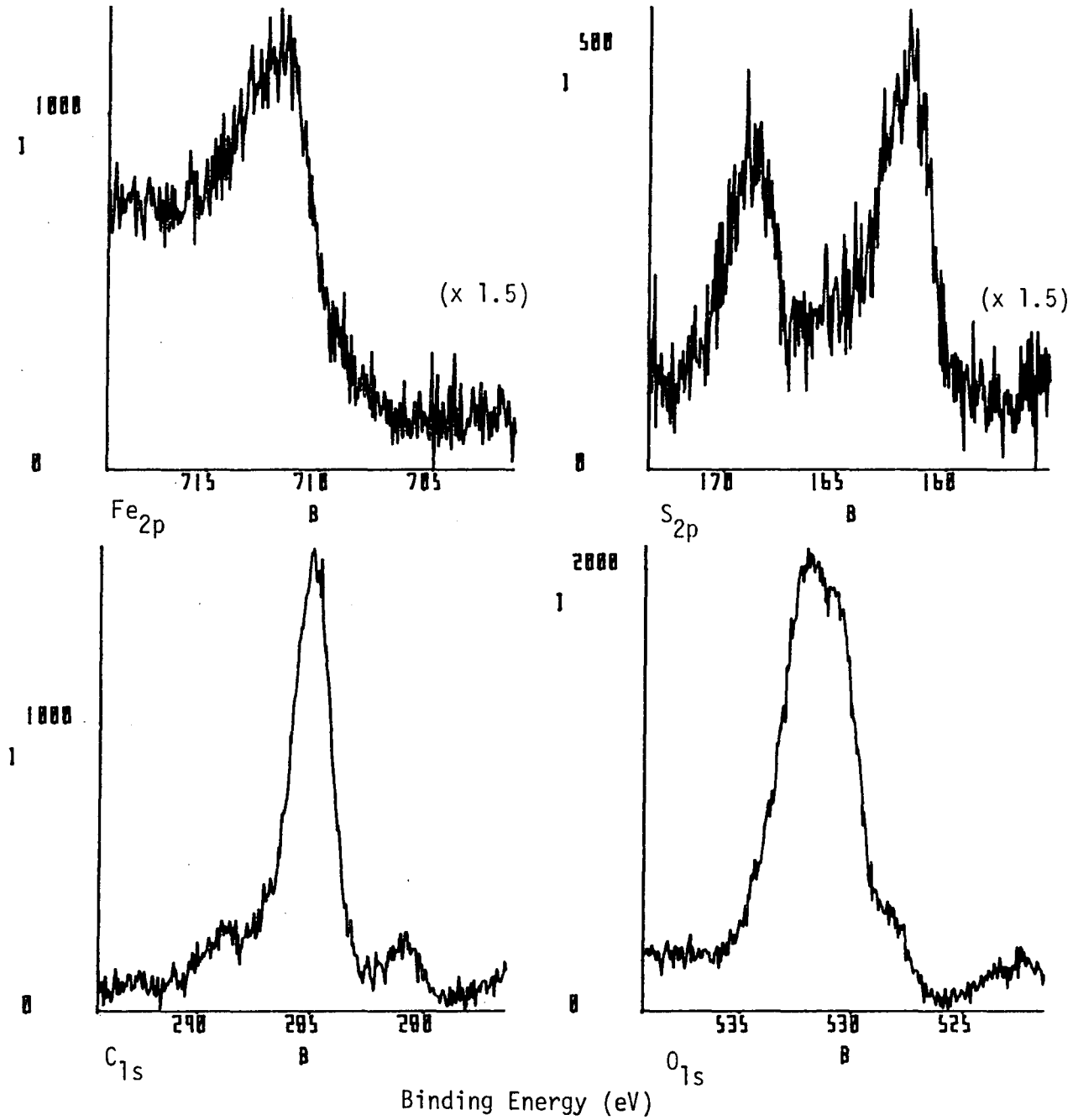

Figure 5.39c Ferrous sulphide, 18 hr U.V.

Table 5.22 Relative peak area measurements for polyphenylene sulphide and ferrous sulphide before and after U.V. irradiation (254nm in air at ~ 30°C).

	C_{1s}	O_{1s}	S_{2p}	S_{ox} †	Fe_{2p}	Si_{2p}
Polyphenylene Sulphide *						
Unexposed	100	16.0	25.0	0.6	-	2.1
½hr U.V.	100	40.0	13.3	31.0	-	-
2hr U.V.	100	80.7	30.7	56.7	-	-
Ferrous Sulphide ‡						
As received	207.1	245.8	72.6	15.2	100	-
2hr U.V.	199.4	264.8	51.1	20.0	100	-
18hr U.V.	234.1	440.7	90.7	36.1	100	-

† S_{ox} refers to oxidised sulphur expressed as per cent total S_{2p} peak area

* Polyphenylene sulphide was analysed in thin film form at electron take-off angle, θ, 30°.

‡ Ferrous sulphide powder (technical grade) was analysed at optimum θ.

The S_{2p} photoionisation signal is centred at 163.9eV binding energy, the expected position for an organic sulphide. Also with the S_{2p} envelope there is a second peak of far lower intensity, to higher binding energy of the predominant sulphide peak (168.6eV) and representative of oxidised sulphur. After 2 hours' exposure to U.V. light considerable oxidation of the S_{2p} envelope has occurred. The oxidised S_{2p} signal corresponds to $\sim$ 57% of the total sulphur envelope. In addition the carbon framework of the polymer system has undergone oxidative attack. Similar observations hold for irradiation for 30 minutes, although the development of the S_{2p} doublet structure is not as well advanced.

The ESCA spectra of ferrous sulphide shows high levels of carbon and oxygen to be present. The inorganic sulphide S_{2p} peak is found at $\sim$ 161.6eV binding energy, somewhat lower than for the organic sulphide. There is little evidence for oxidised sulphur functionality for the unexposed material. Two hours' irradiation with U.V. light produces substantially less oxidation of the inorganic sulphide than was found for polyphenylene sulphide. Even after a period of 18 hours' irradiation the sulphate sulphur S_{2p} peak amounts to just 46% of the total S_{2p} peak intensity.

These differences in reactivity would indicate that the sulphur present in Gilsonite 'selects' and the Oxfordshire coal was present in an organic sulphide form since conversion to oxidised sulphur moieties is complete within a few hours irradiation time. A previous study[169] of the reaction of polyphenylene sulphide and ferrous sulphide when subjected to mild oxygen plasma treatments has been carried out. It was found that, for ferrous sulphide, a 10W, 5 sec. treatment produced oxidation of sulphur with the C_{1s} level showing little oxidation (Figure 5.40). In contrast a weaker plasma treatment (0.4W, 5 sec.)

left the sulphur envelope unchanged whilst causing more extensive oxidation of the C_{1s} signal.

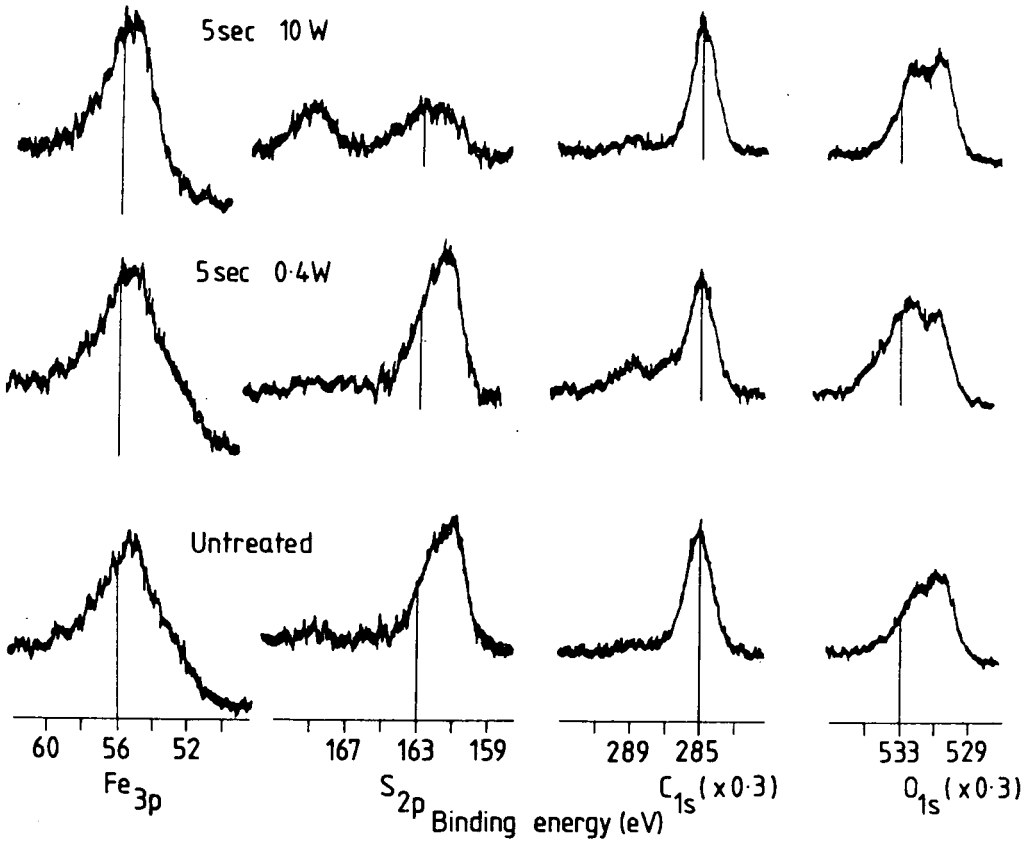

Figure 5.40 Effect of oxygen plasma treatment (0.2 torr) on the core level spectra of ferrous sulphide.

U.V. irradiation of ferrous sulphide for both 2 hour and 4 hour time periods bring about oxidation of the sulphide with comparatively small effect on the carbon component. It may be that sulphur oxidation will occur in preference to carbon oxidation.

5.3.8 Atmospheric Oxidation of Coal

5.3.8a Introduction

Coal is known to undergo rapid deterioration attributable to oxidation even when stored under strictly controlled conditions.[306] Recently studies have been performed to investigate the air oxidation of bituminous coal under ambient conditions.[302] Wet chemical and spectroscopic (Fourier transform infrared and solid state ^{13}C n.m.r.) were used for oxygen functional group analyses.

This work uses the surface sensitivity of ESCA to probe the oxidation of recently mined coal (Illinois No. 6 and Rawhide coal, the analytical characteristics of which are listed in Table 5.23) under two sets of experimental conditions. The first procedure involved simple exposure to air at ambient temperature in the laboratory with periodic mixing of the coal. In the other method, samples were mounted on a spectrometer probe tip and allowed to weather outdoors for one week. Samples of anthracite were also weathered this way over two separate one week time periods.

Throughout this investigation the dual anode facility of the ES300 spectrometer has been used to afford depth profiling of the sample surface. To recap, the respective sampling depths amenable to study using $Mg_{K\alpha}$ and $Ti_{K\alpha}$ x-ray sources are $\sim$ 50Å and $\sim$ 130Å.

5.3.8b Ambient oxidation of Illinois No. 6 and Rawhide coals (indoors)

The $Mg_{K\alpha}$ spectra of Illinois No. 6 and Rawhide coal samples, introduced into the ESCA spectrometer from their sealed glass sample bottles via an N_2 glove bag so as to minimise air contact, are shown in Figures 5.41a and 5.42a respectively. Differences in ESCA derived elemental atomic ratios (Table 5.24) in general reflect those values from standard

Table 5.23 Exxon analyses of Illinois No. 6 and Rawhide coals

	Illinois No. 6	Rawhide
Sample No.	9065-71-1	7793-19-0
% C	68.40	66.96
% H	5.23	4.71
% N	1.26	0.84
% S Total	4.38	0.47
% S pyrite	1.28	-
% S sulphate	0.01	-
% S organic	3.09	-
% O (NAA)†	14.38	22.01
TGA N_2 loss	30.3	41.0
" Air loss	60.3	54.2
" % Ash	9.4	4.8
% Mineral Matter	11.22	5.42
% O (by diff.)	10.80	21.60
Empirical Formula		
Carbon	100	100
Hydrogen	91.75	84.41
Nitrogen	1.58	1.08
Sulphur	1.69	0.26
Oxygen	11.84	24.19

† determined using neutron activation analysis

Figure 5.41a C_{1s}, O_{1s}, N_{1s}, S_{2p}, Si_{2p} and Al_{2p} core level spectra of Illinois No. 6 coal, unexposed

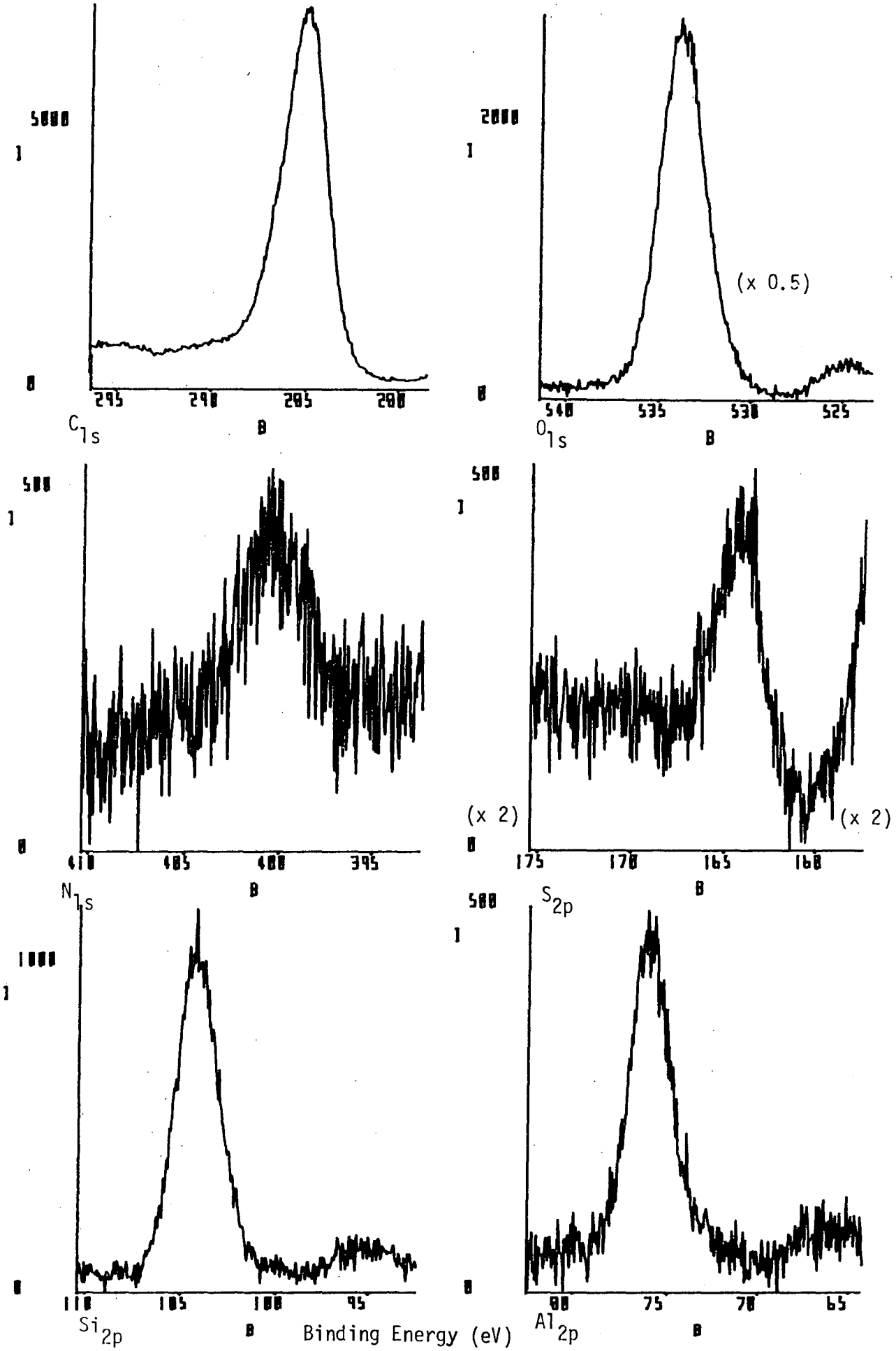

Figure 5.41b Core level spectra of Illinois No. 6 coal, weathered for one week, October 1983.

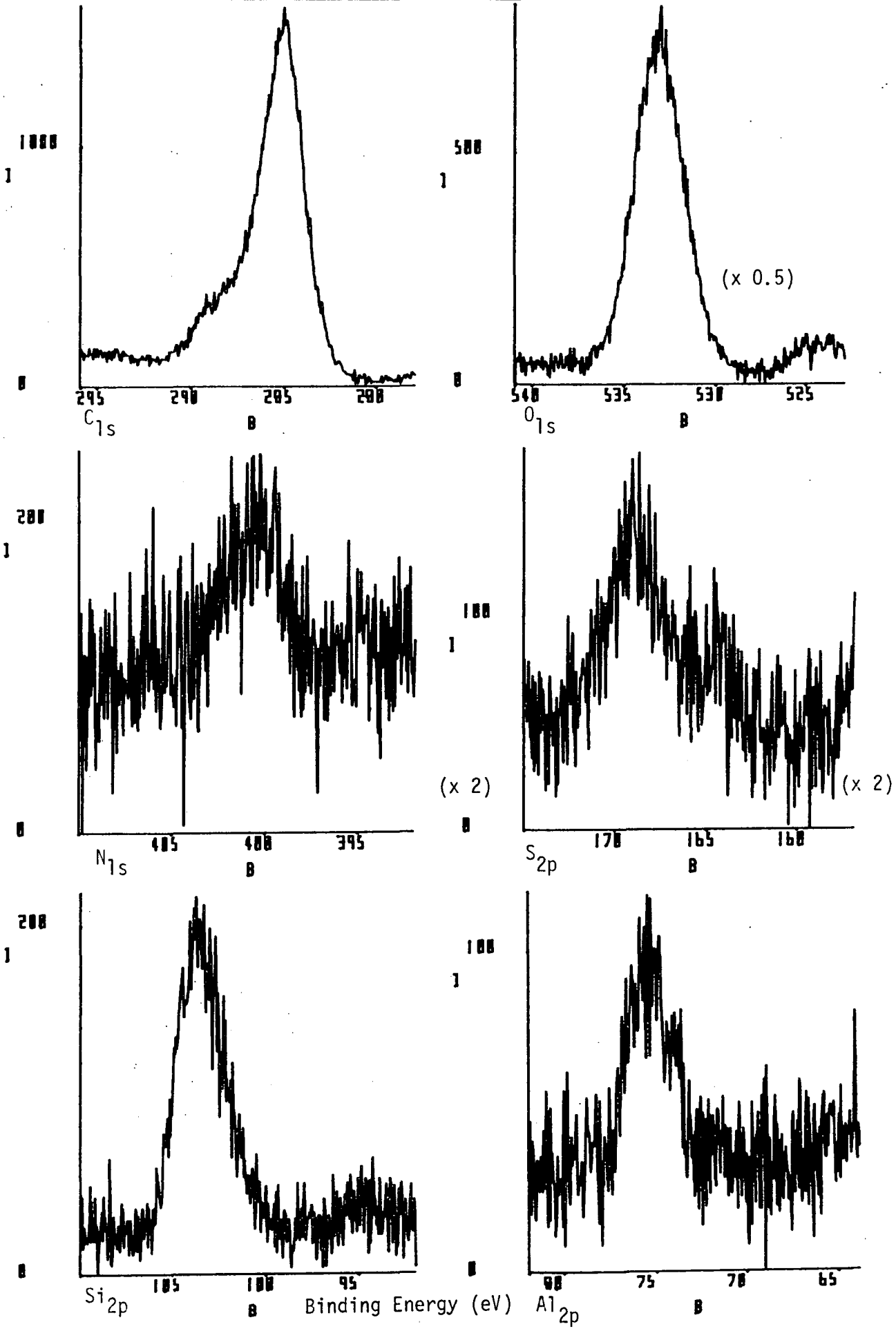

Figure 5.4lc C_{1s} difference spectrum (weathered - unexposed) for Illinois No. 6 Coal, weathered for one week, October 1983

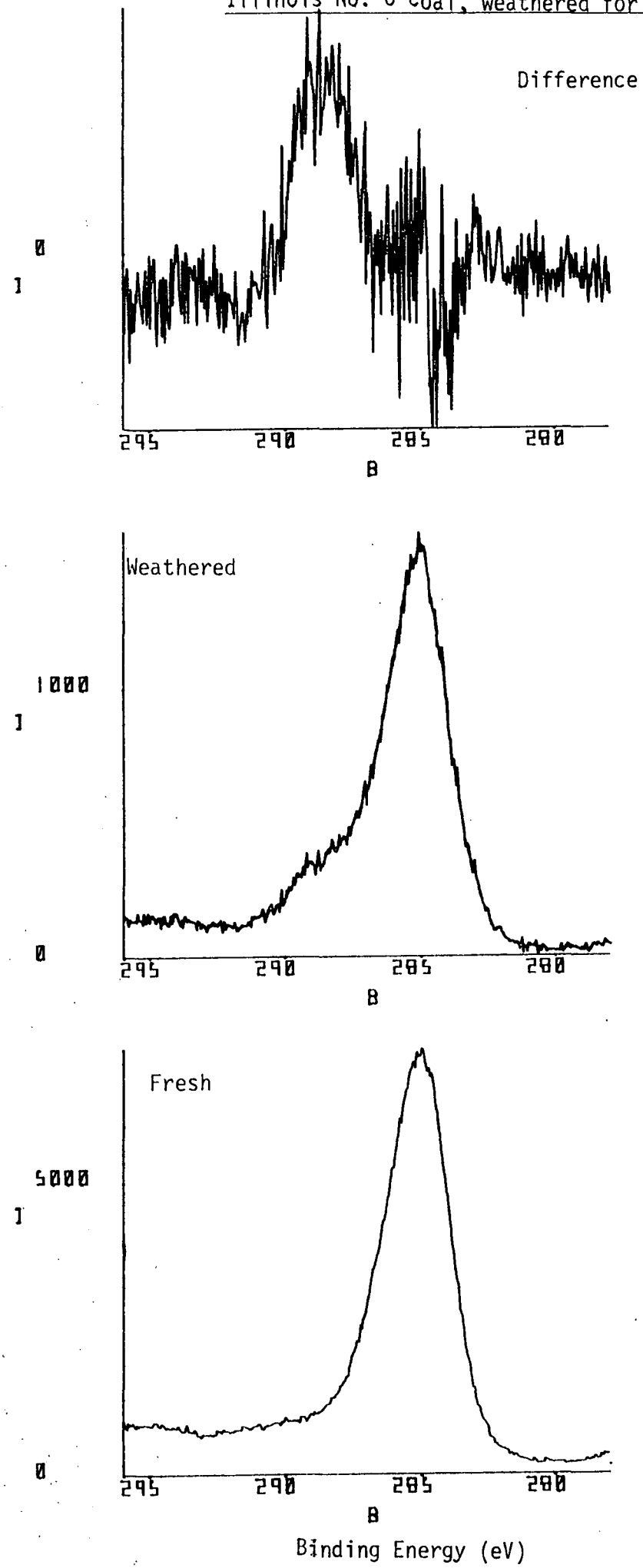

Figure 5.42a C_{1s}, O_{1s}, N_{1s}, S_{2p}, Si_{2p} and Al_{2p} core level spectra of Rawhide coal, unexposed.

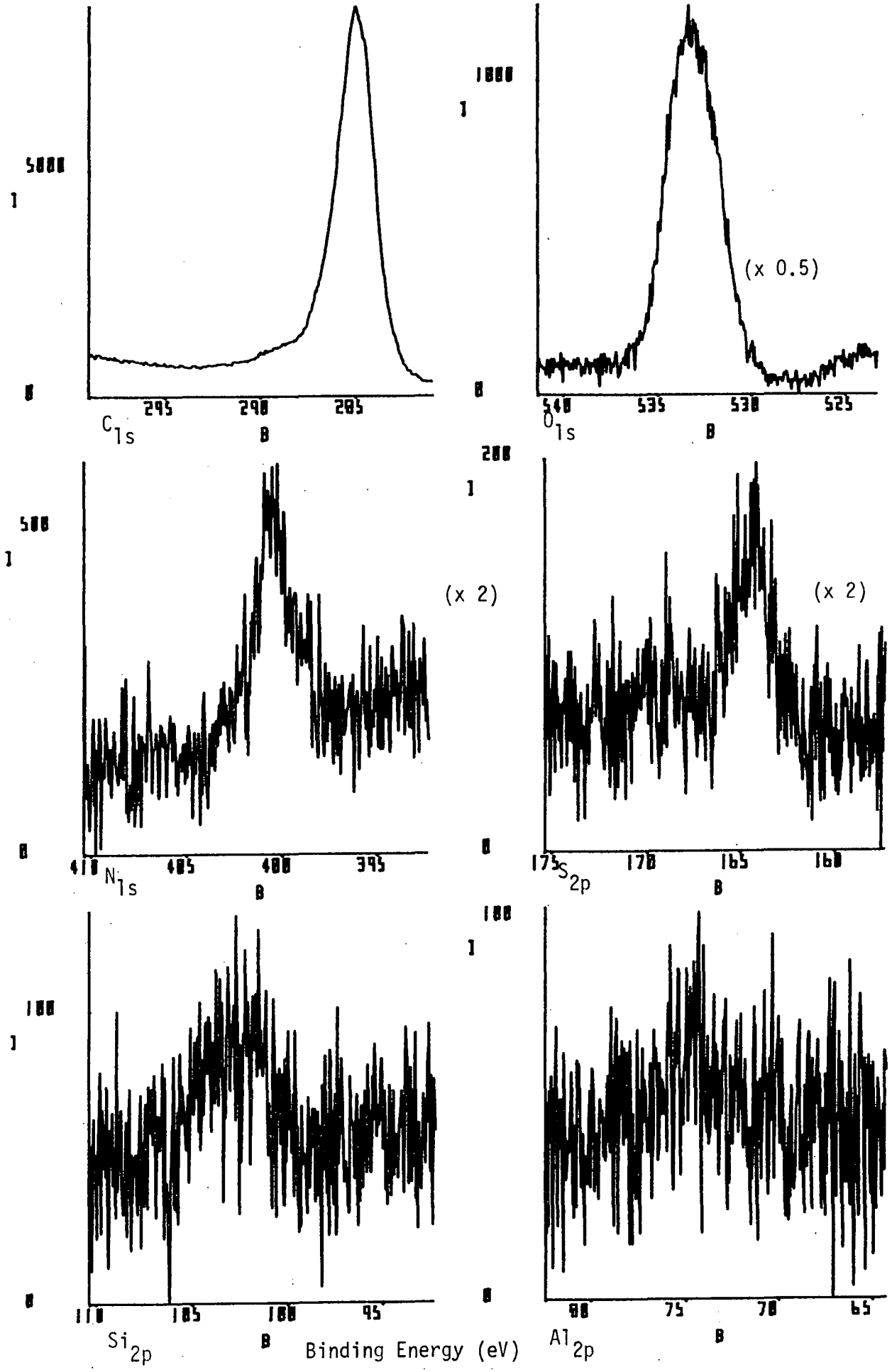

Figure 5.42b Core level spectra of Rawhide coal, weathered for one week, October 1983.

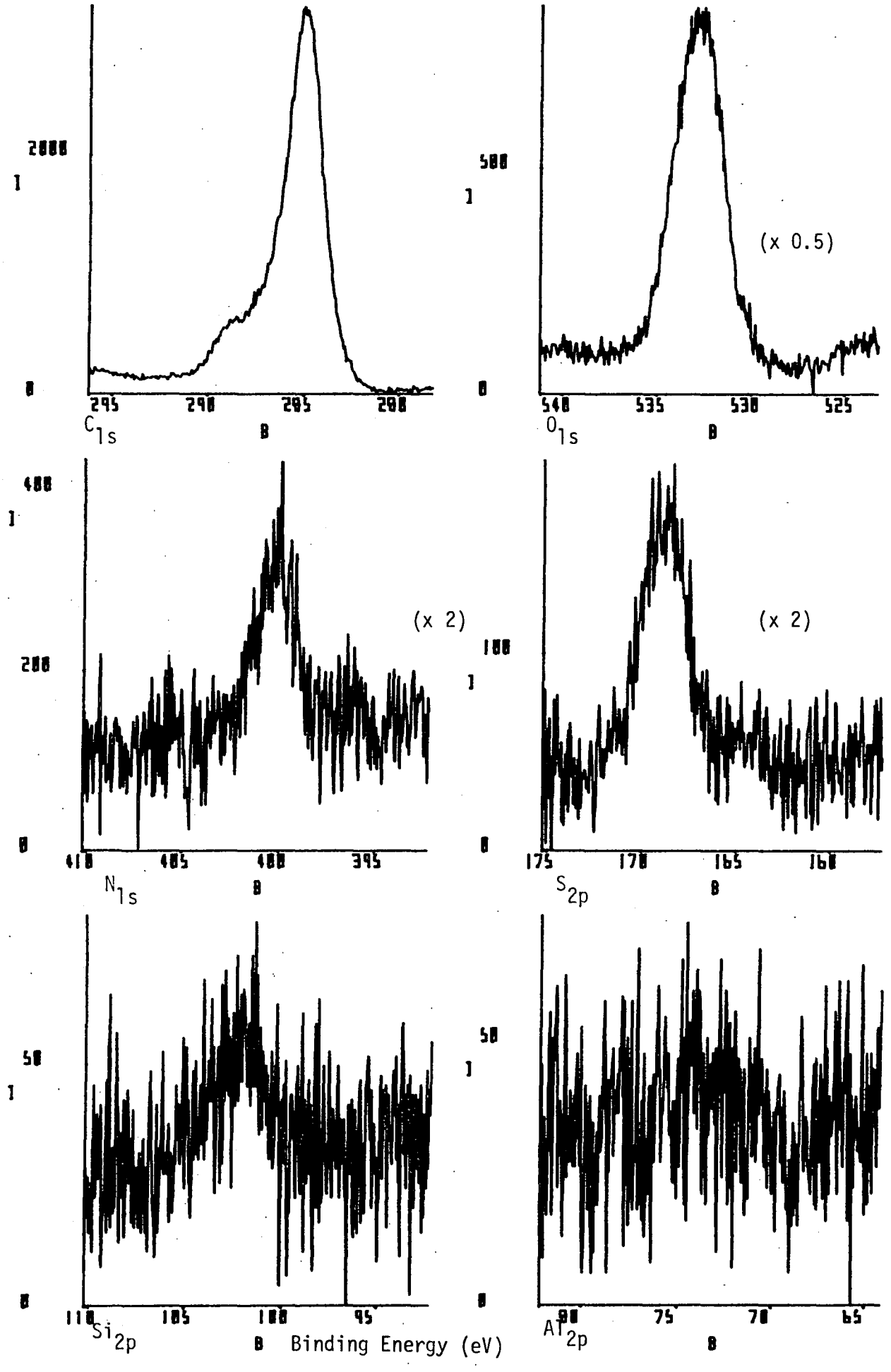

Figure 5.42c C_{1s} difference spectrum (weathered - unexposed) for Rawhide coal, weathered for one week, October 1983.

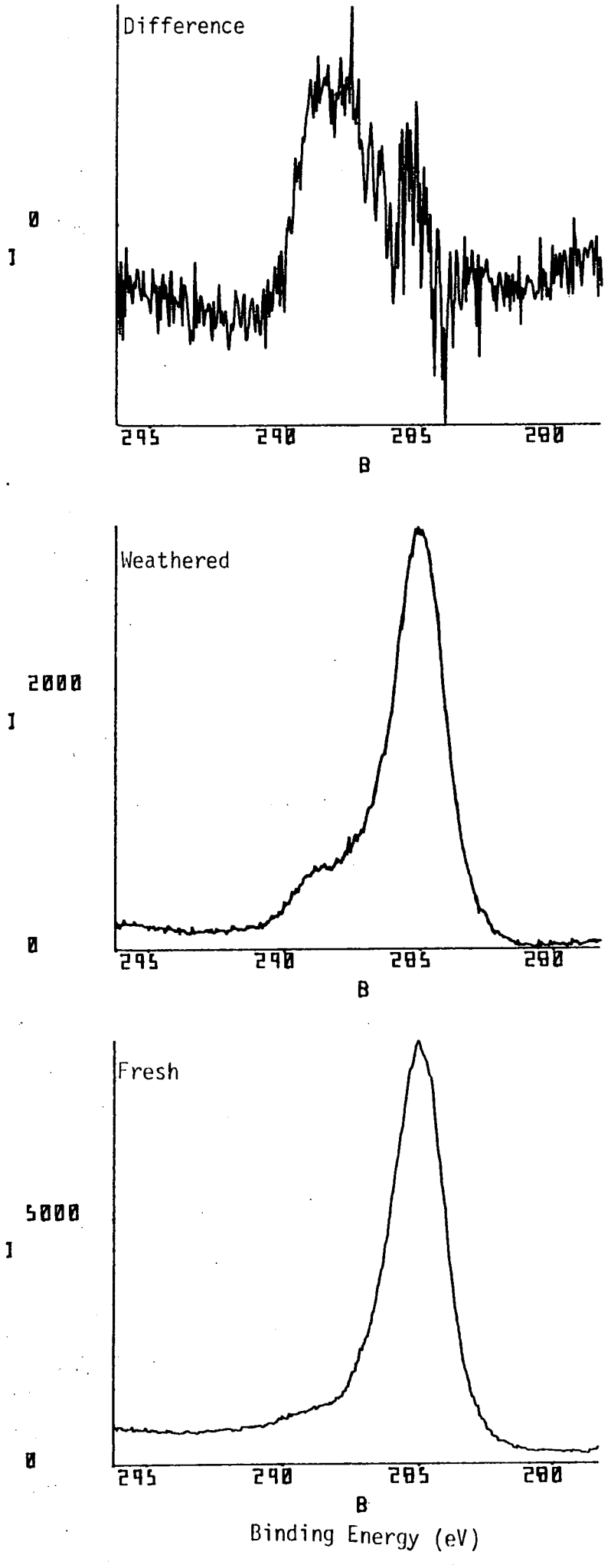

Table 5.24 Atmospheric oxidation studies of coal. Relative atomic concentrations. († indicates that the core level was not analysed.)

		C	O (Total)	N	S	Si	Al	Org. O
Illinois No.6	Mg	100	46.0	1.9	1.5	10.2	4.0	19.6
Unexposed	Ti	100	58.8					
	Mg	100	32.5	-†	1.8	5.8	4.9	13.6
Powdered	Ti	100	78.5					
Exposed One Day	Mg	100	62.6	-	-	14.8	6.0	23.9
Exposed 8 Days	Mg	100	58.0	1.7	1.9	12.6	5.8	24.1
	Ti	100	74.1					
Repowdered	Mg	100	35.6	-	1.7	6.9	3.1	17.1
Weathered one week (October)	Mg	100	65.4	2.7	2.0	7.9	4.8	42.4
	Ti	100	57.4					
Rawhide	Mg	100	21.2	2.1	0.5	1.0	0.0	19.2
Unexposed	Ti	100	30.5					
	Mg	100	19.8	-	0.4	0.5	0.0	18.8
Powdered	Ti	100	28.2					
Exposed One Day	Mg	100	23.1	1.6	-	1.2	0.0	20.8
	Ti		34.6					
Exposed 8 Days	Mg	100	20.3	-	0.6	0.6	0.0	19.1
	Ti	100	29.0					
Repowdered	Mg	100	20.7	-	0.8	0.3	0.4	19.8
Weathered One week (October)	Mg	100	68.3	2.9	2.8	2.5	0.0	63.3
	Ti	100	38.9					
Anthracite	Mg	100	5.0	1.8	0.2	0.1	0.1	4.7
Unexposed	Ti	100	-					
Weathered One Week (August)	Mg	100	20.0	1.9	0.5	1.0	-	18.0
	Ti	100	17.9					
Weathered One Week (October)	Mg	100	30.1	-	1.0	0.8	-	28.5
	Ti	100	22.7					

elemental analyses (Table 5.23). The ESCA spectrum of Illinois No. 6 coal reveals a high silicon and aluminium content, whereas the spectrum of the Rawhide coal sample shows a very weak Si_{2p} signal only. Both coal samples give S_{2p} photoionisation signals, each dominated by organic sulphide. The N_{1s} signal of the Illinois No. 6 coal is broader than that of the Rawhide coal sample, and this suggests nitrogen is present in more than one form in Illinois No. 6 coal. There is no evidence for oxidised nitrogen functionalities for either coal. The C_{1s} spectra of the unexposed coals do show signs of carbon - oxygen functionality (e.g. $-\underline{C} - O$, $\underline{C}(=O) - O$ and possibly $\underline{C} = O$). The small peak at $\sim$ 294.5eV binding energy in the C_{1s} region for Illinois No. 6 coal corresponds to a potassium 2p core level signal.

Repowdering the coal samples using a pestle and mortar and reanalysing yields C : O (Total or organic) atomic ratios lower than for the original ESCA analyses. This observation would suggest that despite the care exercised in the collection, preparation and storage of the coal samples, a degree of surface oxidation is present.

Samples taken from each coal after exposure to the air for just one day show an increased C : O atomic ratio. The results for the coal samples repowdered after 8 days' exposure indicate that the oxidation has penetrated the bulk. The Illinois No. 6 coal shows enhanced surface oxidation from consideration of the $Mg_{K\alpha}$ C : O atomic ratio data before and after repowdering. The Rawhide coal data does not exhibit such wide variation. Inspection of the core level spectra does not reveal marked structural differences between the exposed and unexposed coals.

5.3.8c Weathering Studies

Weather reports for the periods 6th - 13th August, 1983 and 19th - 26th October are shown in Tables 5.25 and 5.26.

Core level spectra for Illinois No. 6 coal and Rawhide coal weathered in October (Figures 5.41b and 5.42b) show that oxidation of the carbon and sulphur moieties has occurred. The tendency is noticed for the S_{2p} and N_{1s} core levels to increase intensity on weathering (Table 5.24). The binding energy and overall peak shape of the N_{1s} signal remains essentially unaltered, indicating that the nitrogen species in the coals are not oxidised. The nature of the silicon and aluminium components within the coal show no signs of chemical alteration, although the Rawhide coal appears to have accumulated a low level of surface silicon from the environment.

These weathering experiments allow the analysis of the very same sample surface as has been directly exposed to the environment. It is not surprising therefore that the measured oxidation is far more pronounced than was found for the laboratory exposed samples in Section 5.3.5b. Depth profiling of the coal surfaces reveals the surface specifity of the oxidation (Table 5.24).

Although the C : O atomic ratios for both Illinois No. 6 and Rawhide coal after weathering are quite similar, respective values being 100 : 65.4 and 100 : 68.3, estimations of the organic oxygen content show a large difference. Hence the Illinois No. 6 coal has a C : O organic of 100 : 42.4 whilst the corresponding value for the Rawhide coal is 100 : 63.3. Deconvolution of the C_{1s} envelopes, the results of which are presented in Table 5.27, show carbon components corresponding to $\underline{C}$ - O, $>\underline{C}$ = O and $\underline{\overset{O}{\overset{\|}{C}}}$ - O functionalities in approximately equal ratios for both coals.

Table 5.25 Daily Observations and Weather for Durham, 6th - 13th August 1983.*

Date	Temperature °C					Rainfall (mm)	Sunshine (hours)	Weather
	Dry† Bulb	Wet† Bulb	R.H. (%)	Max.	Min			
6	20.0	16.4	67	24.0	13.8	-	10.4	Bright and sunny
7	16.9	14.7	78	20.0	10.3	-	6.9	Cloudy at first, sunny later
8	15.4	13.8	83	18.4	13.4	-	0.6	Cloudy, dry, sunny spells
9	14.5	13.2	86	17.1	13.1	-	0.5	Cloudy, dry, with brief sunny spells
10	16.5	14.0	75	20.9	13.3	-	8.0	Cloudy, becoming bright and sunny
11	20.6	17.1	68	26.6	8.8	-	12.0	Bright, sunny, warm
12	16.9	13.4	65	23.4	12.1	-	11.3	Bright and sunny
13	16.9	12.8	60	25.4	9.2	-	11.9	Bright and sunny

* Figures collated by Dr R. Harris, Department of Geography, University of Durham

† Measurements recorded at 9.30 a.m.

Table 5.26 Daily Observations and Weather for Durham, 19th - 26th October 1983.*

Date	Temperature °C					Rainfall (mm)	Sunshine (hours)	Weather
	Dry† Bulb	Wet† Bulb	R.H. (%)	Max.	Min.			
19	10.0	9.1	86	11.3	6.8	-	8.8	Bright, sunny and dry
20	8.4	6.5	74	10.0	5.1	-	6.6	Bright, sunny and dry
21	4.5	3.5	84	10.5	-1.4	-	6.2	Frost, bright and sunny
22	2.3	1.2	80	11.0	-2.1	-	8.6	Frost, bright and sunny
23	10.0	7.5	68	13.1	1.8	-	5.4	Ground frost, bright and sunny
24	5.6	3.5	68	10.5	0.2	1.2	7.6	Ground frost, bright and sunny
25	8.9	7.2	80	12.3	1.0	Tr.	0.1	Cloudy, slight rain, strong SW winds
26	12.1	10.1	76	14.0	8.2	-	4.6	Bright and sunny, becoming cloudy later

* Figures collated by Dr R. Harris, Department of Geography, University of Durham

† Measurements recorded at 9.30 a.m.

Table 5.27 Relative area measurements for the C_{1s} spectra of coals weathered for one week

	C_{1s} Tot.	C - H	C - O	> C = O	O || C - O
			(286.6)	(288.0)	(289.2)
Illinois No. 6	100	70.5	14.8	7.7	7.0
			(286.7)	(288.0)	(289.4)
Rawhide	100	71.0	14.9	7.5	6.6
			(286.5)	(287.8)	(289.2)
Anthracite (October)	100	71.1	14.9	7.4	6.7
			(286.4)	(288.0)	(289.3)
Anthracite (August)	100	73.0	15.3	6.4	5.3

Difference spectra (unexposed - weathered) of the C_{1s} envelopes for Illinois No. 6 coal and Rawhide coal are shown in Figures 5.41c and 5.42c respectively. They highlight the development of the high binding energy shoulder of the C_{1s} signals on weathering, and the variation in the pattern of oxidation for the different types of coal.

The weathering of anthracite is found to follow a similar pattern to that of the lower rank coals discussed, so far as carbon-oxygen functional group and oxidised sulphur development are concerned (Tables 5.24 and 5.27; Figures 5.43a-d). The C_{1s} difference spectrum for anthracite weathered in October (Figure 5.43c) contrasts with those for the Illinois No. 6 and Rawhide coals (Figures 5.41c, 5.42c) and also with the difference spectrum of U.V. irradiated (254nm) anthracite (Figure 5.31). It should be noted however that 254nm ultraviolet light is not a component of the spectrum of natural sunlight : the atmosphere filters out practically all the radiation below 295nm.

Atmospheric conditions prevailing during the exposure period will affect the extent and nature of weathering. This is demonstrated for samples of anthracite weathered for one week time intervals in October

Figure 5.43a C_{1s}, O_{1s}, N_{1s}, S_{2p}, Si_{2p} and Al_{2p} core level spectra of anthracite, unexposed.

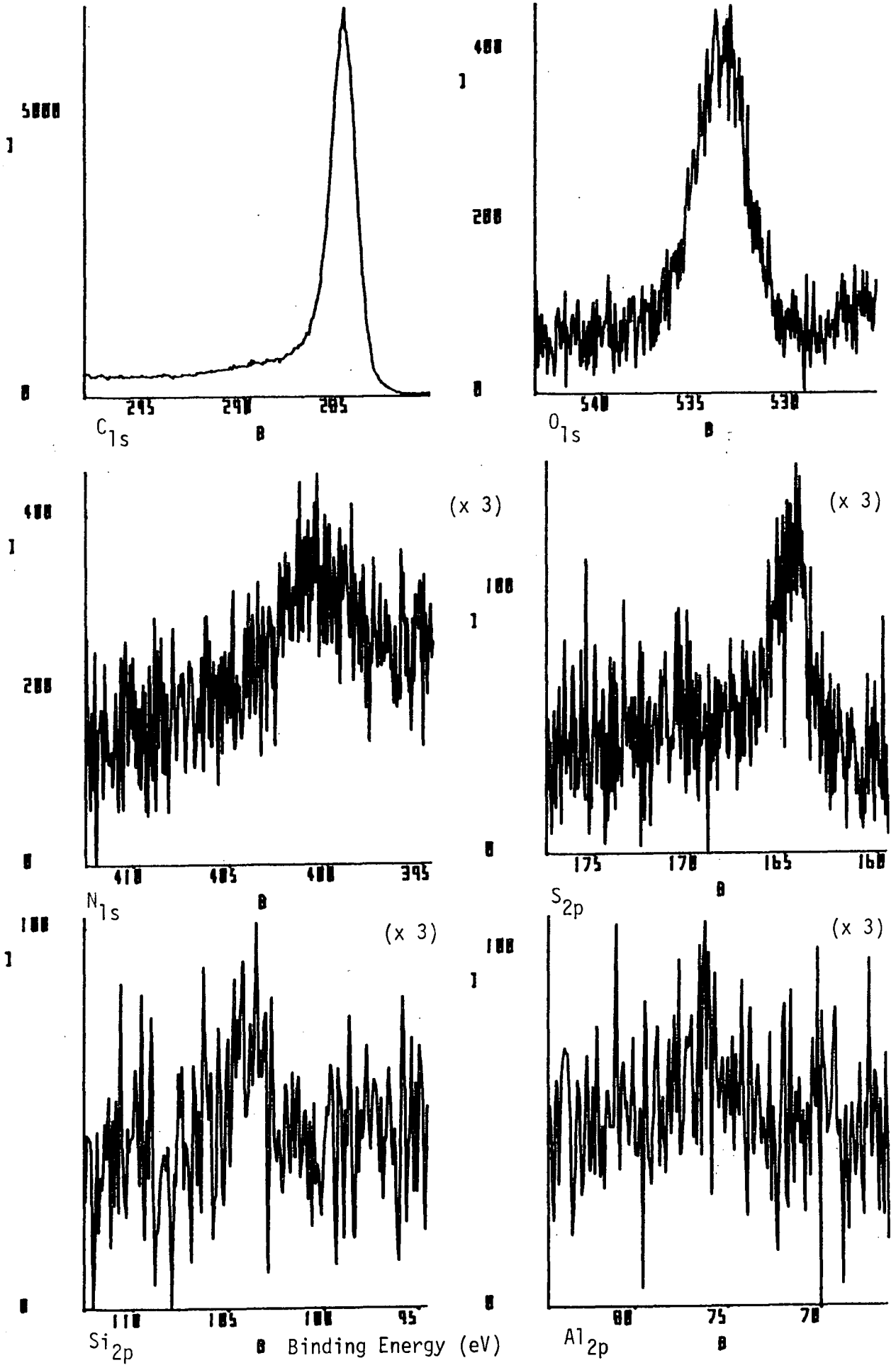

Figure 5.43b Core level spectra of anthracite, weathered for one week, October 1983.

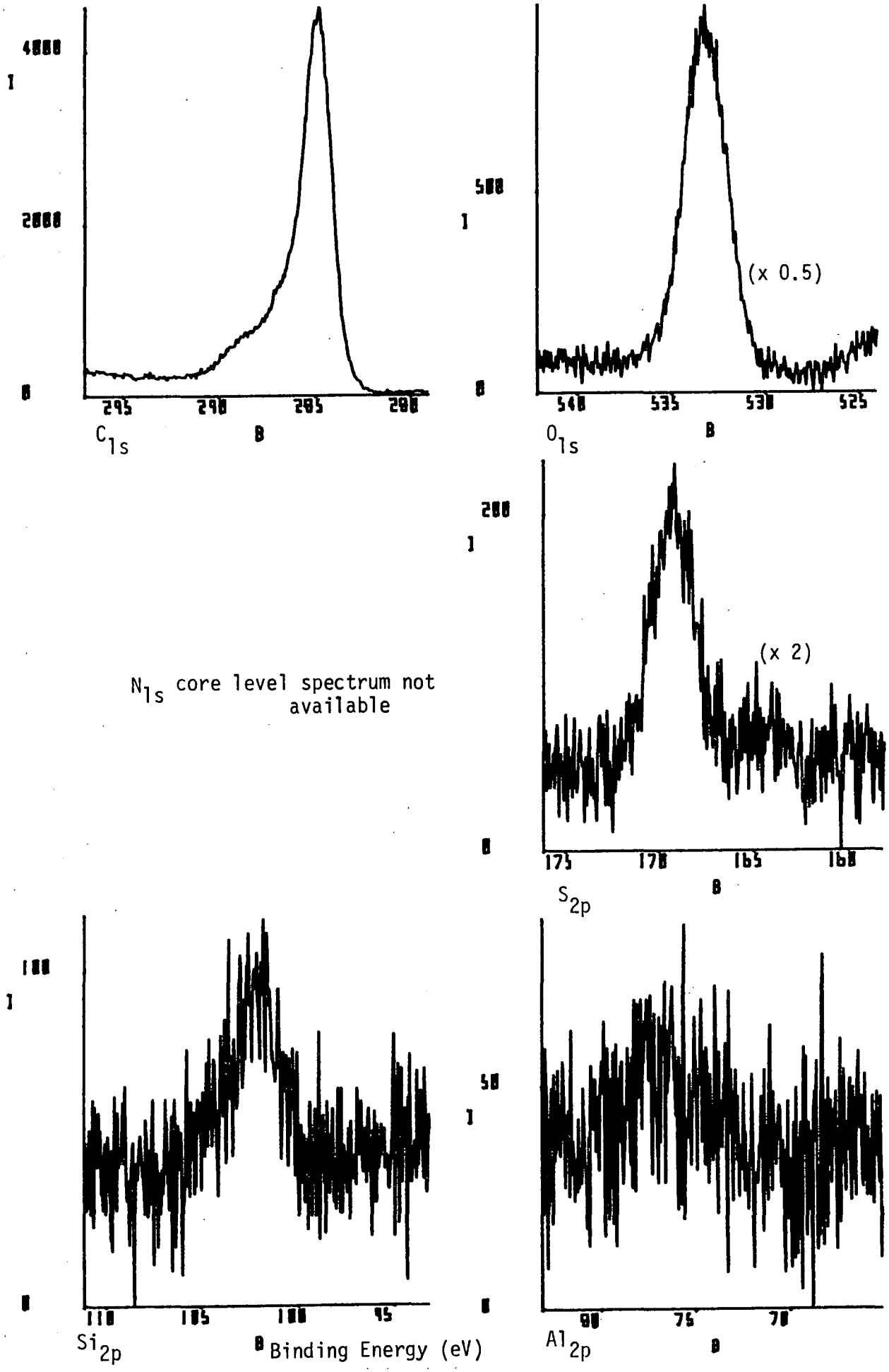

Figure 5.43c C_{1s} difference spectrum (weathered - unexposed) for anthracite, weathered for one week, October 1983.

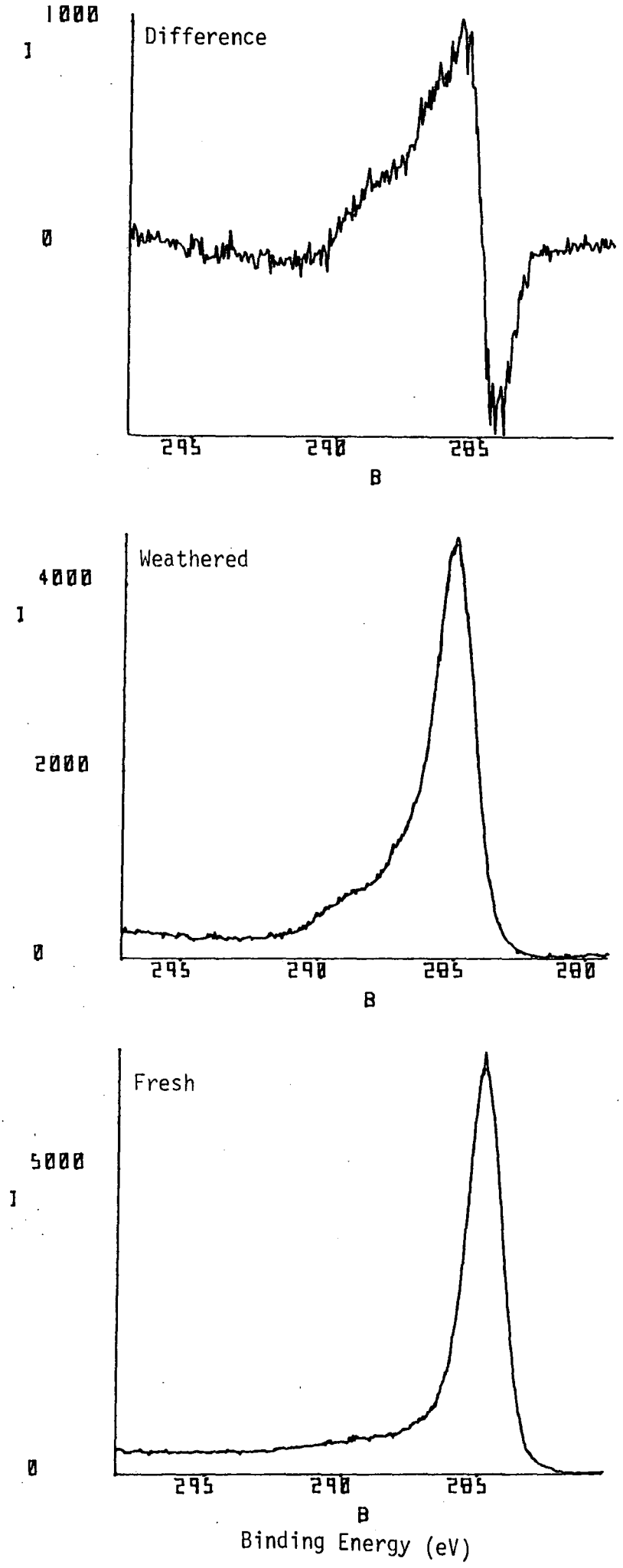

Figure 5.43d C_{1s} difference spectrum (weathered - unexposed) for anthracite, weathered for one week, August 1983.

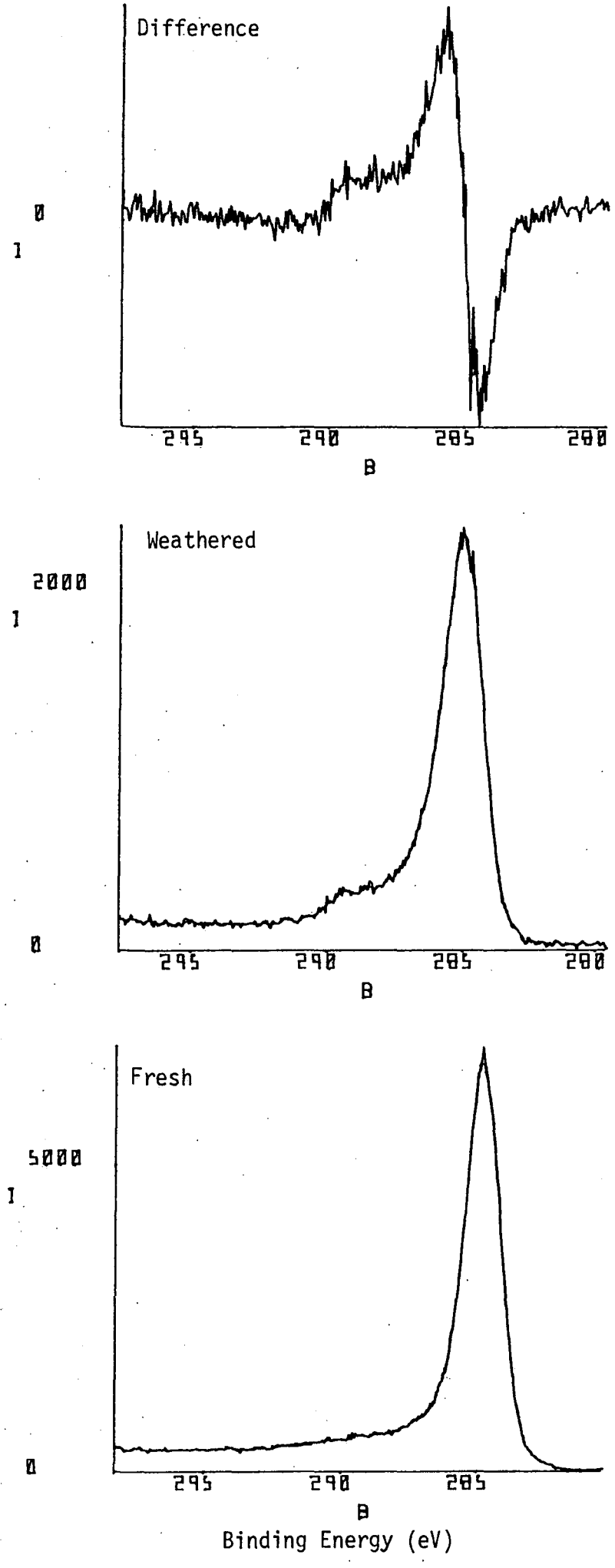

and in August (Tables 5.24, 5.27; Figures 5.43c,d). More extensive oxidation is found for the October period when the relative humidity measurements were higher as opposed to the week in August. The ESCA difference spectra for anthracite reveal different distributions of oxidised carbon functionality for the two weathering conditions.

5.3.9 Incoherent Inelastic Neutron Scattering (IINS) Spectroscopy

In a recent publication Howard and co-workers [320] have applied IINS spectroscopy to the study of coal.

IINS spectroscopy is a vibrational technique in which the scattering mechanism is direct interaction between an incident neutron and a nucleus in the sample. Energy differences between the incident and scattered neutrons correspond to vibrational transitions in the sample. A detailed description of the technique is not required and explanation of the technique is best left to the experts. [320] It is the large neutron scattering cross-section of hydrogen which lends IINS spectroscopy to the observation of the normal modes of vibration of hydrogeneous species in a non-hydrogeneous matrix, provided that the total cross-section of the matrix is such that it may be regarded as effectively transparent.

Coal is a suitable material for study by IINS spectroscopy and may be studied in the solid state with minimal sample preparation, samples being contained in aluminium foil envelopes. The prospects of gaining information on the hydrogen component of the coal network by IINS spectroscopy, complementary to findings from other techniques, Fourier transform infrared, solid state nmr and ESCA for example, have been met with considerable enthusiasm by coal scientists.

Here are presented preliminary IINS spectra for coals which have already been introduced in previous sections of this chapter.

The samples analysed comprise a rank-range of coals (brown coal; Lower Kittanning seam coals PSOC Nos. 308 and 1133 of respective carbon contents (%C, dmmf) 80.2 and 90.7; anthracite); and samples of unaltered coal and natural coke from the Togston open cast site, Northumberland.

The IINS spectra, recorded over the 100 - 750 cm^{-1} region, are presented in Figures 5.44a-f; extended spectra (0 - 4000 cm^{-1}) are yet to be run. The spectra which consist of broad bands do differ significantly in either the number of component bands or the band widths. These observations give further confirmation of the usefulness of IINS spectroscopy in the study of coal. It is of particular interest that differences are seen, not only between samples of different origins and rank, but also for coal before and after carbonisation.

Although at present it is not possible to assign principal bands to specific molecular groups, further programmes of research in this area are envisaged.

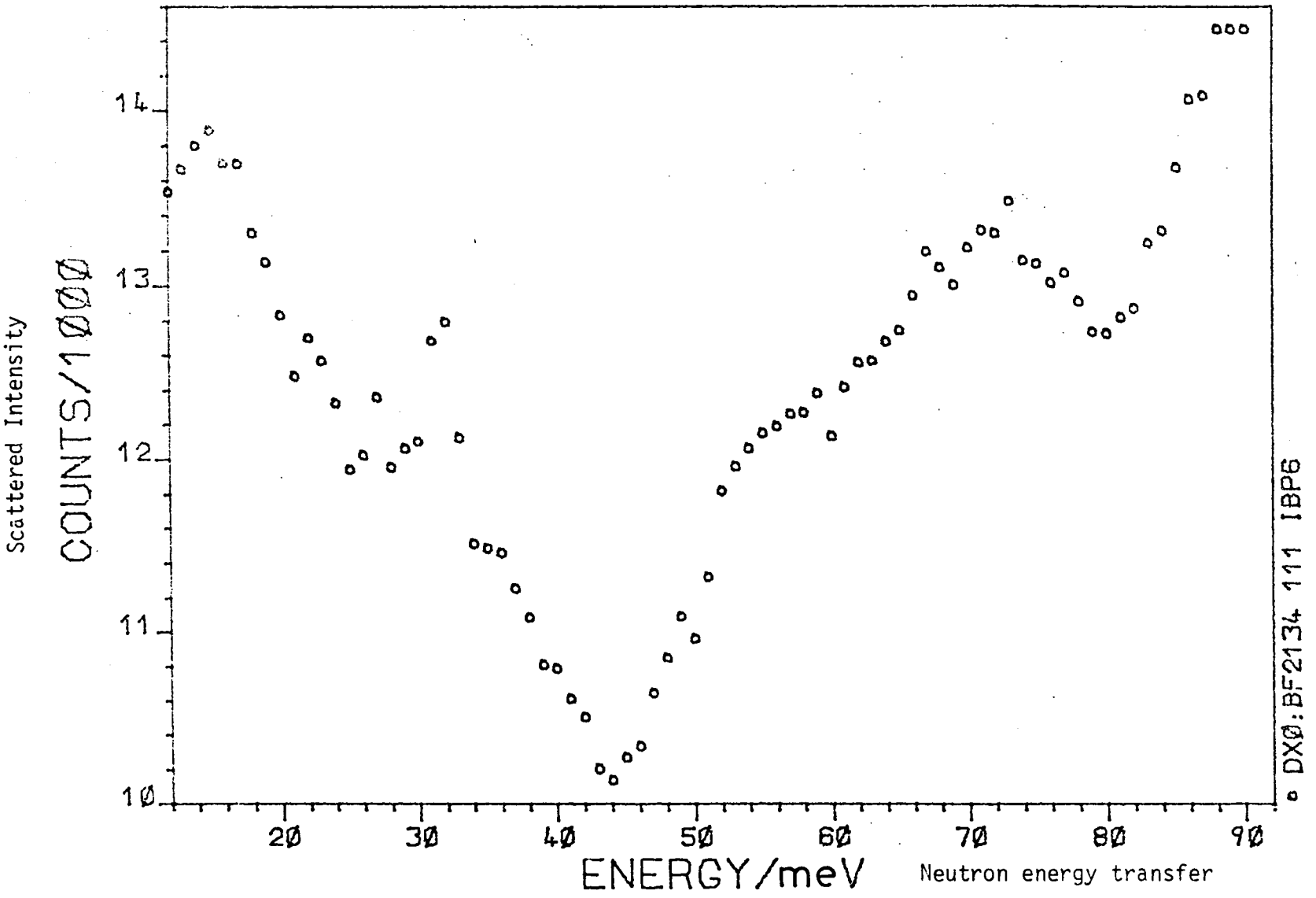

Figure 5.44a IINS spectrum of brown coal

(1meV = 8.06cm^{-1})

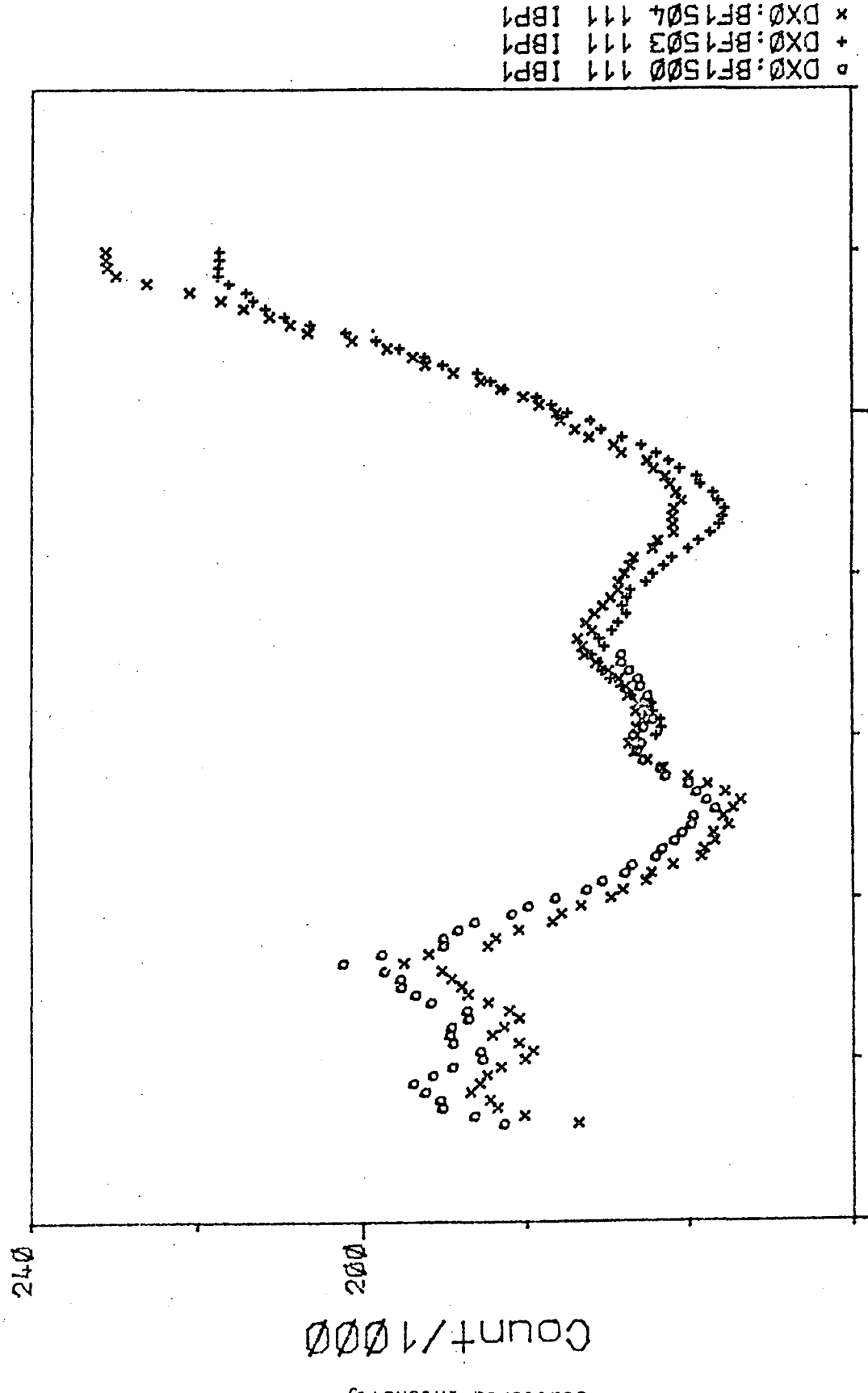

Figure 5.44b IINS spectrum of Lower Kittanning seam coal, PSOC No. 308.
(1meV = 8.06cm^{-1})

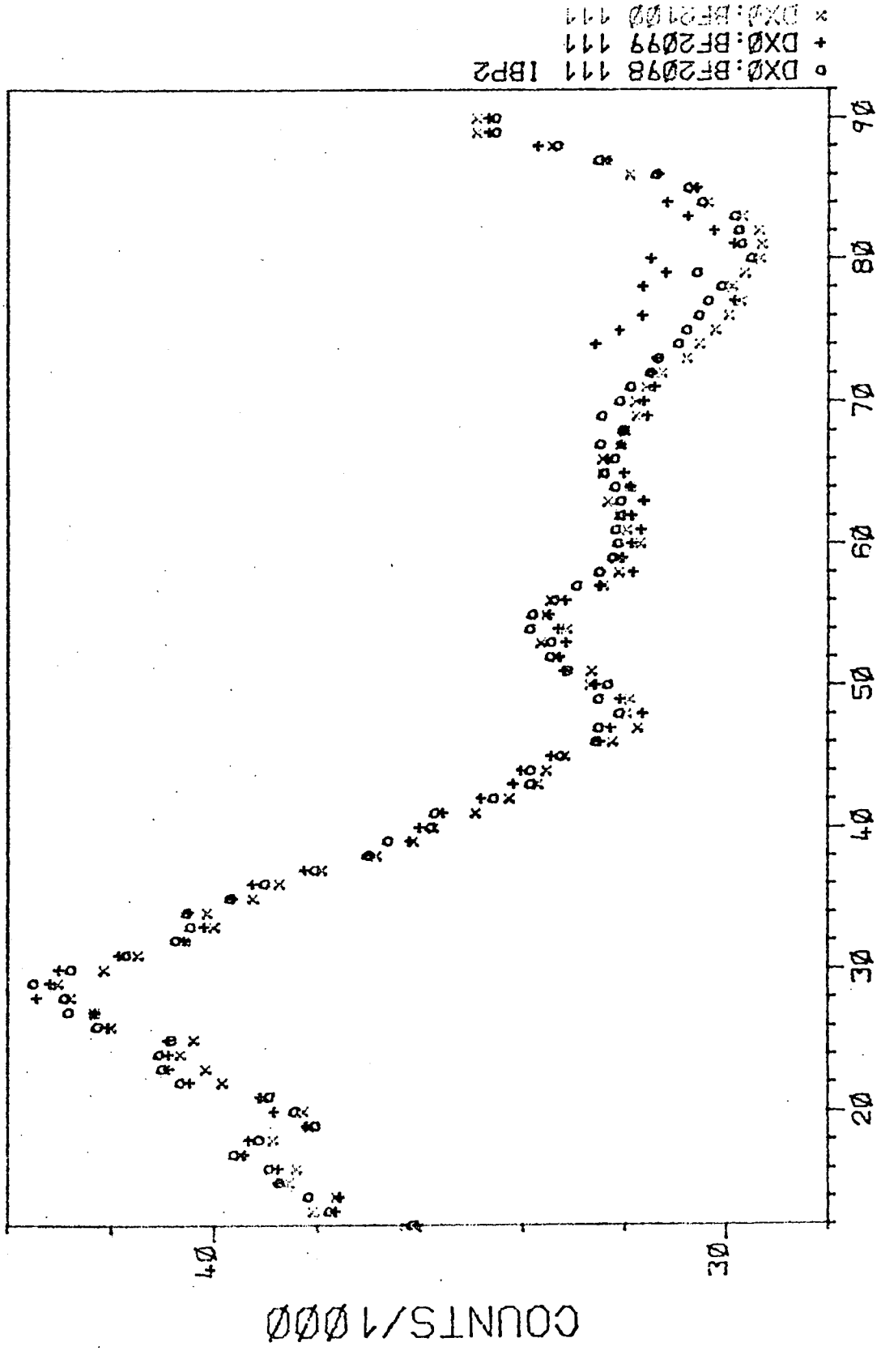

Figure 5.44c IINS spectrum of Lower Kittanning seam coal, PSOC No. 1133.
(1meV = 8.06cm^{-1})

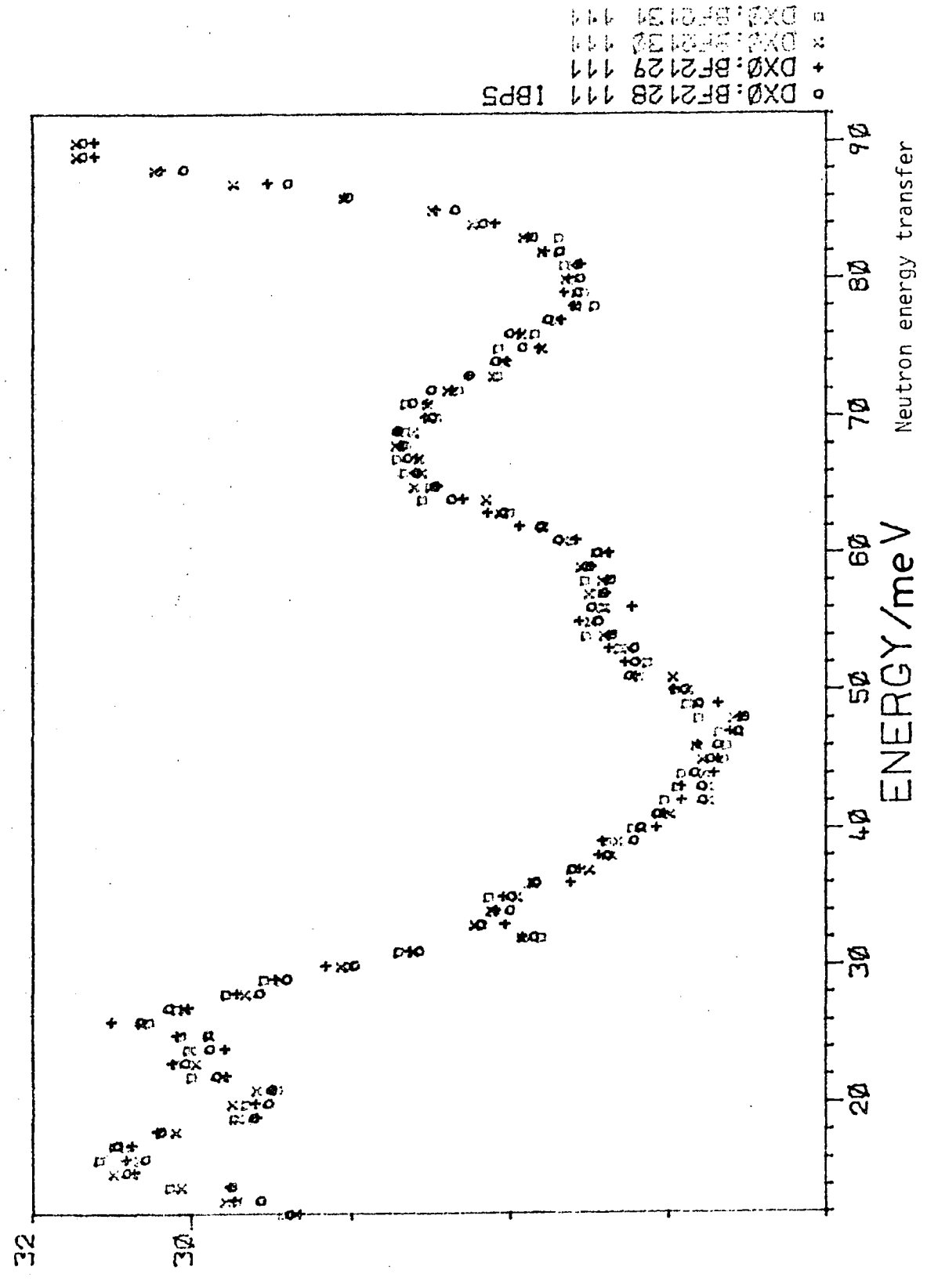

Figure 5.44d IINS spectrum of anthracite

(1meV = 8.06cm^{-1})

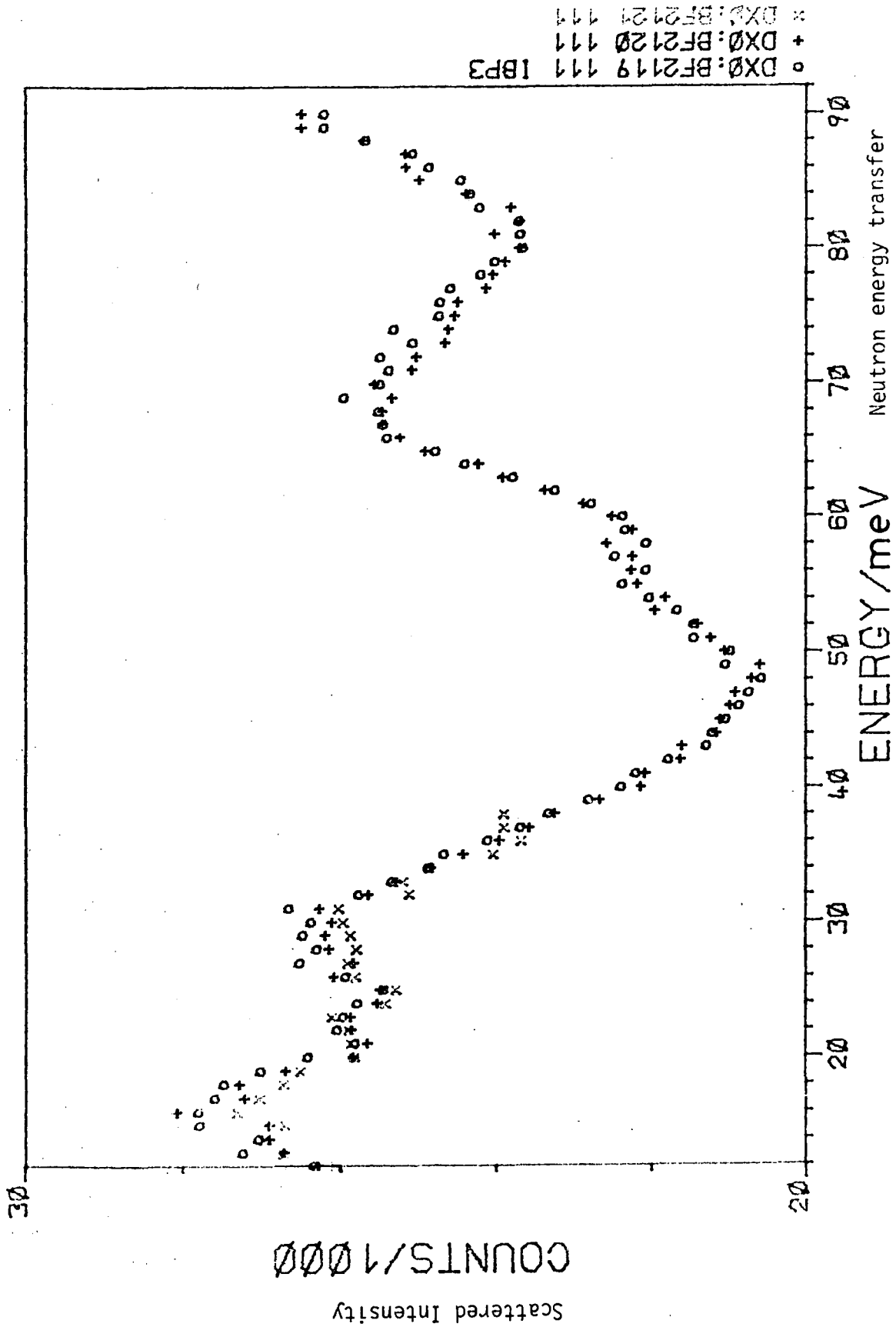

Figure 5.44e IINS spectrum of Acklington Dyke coal, unaltered.

(1meV = 8.06cm^{-1})

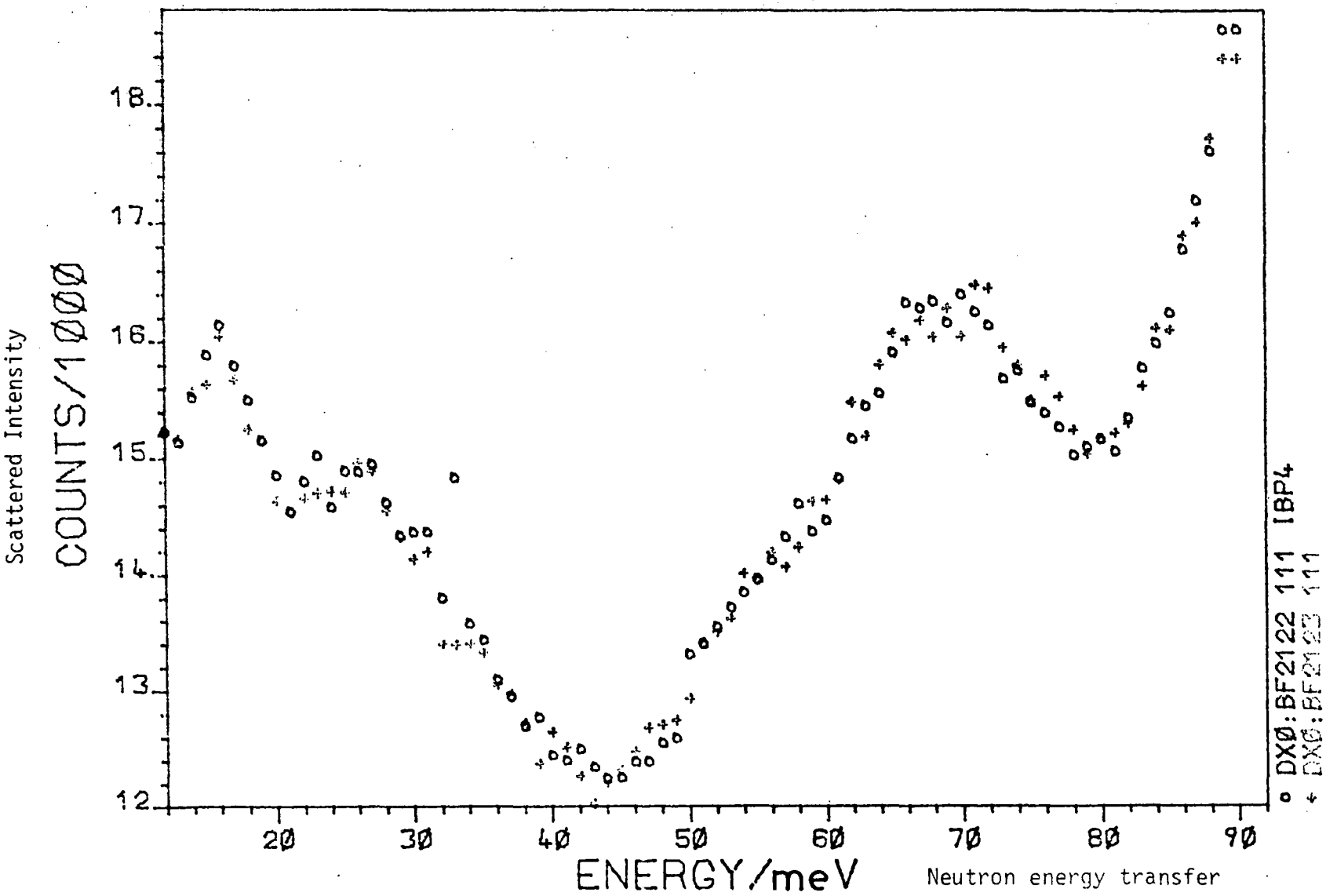

Figure 5.44f IINS spectrum of natural coke, Acklington Dyke.
(1meV = 8.06cm^{-1})

5.4 Conclusions

This chapter has demonstrated the capability of ESCA to probe the surface chemistries of a wide range of naturally occurring carbonaceous materials, particular emphasis being placed on coal. It has been shown that ESCA may provide a wealth of information on the structure, bonding and reactivity of these materials as studied in their solid state.

The use of ESCA as a semi-quantitative analytical tool has been investigated by the analysis of standard coal samples. The surface sensitivity of ESCA has been found to be of special value in the characterisation of surface specific reactions. This has been exemplified by studies of surface oxidation reactions, both naturally occurring through weathering processes and artificially induced. ESCA may provide information, not only on the extent of reaction, but also on the chemical bonding at the reacted surface.

Since the interaction of the solid coal with its immediate environment is known to play a fundamental role in aspects of coal utilisation, it is particularly apposite that such surface reactions be monitored by ESCA. The combined use of ESCA and other analytical techniques, especially solid state nuclear magnetic resonance spectroscopy, Fourier transform infra-red spectroscopy and incoherent inelastic neutron scattering spectroscopy holds considerable promise in the understanding of the structure, bonding and reactivity of coal and coal-related materials.

APPENDIX

APPENDIX

The Board of Studies in Chemistry requires that each postgraduate research thesis contains an appendix listing all research colloquia, seminars and lectures by external speakers held in the department as well as all conferences attended by the author, during the period of research.

Lectures held October 1981 - July 1983

Prof. E. Kluk (Univ. of Katowice) - 'Some Aspects of the Study of Molecular Dynamics', 14 Oct. 1981.

Dr P.J. Corrish (Dunlop Ltd.) - 'What would Life be like without Rubber?', 22 Oct. 1981.

Dr W. Moddeman (Monsanto Ltd.) - 'High Energy Materials', 6 Nov. 1971.

Prof. A.I. Scott (Edinburgh Univ.) - 'An Organic Chemist's View of Life in the n.m.r. tube', 12 Nov. 1981.

Dr W.O. Ord (Northumbrian Water Authority) - 'The Role of the Scientist in a Regional Water Authority', 26 Nov. 1981.

Dr R.E. Hester (York Univ.) - 'Spectroscopy with Lasers', 3 Dec. 1981.

Prof. I. Fells (Newcastle Univ.) - 'Balancing the Energy Equations', 28 Jan. 1982.

Dr D. Pethnick (Strathclyde Univ.) - 'Conformational Dynamics of Small and Large Molecules', 10 Feb. 1982.

Dr D.W. Turner (Oxford Univ.) - 'Photoelectrons in a Strong Magnetic Field', 17 Feb. 1982.

Prof. R.K. Harris (Univ. of East Anglia) - 'N.m.r. in the 1980s', 18 Feb.1982.

Prof. R.O.C. Norman FRS (York Univ.) - 'Turning Points and Challenges for the Organic Chemist', 25 Feb.1982.

Dr P. Banfield (I.C.I. Organics) - 'Computer Aided Synthesis Design: A View from Industry', 3 Mar. 1982.

Dr R. Whyman (I.C.I. Ltd.) - 'Making Metal Clusters work', 4 Mar. 1982.

Prof. D.J. Burton (Iowa Univ.) - 'Some Aspects of the Chemistry of Phosphonium Salts and Phosphates', 28 Jun. 1982.

Prof. Neidlein (Heidelberg Univ.) - 'New Aspects and Results of Bridged Annulene Chemistry', 13 Sept. 1982.

Dr W.K. Ford (Xerox, New York) - 'The Dependence of the Electronic Structure of Polymers on their Molecular Architecture', 27 Sept. 1982.

Prof. H. Suhr (Univ. of Tubingen) - 'Preparative Chemistry in Non-Equilibrium Plasmas', 14 Oct. 1982.

Mr F. Shenton (County Analyst, Durham) - 'There is Death in the Pot', 14 Oct. 1982.

Dr C.E. Housecroft (Notre Dame Univ.) - 'Bonding Capabilities of Butterfly-shaped Fe_4 Units', 27 Oct. 1982.

Prof. M.F. Lappert, FRS (Sussex Univ.) - 'Approaches to Assymetric Synthesis and Catalysis using Electron-rich Olefins and Some of their Metal Complexes', 28 Oct. 1982, and 'The Chemistry of some Unusual Subvalent Compounds of Group IV and V Elements', 28 Oct. 1982.

Dr D.H. Williams (Cambridge Univ.) - 'Studies on the Structures and Modes of Action of Antibiotics', 4 Nov. 1982.

Dr J. Cramp (I.C.I.Ltd.) - 'Lasers in Industry', 11 Nov. 1982.

Dr G. Bertrand (Paul Sabatier Univ., Toulouse) - 'Curtius Rearrangement in Organometallic Series : A Route for New Hybridized Species', 15 Nov. 1982.

Prof. F.R. Hartley (R.M.C.S., Shrivenham) - 'Supported Metal Complex Hydroformylation Catalysts', 24 Nov. 1982.

Dr D.R. Richards (P.E.R.M.E.) - 'Terminally Functional Polymers - their Synthesis and Uses', 25 Nov. 1982.

Dr G. Wooley (Trent Poly.) - 'Bonds in Transition Metal Cluster Compounds', 8 Dec. 1982.

Dr D.C. Sherrington (Strathclyde Univ.) - 'Polymer Supported Phase Transfer Catalysts', 12 Jan. 1983.

Prof. D.W.A. Sharp (Glasgow Univ.) - 'Some Redox Reactions in Fluorine Chemistry', 27 Jan. 1983.

Dr P. Moore (Warwick Univ.) - 'Mechanistic Studies in Solution by Stopped Flow F.T. n.m.r. and High Pressure n.m.r. Line Broadening', 9 Feb. 1983.

Sir G. Allen FRS (Unilever Ltd.) - 'U.K. Research Ltd.', 10 Feb. 1983.

Prof. A.G. MacDiarmid (Pennsylvania Univ.) - 'Metallic Covalent Polymers: $(SN)_x$ and $(CH)_x$ and their Derivatives', 17 Feb. 1983.

Dr D. Bloor (Queen Mary College) - 'The Solid State Chemistry of Diacetylene Monomers and Polymers', 2 Mar. 1983.

Prof. A.C.T. North (Leeds Univ.) - 'The Use of a Computer Display System in Studying Molecular Structures and Interactions', 3 Mar.1983.

Prof. D.C. Bradley, FRS (Queen Mary College) - 'Recent Developments in Organo-Imido Transition Metal Chemistry', 8 Mar. 1983.

Prof. H.G. Viehe (Univ. of Louvain, Belgium) - 'Oxidations on Sulphur', 11 Mar. 1983 and 'Fluorine Substitution in Radical and Biradical Addition Reactions', 11 Mar. 1983.

Dr I. Gosney (Edinburgh Univ.) - 'New Extrusion Reactions : Organic Synthesis in a Hot Tube', 16 Mar. 1983.

Prof. J. Passmore (Univ. of New Brunswick) - 'Novel Selenium - Iodine Cations', 21 Apr. 1983.

Prof. P.H. Plesch (Keele Univ.) - 'Binary Ionisation Equilibria between two ions and two molecules. What Ostwald never thought of', 4 May 1983.

Prof. K. Berger (Munich Univ.) - 'New Reaction Pathways to Partially Fluorinated Heterocyclic Compounds', 10 May 1983.

Dr N. Isaacs (Reading Univ.) - 'The Applications of High Pressures to the Theory and Practice of Organic Chemistry', 11 May 1983.

Dr T.D. Marder (U.C.L.A.) - 'The Chemistry of Metal-Carbon and Metal-Metal Multiple Bonds', 13 May 1983.

Dr J.M. Vernon (York Univ.) - 'New Heterocyclic Chemistry involving Lead Tetra-Acetate', 25 May 1983.

Dr A. Pietrykowski (Warsaw Univ.) - 'Synthetic Structure and Properties of Aluminoxanes', 15 June 1983.

Conferences Attended

1. 'Electrical Breakdown and Discharges in Gases', NATO Advanced Study Institute, 28th June - 10th July 1981, Les Arcs, France.

2. 'Processing and Applications of Polymers'. SERC Summer School, July 1982, Institute of Polymer Technology, Loughborough University of Technology, Loughborough.

3. 99th Annual Miners' Gala, July 1982, Durham.

4. 2nd Durham - Newcastle Graduate Symposium, April 1983, University of Durham, Durham.

5. 'Analytical Methods for Coals, Cokes and Carbons'. Society for Chemical Industry, Industrial Carbon and Graphite Group Symposium, 28-29th April 1983, London. (Paper presented).

6. 'Coal Evaluation Using New Wireline Logging Techniques'. A Schlumberger presentation to the coal industry, 18th May 1983, Barnsley.

7. 'Magnetic Resonance Techniques in Fossil Fuel Problems'. NATO Advanced Study Institute, 3rd-15th July 1983, Crete.

8. 11th International Meeting on Organic Geochemistry, 12-16th September 1983, The Hague, The Netherlands. (Poster presented.)

REFERENCES

References

1. D.T. Clark, 'Chemical Aspects of ESCA' in 'Electron Emission Spectroscopy', Eds. W. Dekeyser and D. Riedel, D. Riedel Publishing Co., Dordrecht, Holland, 373 (1973).
2. M. de Broglie, Compt Rend., 158, 1493 (1914).
3. M. de Broglie, Compt Rend., 163, 87, 353 (1916).
4. H. Robinson and W.I. Rawlinson, Phil. Mag., 28, 277 (1914).
5. H. Robinson, Proc. Roy. Soc., A104, 455 (1923).
6. H. Robinson, Phil. Mag., 50, 241 (1925).
7. K. Siegbahn and K. Edvarson, Nucl. Phys., 1, 137 (1956).
8. K. Siegbahn, 'Alpha, Beta and Gamma Ray Spectroscopy', Chapter 3, Ed. K. Siegbahn, North Holland Publishing Co., Amsterdam (1965).
9. K. Siegbahn, C. Nordling, A. Fahlman, R. Nordberg, K. Hamrin, J. Hedman, G. Johansson, T. Berkmark, S.E. Karlsson, I. Lidgren and B. Lindberg, 'ESCA, Atomic, Molecular and Solid State Structure Studied by means of Electron Spectroscopy', Almquist and Wiksells, Uppsala (1967).
10. K. Siegbahn, C. Nordling, G. Johansson, J. Hedman, P.F. Heden, K. Hamrin, U. Gelius, T. Bergmark, L.D. Werme, R. Manne and Y. Baer, 'ESCA Applied to Free Molecules', North Holland Publishing Co. (1969).
11. J.G. Jenkin, R.C.G. Leckey and J. Liesengang, J. Electron Spectrosc. Rel. Phenom., 12, 1 (1977); 14, 477 (1978).
12. D.W. Turner, C. Baker, A.D. Baker and C.R. Brundle, 'Molecular Photoelectron Spectroscopy', J. Wiley and Sons Ltd. (1970).
13. D.T. Clark, 'Structure and Bonding in Polymers as Revealed by ESCA', in 'Electron Structure of Polymers and Molecular Crystals', Eds. J. Lodik and J.M. Andre, Plenum Press, New York (1975).

14. L.S. Cederbaum and W. Domcke, J. Electron Spectrosc. Rel. Phenom., 13, 161 (1978).

15. H.B. Cullen, Handbook of Physics, Section 8, Chapter 2, McGraw-Hill (1967).

16. A. Rosen and I. Lindgren, Phys. Rev., 176, 114 (1968).

17. P.S. Bagus, Phys. Rev. A., 139, 619 (1965).

18. D.A. Shirley, Advances in Chem. Phys., 23, 85, Eds. I. Prigogini and S.A. Rice, J. Wiley and Sons Ltd., New York (1973).

19. U. Gelius and K. Siegbahn, Faraday Discuss. Chem. Soc., 54, 257 (1972).

20. L.C. Snyder, J. Chem. Phys., 55, 95 (1971).

21. D.B. Adams and D.T. Clark, Theoret. Chim. Act., 31, 171 (1973).

22. M.F. Guest, I.H. Hillier, V.R. Saunders and M. W. Wood, Proc. Roy. Soc., A333, 201 (1973).

23. D.T. Clark, I.W. Scanlan and J. Müller, Theoret. Chim. Act., 35, 341 (1974).

24. D.T. Clark and I.W. Scanlan, J. Chem. Soc. Farad. Trans. 11, 70, 1222 (1974).

25. C.D. Wagner and P. Bilden, Surface Sci., 35, 82 (1973).

26. U. Gellus, Phys. Scr., 9, 133 (1974).

27. H. Basch, J. Electron Spectrosc. Rel. Phenom., 5, 463 (1974).

28. M.E. Schwarz, in M.T.P. Internat. Rev. Sci., Phys. Chem. Ser. 2, Vol. 1 (Theoret. Chem.), Eds. A.D. Buckingham and C.A. Coulson, Butterworths, London, 189 (1975).

29. T.A. Koopmans, Physica, 1, 104 (1933).

30. R. Manne and T. Åberg, Chem. Phys. Lett., 7, 282 (1970).

31. S. Pignatoro and G. Distofaro, Z. Naturforsch. A. 30a, 815 (1975).

32. T. Ohta, T. Fukitawa and H. Furoda, Chem. Phys. Lett., 32, 369 (1975).

33. L. Yin, I. Adler, T. Tsang, L.J. Matienzo and S.O. Grim, Chem. Phys. Lett., 24, 81 (1974).

34. T. Robert and G. Offergeld, Chem. Phys. Lett., 29, 606 (1974).

35. P. Burroughs, A. Hamnett, A.F. Orchard and G. Thornton, J. Chem. Soc. Dalton Trans., 1686 (1976).

36. D.C. Frost, C.A. McDowell and A. Ishitani, Mol. Phys., 24, 861 (1972).

37. D.T. Clark, D.B. Adams, A. Dilks, J. Peeling and H.R. Thomas, J. Electron Spectrosc. Rel. Phenom., 8, 51 (1976).

38. D.T. Clark and A. Dilks, J. Polym. Sci. Polym. Chem. Edn., 15, 533 (1976).

39. D.T. Clark and A. Dilks, J. Polym. Sci. Polym. Chem. Edn., 15, 15 (1977).

40. M.A. Brisk and A.D. Baker, J. Electron. Spectrosc. Rel. Phenom., 7, 197 (1977).

41. A.E. Sandstrom in 'Handbook of Physics', Vol. XXX, 'X-Rays', 164, Ed. S.F. Flugge, Springer-Verlag (1957).

42. P. Auger, J. Phys. Radium, 6, 205 (1925).

43. P. Auger, Compt. Rend., 65, 180 (1925).

44. J.J. Lander, Phys. Rev., 91, 1382 (1953).

45. cf. T.A. Carlson, 'Photoelectron and Auger Spectroscopy', Plenum Press, New York (1975).

46. D. Coster and R. de L. Kronig, Physica, 2, 13 (1935).

47. E.H.S. Burhop, 'The Auger Effect and Other Radiationless Transitions', Cambridge University Press (1952).

48. C.C. Chang, Surface Sci., 25, 53 (1971).

49. J.P. Coad, M. Gettings and J.G. Riviere, Faraday Chem. Soc., 60, 269 (1975).

50. cf. C.D. Wagner, Discuss. Faraday Soc., 60, 291 (1975).

51. S.P. Kowalczyk, R.A. Pollak, F.R. McFeely, L. Ley and D.A. Shirley, Phys. Rev., B8, 3583 (1973).

52. L. Ley, S.P. Kowalczyk, F.R. McFeely, R.A. Pollak and D.A. Shirley, Phys. Rev., B8, 2392 (1973).

53. S.P. Kowalczyk, R.A. Pollak, F.R. McFeely, L. Ley and D.A. Shirley, Phys. Rev., B8, 2387 (1973).

54. S.P. Kowalczyk, L. Ley, F.R. McFeely, R.A. Pollak and D.A. Shirley, Phys. Rev., B9, 381 (1974).

55. C.D. Wagner, Faraday Discuss. Chem. Soc., 60, 291 (1975).

56. C.D. Wagner, L.H. Gale and R.H. Raymond, Anal. Chem., 51, 466 (1979).

57. W.L. Jolly and D.N. Hendrickson, J. Amer. Chem. Soc., 92, 1863 (1970).

58. D.T. Clark, B.J. Cromarty and A. Dilks, J. Polym. Sci. Polym. Chem. Edn, 16, 3173 (1978).

59. D.T. Clark amd A. Harrison, J. Polym. Sci. Polym. Chem. Edn., 19, 1945 (1981).

60. J.N. Murrell and B.J. Ralston, J. Chem. Soc. Faraday Trans. 11, 68, 1393 (1972).

61. M.E. Schwartz, Chem. Phys. Lett., 6, 631 (1970).

62. D.A. Shirley, Chem. Phys. Lett., 15, 325 (1972).

63. C.S. Fadley, 'Basic Concepts of X-ray Photoelectron Spectroscopy', in 'Electron Spectroscopy, Theory, Techniques and Applications', Vol. 2, 1, Eds. C.R. Brundle and A.D. Baker, Academic Press (1978).

64. R.E. Watson and A.J. Freeman in 'Hyperfine Interactions', Eds. A.J. Freeman and R.B. Frankel, Academic Press, New York (1967).

65. C.S. Fadley, D.A. Shirley, A.J. Freeman, P.S. Bagus and J.V. Mallow, Phys. Rev. Lett., 23, 1397 (1969).

66. J.H. van Vleck, Phys. Rev. Lett., 45, 405 (1934).

67. C.S. Fadley in 'Electron Spectroscopy', Ed. D.A. Shirley, 781, North Holland Publishing Co. (1972).

68. T. Novakov, ref. 26 of C.S. Fadley in 'Electron Spectroscopy', Ed. D.A. Shirley, North Holland Publishing Co. (1972).

69. G.M. Bancroft, I. Adams, H. Lampe and T.K. Sham, Chem. Phys. Lett., 32, 173 (1975).

70. R.P. Gupta and S.K. Sen, Phys. Rev. Lett., 28, 1311 (1972).

71. T. Novakov and J.M. Hollander, Bull. Amer. Phys. Soc., 14, 524 (1969).

72. T. Novakov and J.M. Hollander, Phys. Rev. Lett., 21, 1133 (1968).

73. G.K. Wertheim, 'Mössbauer Effect : Principles and Applications', Academic Press, New York (1964).

74. M.F. Ebel and H. Ebel, J. Electron Spectroscop. Rel. Phenom., 3, 169 (1974).

75. A.F. Orchard, Electron Structure Magn. Inorg. Comp., 3 (1974).

76. J.F. McGilp and I.G. Main, J. Electron Spectroscop. Rel. Phenom., 6, 397 (1975).

77. G. Johansson, J. Hedman, A. Berndtsson, M. Klasson and R. Nilsson, J. Electron. Spectrosc. Rel. Phenom., 2, 295 (1973).

78. D.T. Clark in 'Advances in Polymer Science', Springer-Verlag, 24, 125 (1977).

79. T.A. Carlson and G.E. McGuire, J. Electron. Spectrosc. Rel. Phenom., 1, 161 (1972).

80. C.S. Fadley, R.J. Baird, W. Siekhaus, T. Novakov and S.A.L. Burgstrom, J. Electron. Spectrosc. Rel. Phenom., 4, 93 (1974).

81. J.H. Scofield, Lawrence Livermore Laboratory Report UCRL, 51326, Jan (1973).

82. J.H. Scofield, J. Electron. Spectroscop. Rel. Phenom., 8, 129 (1976).

83. D.T. Clark and H.R. Thomas, J. Polym. Sci. Polym. Chem. Edn., 15, 2843 (1977).

84. D.T. Clark and D. Shuttleworth, J. Polym. Sci. Polym. Chem. Edn., 16, 1093 (1977).

85. D.R. Penn, J. Electron. Spectrosc., 9, 29 (1976).

86. D.T. Clark amd H.R. Thomas, J. Polym. Sci. Polym. Chem. Edn., 16, 791 (1978).

87. cf. N. Beatham and A.F. Orchard, J. Electron Spectroscop. Rel. Phenom., 9, 129 (1976).

88. A.F. Carley and R.W. Joyner, J. Electron Spectrosc. and Rel. Phenom., 16, 1 (1979).

89. R.M. Eisenberg in 'Fundamentals of Modern Physics', Chapter 14, J. Wiley and Sons, New York (1961).

90. J.E. Castle, L.B. Hazell and R.D. Whitehead, J. Electron Spectrosc. Rel. Phenom., 9, 247 (1976).

91. C.D. Wagner, J. Electron Spectrosc., 10, 305 (1977).

92. C.D. Wagner, L.H. Gale and R.H. Raymond, J. Vac. Sci. Tech., 15, 518 (1978).

93. B.L. Henke, Adv. X-ray Analysis, 13, 1 (1969).

94. C.D. Wagner, Faraday Discuss. Chem. Soc., 60, 306 (1975).

95. K. Yates, A. Barrie and F.J. Street, J. Phys., E6, 130 (1973).

96. K. Siegbahn, D. Hammond, H. Fellner-Feldegg and E.F. Barnett, Science, 176, 245 (1972).

97. D.T. Clark and P.J. Stephenson, Explosives and Propellants, (Proc. Waltham Abbey conf. 1980), Ed. T.J. Lewis, Plenum Press, in press.

98. I.H. Munro, Chem. in Brit., 15, 330 (1979).

99. M.L. Periman, E.M. Rowe and R.E. Watson, Phys. Today, 27, 30 (1974).

100. E.M. Purcell, Phys. Rev., 54, 818 (1938).

101. J.C. Helmer and N.H. Weichert, Appl. Phys. Lett., 13, 268 (1968).

102. K. Siegbahn, J. Electron Spectrosc. Rel. Phenom., 5, 3 (1974).

103. J.J. Huang, J.W. Rabalais and F.O. Ellison, J. Electron Spectrosc. Rel. Phenom., 6, 85 (1975).

104. D.C. Frost, C.A. McDowell and B. Wallbank, Chem. Phys. Lett., 40, 189 (1976).

105. C.D. Wagner, W.M. Riggs, L.E. Davis, J.F. Moulder and G.E. Muilenberg (Editor), 'Handbook of X-ray Photoelectron Spectroscopy', Perkin Elmer Corporation, Physical Electronic Division (1979).

106. A.D. Baker and C.R. Brundle, 'An Introduction to Electron Spectroscopy', in 'Electron Spectroscopy, Theory, Techniques and Applications'. Vol. 1, Eds. C.R. Brundle and A.D. Baker, 1, Academic Press, London (1977).

107. T.N. Rhodin and J.W. Gadzuk, 'Electron Spectroscopy and Surface Chemical Bonding', in 'The Nature of the Surface Chemical Bond', Eds. T.N. Rhodin and G. Ertl, 112, North Holland Publishing Co., Amsterdam (1979).

108. C.D. Wagner, Anal. Chem., 44, 1050 (1972).

109. N. Berthou and C.J. Jorgensen, Anal. Chem., 47, (1975)

110. V.L. Nefedov, N.P. Sergushin, I.M. Band and M.B. Trzhaskovskaya, J. Electron Spectrosc. Rel. Phenom., 2, 383 (1973); 7, 175 (1975).

111. R.S. Swingle 11, Anal. Chem., 47, 21 (1975).

112. F.M. Chapman and L.L. Lohr, J. Amer. Chem. Soc., 96, 4731 (1974).

113. J.T.J. Huang and J.W. Rabalais, 'X-ray Photoelectron Cross-sections and Angular Distributions' in 'Electron Spectroscopy, Theory, Techniques and Applications', Vol. 2, 225. Eds. C.R. Brundle and A.D. Baker, Academic Press, London (1978).

114. D.M. Wyatt, J.C. Carver and D.M. Hercules, Anal. Chem., 47, 1297 (1975).

115. K.T. Ng and D.M. Hercules, J. Electron Spectrosc. Rel. Phenom., 7, 257 (1975).

116. L.E. Cox and D.M. Hercules, J. Electron Spectrosc. Rel. Phenom., 1, 193 (1972/73).

117. T.E. Madey, C.D. Wagner and A. Joshi, J. Electron Spectrosc. Rel. Phenom., 10, 359 (1977).

118. cf. H. Siegbahn, L. Asplund, P. Kelfve and K. Siegbahn, J. Electron Spectrosc. Rel. Phenom., 7, 411 (1975) and references therein.

119. O. Keski-Rahkonen and M.I. Krause, At. Data Nucl. Data Tables, 14, 139 (1974).

120. D.A. Huchital and R.T. McKeon, Appl. Phys. Lett., 20, 158 (1972).

121. J.S. Brinnen, Acc. Chem. Res., 9, 86 (1976).

122. D.T. Clark, H.R. Thomas and A. Dilks (unpublished data).

123. D.T. Clark, H.R. Thomas and A. Dilks, J. Polym. Sci., Polym. Chem. Ed., 16, 1461 (1978).

124. D.T. Clark and A. Dilks, A.C.S. Centennial Meeting, New York, April 1976, 'International Symposium on Advances in Characterisation of Polymer Surfaces', 101, Ed. L.H. Lee, Academic Press, New York, (1976).

125. D.T. Clark and A. Dilks, J. Polym. Sci. Polym. Chem. Ed., 16, 791 (1978).

126. D.T. Clark and A. Dilks, J. Polym. Sci. Polym. Chem. Ed., 16, 911 (1978).

127. D.T. Clark and A. Dilks, J. Electron Spectrosc. Rel. Phenom., 11, 225 (1977).

128. S. Evans, J.M. Adams and J.M. Thomas, Phil., Trans. Roy. Soc. London Series A, 292, 59 (1979).

129. D. Briggs, D.M. Brewis and M. Konieczko, J. Mater. Sci., 11, 1270 (1976).

130. D. Briggs and D.M. Brewis, Polymer, 22, 7 (1981), and references therein.

131. W.M. Riggs and D.W. Dwight, J. Electron Spectrosc. Rel. Phenom., 5, 447 (1974).

132. D.T. Clark in 'Polymer Surfaces', Eds. D.T. Clark and W.J. Feast, Wiley, Chichester, Chapter 16 (1978).

133. D.T. Clark, A. Dilks and D. Shuttleworth in 'Polymer Surfaces', Eds. D.T. Clark and W.J. Feast, Wiley, Chichester, Chapter 9 (1978).

134. D.T. Clark and A. Dilks, J. Polym. Sci. Polym. Chem. Edn., 15, 2321 (1977).

135. D.T. Clark and A. Dilks, J. Polym. Sci. Polym. Chem. Edn., 17, 957 (1979).

136. D.T. Clark and R. Wilson, J. Polym. Sci. Polym. Chem. Edn., 21, 837 (1983).

137. E.J. Gawne and B.V. Oerke, 'Dress : The Clothing Textbook', 3rd Ed., C.A. Bennet, Illinois (1969).

138. N. Wilson, 'Static Charges on Textile Surfaces' in 'Polymer Surfaces', Eds. D.T. Clark and W.J. Feast, Chapter 7, Wiley, Chichester (1978).

139. C.E. Carraher Jr., W.R. Burt, D.J. Giron, J.A. Schroeder, M.L. Taylor, H.M. Molloy and T.O. Tierman, J. Appl. Polym. Sci., 28, 1919 (1983).

140. D.T. Clark and H.R. Thomas, J. Polym. Sci. Polym. Chem. Edn., 14, 1671 (1976).

141. C.D. Batich and R.C. Wendt in 'Photon, Electron and Ion Probes of Polymer Structure and Properties', Eds. D.W. Dwight, T.J. Fabish and H.R. Thomas, ACS symposium series No. 162, Washington, Chapter 15 (1981).

142. D.T. Clark, A. Dilks and H.R. Thomas, Disc. Faraday Soc., 60, 183 (1975).

143. D.T. Clark in 'Molecular Spectroscopy', Ed. A.R. West, Heyden, Chapter 17 (1977).

144. D.W. Dwight and W.M. Riggs, J. Colloid and Interface Sci., 650 (1974).

145. M. Millard and M. Marsi, Anal. Chem., 46, 1820 (1974).

146. A. Bradley and M. Czuha Jr., Anal. Chem., 47, 1838 (1975).

147. M. Czuha Jr. and W.M. Riggs, Anal. Chem., 47, 1836 (1975).

148. D. Briggs, D.M. Brewis and M.B. Konieczko, J. Mater. Sci., 12, 429 (1977).

149. J.S. Hammond, J.W. Holubka, A. Dursin and R.A. Dickie, Abstract from Colloid and Interfacial Science Section, ACS Meeting, Miami, September 1978.

150. J.S. Hammond, J.W. Holubka and R.A. Dickie, Preprint from Organic Coatings and Plastic Chemistry, ACS Meeting, Miami, September 1978.

151. H.L. Spell and C.P. Christensen, Tappi, 62, 77 (1979).

152. D. Briggs and C. Kendal, Polymer Commun., 20, 1053 (1979).

153. H.S. Munro, Ph.D. Thesis, University of Durham (1982).

154. D.S. Everhart and C.N. Reilly, Anal. Chem., 52, 655 (1981).

155. D.S. Everhart and C.N. Reilly, Surf. Interfaces Anal., 3, 126 (1981).

156. R.A. Dickie, J.S. Hammond, J.E. de Vries and J.W. Holubka, Anal. Chem., 54, 2045 (1982).

157. D.T. Clark, Y.C.T. Fok and G.C. Roberts, J. Electron Spectrosc. Rel. Phenom., 22, 173 (1981).

158. D.T. Clark, M.M. AbuShbak and W.J. Brennan, J. Electron Spectrosc. Rel. Phenom., 28, 11 (1982).

159. K. Siegbahn, 'Electron Spectroscopy - An Outlook', Uppsala University Institute of Physics, Uppsala, Sweden (1974).

160. D.T. Clark in 'Photon, Electron and Ion Probes of Polymer Structure and Properties', Eds. D.W. Dwight, T.J. Fabish and H.R. Thomas, ACS symposium series No. 162, Washington, Chapter 17 (1981).

161. C.D. Wagner in 'Photon, Electron and Ion Probes of Polymer Structure and Properties', Eds. D.W. Dwight, T.J. Fabish and H.R. Thomas, ACS symposium series No. 162, Washington, Chapter 14 (1981).

162. J.R. Rasmussen, E.R. Stedronsky and G.M. Whitesides, J. Amer. Chem. Soc., 99, 4736 (1977).

163. J.R. Rasmussen, D.E. Bergbreiter and G.M. Whitesides, J. Amer. Chem. Soc., 99, 4746 (1977).

164. cf. A.T. Bell, in 'Techniques and Applications of Plasma Chemistry, Eds. J.R. Hollahan and A.T. Bell, Wiley, New York (1974).

165. J.E. Castle and C.R. Clayton, Corrosion Sci., 17, 7 (1977).

166. P.G. Rouxhet, P.G. Cappelle, M.H. Palm-Gennen and R.M. Torres Sanchez, Proc. 9th International Conf. in Organic Coatings Science and Technology, Athens, Greece.

167. D.T. Clark, A. Dilks, D. Shuttleworth and H.R. Thomas, J. Electron Spectrosc. Rel. Phenom., 14, 247 (1978).

168. D.T. Clark and D. Shuttleworth, J. Electron Spectrosc. Rel. Phenom., 17, 15 (1979).

169. R. Wilson, M.Sc. Thesis, University of Durham (1981).

170. D.T. Clark, A. Dilks, J. Peeling and H.R. Thomas, Discuss. Faraday Soc., 60, 183 (1975).

171. V. Stannett, in Diffusion in Polymers, Eds. J. Crank and G.S. Park, Academic Press, London, Chapter 2 (1968).

172. D.T. Clark, Physica Scripta, 16, 307 (1977).

173. H.F. Beer, Ph.D. Thesis, University of Durham (1980).

174. D.T. Clark and Y.C.T. Fok, Thin Solid Films, 78, 271 (1981).

175. D.R. Hutton, Ph.D. Thesis, University of Durham, 1983.

176. P.J. Stephenson, Ph.D. Thesis, University of Durham (1981).

177. D.T. Clark, A.H.K. Fowler and P.J. Stephenson, J. Macromol. Sci. Rev. Macromol. Chem. Phys., C23(2), 217 (1983).

178. D.T. Clark and A.H.K. Fowler, Polymer Comms., 24, 119 (1983).

179. D.T. Clark and A.H.K. Fowler, Polymer Comms., 24, 140 (1983).

180. A.L. Geddes, J. Polym. Sci., 22, 31 (1956).

181. J.M. Tedder, Chem. Revs., 55, 787 (1955).

182. A.H.K. Fowler, unpublished results.

183. G. Wegner, Angew. Chem. Int. Ed. Engl.,20, 361 (1981).

184. I.M. Ward, Phil. Trans. R. Soc. Lond., A294, 473 (1980).

185. D. Bloor, Chem. in Brit., 19, 725 (1983).

186. J.B. Torrance, Acc. Chem. Res., 12, 79 (1979).

187. C.B. Duke and H.W. Gibson, 'Conductive Polymers' in Kirk-Othmer: Encyclopedia of Chemical Technology, 18, 755, 3rd Edn. J. Wiley and Sons Inc. (1982).

188. J.H. Edwards and W.J. Feast, Polymer, 21, 595 (1980).

189. D.C. Bott. J.H. Edwards and W.J. Feast, Polymer, in press.

190. H.W. Gibson and J.M. Pochan, Macromolecules, 15, 242 (1982).

191. M.A. Druy, C.H. Tsang, N. Brown, A.J. Heeger and A.G. MacDiarmid, J. Polym. Sci., Polym. Phys. Edn., 18, 429 (1980).

192. H. Shirakawa and S. Ikeda, Polym. J., 2, 231 (1971).

193. T. Ito, H. Shirakawa and S. Ikeda, J. Polym. Sci., Polym. Chem. Ed., 12, 11 (1974).

194. A.G. MacDiarmid and A.J. Heeger, Synthetic Metals, 1, 101 (1979-80).

195. R.H. Friend, 'Electrical Properties of Some Conjugated Polymers', a Durham University Chemistry Department Colloqium (1983).

196. D.C. Bott, C. Chai, J.H. Edwards, W.J. Feast, R.H. Friend and M.E. Horton, J. de Physique, 44, C3-143 (1983).

197. W.J. Feast and B. Wilson, J. Molecular Catalysis, 8, 277 (1980).

198. T. Ueshima and S. Kobayashi, Japan Plastics, 24, 11 (1974).

199. N. Calderon, E.A. Ofstead and W.A. Judy, Angew. Chem. Int. Ed. Engl., 15, 401 (1976).

200. W.B. Hughes, Chem. Tech., p. 486 (1975).

201. Y. Uchida, M. Hidai and T. Tatsumi, Bull. Chem. Soc. Japan, 45, 1158 (1972).

202. J.M. Basset, Y. Ben Taarit, G. Condurier and H. Praliaud, J. Organometallic Chem., 74, 167 (1974).

203. A.K. Rappé and W.A. Goddard III, J. Amer. Chem. Soc., 102, 5114 (1980).

204. A.K. Rappé and W.A. Goddard III, Nature, 285, 311 (1980).

205. W.J. Feast and J.H. Edwards, personal communication.

206. G.E. McGuire, G.K. Schweitzer and T.A. Carlson, Inorg. Chem., 12, 2450 (1973).

207. C.D. Wagner, W.M. Riggs, L.E. Davis, J.F. Moulder and G.E. Muillenberg, 'Handbook of X-ray Photoelectron Spectroscopy', Perkin Elmer Corporation, Physical Electronic Division (1979).

208. J.C. Fuggle, 'XPS in ultra-high vacuum conditions' in: 'Handbook of X-ray and ultraviolet photoelectron spectroscopy', Ed. D. Briggs,Heyden, Chapter 8, p. 273 (1978).

209. J.M. Pochan, D.F. Pochan, H. Rommelmann and H.W. Gibson, Macromolecules, 14, 110 (1981).

210. D.T. Clark and W.J. Feast, J. Macromol. Sci. - Revs. Macromol. Chem., C12, 191 (1975).

211. W.R. Salaneck, H.R. Thomas, C.B. Duke, A. Paton, E.W. Plummer, A.J. Heeger and A.G. MacDiarmid, J. Chem. Phys., 71, 2044 (1979).

212. W.N. Allen, P. Brant, C.A. Carosella, J.J. De Corpo, C.T. Ewing, F.E. Saalfeld and D.C. Weber, Synthetic Metals, 1, 151 (1979/80).

213. A.F. Orchard, 'Basic principles of photoelectron spectroscopy' in 'Handbook of x-ray and ultraviolet photoelectron spectroscopy', Ed. D. Briggs, Heyden, Chapter 1, p.1 (1978).

214. M.E. Galvin and G.E. Wnek, Polymer, 23, 795 (1982).

215. M.F. Rubner, S.K. Tripathy, J. Georger, Jr. and P. Cholewa, Macromolecules, 16, 870 (1983).

216. J.M. Pochan, H.W. Gibson and J. Harbour, Polymer, 23, 439 (1982).

217. J.M. Pochan, H.W. Gibson, F.C. Bailey and D.F. Pochan, Polymer, 21, 250 (1980).

218. S. Lefrant, E. Rzepka, P. Bernier, M. Rolland and M. Aldissi, Polymer, 21, 1235 (1980).

219. L.R. Dalton, University of Southern California, Los Angeles, USA (in preparation).

220. J.M. Pochan, D.F. Pochan and H.W. Gibson, Polymer, 22, 1367 (1981).

221. H.W. Gibson, F.C. Bailey, A.J. Epstein, H. Rommelmann, S. Kaplan, J. Harbour, Xiao-Quing Yang, D.B. Turner and J.M. Pochan, J. Amer. Chem. Soc., 105, 4417 (1983).

222. W. Deits, P. Cukor, M. Rubner and H. Jopson, Synthetic Metals, 4, 199 (1982).

223. J.C.W. Chien, G.E. Wnek, F.E. Karasz and J.A. Hirsch, Macromolecules, 14, 479 (1981).

224. H.E. Galvin and G.E. Wnek, J. Polym. Sci., Polym. Chem. Ed. 21, 2727 (1983).

225. D.C. Weber, P. Brant, C. Carosella and L.G. Banks, J. Chem. Soc. Chem. Comm., 522 (1981).

226. D.T. Clark, 'ESCA applied to organic and polymeric systems', in 'Handbook of x-ray and ultraviolet photoelectron spectroscopy', Ed. D. Briggs, Heyden, Chapter 6, p. 211 (1978).

227. J.J. Pireaux, J. Riga, R. Caudano and J. Verbist, in 'Photon, Electron and Ion Probes of Polymer Structure and Properties', Eds. D.W. Dwight, T.J. Fabish and H.R. Thomas, ACS symposium series No. 162, Washington, Chapter 13 (1981).

228. R.A. Meyers in 'Coal Structure', Ed. R.A. Meyers, Academic Press, New York, Chapter 1 (1982).

229. R.M. Davidson in 'Coal Science' Vol. 1, Eds. M.L. Gorbaty, J.W. Larsen and I. Wender, Academic Press, New York, pp.83-160. (1982).

230. M.L. Gorbaty, 'Challenges in Fossil Energy Chemistry' in Proceedings of the NATO Advanced Study Institute, 'Magnetic Resonance Techniques in Fossil Energy Problems', 3rd - 16th July, 1983, Crete, Greece, D. Reidel Publishing Co., Dordrecht, Holland (in press).

231. J.M. Hunt, 'Petroleum Geochemistry and Geology, W.H. Freeman and Co., San Francisco (1979).

232. Society of chemical industry conference, 'Analytical Methods for Coals, Cokes and Carbons', 28-29th April, 1983, London, UK, Fuel, 62 (9), (1983).

233. P.G. Rouxhet, P.L. Robin and G. Nicaise, 'Characterisation of kerogens and of their evolution by infrared spectroscopy', in 'Kerogen : Insoluble Organic Matter from Sedimentary Rocks', Technip, Paris, pp. 163-190 (1980).

234. D.W. Kuehn, R.W. Snyder, A. Davis and P.C. Painter, Fuel, 61, 682 (1982).

235. P.C. Painter and M.M. Coleman, Internat. Lab., p. 17, April (1980).

236. B.C. Gerstein, P. Dubois Murphy and L.M. Ryan, 'Aromaticity in Coal' in 'Coal Structure', Ed. R.A. Meyers, Academic Press, New York (1982).

237. Proceedings of the NATO Advanced Study Institute, 'Magnetic Resonance Techniques in Fossil Energy Problems', 3rd-16 July, 1983, Crete, Greece, D. Reidel, Dordrecht, Holland (in press).

238. K.J. Packer, R.K. Harris, A.M. Kenwright and C.E. Snape, Fuel, 62, 999 (1983).

239. Basic Coal Sciences Project Advisory Committee Report, Gas Research Institute, Chicago, Illinois, USA (July 1980).

240. G.R. Dyrkacz and E.P. Horwitz, Fuel, 61, 3 (1982).

241. L. Grainger and J. Gibson, 'Coal Utilisation: Technology, Economics and Policy', Graham and Trotman, London (1981).

242. G.M. Bancroft, J.R. Brown and W.S. Fyfe, Chem. Geol., 25, 227 (1979).

243. P. Canesson in 'Advanced Techniques for Clay Mineral Analysis', Ed. J.J. Fripiat, Elsevier, Amsterdam, p. 211 (1982).

244. M.H. Koppelman in 'Advanced Chemical Methods for Soil and Clay Mineral Research', Eds. J.W. Stucki and W.L. Banwart, D. Reidel Publishing Co., Dordrecht, Holland, p.205 (1980).

245. J.M. Adams and S. Evans, Clays, Clay Miner., 27, 48 (1979).

246. D.C. Frost, B. Wallbank and W.R. Leeder in 'Analytical Methods for Coal and Coal Products', Vol. 1, Ed. C. Karr Jr., Academic Press, London, p. 349 (1978) and references therein.

247. J.R. Brown, B.I. Kronberg and W.S. Fyfe, Fuel, 60, 439 (1981).

248. D.T. Clark, R. Wilson and J.M.E. Quirke, Chem. Geol., 39, 215 (1983).

249. R.B. Jones, C.B. McCourt and P. Swift, Int. Conf. Coal Science, Dusseldorf, p. 657 (1981).

250. A. Grint and D.L. Perry, Proc. 15th Biennial Conf. on Carbon, Philadelphia, p. 462 (1981).

251. A. Grint and D.L. Perry, Carbon '82, 6th London International Carbon and Graphite Conf., London, p. 125 (1982).

252. D.L. Perry and A. Grint, Fuel, 62, 1024 (1983).

253. H. Marsh, P.M.A. Sherwood and D. Augustyn, Fuel, 55, 97 (1976).

254. W.D. Schneider and C.A. Luengo, Energy Research, 2, 123 (1978).

255. T.T.P. Cheung, J. Appl. Phys., 53, 6857 (1982).

256. D.T. Clark, J. Peeling and L. Colling, Biochim. Biophys. Acta, 453, 533 (1976).

257. J. Peeling, D.T. Clark, I.M. Evans and D. Boulter, J. Sci. Food Agric., 27, 331 (1976).

258. J. Peeling, B.G. Haslett, I.M. Evans, D.T. Clark and D. Boulter, J. Amer. Chem. Soc., 99, 1025 (1977).

259. D.W. Van Krevelen, 'Coal', Elsevier, Amsterdam (1961).

260. D.G. Murchison and T.S. Westoll (Editors), 'Coal and Coal-Bearing Strata', Oliver and Boyd, Edinburgh (1968).

261. C. Karr Jr. (Ed.), 'Analytical Methods for Coal and Coal Products', Vols 1 - 111, Academic Press, London (1978, 9).

262. B.P. Tissot and D.H. Welte, 'Petroleum Formation and Occurrence', Springer-Verlag, Berlin (1978).

263. E. Stach, M. -Th. Mackowsky, M. Teichmuller, G.H. Taylor, D. Chandra and R. Teichmuller, 'Stach's Textbook of Coal Petrology', 3rd. Edn., Gebruder Borntraeger, Berlin (1982).

264. W. Francis and M.C. Peters, 'Fuels and Fuel Technology', 2nd Edn., Pergamon Press, Oxford (1980).

265. A. Raistrick and C.E. Marshall, 'The Nature and Origin of Coal and Coal Seams', English Universities Press, London, Chapter 13 (1939).

266. N.H. Bostick, Geoscience and Man, 3, 83 (1971).

267. B.R.T. Simoneit, S. Brenner, K.E. Peters and I.R. Kaplan, Nature, 273, 501 (1978).

268. B.R.T. Simoneit, S. Brenner, K.E. Peters and I.R. Kaplan, Geochim. Cosmochim. Acta, 45, 1581 (1981).

269. L.W. Dennis, G.E. Maciel, P.G. Hatcher and B.R.T. Simoneit, Geochim. Cosmochim. Acta, 46, 901 (1982).

270. J. Perregaard and E.J. Schiener, Chem. Geol., 26, 331 (1979).

271. W. Hopkins, Proc. Geological Assoc. London, 42, 238 (1931).

272. H. Briggs, Trans. Inst. Min. Eng., 89, 187 (1934-5).

273. C. E. Marshall, Trans. Inst. Min. Eng., 91, 235 (1935-6).

274. J.H. Jones, Inst. Fuel War Time Bull., p. 89, Feb. (1945).

275. J.A. Smythe and K.C. Dunham, J. Mineral. Soc., 28, 53 (1947).

276. G. Armstrong and R.H. Price, Trans. Inst. Min. Eng., 113, 974 (1953-4).

277. A.H. Edwards and T.S. Tomlinson, Trans. Inst. Min. Eng., 117, 50 (1957-8).

278. J.M. Jones and S. Creaney, J. Microsc., 109, 105 (1977).

279. B.J. Taylor, I.C. Burgess, D.H. Land, D.A.C. Mills, D.B. Smith and P.T. Warren, 'British Regional Geology - Northern England', 4th Edn., H.M.S.O., London (1971).

280. G.A.L. Johnson, 'Geology of Durham County', Ed. G. Hickling, 2nd. Edn., Trans. Nat. Hist. Soc. Northumberland, Durham and Newcastle Upon Tyne, 41, No. 1, (1972).

281. C.R. Warn, 'Rocks and Scenery from Tyne to Tweed', Frank Graham, Newcastle Upon Tyne (1975).

282. D.A. Robson Ed., 'The Geology of North East England', Nat. Hist. Soc. Northumbria, Newcastle Upon Tyne (1980).

283. A. Holmes and H.F. Harwood, J. Mineral. Soc., 22, 1 (1929).

284. D. Blythe, N.C.B., Personal communication.

285. H.J.Kirsch and G.H. Taylor, Econ. Geol., 61, 343 (1966).

286. D.G. Murchison, 'Optical Properties of Carbonised Vitrinites', Chapter 31 in 'Analytical Methods for Coal and Coal Products', Vol. 2, C. Karr Jr. (Ed.), Academic Press, London (1978).

287. H. Marsh and J. Smith, 'The Formation and Properties of Anisotropic Cokes from Coals and Coal Derivatives Studied by Optical and Scanning Electron Microscopy', Chapter 30 in 'Analytical Methods for Coal and Coal Products', Vol. 2, C. Karr Jr. (Ed.), Academic Press, London (1978).

288. M.C. Stopes, Fuel, 14, 4 (1935).

289. J.M. Jones, personal communication.

290. H.E. Blayden, J. Gibson and H.L. Riley, 'The Ultra-Fine Structure of Coals and Cokes', proc. BCURA Conference, p. 176 (1944).

291. H. Marsh, Fuel, 50, 280 (1971).

292. H.H. Read, 'Rutley's Elements of Mineralogy', 26th Edn., T. Murby, London (1970).

293. R. Hardy, personal communication (JCPDS card 23-64).

294. B. Mukherjee, Econ. Geol., 60, 1451 (1965).

295. P. Kar, J. Geol. Soc. India, 19, 558 (1978).

296. J.C. Crelling, R.H. Schrader and L.G. Benedict, Fuel, 58, 542 (1979).

297. T. Yokono, K. Miyazawa, Y. Sanada and H. Marsh, Fuel, 60, 598 (1981).

298. C.-Y. Chang, J.A. Guin and A.R. Tarrer, J. Chinese Chem. Soc., 28, 155 (1980).

299. A. Grint and D.L. Perry, unpublished results.

300. R.E. Jones and D.T.A. Townend, J. Soc. Chem. Ind. (London), 68, 197 (1949).

301. L. Blom, L. Edelhausen and D.W. Van Krevelen, Fuel, 36, 135 (1957).

302. R. Liotta, G. Brons and J. Isaacs, Fuel, 62, 781 (1983).

303. D.L. Carpenter and G.D. Sergeant, Fuel, 45, 429 (1966).

304. B. Durand and G. Nişaise in 'Kerogen : Insoluble Organic Matter from Sedimentary Rocks', Technip. Paris, pp. 113-142 (1980).

305. P.C. Painter, D.W. Kuehn, M. Starsinic, A. Davis, J.R. Havens and J.L. Koenig, Fuel, 62, 103 (1983).

306. A. Davis, 'A data base for the analysis of compositional characteristics of coal seams and macerals', Quarterly Technical Progress Report, May - June 1980, DOE contract DOE-30013-2.

307. T. Stadnichenko, Econ. Geol., 29, 511 (1934).

308. E.T. Degens, E.G. Williams and M.L. Keith, Bull. Amer. Assoc. Petrol. Geol., 41, 2427 (1957).

309. E.T. Degens, E.G. Williams and M.L. Keith, Bull. Amer. Assoc. Petrol. Geol., 42, 981 (1958).

310. E.G. Williams and M.L. Keith, Econ. Geol., 58, 720 (1963).

311. J.C. Ferm and E.G. Williams, J. Sed. Petrol., 35, 319 (1965).

312. W.E. Edmunds, T.M. Berg, W.D. Sevon, R.C. Piotrowski, L. Heyman and L.V. Richard, 'The Mississippian and Pennsylvanian (Carboniferous) Systems in the United States - Pennsylvania and New York', Ecological Survey Professional Paper 1110-A-L, U.S. Govnt. Printing Office, Washington, pp. B1-B33 (1979).

313. F.T.C. Ting, 'Coal Macerals' in 'Coal Structure', Ed. R.A. Meyers, Academic Press, New York, p. 7 (1982).

314. D.J. Casagrande, K. Siefert, C. Berschinski and N. Sutton, Geochim. Acta, 41, 161 (1977).

315. R. Markuszewski, personal communication.

316. Pennsylvania State University Coal Data Base.

317. J.A. Solomon and G.J. Mains, Fuel, 56, 303 (1977).

318. W.J. Montgomery, 'Standard Laboratory Test Methods for Coal and Coke', in 'Analytical Methods for Coal and Coal Products', Vol. 1, Ed. C. Karr Jr., Academic Press, Chapter 6 (1978).

319. R.E. Dudley and C.A. Fyfe, Fuel, 61, 651 (1982).

320. J. Howard, C.J. Ludman and J. Tomkinson, Fuel, 62, 1097 (1983).

321. D.T. Clark and R. Wilson, unpublished results.

322. D.T. Clark, J.M.E. Quirke and R. Wilson, unpublished results.

323. S.H. Pinner and W.G. Simpson, 'Plastics : Surface and Finish', Butterworths, London (1977).

324. D. Brewis (Ed.), 'Surface Analysis and Pretreatment of Plastics and Metals', Applied Science Publ. Ltd. (1982).

325. H. Schonhorn and R.H. Hansen, J. Appl. Polym. Sci., 11, 1461 (1967).

326. C.B. Jones, Soc. Plast. Eng. Tech. Pap., 25, 724 (1979).

327. B. Budesinsky, Anal. Chem., 37, 1159 (1965).